Ozonation and/or Coagulation - Ceramic Membrane Hybrid for Filtration of Impaired-Quality Source Waters

Dissertation by

Changwon Ha

In Partial Fulfillment of the Requirements
For the Degree of
Doctor of Philosophy

King Abdullah University of Science and Technology
Thuwal, Kingdom of Saudi Arabia

September 2013

EXAMINATION COMMITTEE APPROVALS FORM

EXAMINATION COMMITTEE	NAMES
Committee Chairperson:	Prof. Gary L. Amy
Committee Member:	Prof. Maria D. Kennedy
Committee Member:	Prof. Suzanna Nunes
Committee Member:	Prof. Zhiping Lai

ABSTRACT

Ozonation and/or Coagulation - Ceramic Membrane Hybrid for Filtration of Impaired-Quality Source Waters

Changwon Ha

When microfiltration (MF) and ultrafiltration (UF) membranes are applied for drinking water treatment/wastewater reuse, membrane fouling is an evitable problem, causing the loss of productivity over time. Polymeric membranes have been often reported to experience rapid and/or problematical fouling, restraining sustainable operation. Ceramic membranes can be effectively employed to treat impaired-quality source waters due to their inherent robustness in terms of physical and chemical stability. This research aimed to identify the effects of coagulation and/or ozonation on ceramic membrane filtration for seawater and wastewater (WW) effluent. Two different types of MF and UF ceramic membranes obtained by sintering (i.e., TAMI made of TiO_2+ZrO_2) and anodic oxidation process (i.e., AAO made of Al_2O_3) were employed for bench-scale tests.

Precoagulation was shown to play an important role in both enhancing membrane filterability and natural organic matter (NOM) removal efficacy for treating a high-organic surface water. The most critical factors were found to be pH and coagulant dosage with the highest efficiency resulting under low pH and high coagulant dose. Due to the ozone-resistance nature of the ceramic membranes, preozonation allowed the ceramic membranes to be operated at higher flux, especially leading to significant flux improvement when treating seawater in the presence of calcium and magnesium.

Dissolved ozone in contact with the TAMI ceramic membrane surface accelerated the formation of hydroxyl (˙OH) radicals in WW effluent treatment. Flux restoration of both ceramic membranes, fouled with seawater and WW effluent, was efficiently achieved by high backwash (BW) pressure and ozone in chemically enhanced backwashing (CEB). Ceramic membranes exhibited a pH-dependent permeate flux while filtering WW effluent, showing reduced fouling with increased pH. On the other hand, for filtering seawater, differences in permeate flux between the two membranes was observed under basic pH conditions, showing that the TAMI membrane flux was stable regardless of changes in pH, while the AAO membrane flux was significantly decreased as pH increased to 10.

Consequently, it is expected that ozone and/or coagulation prior to ceramic membrane filtration can play a significant role in treating impaired-quality source waters (e.g., seawater and WW effluent), leading to maintaining sustainable membrane flux in seawater pretreatment before reverse osmosis (RO) or water reuse applications.

Keywords: ceramic membrane, NOM, ozonation, precoagulation, water reuse

ACKNOWLEDGEMENTS

I am glad that this dissertation is successfully completed at the end with supports from many people. First of all, I would like to express my sincere gratitude to my supervisor, Prof. Gary Amy, for granting me his positive response, guidance and consideration at all times, encouraging me to bridge over many facing difficulties while studying from the Netherlands to Saudi Arabia. Also, my mentor, Prof. Maria Kennedy is deeply appreciated for providing me useful guidance not only for research, but also individual problems during stay in the Netherlands.

A doctoral degree could not be achieved by one's own. Colleagues and friends were there to provide scientific idea, technical supports, inspiring advice and constant warmth. The bearers of these were (in alphabetical order) Ahmed Kasmi, Cyril Aubry, Faisal Wali, Juma Hamad, Min Yoon, Sairam Sudhakaran, Sanghyun Jeong, Shereen Bawazeer, Tao Zhang, Tong Zhan, Victor Yangali-Quintanilla and Zhenyu Li.

Last, but not least, I would like to thank my parents, Hanjoon Ha and Heesoon Cho, my wife, Yoonhee Kang, and my lovely two sons, Chi and Chan, for their endless love, support and patience during all my stay abroad. I never thought that I could do it without you all.

Changwon Ha

TABLE OF CONTENTS

LIST OF FIGURES

LIST OF TABLES

Chapter 1

Introduction and Research Objectives

1.1. INTRODUCTION

Application of low pressure membrane (LPM) filtration such as microfiltration (MF) and ultrafiltration (UF) has been developed into a widely established technology for drinking water treatment, with a steady worldwide increase in installed production capacity over the past couple of decades as a result of increasingly stringent discharge standards and increased water reclamation demand. Compared to conventional water treatment, LPMs have many advantages in terms of a stable process with various raw water qualities, the need for a small treatment plant, and highly automatic and safe operation. Most of these full-scale plants have been designed for polymeric membranes because recently technical advances and cost declines in polymer technologies have led to significant increases in the application of membrane processes for water and wastewater treatment.

1.1.1. Statement of Problem

A key constraint to further application of membrane technology is fouling, which is a main factor increasing the costs of operation and maintenance by deteriorating sustainable membrane performance and shortening lifetime (Pontié et al. 2007). In particular, it has been shown that in both drinking water and wastewater applications, a major constraint is organic fouling associated with bulk natural organic matter (NOM) or effluent organic matter (EfOM) causing irreversible fouling (Amy 2008, Huang et al. 2007, Lee et al. 2008, Lee et al. 2004).

One of the techniques that can reduce organic fouling includes coagulation pretreatment in combination with LPM filtration. According to previous research, it has been frequently reported that MF/UF membranes can remove some organic matter with improved membrane performance and reduced fouling when coupled with precoagulation (Dong et al. 2007a, Matsushita et al. 2005, Volk et al. 2000). Nevertheless, some limitations such as the lack of durability against extreme pH and temperature, and relatively premature degradation by biological and chemical agents have been considered as major deficiencies of polymeric membranes (Lee et al. 2005b, Seidel and Elimelech 2002). Eventually, loss of productivity resulting from fouling, low resistance to cleaning chemicals, and low permeability, have limited their widespread usage and performance in drinking water (DW) treatment. That is why there are calls for new approaches for more efficient and economic alternatives.

Ceramic membranes, one of the alternatives to overcome these problems, have recently been introduced into the water-sector marketplace. Ceramic membranes have many attractive attributes in terms of their inherent mechanical, thermal and chemical stability, allowing them to be operated at higher permeability, less frequent cleaning, and a longer lifetime than those of the more conventional polymeric ones (Lee and Cho 2004). They are generally asymmetric structures, consisting of a supporting layer with large pores (having low flow resistance) of sufficient mechanical strength on top of which are layers with gradually decreasing pore size (Burggraaf and Cot 1996). This can be an advantage for obtaining relatively higher fluxes from thin separation layers. The principal chemical properties of ceramic membranes are their hydrophilicity (Dafinov et al. 2002, Larbot et al. 2004) and their negatively-charged surface due to the presence of hydroxyl (OH^-) groups on their metal-oxide surfaces.

These features contribute to high permeability, and influence separation ability and fouling potential as well (Dafinov et al. 2002).

Unfortunately, in spite of these positive features, polymeric membranes have still been employed in the majority of water treatment plants because of higher capital costs involved in ceramic membrane modules. Recently, the production cost has substantially been decreasing due to technological advances. More than a decade ago, the cost of producing ceramic membranes was up to five times as high as polymeric ones (Garmash et al. 1995), whereas, more recent estimates have shown that this has gone down to only twice as expensive (Baruah et al. 2006). The attractive merits, such as higher flux, less frequent cleaning, and the longer lifetime of ceramic membranes, especially for the hybrid process of coagulation and ceramic membrane filtration, are getting more attention as an alternative for surface water treatment.

1.1.2. Recent research studies on ceramic membrane filtration

Recent pilot scale studies have suggested that the coagulation process with monolithic ceramic MF membranes at a constant flux in a direct filtration (dead-end) mode can be optimized to such an extent that their employment was competitive with polymeric hollow fibre membranes (Konieczny et al. 2006, Lerch et al. 2005). Lately, the increase of natural organic matter (NOM) in natural water sources, partly caused by progressing climate change, has become a growing concern in DW treatment applications. Reverse osmosis (RO) or nano-filtration (NF) has been successfully applied as a robust solution to address the problem in recent years. However, coagulation/flocculation pretreatment in combination with MF ceramic membrane

filtration is being emphasized as an effective alternative in terms of less energy consumption and long term operation, resulting in efficient removal of NOM.

The coagulation process has significant effects on the water quality and operating conditions when implemented prior to LPM filtration, especially MF, rather than used alone. Many studies have shown that a coagulation prior to MF membrane hybrid system not only increases the removal of NOM, viruses, and micro-contaminants which are smaller than the membrane pore size, but also improves the membrane performance due to fouling reduction. However, these studies have usually been carried out for polymeric membranes, but have not been closely looked at for ceramic membranes.

Ozone has been frequently employed for oxidation in water and wastewater treatment applications. Because of the robustness of ceramic membranes, ozone as a strong oxidant can be effectively used for pretreatment reducing membrane fouling. (Mori et al. 1998) investigated the effect of ozone prior to MF membrane process for treatment of surface water and secondary treated municipal wastewater. They found that organic gels adhering onto the membrane could be decomposed by ozone, resulting in less fouling and higher flux. It has been demonstrated through a pilot-scale test that a ceramic MF membrane showed stable performance at a filtration flux of 100gfd (170LMH) at 20° C with pretreatment using PACL (1mg/L as Al) and ozone (4mg/L) (Lehman and Liu 2009). They also demonstrated that ozone treatment is effective at degrading colloidal NOM which is likely responsible for the majority of membrane fouling.

The impact of fouling on flux decline is the limiting factor in the operation of membrane filtration. Membrane fouling can be defined as the reduction in permeability or increase in trans-membrane pressure during filtration, caused by the accumulation of foulants on the membrane surface or inside the pores. Therefore, factors affecting fouling, including operational conditions, major foulant types, and physical/chemical cleaning regime, are of primary interest to optimize the membrane performance. The research regarding fouling of polymeric membranes has been quite intensively conducted, but even the major foulants and fouling mechanisms have not been well investigated for ceramic membranes in DW applications. Considering this point, it is very important to identify and characterize these factors in order to optimize ceramic membrane performance. Once primary foulants can be identified for ceramic membranes, the optimal operational conditions for pretreatment such as coagulation and ozonation can be proposed to specifically target these components.

In a hybrid MF membrane system with coagulation or ozone treatment, a fouling layer is generally formed by the deposition of different kinds of particles, colloids, organic (macro) molecules and flocs. For optimizing appropriate operational performances with respect to economic and procedural engineering aspects, it is necessary to determine how limiting factors take place and how they are alleviated by an optimal design and operating conditions. More research is needed and advancements should be found so that ceramic membranes can be more effectively and more widely employed to produce potable drinking water.

1.2. RESEARCH AIMS AND OBJECTIVES

Ceramic membranes represent a new generation of materials as an alternative to polymeric ones that have been being applied to most full-scale plants. Because ceramic membranes are mechanically superior and are more resistant to severe chemical and thermal environments, it is expected that they can provide higher permeability, less frequent cleaning, and a significantly longer lifetime in combination with coagulation and strong oxidants such as ozone. Moreover, these features can play significant roles in effectively treating impaired-quality source waters, seawater and wastewater (WW) effluent.

The research aims to optimize precoagulation with ceramic membrane filtration to not only reduce membrane fouling, but also improve permeability; to investigate ozone (O_3) effects as a pretreatment or chemically enhanced backwashing (CEB) on ceramic membrane filtration for filtration of seawater and WW effluent. Fundamental properties of different types/materials of ceramic membranes and their susceptibility to NOM or EfOM foulants present in impaired-quality water sources (i.e. seawater and WW effluent) are investigated using various the-state-of-the-art technologies.

1.2.1. Expected roles of ceramic membranes

Aforementioned, ceramic membranes can be effectively applied to maximize the removal of dissolved organic carbon (DOC), some organics, viruses, micro-contaminants, as well as improve the membrane performance due to fouling reduction. Aggressive performance possible and expected roles of ceramic membranes in both

drinking water and WW reuse applications are summarized as followings, focused on their inherent mechanical and chemical robustness:

Aggressive performance possible

1. High flux operation (e.g., 200, 300 LMH, or higher for MF/UF performance)
2. Strong oxidants such as ozone (O_3) and/or coagulation under acidic conditions prior to ceramic membrane filtration which is a so-called hybrid
3. Very high pressure backwashing (BW) (e.g., 5 times, 10 times, 20 times, or far higher than operational pressure) for very short time (e.g., 5 sec, or lower)
4. Chemically enhanced backwashing (CEB) using ozone (O_3)

Roles expected in DW applications

1. High productivity by elevating membrane operational flux
2. Significant improvement of membrane filterability by reducing membrane fouling as a result of combination with ozone and/or coagulation pretreatments
3. Increase in fouling reversibility by not only high pressurized BW, but also ozone (O_3)-enhanced backwashing as a CEB
4. High performance in treating impaired-quality source waters (e.g., seawater and wastewater), leading to successful employment as one of the powerful pretreatments before RO in desalination or reuse applications

1.2.2. Key research questions

Many questions are posed to answer for determining the optimal use and better application of ceramic membranes in drinking water-sectors.

1) What are the fundamental properties of ceramic membranes influencing operation, e.g., synthetic layer composition, porous nature (i.e., pore size and distribution), surface roughness, pure water permeability (PWP), contact angle, surface charge, etc.?
2) Does ceramic membrane filtration have benefit(s), compared to polymeric membrane filtration for treating impaired-quality source waters such as seawater and WW effluent? If so, what is (are) the most attractive advantage(s)?
3) Can precoagulation improve ceramic membrane filtration in terms of productivity and filterability for treatment of high-organic surface water and WW effluent? If so, what are the optimal coagulation conditions (i.e., coagulant dosage, mixing intensity (G; s^{-1}) and time (T; sec) and pH) to optimize the membrane performance, to enhance NOM removal and to reduce fouling?
4) Can preozone (O_3) be effectively used with ceramic membrane filtration to reduce membrane fouling and to degrade colloidal NOM fouling? If so, what are the main mechanisms? And, is there any difference between seawater and WW effluent?
5) Can ozone (O_3) be also employed to recover flux for fouled membranes as one of the cleaning agents in CEB? If so, how effectively can it work?

1.2.3. Hypotheses

Several hypotheses are formulated to solve the key research questions mentioned above based on the literature survey (chapter 2) as follows:

1) Ceramic membranes have a longer lifetime and a higher permeability than polymeric membranes allowing for higher operational fluxes and a potentially lower fouling rate. Moreover, further improvement in performance can be realized when employing pretreatment processes, such as coagulation and ozone (O_3) prior to the membrane filtration. In particular, ozone pretreatment allows the ceramic membrane to operate sustainably under optimized conditions because of the ozone-resistant nature of the ceramic materials.
2) Very high backwashing pressure (e.g., up to about 4 bars, corresponding to more than 20 times higher than TMP) can be possibly applied to completely recover fouled-membrane flux, attributed to robustness of the ceramic membrane.
3) When using coagulation and ozonation pretreatment with ceramic MF filtration, the removal of NOM, viruses, and micro-contaminants coupled with liquid-solids separation can be accomplished.
4) Precoagulation can effectively enhance the MF ceramic membrane performance (i.e., permeate flux, TMP, hydraulic resistance, fouling reversibility and NOM removal) rather than by MF alone. This enhancement is possible by enhanced particle transport, reduced pore plugging, reduced compaction of foulants and improved backwashing efficiency attributed to a more porous cake layer formed on the membrane.
5) The higher efficiency of ceramic MF membranes aided by precoagulation can be achieved with the creation of only small flocs, or pin flocs, unlike what is necessary in the conventional coagulation process. These pin flocs being accumulated on the membrane surface with an incompressible porous cake

layer would result in lower modified fouling index (MFI) values, leading to less fouling, improved filterability and backwashability of the membrane.

6) An ozone (O_3) – ceramic membrane *hybrid* can be successfully applied to treat impaired-quality source waters (i.e., seawater and WW effluent). Not only does ozone (O_3) degrade micro-organisms and NOM causing problematical membrane fouling, but it provides ozone-induced coagulation of particles/ colloids and (macro) molecules through binding with metal ions such as calcium (Ca^{2+}) and magnesium (Mg^{2+}), higher in presence in seawater compared to WW effluent.
7) Ozone (O_3) can play an important role in improving ceramic membrane flux, reducing membrane fouling, and enhancing filterability as a pretreatment. Moreover, in the case where ozone is used to clean the fouled membrane as a chemically enhanced backwashing (CEB), recovery rate can be significantly increased with even small amount of ozone dosage and for short BW duration.

1.2.4. Specific objectives

Based on the key research questions and hypotheses stated above, the overall aim and objectives of this research are to identify the effects of coagulation and/or ozonation on ceramic membrane filtration for impaired-quality source waters (i.e., seawater and WW effluent). The optimal conditions for coagulation and ozonation are determined for improving the removal efficiency of contaminants, creating conditions for minimum resistance against the ceramic membrane, and minimizing membrane fouling. Especially, the effects of ozone (O_3) as a pretreatment or CEB on ceramic membrane performance are assessed. Results from the research are expected to further

elevate the advantages of ceramic membranes in both drinking water and wastewater applications, allowing for higher operating fluxes and a potentially lower fouling rate.

The specific objectives of this study are summarized as follows:

1) To investigate fundamental properties of two different kinds of ceramic membranes which are fabricated by sintering (TAMI based on TiO_2+ZrO_2) and anodic oxidation process (AAO based on Al_2O_3).
2) To identify roles of ceramic membranes in treating impaired-quality source waters (i.e., seawater and WW effluent); high operation fluxes up to about 400 LMH are assessed. Ozone and coagulation are used in combination with ceramic membrane filtration, identifying the effects on permeability, fouling, NOM removal, and recovery rate.
3) To optimize coagulation prior to ceramic membrane filtration for improving NOM removal and reducing fouling; various parameters such as coagulant dosage, velocity gradient (G; s-1), mixing time, and pH, are considered to determine the optimal conditions
4) To assess effects of preozonation on ceramic membrane filtration in terms of permeability and fouling reduction; two types of ceramic membranes (i.e., TAMI and AAO) are compared as a function of ozone dose, differentiated for seawater and WW effluent applications in the presence of cationic metal ions such as calcium (Ca^{2+}) and magnesium (Mg^{2+})
5) To evaluate recovery rate of two ceramic membranes fouled with both seawater and WW effluent; very high BW pressures up to 20 times as high as operational pressure and ozone (O_3) as a CEB are applied.

6) To investigate pH-dependent flux behaviors of two ceramic membranes for filtration of seawater and WW effluent; two ceramic membrane performances are compared over a wide range of pH conditions from 4 to 10.
7) To identify the impacts of three NOM types in the presence/absence of calcium on filtration by two ceramic membranes in terms of permeability and removal efficiency, comparing with polymeric membranes such as polyvinylidene difluoride (PVDF) and mixed cellulose ester (MCE).

1.3. OUTLINE OF THE STUDY

1.3.1. Materials and methods

Three types of impaired-quality source waters including a high-organic surface water, a secondary WW effluent, and Red Sea seawater were sampled for the research; relevant water qualities are briefly summarized as follows:

High-organic surface water is taken from the Westvest canal in Delft, the Netherlands, reflecting a high concentration of DOC originating from terrestrial and agricultural sources; turbidity is between 35NTU and 4.5NTU; DOC ranges from 11.86 mg/L to 13.93 mg/L and UVA_{254} (UV absorbance at 254 nm) from 41.8 m^{-1} to 59.6 m^{-1}, corresponding to SUVA (specific UV absorbance) values between 3.5 L/mg·m and 4.3 L/mg·m.

Secondary WW effluent is collected from the Jeddah secondary WWTP which is treated by an anoxic-oxic (AO) activated sludge process; DOC is between 5 mg/L to 7

mg/L and pH ranges from 7.5 to 7.7; SUVA values are between 2.0 L/mg·m and 2.5 L/mg·m.

Seawater is sampled from the Red Sea near Thuwal in Saudi Arabia, characterized by high levels of salts and a low DOC of about 1 mg/L; SUVA is ≈1.0 L/mg·m.

Two kinds of ceramic membranes are used for the study. One (designated as TAMI) is fabricated by sintering from the TAMI INDUSTRIES and another (designated as AAO) by anodic oxidation process from Whatman. Feed water, which is either raw water or pretreated water with coagulation or ozonation, is processed through different filtration modes (mode 1 for the AAO membrane; mode 2 for the TAMI) as shown in Figure 1.1 and Figure 1.2. The filtered water is characterized in terms of both permeability and NOM removal using various analytical tools. Membranes that are fouled with raw water and pretreated raw water are autopsied, imaged using various microscopic analysers.

In more details, the time-dependant permeability, water quality and associated adsorptive retention and capacity of foulants by ceramic membranes are determined. Disc membrane specimens; new, fouled, and cleaned; are characterized according to flux decline, contact angle, surface charge, foulant autopsy and surface morphology/roughness. The modified fouling index (MFI) and Hermia's model is used to predict membrane fouling. A series of measurements are be employed to characterize organic matter and particulate/colloidal components including liquid chromatography with organic carbon detector (LC-OCD), three dimensional excitation-emission matrix (F-EEM), and specific UV absorbance (SUVA =

UVA_{254}/DOC). Several analytical protocols that can be applied to characterize fouled membranes are employed as part of membrane autopsies, including atomic force microscopy (AFM), scanning electron microscopy (SEM), and X-ray diffraction/fluorescence (XRD/XRF).

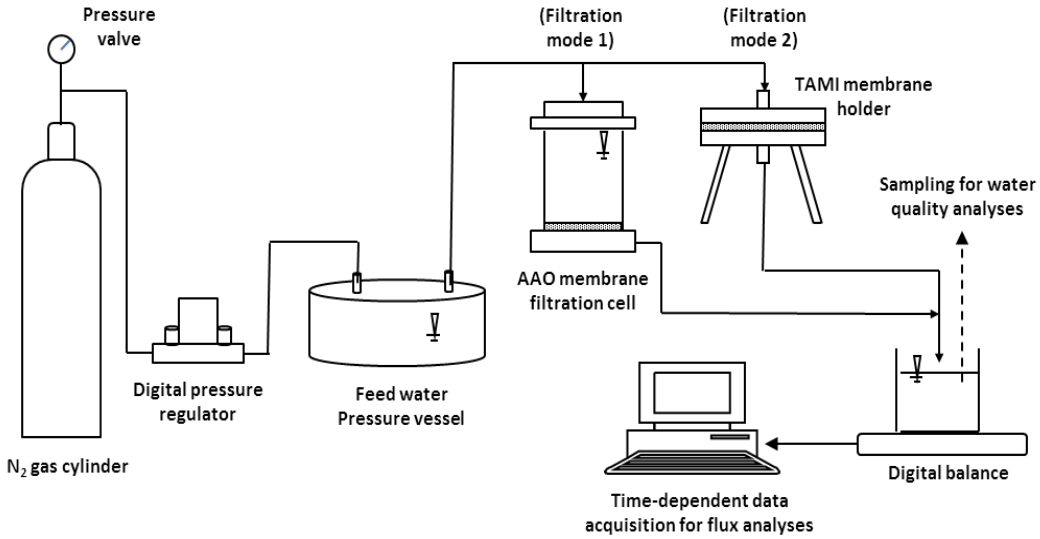

Figure 1.1 - Schematic of ceramic membrane filtration test unit

Figure 1.2 - Photographs of filtration mode 1(left) and mode 2(right)

1.3.2. Thesis structure

This thesis contains five main phases; the chapters are written in journal article format. Chapters 4 and 5 have already been submitted, and Chapters 6, 8, 9, and 10 will be submitted to scientific journals in September 2013.

Chapter 1 is an introduction and research approach section that covers i) research goals and aims; ii) hypotheses and specific objectives; iii) general methodology and approach of the research.

Chapter 2 reviews general background information on ceramic membrane filtration in drinking water-sector applications, including low pressure membrane (LPM) technology, ceramic membranes, pretreatments, membrane fouling mechanisms, cleaning, and sustainable flux.

Chapter 3 (Phase 1) identifies fundamental properties of two different kinds of ceramic membranes that are used for this research. Ceramic membranes which are fabricated by sintering (made of TiO_2 + ZrO_2, designated as TAMI) and anodic oxidation (made of Al_2O_3, designated as AAO) are selected for this phase. Several membrane properties that are necessary for understanding the phenomena of membrane performance, such as pure water permeability (PWP), pore size and distribution, surface roughness, contact angle (°), and zeta potential (ζ) are identified with various analytical methods.

Chapter 4 and 5 (Phase 2) investigates precoagulation effects on ceramic membrane filtration for treatment of impaired-quality source waters, such as a high-organic surface water and WW effluent. This phase is separated into two chapters as follows:

Phase 2-1: Optimization of coagulation prior to ceramic membrane filtration to enhance NOM removal and maintain sustainable flux for treatment of high-organic surface water; Phase 2-2: Effects of enhanced pre-coagulation on ceramic membrane filtration for treatment of secondary WW effluent.

Chapter 6 and 7 (Phase 3) focuses on assessment of an ozone (O_3) - ceramic membrane hybrid on fouling reduction and reversibility in water reuse applications. Ozone is used as a pretreatment and chemically enhanced backwashing (CEB) to reduce membrane fouling for impaired-quality source waters such as seawater and WW effluent. This phase is also separated into two chapters as follows:

Phase 3-1: Effects of ozone-induced flocculation of particles on ceramic membrane filtration in the presence of calcium (Ca^{2+}) and magnesium (Mg^{2+}); Phase 3-2: Effects of ozone on ceramic membrane fouling as a pretreatment and chemically enhanced backwashing (CEB)

Chapter 8 (Phase 4) compares two ceramic membranes performances (i.e., TAMI vs. AAO) for treatment of seawater and secondary WW effluent under wide range of pH conditions. Through this chapter, their fundamental properties, preozonation effects on filterability, and the flux recovery rate are differentiated by membrane autopsies and NOM characterization analysis.

Chapter 9 (Phase 5) aims to identify the impacts of three natural organic matter (NOM) types (i.e., humic acids (HA), bovine serum albumin (BSA), and sodium alginate (SA)) in the presence and absence of calcium on two ceramic membrane filtration in terms of permeability and removal efficiency, comparing with polymeric membranes made of PVDF and MCE.

1.4. REFERENCES

Pontié, M., Thekkedath, A., Kecili, K., Habarou, H., Suty, H. and Croué, J.P. (2007) Membrane autopsy as a sustainable management of fouling phenomena occurring in MF, UF and NF processes. Desalination 204(1-3), 155-169.

Huang, H., Lee, N., Young, T., Gary, A., Lozier, J.C. and Jacangelo, J.G. (2007) Natural organic matter fouling of low-pressure, hollow-fiber membranes: Effects of NOM source and hydrodynamic conditions. Water Research 41(17), 3823-3832.

Lee, E.K., Chen, V. and Fane, A.G. (2008) Natural organic matter (NOM) fouling in low pressure membrane filtration -- effect of membranes and operation modes. Desalination 218(1-3), 257-270.

Lee, N., Amy, G., Croué, J.-P. and Buisson, H. (2004) Identification and understanding of fouling in low-pressure membrane (MF/UF) filtration by natural organic matter (NOM). Water Research 38(20), 4511-4523.

Amy, G. (2008) Fundamental understanding of organic matter fouling of membranes. Desalination 231(1-3), 44-51.

Volk, C., Bell, K., Ibrahim, E., Verges, D., Amy, G. and Lechevallier, M. (2000) Impact of enhanced and optimized coagulation on removal of organic matter and its biodegradable fraction in drinking water. Water Research 34(12), 3247-3257.

Dong, B.-z., Chen, Y., Gao, N.-y. and Fan, J.-c. (2007) Effect of coagulation pretreatment on the fouling of ultrafiltration membrane. Journal of Membrane Science 19, 278-283.

Matsushita, T., Matsui, Y., Shirasaki, N. and Kato, Y. (2005) Effect of membrane pore size, coagulation time, and coagulant dose on virus removal by a coagulation-ceramic microfiltration hybrid system. Desalination 178(1-3), 21-26.

Lee, N., Amy, G. and Lozier, J. (2005) Understanding natural organic matter fouling in low-pressure membrane filtration. Desalination 178(1-3), 85-93.

Seidel, A. and Elimelech, M. (2002) Coupling between chemical and physical interactions in natural organic matter (NOM) fouling of nanofiltration membranes: implications for fouling control. Journal of Membrane Science 203(1-2), 245-255.

Lee, S. and Cho, J. (2004) Comparison of ceramic and polymeric membranes for natural organic matter (NOM) removal. Desalination 160(3), 223-232.

Burggraaf, A.J. and Cot, L. (1996) Fundamentals of inorganic membrane science and technology, Elsevier.

Dafinov, A., Garcia-Valls, R. and Font, J. (2002) Modification of ceramic membranes by alcohol adsorption. Journal of Membrane Science 196(1), 69-77.

Larbot, A., Gazagnes, L., Krajewski, S., Bukowska, M. and Wojciech, K. (2004) Water desalination using ceramic membrane distillation. Desalination 168, 367-372.

Garmash, E.P., Kryuchkov, Y.N. and Pavlikov, V.N. (1995) Ceramic membrane for ultra- and microfiltration (Review). Glass and Ceramic 52(6), 150-152.

Baruah, G.L., Nayak, A. and Belfort, G. (2006) Scale-up from laboratory microfiltration to a ceramic pilot plant: Design and performance. Journal of Membrane Science 274(1-2), 56-63.

Konieczny, K., Bodzek, M. and Rajca, M. (2006) A coagulation-MF system for water treatment using ceramic membranes. Desalination 198(1-3), 92-101.

Lerch, A., Panglisch, S., Buchta, P., Tomita, Y., Yonekawa, H., Hattori, K. and Gimbel, R. (2005) Direct river water treatment using coagulation/ceramic membrane microfiltration. Desalination 179(1-3), 41-50.

Thomas, M. and TorOve, L. (2010) Comparison of optional process configurations and operating conditions for ceramic membrane MF coupled with coagulation/floculation pretreatment for the removal of NOM in drinking water production. Journal of Water Supply: Research and Technology-AQUA 59(2-3), 81-91.

Mori, Y., Oota, T., Hashino, M., Takamura, M. and Fujii, Y. (1998) Ozone-microfiltration system. Desalination 117(1-3), 211-218.

Lehman, S.G. and Liu, L. (2009) Application of ceramic membranes with preozonation for treatment of secondary wastewater effluent. Water Research 43(7), 2020-2028.

Chapter 2

Background Information

2.1. MEMBRANE FILTRATION

A membrane has the ability to transport one component more easily than others due to differences in physicochemical properties between the membrane and the solute, where the transport through the membrane takes place as a result of a driving force to which the permeation rate (i.e., flux) is proportional. The principal fouling mechanism of membrane filtration is to remove certain particles by not only straining through size exclusion (also called sieving or steric exclusion), but also adsorption or as a result of cake formation on the membrane surface (Figure 2.1).

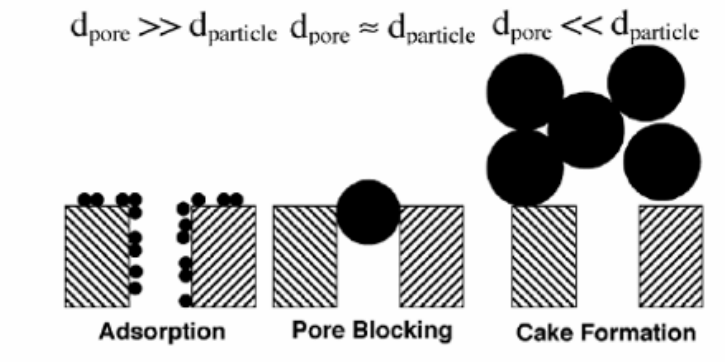

Figure 2.1 - Principal fouling mechanism of membrane filtration [Source: (Hashino et al. 2011b)]

Cake filtration means that each particle settles on other particles previously deposited and already blocking the pores, but when there is no room for particles to directly block membrane area. The cake can be classified as compressible or incompressible depending on the nature of the particles, such as shape, size distribution and rigidity. When the cake material is compressible, then the specific resistance is pressure dependent and the porosity will change with pressure. Conversely, the specific

resistance of incompressible cake will be constant over time as the porosity is pressure and time independent.

2.1.1. Classification of membranes

Membrane separation processes used for water production are mainly classified into four types - microfiltration (MF), ultrafiltration (UF), nanofiltration (NF), and reverse osmosis (RO) - in drinking water treatment applications. The major characteristics of these membrane types are summarized in Table 2.1. These four kinds of membranes are generally categorized into low pressure membranes (LPM), such as MF and UF, and high pressure membranes (HPM), such as NF and RO, depending on the application of hydraulic pressure to induce water transport through the membranes.

Table 2.1 - Characteristics of different pressure-driven membranes
[Source: (Kim and Dempsey 2013) et al., 2004]

Membrane process	Applied pressure KPa	Minimum particle size removed	Rejection/application
Microfiltration (MF)	10 ~ 100 (0.1 ~ 2 bar)	0.1 ~ 3 ㎛	Particle/turbidity, bacteria, algae, protozoa
Ultrafiltration (UF)	50 ~ 500 (0.1 ~ 5 bar)	0.001 ~ 0.1 ㎛ > 1,000 Dalton	Small colloids, macromolecule, viruses
Nanofiltration (NF)	500 ~ 1,000 (3 ~ 20 bar)	200 ~ 400 Dalton Multivalent ions	Dissolved organic matter, multivalent ions, softening
Reverse osmosis (RO)	1,000 ~ 8,000 (5 ~ 120 bar)	50 ~ 400 Dalton All ions	Monovalent ions, desalination

LPM has been employed more widely than HPM for primary DW treatment applications over the last couple of decades around the world. That is because LPM needs relatively less energy and can effectively remove microorganisms and suspended or colloidal particles as primary targets for surface water treatment, even though having no effect on removal of dissolved substances (e.g., molecules and ions). For this reason, many kinds of hybrid LPM technologies in combination with pre and post-treatment processes and various membrane materials including ceramic ones have been continuously developed for surface water treatment.

The discussion focuses on LPM, such as MF and NF, although HPM has many features in terms of removal efficiency of contaminants more difficult to remove by means of usual treatment technologies including LPM filtration.

2.1.2. Materials and properties of membranes

MF and UF membranes can be made from organic polymers and inorganic materials (e.g., ceramic, glass or metal or organic polymers). A number of different techniques are employed to manufacture synthetic membranes; the most important are phase inversion, coating, sintering[1)], and track etching.

Synthetic polymeric membranes can divided into two classes i.e., hydrophobic and hydrophilic. Hydrophilic polymers, such as cellulose and its derivatives, have been used widely for the manufacture of MF and UF membranes. However, cellulose

---

[1)] Heating a mixture of powered metals, sometimes under pressure, to the melting-point of the metal in the mixture which has the lowest melting-point, which then binds together the harder particles

acetate is sensitive to acid or alkaline hydrolysis, temperature, and biological degradation. Polysulfone (PS) and polyethersulfone (PES) are also hydrophilic and used for UF membranes and a support for composite RO membranes. Hydrophobic membranes, such as polytetrafluoroethylene (PTFE), polyvinylidene (PVDF), polyethylene (PE), or isotactic polypropylene (PP), are commonly used for MF membranes. These membranes are usually modified to reduce membrane fouling by blending with hydrophilic polymers.

Ceramics are widely used for the manufacture of inorganic membranes. They are available as metal oxides, composites, and sintered clay. The most common materials used for ceramic membranes are metal oxides, such as aluminium oxide or alumina (α-Al_2O_3 and γ- Al_2O_3), zirconium dioxide (ZrO_2), titanium dioxide (TiO_2), and silicon dioxide (SiO2) or a combination of these. They are usually of asymmetric construction, where there is a distinct transition between the dense filtration layer and the support structure. Inorganic membranes, such as ceramic ones, have outstanding stability at high temperatures and at extreme pH, but are relatively mechanically weak. After expiration of operation life, the membrane could be reused as raw material for ceramic membranes, which means no waste will be generated. This membrane is therefore environmentally friendly. In other words, this is a filtration system that also conserves energy with low power consumption.

Membrane surfaces have hydrophilic or hydrophobic properties based on the chemical characteristics of the membrane material. Hydrophobicity can be estimated by contact angle using the sessile drop method with a goniometer. A goniometer measures the angle of a droplet of 1 $\mu\ell$ of pure water on a membrane surface as shown in

Figure 2.2. Hydrophobic membrane surfaces are often modified by blending with hydrophilic materials. The fouling potential of hydrophobic membranes is higher than that of hydrophilic ones because of the high binding affinity of proteins and humic substances.

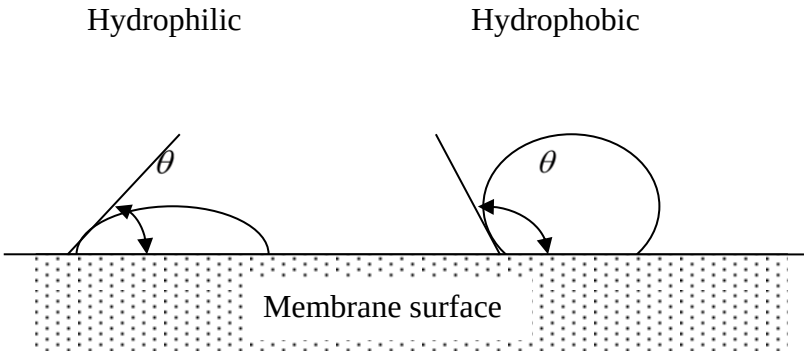

Figure 2.2 Contact angle of membrane surface

The measurement of water contact angle is affected by many factors including material, manufacturing process, roughness of the membrane surface, the purity of water, and even the techniques used by individual investigators. A plot according to the data from Cheryan (1998) is depicted as shown in Figure 2.3, which represents an approximate order of hydrophobicity of various membrane materials.

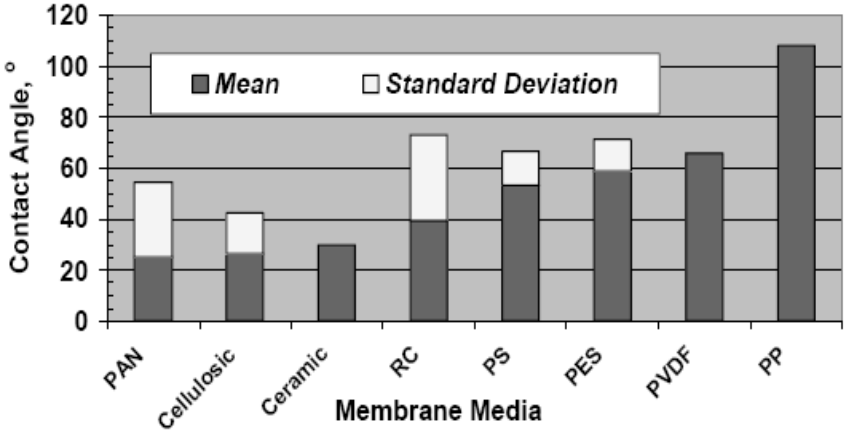

Figure 2.3 Contact angle of different kinds of membranes

Zeta potential (ξ) indicates the surface charge of a membrane and can be observed by measuring the streaming potential across a fluid shear plane at the surface. The isoeletric point is the pH at which the surface charge is zero. A streaming potential is generated when an ionic solution is forced to flow between two parallel membranes, and electrodes detect the difference in streaming potential. Zeta potential can be derived by the Helmholtz-Smoluchowski equation.

$$\frac{\Delta\phi}{\Delta P} = \frac{\varepsilon \cdot \xi}{\mu \cdot k}$$

Where, $\Delta\phi$ is streaming potential (mV), Δp is forced pressure (Pa), ε is the permittivity of the solution (s/m), μ is viscosity (Pa · s), k is the electrical conductivity of the solution (ms/m). The surface charge implies different fouling tendencies. Generally, membrane materials carry a negative charge or are modified to have a negative charge because NOM in water is negatively charged at neutral pH, due to phenolic and carboxylic functional groups. A negatively charged membrane, therefore, prevents deposition on the membrane surface by charge repulsion.

The retention rate or size of materials retained by membranes can be expressed as pore size or molecular weight cut-off (MWCO). Pore size and its distribution are determined by bubble point analysis, microscopic technique (i.e., atomic force microscopy), mercury porosimetry, solute transport, thermometry, and others (Alazmi et al. 2010, Hao et al. 2013, Katsoufidou et al. 2008, Katsoufidou et al. 2010). On the other hand, MWCO expressed in Daltons is a measure of the atomic weight of mass of the material retained. The nominal MWCO is a performance-related parameter defined as the lower limitation of a solute molecular weight such as dextran for which

the rejection is 95 – 98%. This value gives only a rough indication or the membranes characteristics and rejection potential due to differences in molecular shapes and possible steric interaction. A significant difference can exist in terms of retention between UF membranes with the same MWCO but originating from different manufactures as a result of the use of different molecular weight markets and test conditions, such as pH, ionic strength, pressure, temperature, etc.

2.2. CERAMIC MEMBRANES

2.2.1. Ceramic materials and properties

Ceramic membranes can be made using metal oxides, composites and sintered clay. The most usual ones are composed of metal oxides, such as aluminium oxide, or alumina (α-Al_2O_3 and γ- Al_2O_3), titanium dioxide (TiO_2), zirconium dioxide (ZrO_2), and silicon dioxide (SiO_2) or a combination of these. It is also possible to combine with different kinds of metal oxides such as Al_2O_3, ZrO_2, SiO_2, ZrO_2 and SiO_2-TiO_2, ZrO_2- TiO_2 (Kelly and Zydney 1995). Ceramic membranes are constructed from multiple layers into an asymmetric, multichannel element, where there is a distinct transition between the dense filtration layer and the support. The layers can be made of one or more of the constituent oxides. Generally, they consist of a microporous top layer, mesoporous intermediate layer and a macroporous support as shown in Figure 2.4.

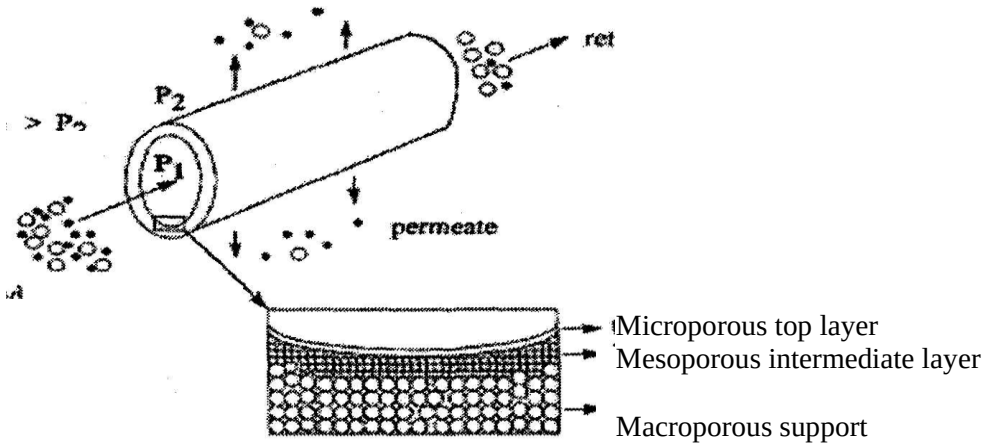

Figure 2.4 - Schematic diagram of tubular asymmetric membrane
[Source: Adapted from Vercauteren et al. 1998]

The pore size distribution of ceramic membranes is generally smaller than that of polymeric ones (Fu et al. 2008). The pore size distribution determines the permeability of membranes, as well as their separation efficiency by size (or steric) exclusion. Therefore, the separation efficiency of ceramic membranes based on steric exclusion is relatively higher.

Ceramic membranes are manufactured by the sol-gel process, which can allow them to make thin porous films in relatively simple way, at low cost and with good control over the whole process (Sekulić-Kuzmanovic 2004). Basically, the sol-gel process is what converts a colloidal solution called a sol to a gelatine-substance called a gel. A representative method to make ceramic membranes is sintering that can make powder into the object by means of heating the material until its particles adhere to each other. For this reason, ceramic membranes have rougher surface than polymeric ones made by phase inversion, stretching, track etching, etc. Also, the phases of aluminium oxides, α - Al_2O_3 and γ - Al_2O_3, depend on the sintering temperature of 1100 and 400℃, respectively.

It is generally known that ceramic membranes are physically superior to polymeric membranes and are more resistant to severe chemical environments (Burggraaf and Cot 1996, Lee and Cho 2004). As a result, ceramic membranes have been found to be able to operate at high permeate fluxes, high feed water recoveries, and with less frequent chemical cleaning as compared to conventional polymeric ones. The attributes and deficiencies of ceramic membranes compared to polymeric ones are summarized in

Table 2.2.

Table 2.2 - Main features of ceramic membranes (Vs. polymeric membranes) [Source: Adapted from Gary 2009]

Attributes	Deficiencies
• High flux (up to 400 lmh) at relatively low pressure – high permeability • High recovery (99%) • Very high backwash flux possible (50 times than forward flux) – water: up to 5 bar; air: up to 2 bar; strong CEB possible) • High durability against oxidants, strong acids, bases, and temperature – can be aggressively cleaned • Hydrophilic membrane surface • High security regarding membrane integrity – resistance to physical breakage • Long service life/wear-resistant (approximately 20 years)	• Relatively small packing density (m^2/m^3) • Relatively high price (per m^2) • Sensitive to crack formation

The principal properties of ceramic membranes are their hydrophilicity (Dafinov et al. 2002, Larbot et al. 2004) and negative charge of their surface due to the presence of hydroxyl (OH^-) groups on their surface. A hydrophilic membrane possesses a high surface tension and is easily wetted upon contact with water because of its ability to

form “hydrogen-bonds” with water. The greater a material tends to associate with water hydrogen bonding, the more hydrophilic the material is. The chemical features of being hydrophilic surface make the membrane develop high permeability (Dafinov et al. 2002) in terms of forming a water film or coating on its surface. The surface charge of membranes is able to influence not only their separation ability, but also fouling potential. Particularly, when some species having a negative charge on their surface encounter with a negatively charged membrane, electrostatic repulsion takes place. Some researchers have shown that the negative charge on membrane surface helps to alleviate deposition of foulants on the membrane, thus leading to less fouling (Xiao et al.).

The pH of solvents has a great influence on the surface charge of ceramic membranes. It has been reported that surface charge density and sign of ceramic membranes react as function of pH because the ceramic materials have amphoteric oxides (Kosmulski 2011, Moritz et al. 2001a, Moritz et al. 2001b, Zhou et al. 2009). This indicates that the electric surface charge of ceramic membranes depend on the pH of their surrounding environment (i.e., the solution) and thus, a repulsion or attraction phenomenon occurs between ionic species present in the solution and the isoelectric point, or zero point charge of the materials.

Table 2.3 - Point of zero charge (PZC) of ceramic membranes
[Source: (Moritz et al. 2001b, Nazzal and Wiesner 1994, Zhou et al. 2009)]

Material	PZC
Al_2O_3	9
TiO_2	4.0 – 6.1
ZrO_2	5.5 – 6
SiO_2	2 – 2.5

Table 2.3 shows the point of zero charge (PZC) of ceramic materials. If the pH of the solution is lower than the ZPC of the certain material, the material is positively charged, and vice versa.

2.2.2. Ceramic membranes in surface water treatment applications

MF and UF are low-pressure membrane (LPM) processes that can be applied to remove microorganisms and suspended or colloidal particles. However, they have no effect on removing other dissolved substances and ions like salts. In particular, as shown in Table 2.1, microfiltration has not guarantee an absolute barrier against all kinds of microorganisms due to its pore size. Since the smallest pore size of MF membranes is bigger than viruses, their removal is not guaranteed in sufficient log-removal for most regulations. Besides viruses, NOM and micro-contaminants cannot be effectively removed by MF due to their smaller size compared to the pore size. However, ultrafiltration membranes alone can remove viruses but cannot efficiently reject NOM and micro-contaminants because of their size compared to the pore size as well. For these reasons, LPM, such as MF and UF, are often applied with pre-treatment processes such as coagulation, PAC, and ozonation, rather than membrane filtration alone. According to previous research, it has been reported that these kinds of hybrid LPM process could increase the removal ability of dissolved organic carbon (DOC), some organics, viruses, micro-contaminants, as well as improve membrane performance due to its ability to reduce fouling.

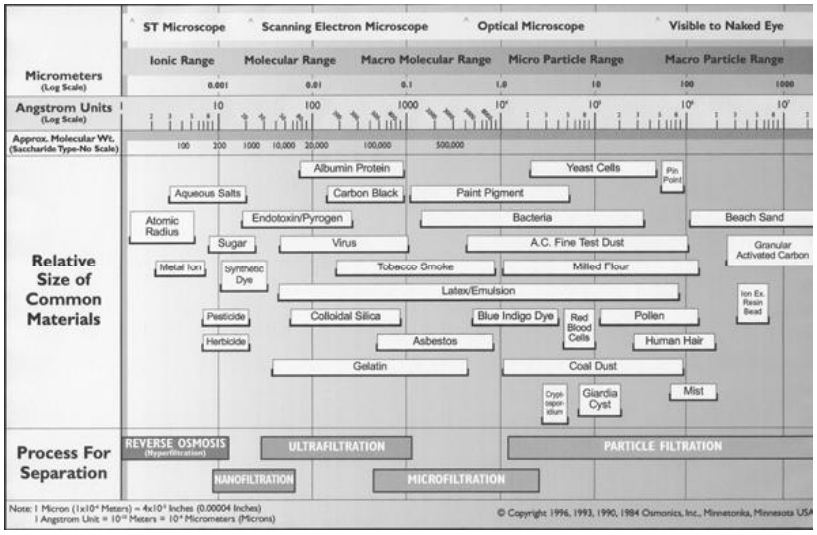

Figure 2.5 - Size range of contaminants

[Source: Adapted from applied water solution 2006]

Ceramic membranes applied for water treatment and wastewater reclamation/reuse treatment are mostly MF and UF membranes. The following discussion summarizes studies that have applied ceramic membranes in combination with different kinds of pre-treatment processes for filtration of various surface waters. Pre-coagulation involves the addition of coagulants such as $FeCl_3$ or $FeSO_4$, alum, polyaluminium chloride, etc. in order to agglomerate suspended and colloidal particles in the feed water prior to UF or MF. Coagulation, which is the most popular pre-treatment process applied before membrane filtration, has a significant effect on the water quality, as well as the operating conditions of the membrane. Particularly, in ceramic MF, coagulation pre-treatment is essential in maintaining high permeate flux which is one of the most attractive features of ceramic membranes.

Coagulation process followed by LPM filtration can help permeate flux improvement by three mechanisms with varying efficiency. First, it is possible to be enhanced by reducing foulants penetration into membrane pores. Secondly, it can be due to

conditioning of the layer of material deposited on the membrane. That is because more porous cake by coagulation decreases the specific resistance of the cake layer against the membrane. Finally, it can be helped by improving particle transport characteristics that could reduce particle deposition on the membrane surface due to shear forces moving particles away from membrane (Mallevialle *et al.* 1996). The combination of coagulation with filtration can decrease fouling for both polymeric and ceramic membranes by minimizing pore blocking and pore adsorption, and allow the membrane performance to be stable due to pure cake filtration, as well as improve rejection (e.g., viruses) to increase permeate quality (Carroll *et al.* 2000; Lerch *et al.* 2005; Matsushita *et al.* 2005).

Coagulation pre-treatment combined with ceramic MF membranes has been shown to be effective in increasing removals and decreasing membrane fouling. Konieczny et al. (2006) investigated the effects of when ceramic MF membranes are used with coagulation pre-treatment, the removal efficiency of TOC was higher than coagulation alone. They used two ceramic membranes (nominal pore size 0.1 and 0.2 μm) and compared TOC (7 and 10mg/L) removal by coagulation alone, MF alone, and pre-coagulation with MF. The TOC was synthetically simulated with humic acid. TOC removal by both ceramic membranes, regardless of pre-coagulation, showed complete removal (100%). In spite of this significantly greater flux decline was observed. This means that performance by MF alone is not suitable for optimal operation, and when used with pre-coagulation, it can be improved with stable fluxes. Interestingly, the complete removal of humic acids by MF membranes alone was achieved, but the mechanism was not closely investigated. It is likely some form of binding interaction occurred between humic acid and the membrane surface (inherent

property of a ceramic membrane). They used three types of coagulants such as ferric chloride, alum, and ALF (combination of both). All three coagulants used showed comparable flux decline, however, residual aluminium in the permeate water exceeded drinking water standards. This might be indicative of improper coagulation conditions or over-dosing.

Loi-Brügger *et al.* (2006) investigated flux, recovery, and DOC removal using ceramic membranes (nominal pore size 0.1 μm) for a raw water DOC of 2~3.5 mg/L. Membrane flux was increased stepwise from 80 to 300 L/m^{2}h, resulting in recoveries between 95.9 and 98.9%. A dosage of 3.5 mg/L Al^{+3}/L as pre-treatment resulted in a DOC reduction of 20~35%. The turbidity of filtrate was always below 0.01 NTU. Also, the results indicated that with proper coagulation and chemically enhanced backwash (CEB) condition, the membrane performance was stable regardless of either temperature variation or turbidity peak (3~100 FNU). It was shown that if membrane operation was kept at optimal fluxes (less than 200 L/m^{2}h), the application of CEB could not be necessary, but might be useful in case of high organic loading or to extend the clean-in-place (CIP) interval. The use or frequency of CEB for moderate flux operation can be determined depending on the relationship between chemical consumption, energy consumption, and CIP period (Loi-Brügger *et al.* 2007).

Meyn *et al.* (2007) investigated the removal efficiency of NOM when adding coagulants, such as polyaluminium chloride (PAX-18) and iron chloride (PIX-111), prior to ceramic membrane filtration under Norwegian conditions, which are typically characterised by a high content of NOM, high colour, very low turbidity, low alkalinity and low hardness. In this study, multi-channel ceramic membranes were

operated in a dead-end, inside-out mode with a nominal pore size of 0.1 μm with rapid and slow mixing processes (i.e., flocculation). They evaluated the influences of coagulant dosage and pH variation. The DOC and colour removal could be achieved at relatively low dosage, but the removal was greatly dependent on pH value. At lower pH values (between 4 and 6), the DOC removal was higher due to a better formation of polyhydroxocomplexes. However, an increase in residual metal concentrations at those ranges of pH had to be taken into account when determining the optimal operational conditions.

Additionally, several studies have shown that in-line coagulation could be more effective than conventional flocculation (Milton *et al.* 2007; Matsushita *et al.* 2005). This is considered to be possible because of the fact that coagulation (i.e., adsorption to colloidal particles) occurs within a very short time after adding metal coagulants, such as alum and ferric chloride, and subsequent agglomeration immediately reaches larger sizes than those of the membrane pore. Milton *et al.* (2007) used a 0.1 μm MF ceramic membrane to treat a Scandinavian water of low turbidity and high TOC (between 6 and 8 mg/L) under a variety of coagulation and flocculation conditions. They evaluated the effect of different operation conditions for coagulation by varying coagulation pH (5.6~6.9), coagulant type ($FeCl_3$ vs. PACl) and dosage (2.7~5.5 mg/L), and mixing configuration. For their tests, they used two types of flocculation configurations. Those were i) two-tank mixing for which coagulants and pH adjustment agents are added in the first tank and flocculated in the second tank, or ii)in-line mixing for which the coagulant is injected upstream of the membrane feed pump, and flocs are allowed to form in an in-line hose between the pump and the membrane. Coagulation using ferric chloride was optimized, and removed up to 40%

of TOC at a coagulant dosage of 5.5 mg Fe/L. The results showed that coagulation conditions had an effect on the membrane performance. A lower pH resulted in a higher rate of increase in TMP and higher removal of TOC, but less TMP recovery after a hydraulic backwash due to more iron-organic complexes formed. On the other hand, high coagulation pH formed more hydroxide flocs that were easier to remove by hydraulic backwash. In-line coagulation appeared to more effective than conventional coagulation in terms of permeability decline because flocs formed in the latter were sheared by the membrane feed pump resulting in increased membrane resistance. However, a clean-in-place (CIP) chemical cleaning completely recovered the membrane permeability.

Matsushita *et al.* (2005) investigated the effects of coagulant dose (0.54, 1.08, and 1.62 mg/Al/L), pore size of monolithic ceramic MF membrane (0.1, 0.5, and 1.0 μm), and coagulation time (1.1, 2.4, and 60 s using in-line static mixer) on virus removal in a coagulation and MF hybrid system. They used bacteriophage Qβ (NBRC 20012) as a model virus. Coagulant dose strongly affected virus removal, showing the larger the coagulant dosage, the higher the virus removal. Pore size of the membrane also had an influence on virus removal, indicating that the membranes whose pore sizes were 0.5 and 1.0 μm showed some l log less removal than the 0.1 μm one. That might be because a wide range of aggregates formed by coagulation pre-treatment, or the particle-size distribution determined the removal efficiency of virus achieved by the membranes. However, coagulation time slightly contributed to the virus removal, with the longer mixing time, the better the virus rejection, but the effect was not large. Overall, the results indicated that in-line coagulation prior to ceramic membrane filtration was able to create a nearly comparable effect as did conventional process

(i.e., back-mixer type) with the membrane filtration in terms of removing virus, showing that dosing with at least 1.08 mg/Al/L in those system allowed the coagulation time to be shortened to only 2.4 seconds.

The robustness of ceramic membranes can allow strong oxidants, such as ozone (O_3), to be used as pre-treatment process to increase the treatment efficiency of bulk organic matter and to reduce the membrane fouling. Few researchers have investigated the use of ozone as a pre-treatment prior to conventional polymeric membranes, because of the destruction of polymeric ones by residual ozone. As previously mentioned, ceramic membranes are physically superior to polymeric ones and are more resistant to severe chemical environments. In particular, when treating WWTP effluent, ceramic membranes could achieve enhanced filtration performance for at least two reasons. First, the ceramic membrane provides excellent backwash efficiency as the material itself can withstand high backwash pressure. Second, the incorporation of chemical treatment, such as ozone, as a pre-treatment process with ceramic membranes greatly mitigates fouling by natural organic matter (Karnik *et al.* 2005).

Lehman *et al.* (2009) evaluated the effect of ozonation and coagulation pre-treatment with a ceramic membrane module (nominal pore size 0.1 μm ; monolith METAWATER element; pressurized configuration) to investigate how to optimize the membrane operation for WWTP effluent treatment (pH: consistently 6.8; temperature: 21~ 30℃; turbidity: 0.4~1.8 NTU; TOC: 3.8~5.9mg/L). The pilot system consisted of three parts which is pre-ozonation, coagulation/flocculation pre-treatment and the ceramic membrane module in sequence. Ozone was added between

0 and 6 mg/L. Coagulation and flocculation was performed via inline coagulation using a static mixer positioned after the feed pump to distribute a coagulant (PACl 1~3.5 mg/L Al) in the feed pipe. For membrane performance with pre-ozonation, they fixed PACl dosage at 3.5 mg/L and increased ozone doses from 0 to 6 mg/L in a first experiment. It showed that, with no ozone, the membrane specific flux decreased to 29% of the initial flux after 5 days, with 6 mg/L ozone, the flux was stabilized between 97~ 100%. The results with no ozone would be because the coagulation using PACl was not optimized. However, it was remarkable in that membrane fouling was fully controlled with ozone. In a second test, they fixed ozone dose at 6 mg/L and decreased PACl dosages (3.5 to 1 mg/L). It was shown that the membrane specific flux was stabilized at 88~100% of the initial specific flux regardless of the variation of coagulant dosages. The fouling was still well controlled under that condition. In a third test, while PACl was fixed at 1 mg/L, ozone was decreased to 2.7 mg/L dose. The membrane experienced increased fouling with decreased pre-ozonation. The results exhibited that the membrane operation could be stabilized at an ozone dose of 3.5 mg/L.

In conclusion, while typical polymeric membrane operation conditions are flux of 17~68 L/m^2h (10~40gfd), recovery of 90~98%, backwash every 15~60 min, and maintenance clean every 1~2 days (Metcalf & Eddy, Inc. 2003), ceramic membrane operation demonstrated that even when operated under rigorous conditions (i.e., 170 L/m^2h (100gfd) at 20℃, 120 min backwash interval and no CEB), membrane fouling could be stabilized at a lower PACl dose of 1 mg/L and ozone dose as low as 3.5 mg/L (Lehman *et al.* 2009), as aforementioned . Interestingly, the optimal pre-ozone dose corresponded to the ozone demand of the source water, at which point a majority

of high molecular weight NOM was degraded. Lehman *et al.* (2009), in order to understand the effects of ozone and coagulation pre-treatment on organic foulants, also characterized natural organic matter (NOM) in four waters using high performance size exclusion chromatography (HPSEC). The HPSEC analysis demonstrated that ozone treatment is effective at degrading colloidal NOM which is likely responsible for the majority of membrane fouling. The results concerning the characterization of NOM fouling on the ceramic membrane will be discussed in more detail in Section 2.4.4.

2.3. MEMBRANE FOULING

One of the major problems in operating membrane processes in drinking water treatment and wastewater reclamation/reuse is fouling. Membrane fouling is referred to as the flux decline of a membrane filter caused by the accumulation of certain constituents in the feed water on the membrane surface or in the membrane matrix. When a membrane is fouled, both its porosity and pore size decrease, but effective thickness of the membrane increases. It should be noted that the increase in membrane thickness caused by the accumulation of foulants does not mean physical thickness of the fouling layer, but a hydraulically equivalent of an increase in the thickness of clean membrane. That is because the fouling layer and a clean membrane may have different permeability.

Fouling can be characterized by what the bulk materials causing fouling are (i.e., particulate, organic, inorganic, or biological), whether foulants can be removed (i.e.,

reversible or irreversible), and what the mechanism of formation is (i.e., pore adsorption, cake formation, or pore blockage) (MWH, 2005). The extent to which fouling occurs depends upon the source water quality, such as pH, ionic strength and calcium concentration, and the membrane surface properties, such as zeta potential, roughness, pore size and hydrophobicity (Howe and Clark, 2002).

2.3.1. Classification of membrane fouling

A general classification of membrane fouling includes inorganic fouling (scaling), particulate/colloidal fouling, microbial fouling, and organic fouling.

Inorganic fouling (scaling)

Scaling is caused by the accumulation of inorganic precipitates, such as calcium carbonate, calcium sulphate, barium sulphate, and metal (e.g., iron, aluminium, and silica) oxides/hydroxides on membrane surfaces or within the pores structure. Precipitates are formed when the concentration of chemical species exceeds their saturation concentration. For MF and UF, fouling can occur due to interactions between ions and other fouling materials, such as organic polymers, via chemical bonding. Some pre-treatment processes for membrane filtration such as coagulation and oxidation may contribute to scaling by inducing metal hydroxides on the membrane surface or within the pore structure if are not designed or operated properly.

The precipitation of inorganic scalants can reduce the permeate flux, damage the membrane surface and cause irreversible pore blocking. Parameters that impact the extent of scaling are ion concentration, temperature, pH, and membrane material.

Membrane fouling caused by inorganic precipitation may be recovered using acidic cleaning agents such as citric acid (Laîné *et al.* 2003). Scanning electron microscopy (SEM) is a technique that can be used to detect scaling on the membrane surface.

Colloidal/particulate fouling

Colloidal and particulate fouling is caused by deposition and accumulation of suspended and colloidal solids in the feed water on the membrane surface or inside the pores, resulting in flux decline. Colloids are fine suspended particles and their presence in natural surface waters is ubiquitous. Colloid foulants impacting UF membranes include inorganic matter (e.g., clays, silica, salt precipitates, and metal oxides), organic matter (e.g., natural and synthetic substances, and biological matter (e.g., bacteria, viruses, and proteins) (AWWA 2005).

Colloidal matter typically exhibits a charge in aqueous solutions due to the presence of charged functional groups on its surface or through the adsorption of ions from the surrounding water. The resulting cake structure porosity and the hydraulic resistance are influenced by the surface charge of colloids, which can be measured by zeta potential.

Microbial fouling

Microbial fouling (biofouling) is a result of formation of biofilms on membrane surfaces. Once bacteria attach to the membrane, they start to multiple and produce extracellular polymeric substances (EPS) to form a viscous, slimy and hydrated gel, which reduces permeability, causes flux decline, and leads to pore blocking. Microbial adhesion to the membrane surface is affected by several factors including

microbial characteristics, properties of membrane surface, chemistry of feed water solution, and hydrodynamic operational conditions. EPS typically consists of hetero-polysaccharides and have high negative charge density. This gel structure protects bacterial cells from hydraulic shearing and from chemical attacks of biocides such as chlorine.

Controlling biofouling involves the removal of biodegradable matter from the feed water, ensuring the use of pure chemicals, and performing effective cleaning procedures (Vrouwenvelder *et al.* 1999). A cleaning strategy generally requires two steps: weakening of the biofilm matrix by chemical oxidants, such as chlorine, ozone, hydrogen peroxide, etc., alkaline treatment, enzymes, complex-forming substances, biodispersants, or some combination of these agents; and the mechanical removal of the biofilm, such as air, steam, rinsing with water, or a combination of these (Flemming 1997).

Organic fouling

Besides particulate and colloidal fouling, another major cause of fouling in membrane filtration of various natural waters is dissolved naturally existing organic substances. Organic fouling is profound in membrane filtration with source water containing relatively high natural organic matter (NOM). Surface waters (rivers and lakes) typically contain higher NOM than ground water, with exceptions. The rejection of NOM using membranes is primarily a physical removal process that is dependent on the chemical molecular size. However, the charged functional groups of both the membrane and NOM can also have a significant impact on rejection (Cho *et al.* 2000). While the majority of dissolved NOM will pass through MF/UF membranes due to

their smaller size, organic constituents can still contribute considerably to fouling by plugging membrane pores, adsorbing to the matrix of the membrane, and forming a cohesive gel on the cake layer (AWWA 2005).

The organic fouling may also encourage biofouling by acting as a nutrient. The mechanism of organic fouling is very complex and the rate and extent are influenced by many factors, such as membrane characteristics, properties of organic matter, feed water solution characteristics, and membrane module hydrodynamics (Aoustin *et al.* 2001; AWWA 2005). In particular, more fundamental and specific understanding of organic matter fouling is needed for these reasons.

2.3.2. Understanding of organic fouling of membranes

As previously mentioned, a general classification of membrane fouling includes colloidal fouling, biofouling, organic fouling, and inorganic fouling (scaling). Among the different classifications of membrane fouling, organic fouling associated with bulk organic matter is perhaps the most poorly understood, with relationship to organic colloidal fouling and biofouling, the most significant factors contributing to flux decline, in both drinking water and wastewater reclamation/reuse applications (Mallevialle *et al.* 1989). Problematical foulants have been identified as polysaccharides and proteins but these components occur in both abiotic macromolecular and colloidal forms (Gary 2008).

OM fractions and characterization

There are three types of bulk organic matter of interest in drinking water treatment and wastewater applications: (i) allochthonous natural organic matter (NOM)

dominated by humic substances derived from runoff and leaching of vegetative debris from terrestrial sources within a watershed; (ii) autochthonous or algal organic matter (AOM) consisting of extracellular and intracellular macromolecules and cellular debris; and (iii) wastewater effluent (EfOM) consisting of background (drinking water) NOM plus soluble microbial products (SMPs) derived from biological wastewater treatment. A more simple classification is between microbially-derived OM (AOM, EfOM) versus terrestrially-derived OM (NOM). However, the term NOM is more widely used in a general context with distinction between autochthonous NOM versus allochthonous NOM (Gary 2008). The different fractions of NOM are categorized in Table 2.4

Table 2.4 - Different fractions of NOM
[Source: Adapted from Edzwald 1993]

Category	Acid/Base	Chemical groups
Hydrophobic	Strong acid	Humic & fulvic acid
	Weak acid	Alkyl monocarboxylic acid & dicarboxylic acids
Transphilic	Weak hydrophilic acid	Hydroxyl acid, sugar acids & sulfonic acids
Hydrophobic	Hydrophilic neutrals	Polysaccharides, low MW alkyl alchols & amides
	Hydrophilic bases	Low MW alkyl amines & amino acids

Organic compounds come from degradation of plants and animals in aquatic environments. Humic substances (humic/fulvic acids) contain mainly carboxylic and phenolic groups. They comprise a large fraction of NOM (over 50% of dissolved organic carbon (DOC)) and are generally negatively charged due to the dissociation of carboxylic and hydroxyl functional groups. Non-humics are composed of proteins, amino acids and carbohydrates, which account for 20-40 % of the DOC.

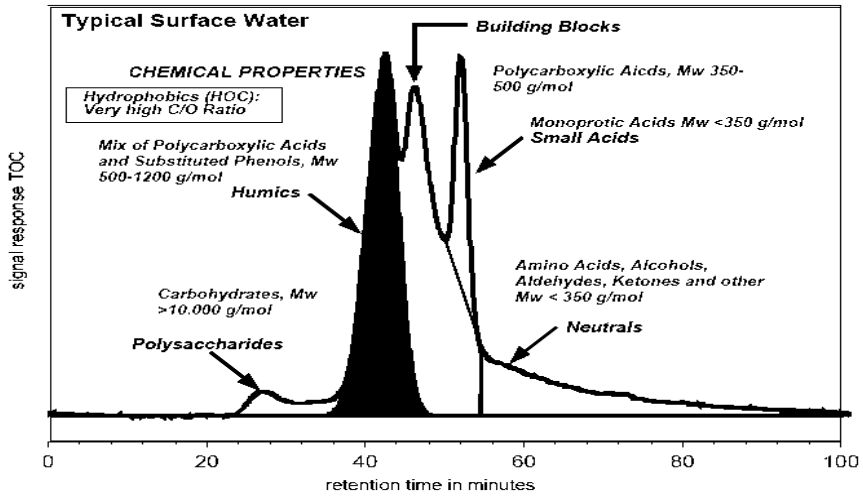

Figure 2.6 - LC-OCD chromatogram of NOM of typical surface water [Source: Doc-Labor 2005]

Table 2.5 - NOM characterization by LC-OCD [Source: Adapted from Kenney 2007]

Fraction category	Definition
Polysaccharides (including amino sugars, polypeptides and proteins)	Associated with peptides of proteins and originated from algae and bacteria; Hydrophilic High molecular weight (>10 kDa)
Humics	Humics and fulvic acids Molecular weight of 1 ~ 10 kDa
Building blocks (HS-hydrolysates)	Weathering and oxidation products of humics Molecular weight of 300 ~ 500 Da
Low molecular weight (LMW) organic acids	Fraction for all aliphatic low molar weight organic acids (MW < 350 Da)
Neutrals	Alcohols, aldehydes, and ketones (MW < 350 Da) Transphilic, non-biodegradable

Important characteristics that affect the interaction of NOM with a membrane are hydrophobicity (aromatic) versus hydrophilicity (aliphatic) nature of the NOM, size (MW and MW distribution) of the NOM, and it's content in terms of functional groups. Figure 2.6 and Table 2.5 show typical NOM characterization of surface water by liquid chromatography-organic carbon detection (LC-OCD) that provides both quantitative and qualitative information of NOM.

Organic Matter measurements and characterization

There are a number of organic matter measurements and characterization protocols that can be applied to characterization of bulk samples of feed water as shown Table 2.6.

Table 2.6 – Organic Matter measurement and characterization

[Source: Adapted from Gary 2008]

Measurement	Characterization
Dissolved organic carbon (DOC)	Representing the amount of organic matter
Dissolved organic nitrogen (DON)	Embodying the nitrogen content of organic matter
UV absorbance at 254 nm (UVA_{254})	Reflecting the aromatic character of organic matter
Specific UVA ($SUVA = UVA_{254}/DOC$)	Revealing the relative amounts of humic (higher SUVA) versus non-humic organic matter (lower SUVA)
Molecular weight (MW) distribution by size exclusion chromatography with on-line DOC detection (SEC-DOC)	Describing organic matter in terms of chromatographic peaks corresponding to high MW polysaccharides (PS), medium MW humic substances (HS), and low MW acids Conceptually equivalent to LC-OCD
Hydrophobic/transphilic/hydrophilic DOC distribution by XAD-8/XAD-4 resin adsorption chromatography	Revealing a polarity distribution of organic matter
Fluorescence excitation-emission matrix (EEM) in the form of 3-dimensional spectra	Distinguishing between humic-like and protein-like organic matter Providing fluorescence index (FI) that is related to organic matter source (i.e., terrestrial of microbial)
Pyrolysis gas chromatography/mass spectrometry (P-GC/MS)	Describing organic matter biopolymer composition in terms of polyhydroxyaromatics, polysaccharides, proteins, and amino sugars

There are also several analytical methods that can be used to investigate the characterization of fouled membranes as part of an autopsy, including:

- Atomic force microscopy (AFM), describing foulant layer morphology and roughness in terms of membrane surface topography and pore distribution
- Infrared spectrophotometry (FTIR), revealing foulant layer composition in terms of organic functional groups including amines (proteins), carbohydrates (polysaccharides), and carboxylic acids (humic substances)
- Scanning electron microscopy (SEM), visually revealing foulant layer morphology

2.3.3. Interaction between fouling materials and membranes

Membrane fouling is a complicated phenomenon of which causes are multiple and poorly understood. The core of the issue is interactions between fouling materials and membrane, and between fouling materials themselves. Electrostatic and hydrophobic/hydrophilic interactions between membranes and fouling materials have a significant bearing on membrane fouling. The balance between the forces of electrostatic repulsion and hydrophobic adhesion determines the outcomes of membrane fouling, as well as the efficiency of chemical cleaning.

Many natural materials have negative charge wholly or partially due to dipole or multiple chemical bonds in their structure. Particles that foul membranes in aqueous media tend to have hydrophobic (Shan 2004). Hydrophobic interactions can be described as “like attracts likes”. In order words, there is a natural tendency of attraction between membranes and solutes with similar chemical structures. Hydrophobic attraction results from van der Walls between molecules each other. It is

also an important mechanism causing NOM fouling because of the high molecular weight of NOM compared with their charge density, providing great potential for hydrophobic adhesion (Kennedy 2008).

Hydrophilic membrane materials with a highly negative surface charge are important in preventing adsorption of organic matter and colloids. There is a tendency of electrostatic repulsion between membrane with a negative surface charge and NOM constituents with a high charge density. Research has shown that the more hydrophobic and less negatively charged membranes adsorb organics which tend to irreversibly foul MF/UF membranes. Membrane permeability is very sensitive to the number of large pores and their loss via plugging, adsorption, etc., results in rapid flux decline. Therefore, membrane porosity, pore size distribution, surface roughness and charge are very important.

The balance between hydrophobic attraction and electrostatic repulsion essentially determines if a membrane is being fouled or being cleaned. As molecular weight and mass/charge ratio of solutes, ionic strength, and the concentration of divalent cations increase, hydrophobic attraction tend to increase, so does the potential of membrane fouling. On the other hand, increases in charge density and polarity of solutes, and pH will increase electrostatic repulsion between the membrane and solutes, which reduces the adhesion between membrane and fouling materials and enhances the cleaning efficiency (Kennedy 2008).

2.3.4. NOM fouling in ceramic membranes applications

Lee and Cho (2004) tested two polymeric membranes (8KDa UF and 250Da NF) and two ceramic membranes (8KDa and 1KDa) to compare their removal efficiency of NOM and haloacetic acid formation potential (HAAFP). The results showed that the ceramic membranes had relatively several advantages. The ceramic membranes exhibited the potential to more effectively remove DBP precursors (i.e., HAAFP) than NOM in terms of DOC versus the tested polymeric ones, and also showed higher permeability than the equivalent polymeric.

Kennedy *et al.* (2007) investigated NOM fouling reversibility and irreversibility of a ceramic membrane in a surface water treatment application. Coagulated surface water ($FeCl_3 \cdot 6H_2O$ in an equivalent of 4 mg/L as Fe^{3+}; pH of 8.2; turbidity of 10.3 NTU; UVA_{254} of 0.467 cm^{-1}; DOC 11.01 mg/L; TSS 22.2 mg/L;) was filtered through a monolithic tubular ceramic membrane (nominal pore size 0.1 μm). Filtration of the feed water resulted in almost removal of turbidity and TSS. The rate of DOC removal amounted to only about 10%, which is reasonable since DOC molecules are much smaller compared to the nominal membrane pore size of 0.1 μm. Reduction in UVA_{254} amounted to about 30%, which suggested better rejection of humics, as UVA_{254} has been correlated to the aromatic or humic content in NOM (Laine 2003). For fluxes of 150~210 L/m^2h, the normalized permeability decreased significantly in the first few filtration cycles due to membrane fouling. Non-backwashable fouling increased with each filtration cycle and accounted for 40% of the total fouling after 10 filtration cycles. NOM fractions that caused reversible and irreversible fouling were characterized using LC-OCD. Although all the NOM fractions have significantly

smaller molecular weight than the nominal membrane pore size used (approximately 1,000kDa, with the largest fraction – hydrophobics – having 20,000 Da), NOM rejection occurred. It is most likely caused by interaction of membrane surface properties (i.e., adsorption) and the DOC molecules, as suggested by Fettig (1999). NOM (DOC) removal by a ceramic membrane is possible because their surfaces are predominantly covered with hydroxyl groups, which can bind the weak acid groups found in NOM. The hydrophobic fraction of DOC was even better removed (by 61%) than any other fraction, followed by biopolymers (25%) and LMW acids (20%). LC-OCD analysis of the backwash water revealed mainly humic substances (45%) and neutral (23%) fractions. However, both hydrophobic and biopolymers were almost completely absent in the backwash water, suggesting that they might be responsible for non-backwashable fouling. Biopolymers are made up of, among others, polysaccharides, which were involved in the evolution of irreversible fouling on polysulfone membranes by Kimura *et al.* (2004). The results of this study seemed to suggest that this is also true for ceramic membranes (Kennedy *et al.* 2007).

As aforementioned in Section 2.2.2, (Lehman and Liu 2009), to understand the effects of ozone and coagulation pre-treatment with ceramic membrane (0.1 μm MF) filtration on organic foulants, natural organic matter (NOM) in four waters – raw, ozone treated, coagulation treated, and ozone prior to coagulation treated – were characterized using HPSEC with ultraviolet absorbance detection from 200 to 300 nm. The molecular weight (MW) distributions of NOM after various pre-treatments were compared. In the case of pre-ozone, the NOM of the entire range from greater than 67kDa to less than 1.8kDa (i.e., biopolymers and humic substances) decreased as a result of oxidation. On the other hand, in the case of pre-coagulation only, the

reduction of NOM was observed to be of a slightly less extent compared with pre-ozonation in the colloidal portion (i.e., biopolymers), but the majority of the humic NOM remained the same as feed water. Herein, the result in terms of removing humic substances would be because the coagulation using PACl was not optimized. Nevertheless, when ozone and coagulation were combined, the peak of the colloidal materials was almost completely removed, these results confirming that ozone enabled the membrane fouling to be greatly reduced as mentioned in section 2.2.2 via degradation of organic foulants, especially the colloidal NOM which is likely responsible for primary membrane fouling (Lehman *et al.* 2009).

2.3.5. Fouling prediction

Membrane fouling results in reduced productivity and therefore, it is very important to predict and control it. Silt density index (SDI), modified fouling index (MFI) and unified membrane fouling index (UMFI) have been developed to characterize the fouling potential of feed waters. Silt density index (SDI) is commonly applied as a parameter for the fouling potential of a feed water by evaluating the linear relationship between particle contents of feed water and flux decline. It is based on the measurement of plugging a membrane filter having 0.45 μm pores at a pressure of 210kPa (30psi). The SDI measures the flux decline rate in minutes (% per minute).

The measurement of SDI is taken as follows;

- The time (t_1) is noted, which is required to filter the first 500ml.
- 15 minutes (T) after the start of this measurement time (t_2) is noted, which is required to filter 500ml (V)
- The index is calculated with the following formula:

$$SDI = \left[\frac{1-\frac{t_1}{t_2}}{T}\right]\times 100 = \left[\frac{1-\frac{t_1}{t_2}}{15}\right]\times 100$$

A disadvantage of this index is that it does not measure the rate of change of resistance throughout the test and only evaluates the system at pre-set intervals, making it a simplistic measure of particulate fouling (MWH 2005). Also, in spite of the general usefulness of the SDI as a qualitative indicator of the need for pre-treatment and treatability of feed water, it is unable to capture the interactions between foulants and the membrane, thus an inadequate indicator of membrane performance. Even though the SDI is the least sensitive of the fouling indices, it is the most widely used (Mallevialle *et al*. 1996, Park *et al.* 2006). However, the SDI does not distinguish between pore blocking and cake filtration mechanisms, and therefore it cannot be used to predict the rate of flux decline resulting from particulate fouling.

The modified fouling index (MFI) has been developed to overcome the deficiencies of SDI. The MFI has been derived from the fouling index (SDI) and makes use of the same equipment when flat-sheet membrane specimens are applied. Unlike the SDI, It is based on the occurrence of cake filtration during a distinct part of the test, since cake filtration is most likely, the dominant filtration mechanism in RO and NF. It is also dependant on particle size, thus smaller particles generally result in higher MFI values (Park *et al.* 2006). The MFI considers the observation that 1) during the initial stage of the filtration of blocking occurs, 2) pore blocking is being followed by cake filtration and 3) finally cake compression and/or depth filtration occurs.

The filtrate volume is recorded in 30 second intervals at a pressure of 30 psi over a 15 minute filtration period. The flow rate is calculated from the volume and time data, and then the inverse of the flow rate (dt/dV) is plotted as a function of volume filtered. A section of this graph is linear, and the MFI is the slope in this region.

$$\frac{\Delta t}{\Delta V} = \frac{1}{Q} = (MFI) \cdot V + b$$

Where V is the volume of permeate (L), b is the intercept of the linear portion of the graph, and MFI is expressed in units of s/L^2. The MFI is a function of the dimension and nature of the particles forming a cake on the membrane and directly correlated to the particle concentration in the feed water (Boerlage *et al.* 2002). The SDI and MFI have been developed to predict fouling of NF/RO membranes and are not applicable to MF/UF membranes. Only the fouling caused by materials lager than its pore size can be measured, but the various fouling mechanisms of NF/RO membranes cannot be reflected. That is because both methods use a 0.4 ㎛ filter (Park et al. 2006). Particulate fouling in MF/UF occurs by pore blocking and cake filtration mechanisms, while NF/RO particulate fouling is mainly dominated by cake layer formation.

Recently, to overcome these kinds of problems, a study using MFI-UF has been carrying out. This research focused on improving the predictability of fouling indices by using UF membranes instead of a 0.45 ㎛ filter used in the SDI and MFI (Boerlage *et al.* 2002; Boerlage *et al.* 2003; Boerlage *et al.* 2004). According to these studies, the most suitable reference membrane for the MFI test was the polyacrylonitril (PAN) MWCO 13kDa membrane.

Hung *et al.* (2008) developed a unified membrane fouling index (UMFI) in order to simplify and standardize bench-scale testing of membrane fouling potential by directly using the commercial LPM of interest. Because the extent of fouling is dependent on each type of membranes and raw water quality, it is difficult to quantify and assess their fouling potential based on a single membrane test (Huang *et al.* 2007, Huang *et al.* 2008). The UMFI is used to modify Hermia model applied to both filtration of constant pressure and constant flux. Complete pore blocking was considered unimportantly and excluded in the derivation of UMFI because of the fact that it is an idealized scenario for pore blocking that requires all foulants to accumulate solely on membrane pores. The rest of the models of pore blocking (i.e., intermediate and standard) were assessed as being more relevant in long-term performance of LPM systems than cake layer formation because they are more likely to contribute to irreversible fouling. The equations for both pore blocking models were subsequently expanded as Taylor series, which ultimately proved to be approximations to the equation for cake layer formation. Therefore, the UMFI could be defined using a single equation based on the cake layer formation equation as following;

$$\frac{1}{J'_s} = P' = 1 + (UMFI) \cdot V_s$$

Where J'_s is the normalized specific flux (dimensionless); here P' = P/P_0 where P_0 is the initial trans-membrane pressure (Pa). Then, the normalized V_s is the specific permeate throughput (L/m^2) and UMFI is in units of m^2/L. The UMFI is the slope of the regression line from typical fouling results acquired through bench scale fouling experiments. The UMFI allows for the quantitative comparison of numerous fouling

results and the evaluation of fouling potential under different conditions, regardless of membrane type, water source, and operational mode and scale.

2.4. MEMBRANE CLEANING

Cleaning is an integral part of membrane process operation, and has a profound impact on the performance and economics of membrane processes. Membrane cleaning is the removal of different kinds of materials, such as foulants discussed in section 2.4 above, from the surface and matrix of the membrane. Figure 2.7 shows a schematic representation of trans-membrane pressure (TMP) drop under constant flux conditions after periodic hydraulic (i.e., backwashing) and chemical cleaning. Membrane cleaning can be mainly classified into hydraulic cleaning (backwashing), which is sometimes used with chemically enhanced backwashing whereby a chemical is added to the permeate, and chemical cleaning.

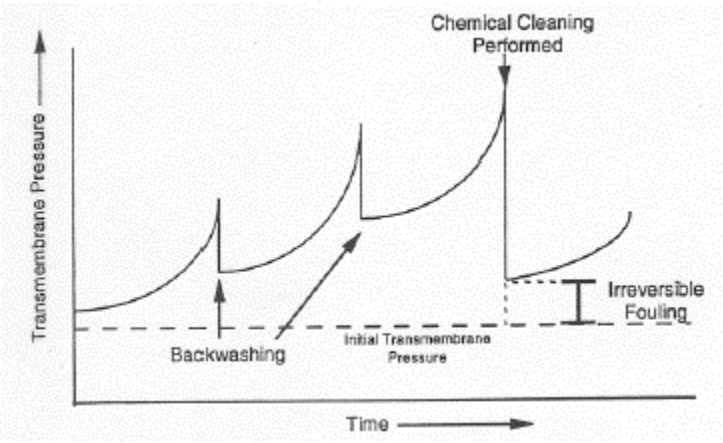

Figure 2.7 - TMP drop after cleaning vs. operation time/volume
[Source: Amy 2005b]

2.4.1. Hydraulic cleaning (backwashing)

Incorporating a backwashing (BW) step into the operation cycle of membrane filtration can dramatically reduce its fouling. Backwashing is performed by automatically reversing the flow of permeate. Usually, the frequency of BW can range every between 30 and 120 minutes and last for a duration of 30 seconds to 5 minutes (AWWA 2005; MWH 2005). Both liquid and gas backwashing can be employed with LPMs. Additionally, combined with air backwashing in a submerged membrane tank, the flux can be increased up to fivefold (Hilal *et al.* 2005). The ideal situation regarding backwash flux and frequency is to use a high flux as frequently as possible. However, such practice results in a very low net flux because permeate is consumed in backwashing. It is therefore desirable to optimize the BW flux and frequency. The frequency of BW is not only dependent upon the feed water quality, but also can be influenced by the operating flux. It has been suggested that if the membrane were operated at lower fluxes, less energy would be required to control fouling and less chemical cleaning would be needed (Fane *et al.* 2005).

For ceramic membranes, the BW pressure can be typically 20 to 40 psi higher that the feed water pressure or 2 to 3 times the TMP (Hsieh 1996). Flux enhancement via BW can control fouling in ceramic membranes and consequently reduce the operation cost. Gray *et al.* (2008) observed that a hydrophilic membrane had greater flux recovery after backwashing than a hydrophobic membrane, and that alum coagulation prior to filtration only significantly increased the efficiency of BW for a hydrophilic membrane while no impact was observed for a hydrophobic membrane. This appears

to be due to the different types of membrane fouling occurring on the hydrophobic membrane, which could not be removed by backwashing.

It is generally effective in removing particle cakes from the membrane surface, and it can also remove foulants from the membrane interior, particularly when performed with a chemical cleaning solution called chemically enhanced backwashing (CEB). An enhanced backwash comprises three steps: firstly a backwash with permeate is performed to remove accumulated particles from the membrane during approximately 30 seconds. Secondly, a short soak during 10 to 15 minutes with a low dose of oxidant/disinfectant to remove adsorbed foulants from the membrane, and finally another short backwash with permeate to remove the chemicals from the systems. CEB can be optimized in terms of chemical dose, frequency and soakage time.

The current trend is toward the merging of chemical cleaning and backwashing. To enhance the efficiency of the BW, the liquid stream is added with chemicals, such as chlorine to clean the membrane surface, aid in oxidation of adsorbed organic materials, and control biological growth on the membrane skin or support material (AWWA 2005).

Table 2.7 shows the effects of various operating strategies against different kinds of fouling. Chemical cleaning is an effective control strategy for all types of membrane fouling. However, this step is preferably avoided or minimized due to the use of chemicals and temporary loss in production.

Table 2.7 - Effects of operating strategies on membrane fouling[2)]

[Source: adapted from Pall 2006]

Type of fouling	Effects of operating strategy			
	Hydraulic cleaning	Feed chlorination	Feed acidification	Chemical cleaning
Inorganic	-	-	++	++
Particulate	++	-	-	++
Microbial	+	++	+*	++
Organic	-	+	-	++

2.4.2. Chemical cleaning

Chemical cleaning is performed when flushing and/or backwashing are/is not able to restore the flux. Compared to an CEB, the chemical dosage is higher than when performing CEB, the duration of chemical cleaning is longer (i.e., a few hours) and the frequency of chemical cleaning is usually much lower (i.e., from a few days to several months depending on the characteristic of the membrane system and source water quality) (MWH 2005). The CEB can be fully automated as it is performed simultaneously with the routine backwash. However, chemical cleaning involves labour to make up the chemicals, fill and flush the system, etc. A cleaning agent can affect fouling material present on a membrane surface in three ways (Hilal *et al.* 2005): i) removal of the foulants; ii) changing morphology of the foulants, e.g., by swelling or compaction; iii) an alteration in surface chemistry of the deposit so that the hydrophobicity or charge is modified. Once the cause of membrane fouling is

[2)] '-': no effects/negative effects; '+': some positive effects; '++': positive effects; '*': together with feed chlorination.

identified, various cleaning chemicals can be used to remove fouling materials from the membrane and to restore the membrane flux. Table 2.8 summarized major categories of membrane cleaning chemicals.

Table 2.8 - Major categories of various cleaning chemicals

[Source: Liu et al. 2001]

Category	Major functions	Typical chemicals
Caustic	Hydrolysis, solubilization	NaOH
Oxidants/disinfectants	Oxidation, disinfection	NaOCl, Ozone, H_2O_2, peroxyacetic acid
Acids	Solubilization	Citric acid, nitric acid, hydrochloric acid
Chelating agents	Chelation	Citric acid, EDTA
Surfactants	Emulsifying, dispersion, surface conditioning	Surfactants, detergents

Caustic

Caustic chemicals are typically used to clean membranes fouled by organic and microbial foulants through hydrolysis and solubilization. There are a number of organic materials including polysaccharides and proteins that can be hydrolysed by caustic. Tertiary structures of proteins are likely to be disrupted and reduced to peptides. Fats and oils also react with caustic through saponification, generating water-soluble soap micelles.

A very important function of caustic is to increase the negative charge of humic substances. During caustic cleaning, the pH of the cleaning solution can be as high as 13. At this pH, even the weakest phenolic groups would be dissociated up to 50%. As a result, the negative charges on organic molecules increase to a great extent, as does their solubility. Molecules of NOM are likely to have a stretched, linear configuration

due to the repulsion between negative charged functional groups (Hong and Elimelech 1997) at high pH. This change in molecule configuration creates a loose fouling layer that allows an easier access for chemicals to penetrate the inner portion of fouling layer, therefore, facilitates mass transfer, and enhances the efficiency of cleaning (Liu *et al.* 2001). In a study by Lee *et al.* (2001), both caustic (NaOH) and acidic (citric acid) agents were more effective in cleaning foulants, in terms of flux recovered, resulting from a hydrophobic NOM source compared to a relatively hydrophilic one. In particular, the caustic agent was more effective than the acidic agent in removing the hydrophobic NOM, and the acidic agent performed slightly better in the removal of hydrophilic NOM.

Oxidants/disinfectants

The most common oxidants used for membrane cleaning include chlorine and hydrogen peroxide. The oxidation of organic polymers generates more oxygen containing functional groups such as ketones, aldehydes, and carboxyl acids. The existence of these functional groups generally increases hydrophilicity of their parent compounds. Therefore, oxidation reduces the adhesion of fouling materials to membranes (Liu *et al.* 2001). The use of oxidants is also better than acids or caustic to remove organic hydrophilic foulants, but is not applicable for hydrophobic and inorganic compounds (Strugholtz *et al.* 2005). Oxidants/disinfectants can also inactivate or kill bacteria that may cause microbial fouling.

Oxidants are often mixed with caustic to form a cleaning cocktail. There are three reasons to mix oxidants, specifically, chlorine with caustic: First, it is to enhance cleaning efficiency, the mixture provides a synergy for NOM dominated fouling

because the fouling layer tends to have more open structure at caustic conditions. This synergy can provide more access to chlorine to reach inner layer of fouling materials, facilitate the mass transfer and reactions between chlorine and fouling materials, and enhance the cleaning efficiency. Second, it is to control excess oxidation to membranes and other module components. At acidic conditions, chlorine is such a strong oxidant that the potential of damage to the membrane and other filter components increases to a great extent. Mixing chlorine with caustic can mitigate excess oxidation by chlorine. The last reason is to simplify the equipment and operation of membrane cleaning. Both caustic and oxidants are needed for efficient membrane cleaning. Mixing them can allow the cleaning to be conducted in one step.

A polymeric membrane of polypropylene (PP) is sensitive to chlorine, while others such as polysulfone (PS) or PVDF can handle concentrations up to 200 mg/L (MWH 2005). One of the advantages of ceramic membrane is their inherent tolerance to high concentrations of oxidants and disinfectants. This potentially can allows for enhanced cleaning of ceramic membranes due to a greater number of options to suit specific needs and at higher concentrations, including ozone (O_3).

Acids and chelating agents

Acids are primarily used to remove scales and metal dioxides from fouling layers. When a membrane is fouled by iron oxides, citric acid is very effective because it not only dissolves iron oxides precipitates, but also forms a complex with iron (Liu *et al.* 2001). If there is coexistence of divalent cations (e.g., calcium) and NOM, the-salt-bridge-effect of divalent cations can cause a denser and more adhesive fouling layer. The removal of divalent cations by either acids or chelating reagent, such as EDTA,

can also improve the cleaning of membranes fouled by organic foulants (Hong and Elimelch 1997).

Surfactants

Surfactants are compounds which have both hydrophilic and hydrophobic structures, and decrease the surface tension of the solutions that are in contact with membranes. They can form micelles with fats, oils, and proteins in water and help to clean the membranes fouled by these materials. Some surfactants may also interfere with hydrophobic interaction between bacteria and membranes. In addition, surfactants can disrupt functions of bacteria cell walls. Therefore, surfactants affect fouling dominated by the formation of biofilms (Liu *et al.* 2001).

2.4.3. Effect on chemical cleaning of ceramic membranes

Kennedy *et al.* (2007) investigated the effect on chemical cleaning of a ceramic membrane (a monolithic tubular ceramic membrane having nominal pore size 0.1 μm) fouled by the Delft Canal water(pH of 8.2; turbidity of 10.3 NTU; UVA_{254} of 0.467 cm^{-1}; DOC 11.01 mg/L; TSS 22.2 mg/L). The fouled membranes was first soaked in 3,000 ppm sodium hypochlorite (NaOCl) solution overnight at alkaline conditions of pH 12, followed by 0.1M solution of sodium hydroxide (NaOH) and finally, 1% solution of citric acid, all at ambient temperature. It was effectively conducted at very high concentrations compared to those performed for polymeric membranes. Sodium hypochlorite, sodium hydroxide and citric acid were able to restore the membrane permeability by 25%, 32% and 14%, respectively. The combination of these chemicals was able to fully restore membrane permeability including backwash (30%).

Caustic (i.e., NaOH) cleaning was more effective (32%) than either NaOCl or citric acid cleaning, due to the fact that it can change the configuration of NOM into a looser and more open structure that is easily detached (Liu *et al.* 2001). Sodium hypochlorite can allow the ceramic membrane to restore flux by 25%, suggesting that microbial fouling was significant since sodium hypochlorite is an effective disinfectant. LC-OCD analyses revealed their effect on the various NOM fractions in the membrane. Hydrophobics, biopolymers and low molecular weight (LMW) acids fractions were well cleaned by NaOCl. The high rejection rate of LMW acid fraction occurred, which was estimated as a result of being removed because they are oxidation products of neutrals, building block and humic substances (Liu *et al.* 2001). NaOH mainly could remove neutrals, which comprises almost 50% of NOM and building blocks. Critic acid was most effective in removing humic substances up to approximately 40%, but was unable to significantly remove the other fractions.

2.5. SUSTAINABLE FLUX

One of the main objectives of membrane filtration is stable operation with minimal fouling during its performance. Sustainable flux allows the membrane filtration to operate at fluxes that result in low levels of fouling, which ultimately increases the lifetime of the membrane and decreases the frequency of cleaning.

The concept of critical flux describes the relationship between flux and the rate of fouling in a controlled steady state environment (Pearce and Field 2007). The critical flux can be generally defined as the “threshold” flux between which fouling does not

occur, and above which fouling becomes noticeable. This concept might be of use in understanding and improving the operation of membrane filtration system (Bacchin *et al.* 2006). There are several different approaches that have been utilized to identify the sustainable flux. The most common method was either stepwise increases in the permeate flux or TMP and maintaining each for a certain amount of time. For example, Choi and Dempsey (2005) performed flux stepping experiments in 10 minutes, while continuously recording the flux and TMP. Similarly, the TMP can be increased stepwise as well at regular intervals. This experiment can be repeated for 20 or 30 minutes for each step. In addition, both subcritical and supercritical fluxes can be applied for 120 minutes to observe the fouling behaviour in longer-term operations. Chan *et al.* (2002) examined the linearity in the plot of TMP averaged over each 15 minutes flux step versus the applied flux. The last value of flux remaining on the straight line was considered as the apparent critical flux, or sustainable flux.

Lehman and Liu (2009) performed flux stepping experiments in a 30 minutes filtration cycle to establish the critical flux for the operation of a ceramic membrane. In each cycle, the flux was kept constant while an increase in TMP was recorded if the membrane fouled. A normal backwash was applied between each cycle before stepping up to higher flux. As shown Figure 2.7, the TMP started to increase within the filtration cycle at second flux. The rate of TMP increase versus time, i.e., the slope of TMP curve in Figure 2.8-a started to increase dramatically once flux exceeded 255 L/m^2h (150 gfd). Figure 2.8-b shows the flux-TMP gradient of the 30-min filtration cycle. The authors determined that the critical flux, or sustainable flux, by general definition, was at TMP of 122 L/m^2h (72 gfd) at which the flux-TMP relationship became non-linear.

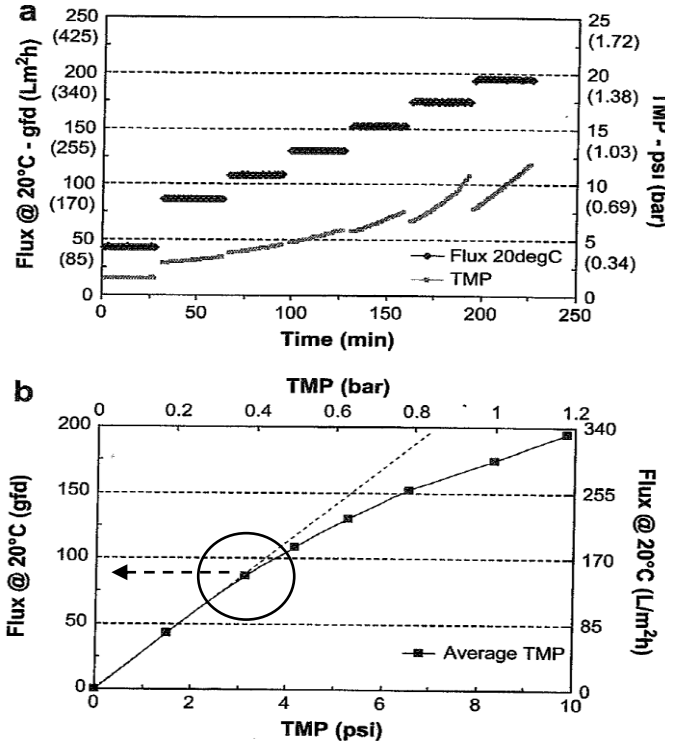

Figure 2.8 Flux vs. TMP to evaluate the critical flux

[Source: (Lehman and Liu 2009)]

2.6. REFERENCES

Alazmi, R., Nassehi, V. and Wakeman, R. (2010) Calcium cation interactions with polysaccharides and proteins in wastewater UF membrane fouling. Membrane Technology 2010(1), 6-12.

Burggraaf, A.J. and Cot, L. (1996) Fundamentals of inorganic membrane science and technology, Elsevier.

Dafinov, A., Garcia-Valls, R. and Font, J. (2002) Modification of ceramic membranes by alcohol adsorption. Journal of Membrane Science 196(1), 69-77.

Fu, X., Maruyama, T., Sotani, T. and Matsuyama, H. (2008) Effect of surface morphology on membrane fouling by humic acid with the use of cellulose acetate butyrate hollow fiber membranes. Journal of Membrane Science 320(1–2), 483-491.

Hao, Y., Moriya, A., Ohmukai, Y., Matsuyama, H. and Maruyama, T. (2013) Effect of metal ions on the protein fouling of hollow-fiber ultrafiltration membranes. Separation and Purification Technology 111(0), 137-144.

Hashino, M., Katagiri, T., Kubota, N., Ohmukai, Y., Maruyama, T. and Matsuyama, H. (2011) Effect of membrane surface morphology on membrane fouling with sodium alginate. Journal of Membrane Science 366(1–2), 258-265.

Katsoufidou, K., Yiantsios, S.G. and Karabelas, A.J. (2008) An experimental study of UF membrane fouling by humic acid and sodium alginate solutions: the effect of backwashing on flux recovery. Desalination 220(1–3), 214-227.

Katsoufidou, K.S., Sioutopoulos, D.C., Yiantsios, S.G. and Karabelas, A.J. (2010) UF membrane fouling by mixtures of humic acids and sodium alginate: Fouling mechanisms and reversibility. Desalination 264(3), 220-227.

Kelly, S.T. and Zydney, A.L. (1995) Mechanisms for BSA fouling during microfiltration. Journal of Membrane Science 107(1–2), 115-127.

Kim, H.-C. and Dempsey, B.A. (2013) Membrane fouling due to alginate, SMP, EfOM, humic acid, and NOM. Journal of Membrane Science 428(0), 190-197.

Kosmulski, M. (2011) The pH-dependent surface charging and points of zero charge: V. Update. Journal of Colloid and Interface Science 353(1), 1-15.

Larbot, A., Gazagnes, L., Krajewski, S., Bukowska, M. and Wojciech, K. (2004) Water desalination using ceramic membrane distillation. Desalination 168, 367-372.

Lee, S. and Cho, J. (2004) Comparison of ceramic and polymeric membranes for natural organic matter (NOM) removal. Desalination 160(3), 223-232.

Lehman, S.G. and Liu, L. (2009) Application of ceramic membranes with pre-ozonation for treatment of secondary wastewater effluent. Water Research 43(7), 2020-2028.

Moritz, T., Benfer, S., Arki, P. and Tomandl, G. (2001a) Investigation of ceramic membrane materials by streaming potential measurements. Colloids and Surfaces A: Physicochemical and Engineering Aspects 195(1–3), 25-33.

Moritz, T., Benfer, S., Árki, P. and Tomandl, G. (2001b) Influence of the surface charge on the permeate flux in the dead-end filtration with ceramic membranes. Separation and Purification Technology 25(1–3), 501-508.

Nazzal, F.F. and Wiesner, M.R. (1994) pH and ionic strength effects on the performance of ceramic membranes in water filtration. Journal of Membrane Science 93(1), 91-103.

Sekulić-Kuzmanovic, J., 2004. Mesoporous and Microporous Titania Membranes. PhD thesis, University of Twente, Enschede, the Netherlands

Xiao, F., Xiao, P., Zhang, W.J. and Wang, D.S. Identification of Key Factors Affecting the Organic Fouling on Low-Pressure Ultrafiltration Membranes. Journal of Membrane Science (0).

Zhou, J., Zhang, X., Wang, Y., Hu, X., Larbot, A. and Persin, M. (2009) Electrokinetic characterization of the Al2O3 ceramic MF membrane by streaming potential measurements. Desalination 235(1–3), 102-109.

Chapter 3

Phase 1: Identification of Fundamental Properties of TAMI and AAO Ceramic Membranes

3.1. INTRODUCTION

Most ceramic membranes are made from oxide powders, such as Al_2O_3, ZrO_2, TiO_2 and various combination, and generally asymmetric structures, consisting of a supporting layer with large pores of sufficient mechanical strength on top of which are layers with gradually decreasing pore size (Burggraaf and Cot 1996). This can be an advantage for obtaining relatively higher fluxes from thin separation layers. It has been reported that the principal chemical properties of ceramic membranes are their hydrophilicity (Dafinov et al. 2002, Larbot et al. 2004) and amphoteric surface charge due to the presence of hydroxyl (OH^-) groups on their surface. These characteristics allow the ceramic membrane to contribute to high permeability, and influence separation ability, filterability, and fouling potential as well (Dafinov et al. 2002).

This chapter is aimed at identification of fundamental properties and morphologies of two different types of MF and UF ceramic membranes with different characteristic: a TiO_2+ZrO_2-based commercial TAMI membrane and a Al_2O_3-based AAO membrane. The TAMI ceramic membrane is obtained by sintering a packing of particles in each layer of the multi-layered system and the latter is fabricated by anodic oxidation of Al metal foil, resulting in porous (amorphous) alumina membranes (Burggraaf and Cot 1996). Important membrane properties including pure water permeability (PWP; $L/m^2h \cdot bar$), material and synthetic layer composition, porous nature (i.e., pore size and distribution, and surface roughness), contact angle (CA; °) as an index of hydrophobicity, and zeta potential (ζ; mV) as an index of surface charge were closely evaluated using various analytical methods. This chapter is expected to serve as a background to analyze and understand experimental results in subsequent chapters.

3.2. MATERIALS AND METHODS

3.2.1. Membranes

Simple specifications of the TAMI ceramic membrane (INSIDE DISRAM™, TAMI INDUSTRIES, France) and the AAO membrane (Anodisc™, Whatman, USA) used for the study are summarized in Table 3.1.

Table 3.1 – Simple specification of two ceramic membrane discs used for bench-scale experiments

	TAMI		AAO	
	MF	UF	MF	UF
Pore size, or MWCO	0.14μm	150kD	0.1μm (100nm)	20nm
Materials	ZrO_2 + TiO_2	ZrO_2 + TiO_2	Al_2O_3	Al_2O_3
Effective surface area (cm^2)	17.4	17.4	17.4	3.14

3.2.2. Morphology analyses and measurements

3.2.2.1. Scanning electron microscopy (SEM)

Membrane specimens were cryogenically preserved in slush nitrogen at −210°C followed by controlled dehydration in a freeze drying instrument (K775X Turbo; Quorum, UK). Scanning electron microscope (SEM) (FEI, USA) equipped with cryo stage and cryo preparation chamber (Quorum, UK) was used to image virgin ceramic membranes. Focused Ion Beam (FIB) technique in combination with SEM was used for cross sectional imaging of the samples. Energy Dispersive X-ray Spectroscopy (EDS or EDX) was used for elemental analysis conducted as spot or mapping analysis.

3.2.2.2. Atomic force microscopy (AMF)

AFM scans the material surface with a very fine tip and generates three-dimensional maps by detection of deflection of a laser beam reflected by cantilever (Alldredge et al.). The AFM employed is made by Digital Instruments, and data are analyzed by built-in software in the analyzer. The tip size is 4~10 nm made of etched single crystal silicon. AFM was performed with a tapping mode. Tapping provides several advantages: higher lateral resolution on most samples, lower forces and less damage to soft samples imaged in air, and lateral forces are virtually eliminated (there is no scraping), but it provides slightly slower scan speed than contact mode AFM. Clean membrane specimens were prepared with MQ water (≈18Ω) filtration and dried at room temperature to obtain an actual surface. Sample specimens were fixed on a glass slide and scanned over 5μm × 5μm for membranes. Images were obtained in amplitude mode and height mode at the same time. Amplitude mode provides a more detailed topographical view of the membrane surface in voltage units of the *Z*-axis range, and height mode offers nanometer scaled image analysis. A scan rate of 1~2 Hz was applied considering image features, membranes, and scan sizes.

3.2.2.3. Contact angle

Contact angle of ceramic membrane surfaces was measured using an optical tensiometer (Theta Lite, attention, Finland). The sessile drop method was selected for the measurement because it is a highly accurate and reproducible optical method, especially for contact angle measurement. The optical tensiometer records drop images, and automatically analyzes the drop shape as a function of time; The captured images are analyzed with a drop-profile fitting method in order to determine contact angle.

3.2.2.4. Zeta potential (ζ)

The ζ potential value of ceramic membranes were determined from electrophoretic mobility measurements using a commercially available electrophoresis measurement apparatus (ELS-Z, Photal, Electronics, Japan) with a plate sample cell. Polystyrene latex particles (diameter 520 nm, Otsuka Electronics, Japan) coated with hydroxyl propyl cellulose (HPC) and with a molecular weight of 300,000 (Scientific Polymer Products, Japan) were used as mobility-monitoring particles. These were dispersed in a 0.01MKCl solution to prevent the interactions with (or adsorption on) the quartz cell surface during measurement.

3.3. RESULTS AND DISCUSSION

3.3.1. Pure water permeability (PWP) and contact angle (CA)

Pure water permeability (PWP) of the two ceramic membranes (i.e. TAMI and AAO) with MQ water (≅18Ω) was investigated. Both the TAMI and AAO membrane performed stable operation at a transmembrane pressure (TMP) of 1 bar, exhibiting constant flux without any fluctuation as shown in Figure 3.1. The AAO MF membrane showed higher permeability than the TAMI membrane, resulting in 4,500 $L/m^2h \cdot bar$ and 1,500 $L/m^2h \cdot bar$ for the AAO and TAMI, respectively. For the UF membranes, result showed that the AAO permeability was significantly higher than the TAMI membrane, showing 2,200 $L/m^2h \cdot bar$ and 250 $L/m^2h \cdot bar$ for the TAMI and the AAO, respectively.

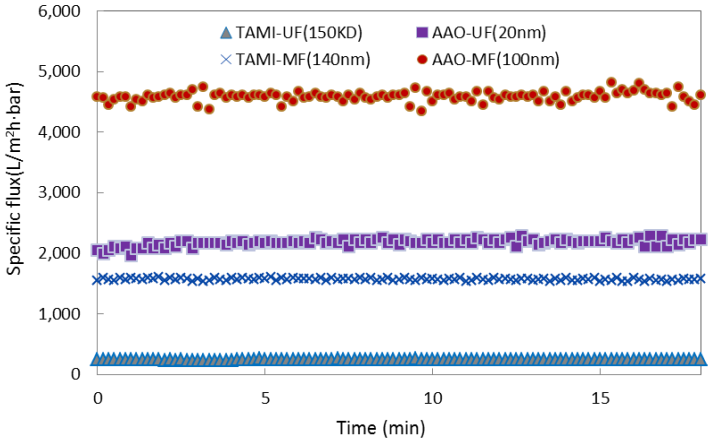

Figure 3.1 - PWP measurement of TAMI and AAO ceramic membranes

Contact angles (CA) were measured. Results showed that both AAO and TAMI membranes were hydrophilic, resulting in 35° (UF) and 25° (MF) for the AAO and 42° (UF) and 50° (MF) for the TAMI. The AAO showed slightly higher hydrophilicity. Table 3.2 summarizes PWP and CA of the TAMI and AAO ceramic membranes, compared to polymeric membranes reported from a literature (Lee et al. 2004).

Table 3.2 – Specifications and properties of TAMI and AAO ceramic membranes, compared with polymeric membranes

	Ultrafiltration (UF) membranes				Microfiltration (MF) membranes			
	AAO	TAMI	PES, Orelis	YM100, Millipore	AAO	TAMI	GVHP, Millipore	GSWP, Millipore
Pore size	20nm	150KDa	100KDa	100KDa	0.1µm	0.14µm	0.22µm	0.22µm
Materials	Al_2O_3	ZrO_2+ TiO_2	PES	Re-generated cellulose	Al_2O_3	ZrO_2+ TiO_2	PVDF	Mixed cellulose ester
PWP ($L/m^2h \cdot bar$)	2200	250	122	372	4500	1500	856	3770
CA (°)	35	42	58	18	25	50	83	19

3.3.2. Zeta Potential (ZP)

Zeta potential (ζ) measurement of two ceramic MF membranes (TAMI and AAO) was achieved in a 0.01MKCl solution under a wide range of pH values from 3 to 11. Both membranes exhibited pH-dependent surface charge, as shown in Figure 3.2. It was clearly observed that the TAMI membrane has a positive charge below pH 4, and negatively charged at higher pH values, with a point of zero charge (PZC) near pH 4, while the PZC of the AAO membrane was observed near pH 10. The result confirmed that both ceramic membranes are amphoteric, so their surface charges varied in accordance with pH, that is, decrease in ZP with increased pH.

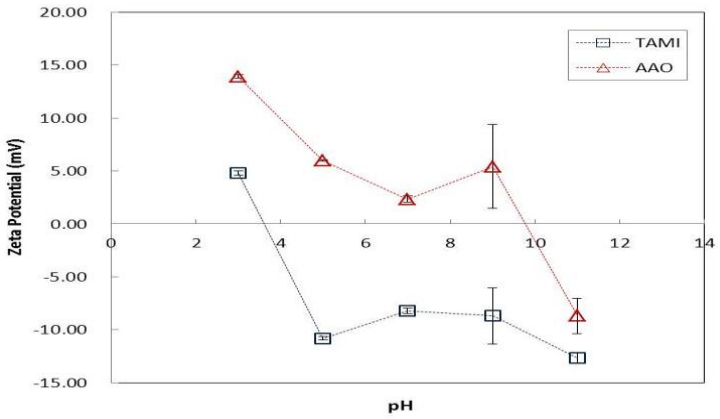

Figure 3.2 – Zeta potentials (ζ) of TAMI and AAO MF membranes in a 0.01MKCl solution as function of pH from 3 to 11

3.3.3. Membrane morphology and material composition

The morphology of TAMI and AAO membranes was identified using scanning electron microscopy (SEM). X-ray crystallography or X-ray diffractometry (XRD) and X-ray fluorescence (XRF) characterized the two membranes in terms of material structure and elemental composition, respectively.

3.3.3.1. TAMI ceramic membrane

SEM images demonstrated that the TAMI membrane that is fabricated by sintering/sol-gel process was asymmetric and multilayered with interconnected pores as shown in Figure 3.3 and Figure 3.4. The TAMI membrane was largely composed of three layers that were the smallest porous active layer at the top supported by an intermediate layer and a macro-porous supporting layer at the bottom. In particular, the UF membrane consisted of a double-coated active layer (Figure 3.3), while the MF represented a single active-separation layer (Figure 3.4). However, each layer was not uniform, representing uneven thickness and level.

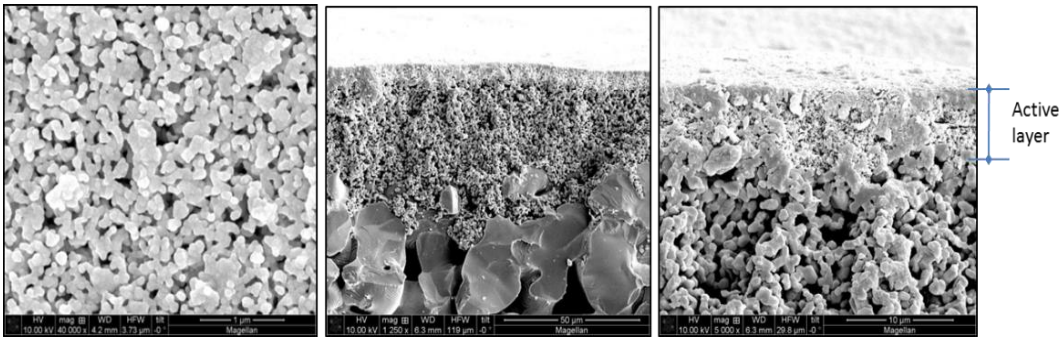

Figure 3.3 – SEM images of a TAMI MF ceramic membrane (left: top view; middle: cross section; right: cross section in higher magnification)

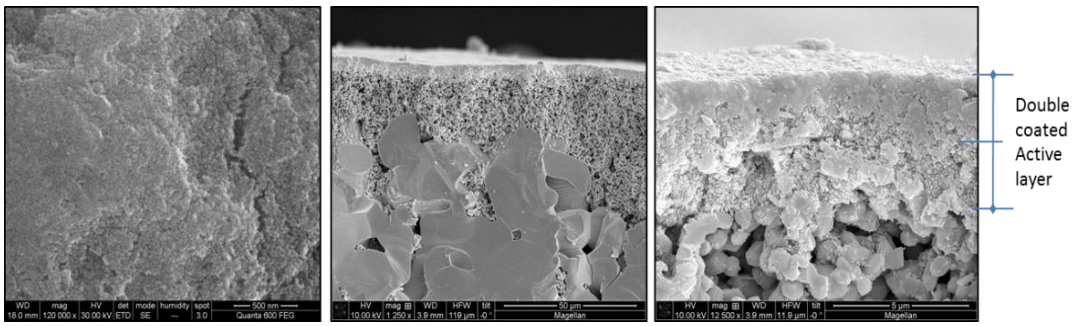

Figure 3.4 – SEM images of a TAMI UF ceramic membrane (left: top view; middle: cross section; right: cross section in higher magnification)

Material structure and composition of TAMI membrane was revealed with X-ray diffraction (XRD) and X-ray fluorescence (XRF). XRD demonstrated that TAMI ceramic are composed of TiO_2 and ZrO_2, presenting two distinctive peaks in terms of TiO_2 and ZrO_2 as shown in Figure 3.5. XRF analysis confirmed that TAMI ceramic membrane consists of heterogeneous material differentiating an active layer and a support layer, characterizing Zr (38.7%), O (32.7%), Ti (23.9%) and Y (3.8%) for a separation layer and Ti (52.8%) and O (46.4%) for a supporting layer.

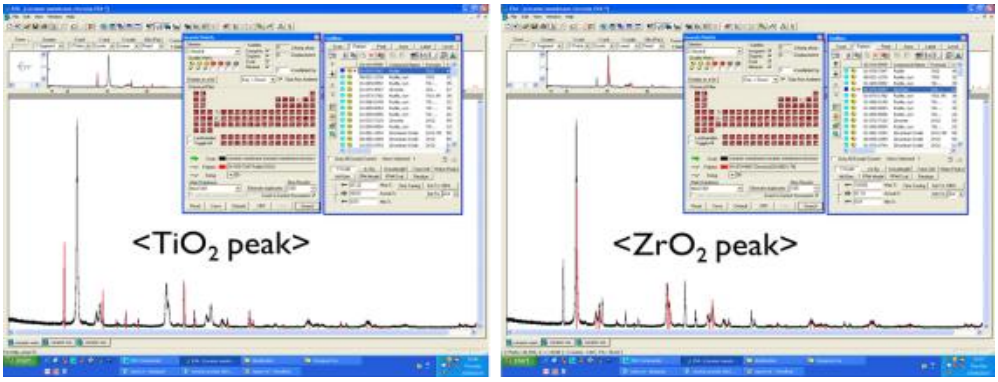

Figure 3.5 – Images of XRD peaks of TAMI MF/UF ceramic membranes: Note that peaks in the figure present the TAMI MF membrane

3.3.3.2. AAO ceramic membrane

Figure 3.6 presents SEM images of an AAO MF/UF ceramic membrane in terms of top view and cross section. The SEM photograph revealed that the AAO ceramic membrane has a simple pore morphology. AAO membranes are fabricated by anodic oxidation process, immersing a piece of aluminium foil in an acidic electrolyte batch, and applying an appropriate potential across it. Different acids yield membranes with different pore size because the rate of field assisted dissolution that results in pore formation depends upon the nature of the electrolyte. Phosphoric and oxalic acids are

generally used to produce the commercially available anodic alumina membranes of AAO (Hernández et al. 1997).

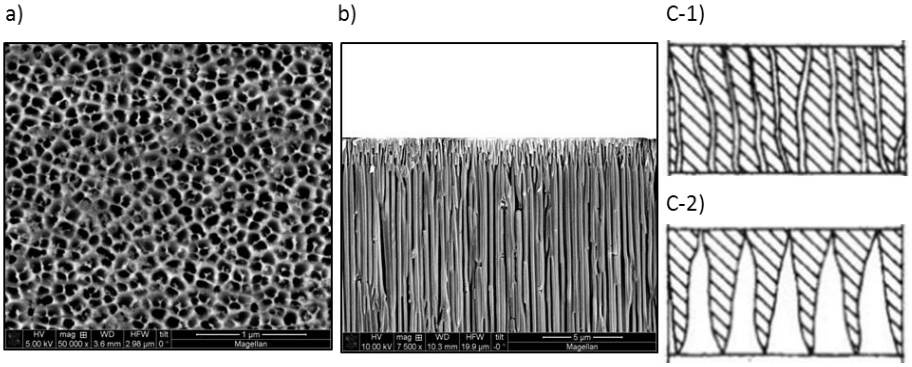

Figure 3.6 - SEM images of an AAO ceramic membrane (based on Al_2O_3) which is fabricated by anodic oxidation process: a) top view; b) cross section; c-1) illustration of the MF cross section; c-2) illustration of the UF cross section

As described in Figure 3.6, the AAO membrane was characterized by uniform pore-structure ceramic membrane, with more or less straight cylindrical-shaped pores for the MF and conical-shaped pores for the UF. An SEM image of the cross section (Figure 3.6-b) revealed that an AAO MF membrane is symmetric, consisting of single wall instead of multilayered composition (i.e., no intermediate and supporting layer), while pore shapes of an AAO UF membrane were asymmetric with conical pore shape. Figure 3.6-c-1) and c-2) illustrate pore shapes of an AAO MF and UF membrane which are observed with SEM, respectively.

X-ray crystallography or diffraction (XRD) revealed that AAO membrane is amorphous instead of crystalline, resulting in no peak observed from the analysis as shown in Figure 3.7. Because XRD is a method used for determining the atomic and molecular structure of a crystal, no peak was observed from the AAO membrane.

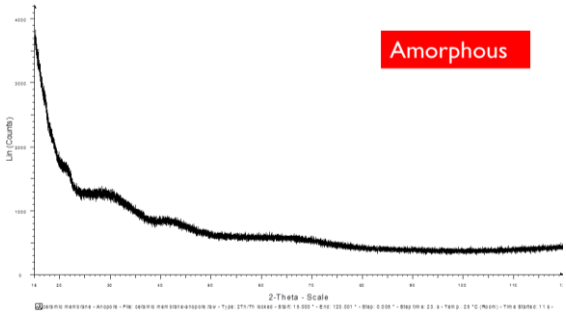

Figure 3.7 – Image of XRD analysis of AAO MF/UF ceramic membranes: The image presents the AAO MF membrane

3.3.4. Measurement of pore nature

3.3.4.1. Pore size (or MWCO)

AAO ceramic membrane

Pore size of AAO MF (a nominal pore size of 100 nm reported by a manufacturer) and UF membrane (a nominal pore size 20nm) were analyzed using SEM images along with built-in software in the analyser measuring randomly seven times per each picture as shown in Figure 3.8. From the MF membrane image (Figure 3.8-a)), size ranges of pores were clearly observed, showing 77.2, 79.3, 122.5, 129.8, 138.2, 164.5 and 182.6 nm, while all pores observed from the UF surface image (Figure 3.8-b)) were bigger than 20 nm, resulting in 25.0, 25.5, 39.2, 42.7, 42.8, 44.9, and 46.7 nm. Pore size of the bottom of the UF membrane measured ranged from 150 nm to 200 nm as shown in Figure 3.8-c), verifying that the AAO UF membrane pore shapes are asymmetric, conical pore structure (i.e., pore shapes are increased from the top to the bottom) as illustrated in Figure 3.6-c-2).

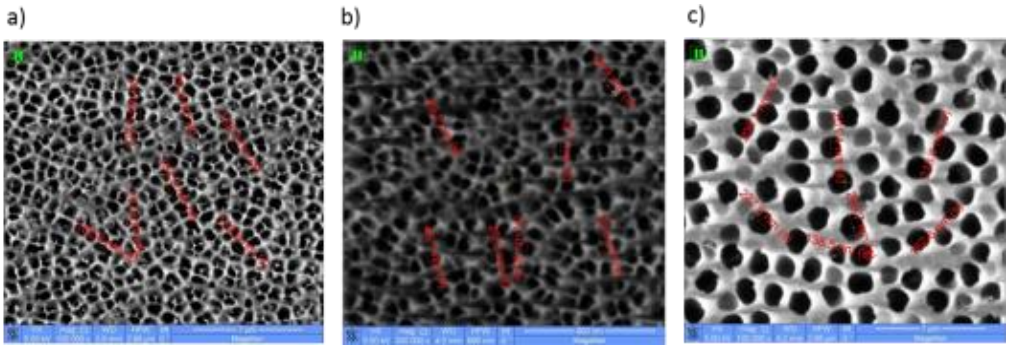

Figure 3.8 - SEM images of AAO MF and UF ceramic membranes: a) top view of MF (bar scale: 1 µm); b) top view of UF active layer (bar scale: 0.4 µm); c) top view of UF bottom layer (bar scale: 0.1 µm)

TAMI ceramic membrane

An attempt was made to measure pore size of the TAMI MF and UF ceramic membranes using SEM in the same way as applied to the AAO membrane. However, no representable measurement was achieved, because pore shapes imaged with SEM are irregular and interconnected with each other as shown in Figure 3.9. Other methods would be possible to measure pore size of the TAMI membrane instead of SEM image analysis software, but further measurement using alternative methods was not carried out.

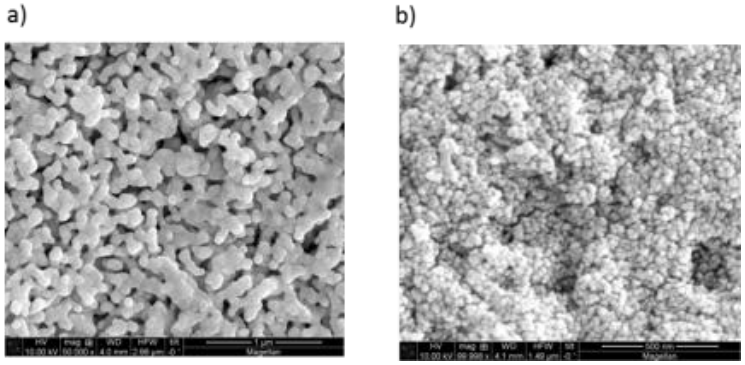

Figure 3.9 - SEM images of TAMI MF and UF ceramic membranes: a) top view of MF (bar scale: 1 µm); b) top view of UF (bar scale: 0.5 µm)

3.3.4.2. Pore distribution

AAO ceramic membrane

SEM along with computerized image analysis (CIA) was applied to identify pore distribution. The statistical distributions of pore areas and perimeters along with equivalent pore diameters and shapes are considered to determine average pore size and distribution (Hernández et al. 1997). SEM photography is digitalized with a resolution of 1024×768 pixels, assigning a grey level ranging from 0 (black) to 255 (white) to each one. Figure 3.10 presents the SEM image digitalization of an AAO MF membrane in order to analyze pore diameter and distribution. First of all, pores are picked up from the image (Figure 3.10-b)) and were used for calculating areas and perimeters, acquiring equivalent diameters, counting the number, and finally yielding the average pore diameter and distribution as summarized in Table 3.3. Results shows that average pore size of the MF membrane analyzed is 76 nm (i.e., 0.076 µm), which is smaller than a nominal pore size of 0.1 µm provide by manufacturer. The pore diameter distribution analyzed is graphically shown in Figure 3.11.

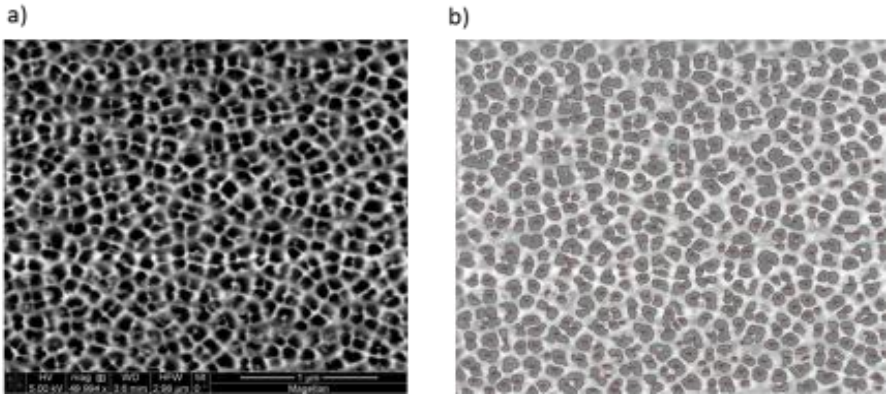

Figure 3.10 - SEM image digitalization of the AAO MF membrane for pore size and distribution analyses; red dots in b) are pores detected

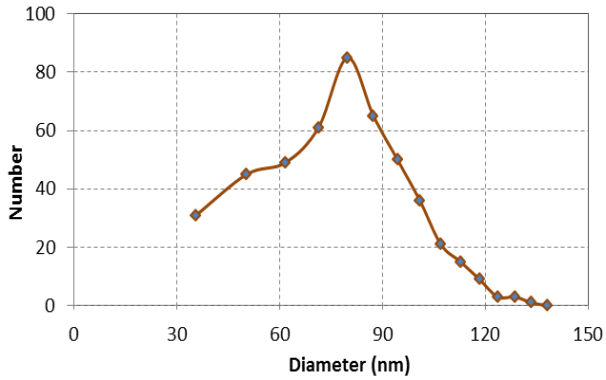

Figure 3.11 - Pore diameter distribution of the AAO MF membrane

Table 3.3 – Pore number of an AAO MF membrane as function of diameter, yielding the average pore diameter and distribution

Area(μm^2)	Equivalent diameter (nm)	Number	Dia.*Num.
0.001	35.68	31	1106
0.002	50.46	45	2271
0.003	61.80	49	3028
0.004	71.36	61	4353
0.005	79.79	85	6782
0.006	87.40	65	5681
0.007	94.41	50	4720
0.008	100.93	36	3633
0.009	107.05	21	2247
0.01	112.84	15	1693
0.011	118.35	9	1065
0.012	123.61	3	371
0.013	128.66	3	386
0.014	133.51	1	134
0.015	138.20	0	0
Average			76nm

For UF membrane analyses, the same procedure as applied to MF membrane was used. Figure 3.11 presents SEM image digitalization of an AAO UF membrane. Consequently, the area and perimeter of each pore are measured; acquiring equivalent diameter, finally yielding the average pore size and distribution as summarized in Table 3.4.

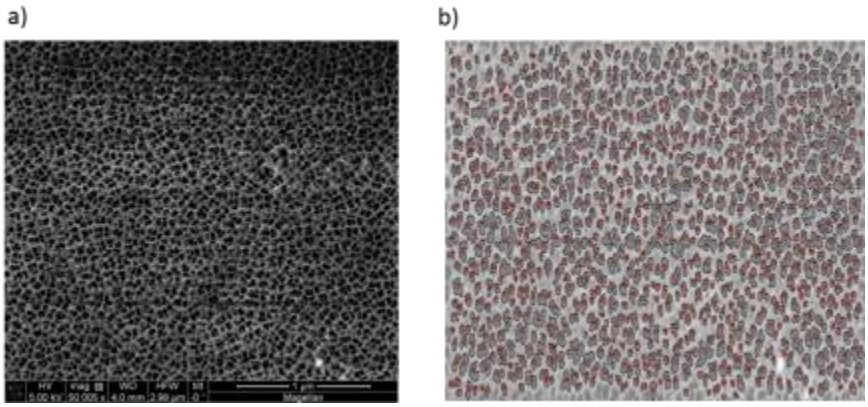

Figure 3.12 - SEM image digitalization of AAO UF membrane for pore size and distribution analyses; red dots in b) are pores detected

The computerized results show that average pore diameter of the UF membrane is 76nm, which is lower than a nominal pore size of 20 nm reported by manufacturer. The pore diameter distribution is graphically shown in Figure 3.13. However, it is considered that since the curve did not show bell shape like MF, detection of pores below 20 nm were limited in the software.

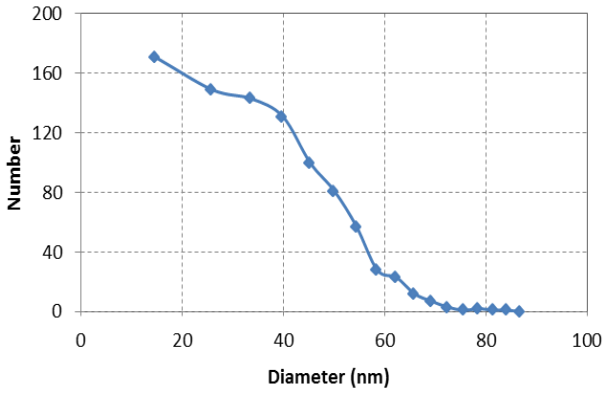

Figure 3.13 - Pore distribution of an AAO UF ceramic membrane

Table 3.4 - Pore number of an AAO UF membrane as function of diameter, yielding the average pore diameter and distribution

Area(μm^2)	Equivalent diameter (nm)	Number	Dia.*Num.
0.000168	14.63	171	2501
0.0005278	25.92	149	3863
0.0008875	33.62	143	4807
0.0012474	39.85	131	5221
0.0016072	45.24	100	4524
0.001967	50.04	81	4054
0.0023268	54.43	57	3102
0.0026866	58.49	28	1638
0.0030464	62.28	23	1432
0.0034062	65.86	12	790
0.003766	69.25	7	485
0.0041258	72.48	3	217
0.0044856	75.57	1	76
0.0048454	78.55	2	157
0.0052052	81.41	1	81
0.005565	84.18	1	84
Average			36nm

3.3.4.3. Surface roughness and profile

Surface roughness and distribution of TAMI and AAO membranes were determined with atomic force microscopy (AFM). There are three commonly used AFM techniques: contact mode, noncontact mode, and tapping mode. In this study, *tapping mode* AFM was used because the mode allows high-resolution topographic imaging of sample surfaces by alternately bringing the tip into contact with the surface to provide high resolution and then lifting it off the surface to avoid dragging the tip across the surface (Boussu et al. 2005). Figure 3.14 shows comparison of AFM topographical section images of TAMI and AAO MF membranes. AFM section images revealed that the TAMI membrane surface is rough and relatively deep, having a large roughness deviation, while the AAO membrane resulted in having smoother surface and smaller roughness deviation.

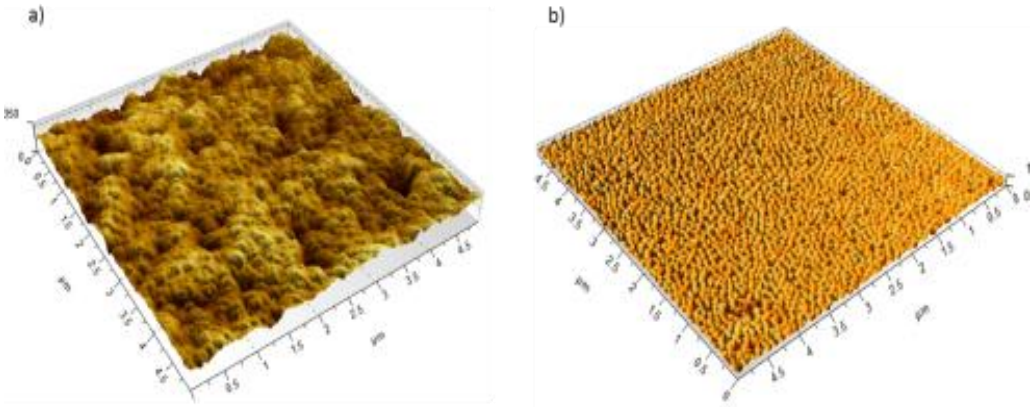

Figure 3.14 – AFM section images of TAMI MF (a) and AAO MF (b): a) 0.5 × 0.5 µm; b) 0.5 × 0.5 µm; note that z-scale of a) and b) is 250 and 1 µm, respectively

Table 3.5 summarizes surface roughness deviation of the two MF membranes in terms of arithmetic mean deviation (Ra) and root-mean-square deviation (Rq), confirming that AAO MF surface is smoother than TAMI. The surface roughness profile and distribution measurement were obtained as shown in Figure 3.15. The TAMI MF surface observed presented wide roughness distribution ranging from 30nm to 320nm, a deep surface, while the AAO MF showed narrow distribution ranging from 30nm to 120 nm, less deep.

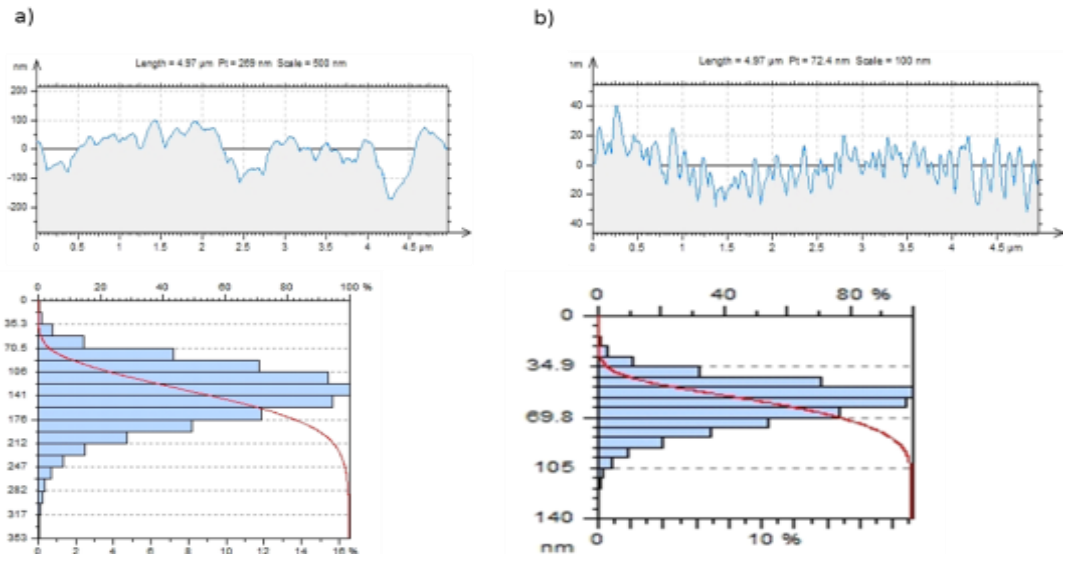

Figure 3.15 – Roughness profile/distribution of TAMI MF (a) and AAO MF (b)

Table 3.5 – Surface roughness deviation of TAMI MF and AAO MF membrane

	Roughness Deviation	*TAMI-MF 140nm*	*AAO-MF 100nm*
Ra	Arithmetic mean deviation	19.4 nm	6.94 nm
Rq	Root-mean-square deviation	24.4 nm	8.72 nm

AFM surface section images of the TAMI and AAO UF membrane were obtained with the same approach as tried for AAO MF. As shown in Figure 3.16, AFM images revealed that the TAMI UF membrane surface (Figure a.) was rough with larger deviation, while the AAO UF membrane (Figure b.) has a relatively smoother surface with a smaller deviation, the same as observed for the AAO MF membrane.

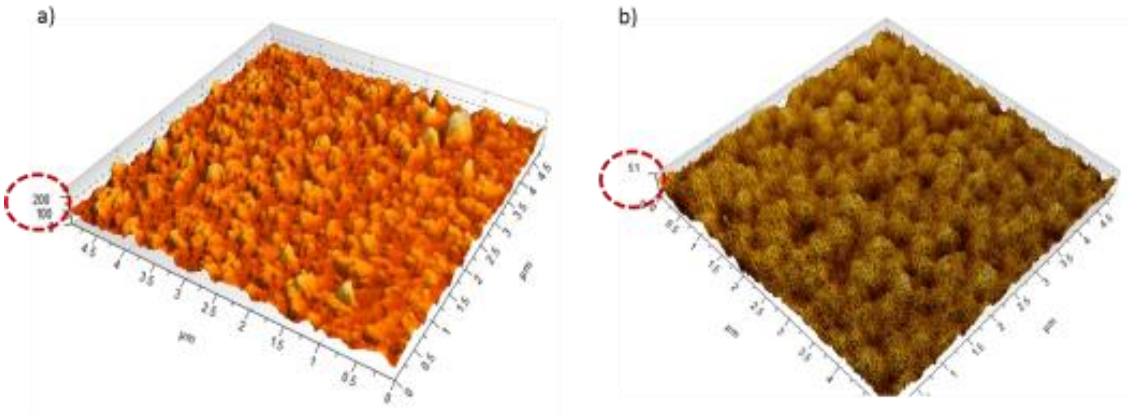

Figure 3.16 - AFM section images of TAMI UF (a) and AAO UF (b): a) 0.5 × 0.5 µm; b) 0.5 × 0.5 µm; note that z-scale of a) and b) is 200 and 51 µm, respectively

Surface roughness deviation of TAMI and AAO UF membranes in terms of arithmetic mean deviation (Ra) and root-mean-square deviation (Rq) were measured, resulting in 12.4 nm and 15.4 nm for TAMI UF and 2.78 nm and 3.45 nm for AAO UF, respectively. The surface roughness profile of both UF membranes were obtained as shown in Figure 3.17. The TAMI UF surface roughness was widely distributed

ranging from 50nm to 250nm, while the AAO UF presented a narrow distribution from 10nm to 45 nm; less deep than the TAMI.

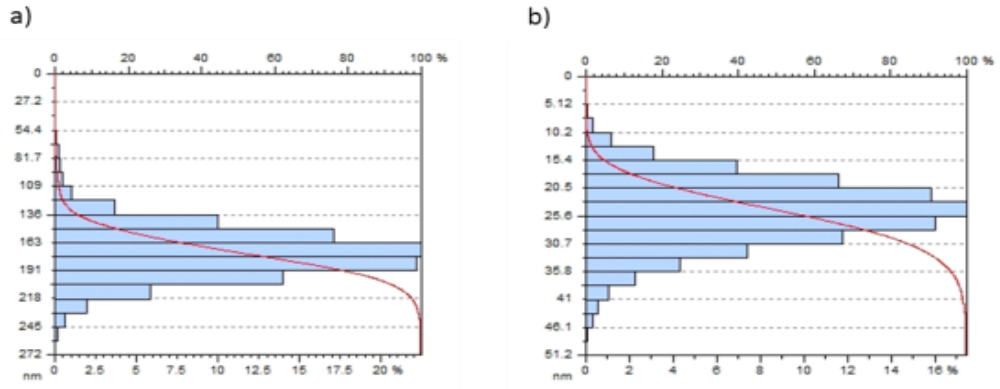

Figure 3.17 – Surface roughness distribution of TAMI UF (a) and AAO UF (b) ceramic membranes

Taking results on SEM and AFM analyses in terms of surface morphology and topology into account, it can be hypothesized that the reason why AAO membrane experienced in much higher permeability than TAMI membrane as shown in Figure 3.1, is that the AAO membrane has narrower surface roughness distribution and possesses a more uniform pore-structure.

3.4. SUMMARY

Pure water permeability (PWP) of AAO and TAMI ceramic membrane was measured, resulting in 4,500 L/m^{2}h·bar (AAO) and 1,500 L/m^{2}h·bar (TAMI) for MF and 2,200 L/m^{2}h·bar (AAO) and 250 L/m^{2}h·bar (TAMI) for UF. The results indicate that the AAO membrane can be operated at higher flux than the TAMI membrane. However,

both ceramic membranes have relatively higher permeability than common polymeric membranes.

Contact angles (CA) measured showed that both AAO and TAMI membranes were hydrophilic, resulting in 35° (UF) and 25° (MF) for the AAO and 42° (UF) and 50° (MF) for the TAMI. It was observed that the hydrophilicity of AAO membrane is slightly higher that TAMI membrane.

Zeta potential (ζ) measurements were performed over a wide range of pH values from 3 to 11. Both TAMI and AAO membrane surface charge showed pH-dependent behaviour. The PZC of the TAMI membrane was observed near pH 4, while the AAO membrane was near pH 10. The result confirmed that both ceramic membranes are amphoteric, so their surface charges are dependent on pH value.

SEM images demonstrated that the TAMI membrane is an asymmetric structure, composed of three layers, the smallest porous active layer at the top supported by an intermediate layer and a macro-porous supporting layer at the bottom. The TAMI UF membrane consisted of a double-coated active layer, while the TAMI MF represented a single active-separation layer.

SEM along with computerized image analysis (CIA) identified that average pore diameter of both AAO MF and UF membranes, determined to be smaller than nominal pore sizes that are provide by the manufacturer.

AFM image analyses revealed that the TAMI membrane surface is rough and deep, having a large roughness deviation, while the AAO membrane resulted in relatively smoother and smaller roughness deviation. These observations were the same for both MF and UF.

3.5. REFERENCES

Pontié, M., Thekkedath, A., Kecili, K., Habarou, H., Suty, H. and Croué, J.P. (2007) Membrane autopsy as a sustainable management of fouling phenomena occurring in MF, UF and NF processes. Desalination 204(1-3), 155-169.

Huang, H., Lee, N., Young, T., Gary, A., Lozier, J.C. and Jacangelo, J.G. (2007) Natural organic matter fouling of low-pressure, hollow-fiber membranes: Effects of NOM source and hydrodynamic conditions. Water Research 41(17), 3823-3832.

Lee, E.K., Chen, V. and Fane, A.G. (2008) Natural organic matter (NOM) fouling in low pressure membrane filtration -- effect of membranes and operation modes. Desalination 218(1-3), 257-270.

Lee, N., Amy, G., Croué, J.-P. and Buisson, H. (2004) Identification and understanding of fouling in low-pressure membrane (MF/UF) filtration by natural organic matter (NOM). Water Research 38(20), 4511-4523.

Amy, G. (2008) Fundamental understanding of organic matter fouling of membranes. Desalination 231(1-3), 44-51.

Volk, C., Bell, K., Ibrahim, E., Verges, D., Amy, G. and Lechevallier, M. (2000) Impact of enhanced and optimized coagulation on removal of organic matter and its biodegradable fraction in drinking water. Water Research 34(12), 3247-3257.

Dong, B.-z., Chen, Y., Gao, N.-y. and Fan, J.-c. (2007) Effect of coagulation pretreatment on the fouling of ultrafiltration membrane. Journal of Membrane Science 19, 278-283.

Matsushita, T., Matsui, Y., Shirasaki, N. and Kato, Y. (2005) Effect of membrane pore size, coagulation time, and coagulant dose on virus removal by a coagulation-ceramic microfiltration hybrid system. Desalination 178(1-3), 21-26.

Lee, N., Amy, G. and Lozier, J. (2005) Understanding natural organic matter fouling in low-pressure membrane filtration. Desalination 178(1-3), 85-93.

Seidel, A. and Elimelech, M. (2002) Coupling between chemical and physical interactions in natural organic matter (NOM) fouling of nanofiltration membranes: implications for fouling control. Journal of Membrane Science 203(1-2), 245-255.

Lee, S. and Cho, J. (2004) Comparison of ceramic and polymeric membranes for natural organic matter (NOM) removal. Desalination 160(3), 223-232.

Burggraaf, A.J. and Cot, L. (1996) Fundamentals of inorganic membrane science and technology, Elsevier.

Dafinov, A., Garcia-Valls, R. and Font, J. (2002) Modification of ceramic membranes by alcohol adsorption. Journal of Membrane Science 196(1), 69-77.

Larbot, A., Gazagnes, L., Krajewski, S., Bukowska, M. and Wojciech, K. (2004) Water desalination using ceramic membrane distillation. Desalination 168, 367-372.

Garmash, E.P., Kryuchkov, Y.N. and Pavlikov, V.N. (1995) Ceramic membrane for ultra- and microfiltration (Review). Glass and Ceramic 52(6), 150-152.

Baruah, G.L., Nayak, A. and Belfort, G. (2006a) Scale-up from laboratory microfiltration to a ceramic pilot plant: Design and performance. Journal of Membrane Science 274(1-2), 56-63.

Konieczny, K., Bodzek, M. and Rajca, M. (2006) A coagulation-MF system for water treatment using ceramic membranes. Desalination 198(1-3), 92-101.

Lerch, A., Panglisch, S., Buchta, P., Tomita, Y., Yonekawa, H., Hattori, K. and Gimbel, R. (2005) Direct river water treatment using coagulation/ceramic membrane microfiltration. Desalination 179(1-3), 41-50.

Thomas, M. and TorOve, L. (2010) Comparison of optional process configurations and operating conditions for ceramic membrane MF coupled with coagulation/floculation pre-treatment for the removal of NOM in drinking water production. Journal of Water Supply: Research and Technology-AQUA 59(2-3), 81-91.

Mori, Y., Oota, T., Hashino, M., Takamura, M. and Fujii, Y. (1998) Ozone-microfiltration system. Desalination 117(1-3), 211-218.

Lehman, S.G. and Liu, L. (2009) Application of ceramic membranes with pre-ozonation for treatment of secondary wastewater effluent. Water Research 43(7), 2020-2028.

Hong, S., Krishna, P., Hobbs, C., Kim, D. and Cho, J. (2005) Variations in backwash efficiency during colloidal filtration of hollow-fiber microfiltration membranes. Desalination 173(3), 257-268.

Boerlage, S.F.E., Kennedy, M., Tarawneh, Z., De Faber, R. and Schippers, J.C. (2004) Development of the MFI-UF in constant flux filtration. Desalination 161(2), 103-113.

Lee, S., Park, G., Amy, G., Hong, S.-K., Moon, S.-H., Lee, D.-H. and Cho, J. (2002) Determination of membrane pore size distribution using the fractional rejection of nonionic and charged macromolecules. Journal of Membrane Science 201(1–2), 191-201.

Zhao, C., Zhou, X. and Yue, Y. (2000) Determination of pore size and pore size distribution on the surface of hollow-fiber filtration membranes: a review of methods. Desalination 129(2), 107-123.

Hernández, A., Calvo, J.I., Prádanos, P. and Tejerina, F. (1998) Pore size distributions of track-etched membranes; comparison of surface and bulk porosities. Colloids and Surfaces A: Physicochemical and Engineering Aspects 138(2–3), 391-401.

Crispin, T. and Halász, I. (1982) Determination of the pore size distribution, by exclusion chromatography, of ion-exchange polymers which swell in water. Journal of Chromatography A 239(0), 351-362.

Guizard, C., Ayral, A. and Julbe, A. (2002) Potentiality of organic solvents filtration with ceramic membranes. A comparison with polymer membranes. Desalination 147(1–3), 275-280.

Baruah, G.L., Nayak, A. and Belfort, G. (2006b) Scale-up from laboratory microfiltration to a ceramic pilot plant: Design and performance. Journal of Membrane Science 274(1–2), 56-63.

Hong, S. and Elimelech, M. (1997) Chemical and physical aspects of natural organic matter (NOM) fouling of nanofiltration membranes. Journal of Membrane Science 132(2), 159-181.

Kosmulski, M. (2011) The pH-dependent surface charging and points of zero charge: V. Update. Journal of Colloid and Interface Science 353(1), 1-15.

Zhou, J., Zhang, X., Wang, Y., Hu, X., Larbot, A. and Persin, M. (2009) Electrokinetic characterization of the Al2O3 ceramic MF membrane by streaming potential measurements. Desalination 235(1–3), 102-109.

Moritz, T., Benfer, S., Arki, P. and Tomandl, G. (2001a) Investigation of ceramic membrane materials by streaming potential measurements. Colloids and Surfaces A: Physicochemical and Engineering Aspects 195(1–3), 25-33.

Moritz, T., Benfer, S., Árki, P. and Tomandl, G. (2001b) Influence of the surface charge on the permeate flux in the dead-end filtration with ceramic membranes. Separation and Purification Technology 25(1–3), 501-508.

Nazzal, F.F. and Wiesner, M.R. (1994) pH and ionic strength effects on the performance of ceramic membranes in water filtration. Journal of Membrane Science 93(1), 91-103.

Alldredge, A.L., Passow, U. and Logan, B.E. (1993) The abundance and significance of a class of large, transparent organic particles in the ocean. Deep Sea Research Part I: Oceanographic Research Papers 40(6), 1131-1140.

Hernández, A., Calvo, J.I., Prádanos, P., Palacio, L., Rodríguez, M.L. and de Saja, J.A. (1997) Surface structure of microporous membranes by computerized SEM image analysis applied to Anopore filters. Journal of Membrane Science 137(1–2), 89-97.

Boussu, K., Van der Bruggen, B., Volodin, A., Snauwaert, J., Van Haesendonck, C. and Vandecasteele, C. (2005) Roughness and hydrophobicity studies of nanofiltration membranes using different modes of AFM. Journal of Colloid and Interface Science 286(2), 632-638.

Chapter 4

Precoagulation Effects on Ceramic Membrane Filtration

Phase 2-1: Optimization of coagulation prior to ceramic membrane filtration to enhance NOM removal and maintain sustainable flux for treatment of high-organic surface water

Optimization of coagulation prior to ceramic membrane filtration to enhance NOM removal and maintain sustainable flux for treatment of high-organic surface water[3]

ABSTRACT

Precoagulation effects on membrane fouling and NOM removal with a TAMI membrane (made of TiO_2+ZrO_2) for filtration of high-organic surface water were investigated. Different pH conditions, coagulant dosages as Fe^{3+}, and mixing conditions (i.e., velocity gradient (G) and time (T)) were considered. The modified fouling index (MFI) was computed to predict membrane fouling. The point of zero surface charge (PZC) of the TAMI MF was found to be near pH 4. Coagulation can play an important role in reducing the MF membrane fouling and improving NOM removal. The most critical factors were found to be pH and coagulant dose, with the highest efficiency resulting under a low pH of 5.5 and a high dose of 10 mg/L as Fe^{3+}, designated as enhanced coagulation conditions. Under a $G_{800}T_{10}$ (i.e., high mixing intensity and short mixing time) and a pH 5.5, the MFI increased with an increase in dose, implying more fouling by increased dosage. However, as coagulant dose increased up to a certain level of 5.0 mg/L, the MFI rapidly started to decrease back to a considerably lower value. UVA_{254} removal was higher than DOC, implying preferential removal of humics over non-humics by coagulation. It is expected that the

[3] This chapter was submitted to Journal of membrane science

TAMI ceramic membrane with precoagulation can be effectively employed to treat impaired-quality source waters in water reuse applications.

Keywords

Ceramic membrane; precoagulation; modified fouling index (MFI); NOM; zeta potential

4.1. INTRODUCTION

Application of microfiltration (MF) and ultrafiltration (UF) has been developed into a widely established technology with a steady worldwide increase in installed production capacity over the past couple of decades. The use of MF/UF has been almost exclusively focused on membranes made of various polymeric materials because of recent advances and cost declines in polymer technologies, leading to significant increases in the application of membrane processes. However, one of the main obstacles to further application of membrane technology is the permeate flux decline occurring during a long-term operation, i.e. membrane fouling, which is a main factor increasing the costs of operation and maintenance by deteriorating sustainable membrane performance and shortening their lifetime (Amy 2008, Huang et al. 2007, Lee et al. 2004, Lehman and Liu 2009, Pontié et al. 2007). In particular, it has been shown that a major constraint is organic fouling associated with bulk natural organic matter (NOM), further influenced by interactions between NOM and particles, causing irreversible fouling (Amy 2008, Huang et al. 2007, Lee et al. 2008, Lee et al. 2004, Zularisam et al. 2011). Research has shown that NOM is able to bridge inorganic particles, increasing the stability of the fouling layer against physical cleaning and decreasing a membrane porosity (Jermann et al. 2008). Several studies have indicated that NOM, particularly the hydrophobic fraction of NOM and high molecular mass (HMM) compounds, have a great impact on membrane fouling and flux decline (Dong et al. 2007b, Jung et al. 2006, Perdue 2009, Zularisam et al. 2007).

One of the techniques that can effectively reduce organic fouling includes coagulation pretreatment with MF or UF. The coagulation process is generally perceived as the

most successful treatment to control membrane fouling for surface waters with high-NOM contents, resulting in high removal efficiency of the NOM. With coagulation pretreatment the fraction of small particles that causes pore blockage is decreased while coagulated aggregates larger than the pores are increased and dominate fouling mechanism (i.e., cake filtration). It has been frequently reported that MF/UF membranes could remove some organic matter with improved membrane performance and reduced fouling when coupled with precoagulation (Choi and Dempsey 2004, Dong et al. 2007a, Hatt et al. 2011, Matsushita et al. 2005, Volk et al. 2000). Dong et al. found that with the coagulated flocs formed on the membrane surface, the flux decline could be improved as a consequence of adsorbing neutral hydrophilic compounds effectively (Dong et al. 2007a) which are difficult to be removed by MF or UF alone. However, the optimization of coagulation conditions is necessary otherwise it may cause exacerbated fouling (Hofs et al. 2012, Huang et al. 2009, Wang et al. 2010). Furthermore, some limitations, such as the lack of durability against extreme pH and temperature, and relatively premature degradation by biological and chemical agents have been considered as major deficiencies of polymeric membranes (Lee et al. 2005b, Seidel and Elimelech 2002).

Ceramic membranes, one of the alternatives to overcome these problems, have recently been introduced into the water-sector marketplace. Ceramic membranes have many attractive attributes in terms of their inherent mechanical, thermal and chemical stability, allowing them to be designed and operated at higher permeability, less frequent cleaning, and a longer lifetime than those of the more conventional polymeric ones (Lee and Cho 2004). Ceramic membranes are made of metal oxides, such as Al_2O_3, ZrO_2, TiO_2 and various combinations, and generally asymmetric

structures, consisting of a supporting layer with large pores (low flow resistance) of sufficient mechanical strength on top of which are layers with gradually decreasing pore size (Burggraaf and Cot 1996). This can be an advantage for obtaining relatively higher fluxes from thin separation layers. The principal chemical properties of ceramic membranes are their hydrophilicity (Dafinov et al. 2002, Larbot et al. 2004) and amphoteric surface charge due to the presence of hydroxyl (OH^-) groups on their surface. These characteristics contribute to high permeability, and influence separation ability and fouling potential as well (Dafinov et al. 2002). Differences in fouling behaviour of polymeric and ceramic membrane can be expected, as the surface groups of them are different. Some researchers have found that reversible fouling decreases in order of polymeric $\approx Al_2O_3 \approx ZrO_2 > TiO_2 > SiC$, and for irreversible fouling of polymeric $> ZrO_2 > Al_2O_3 > TiO_2 > SiC$ (Hofs et al. 2011).

It is highly expected that in the context that the increase of natural organic matter (NOM) in natural surface water sources is becoming a growing concern for drinking water treatment, these features of ceramic membranes can help to more effectively achieve enhanced filtration performance for treating impaired-quality source waters (e.g., high-organic natural surface water, wastewater effluent and seawater). A ceramic membrane can provide excellent backwash efficiency and mitigate NOM fouling with incorporation of various chemical treatments such as coagulation under various conditions and/or ozone (O_3) treatment (Konieczny et al. 2006, Lehman and Liu 2009, Meyn and Leiknes 2010).

Coagulation/flocculation pretreatment with ceramic MF membrane filtration has been especially emphasized as an effective alternative in terms of less energy consumption

and long term operation, resulting in efficient removal of NOM. Recent pilot scale studies have suggested that the coagulation process with monolithic ceramic MF membranes (made of Al_2O_3) at a constant flux in dead-end mode can be optimized to such an extent that their employment was competitive with polymeric hollow fibre membranes (Konieczny et al. 2006, Lerch et al. 2005). In addition, a research have shown that in terms of irreversible fouling development, coagulation pretreatment was effective for Al_2O_3 based MF membrane fouling control in the advanced treatment of secondary effluents (Xu et al. 2010).

This research focused on the identification of the effects of coagulation prior to ceramic MF membrane filtration for treating impaired quality surface water with an elevated level of organic matter. Instead of Al_2O_3 based membrane widely used for drinking water treatment, TiO_2+ZrO_2 based commercial TAMI membrane was employed for the research. To understand fundamental properties of the TAMI ceramic membrane, synthetic layer composition, zeta potential (ζ), and pure water permeability (PWP) were closely evaluated. The flux decline curve and modified fouling index (MFI) was computed in order to predict membrane fouling under different coagulation conditions with simple recording of time-dependent flux. DOC and UVA_{254} were analysed to characterize NOM removal in terms of humics and non-humics. The specific objectives of this study were to identify the optimal coagulation conditions (i.e., pH, coagulant dosage, and mixing intensity and duration) in combination with the ceramic MF membrane filtration to improve NOM removal efficiency, to create flocs with minimum resistance, and to reduce membrane fouling.

4.2. MATERIALS AND METHODS

4.2.1. Source water

The feed (surface) water used for this study was taken from the Westvest canal in Delft, the Netherlands, reflecting a high concentration of DOC originating from terrestrial and agricultural sources. Throughout the experimental period, the pH ranged from 7.55 to 7.96. The temperature used for the experiments was adjusted to room temperature, between 19.5°C and 22.5°C, which was established after water was removed from cold storage for a half-day before starting a test. Turbidity was between 35 NTU and 4.5 NTU, while the DOC ranged from 11.86 mg/L to 13.93 mg/L and UVA_{254} from 41.8 m^{-1} to 59.6 m^{-1}, corresponding to SUVA values between 3.5 L/mg·m an 4.3 L/mg·m. During the winter season, turbidity was relatively higher, but DOC and UVA_{254} were lower than other seasons, resulting from run-off from agricultural areas. Conversely, from April, DOC and UVA_{254} started increasing while turbidity decreased. The alkalinity ranged from approximately 220 mg/L to 250 mg/L as $CaCO_3$. The raw water sample was prefiltered with a 38μm sieve to screen coarse particles instead of removing all particulates bigger than 0.45μm.

4.2.2. Ceramic membrane specification

A ceramic disc membrane (INSIDE DISRAM^{TM}) fabricated by TAMI INDUSTRIES was used for this study. The TAMI ceramic membrane is asymmetric, consisting of an active surface layer of titanium dioxide/zirconium dioxide (TiO_2+ZrO_2) and a support layer of TiO_2, and available in two types of diameters: 47 mm and 90 mm with a

thickness of 2.2 mm. A membrane disc, which is 47mm in diameter with an effective area of 0.00131 m^2, was adopted for this study. Ceramic membranes included a MF-0.14μm and a tight UF-50kDa of nominal pore size and molecular weight cut off (MWCO); these were tested with a special holder, where feed water was filtered through each membrane disc placed inside the holder in a dead-end filtration mode. The MF membrane was used for precoagulation tests, and the UF membrane was compared with the MF membrane for comparison of morphology, resistance, and prefiltration effects with a 38 μm coarse sieve.

4.2.3. Experimental configuration

A schematic of the ceramic membrane filtration test unit is shown in Figure 4.1. Raw water, which was prefiltered with a 38μm of coarse sieve, and coagulated waters which were filtered through different ceramic membranes, were characterized in terms of permeability and filterability by a modified fouling index (MFI). Flux decline (under constant pressure mode), dissolved organic carbon (DOC), and ultraviolet absorbance (UVA_{254}) were monitored. A jar test unit was used for coagulation tests. This unit consists of 6 round jars of 1.8L with 4 baffles and a flat-bladed stainless steel mixer, where mixing intensity can be adjusted with rotational speed set as rpm. In order to simulate in-line coagulation, mixing intensities higher than conventional design values for mechanical flash mixing were adopted as follow: $400s^{-1}$ and 800 s^{-1} for the velocity gradient (G) and 10 s and 30 s of mixing time (t), where no additional flocculation was applied. Different types of in-line mixers can be installed prior to a membrane for precoagulation, including a static mixer or a simple pipe, providing mixing intensity and flash dispersion in a short time. Ferric chloride

($FeCl_3 \cdot 6H_2O$) was used as a coagulant and various coagulation conditions such as pH, mixing (G and t), and coagulant dosage were considered to identify optimal operational conditions prior to ceramic membrane filtration, as shown in Table 4.1.

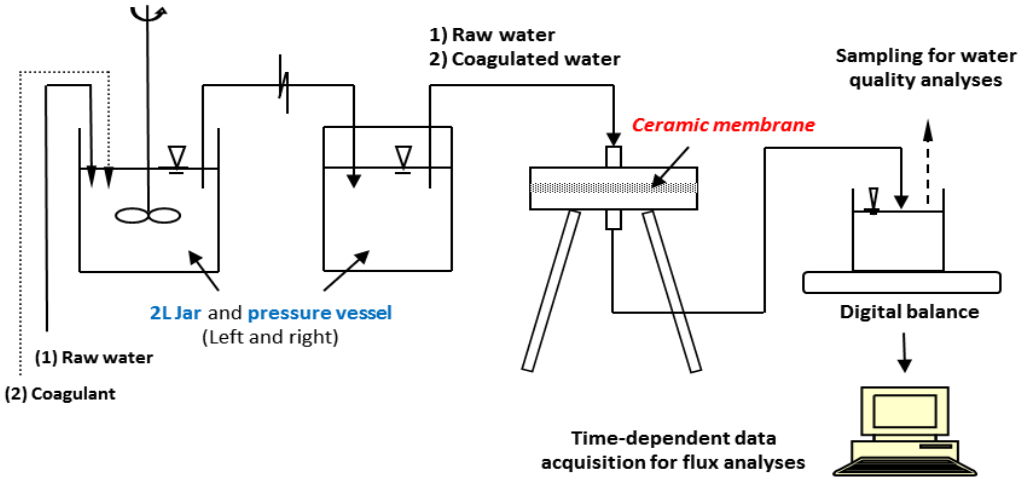

Figure 4.1 - Schematic of TAMI ceramic membrane filtration test unit

Table 4.1 - Parameters/conditions for coagulation prior to ceramic membrane filtration: ferric chloride ($FeCl_3 \cdot 6H_2O$) was used as a coagulant.

Mixing intensity (G; s^{-1})	Mixing time (sec)	pH	Dose (mg/L as a Fe^{3+})
400, 800	10, 30	5.5, 6, 7, 7.5, 8	0, 2, 3.5, 5, 10

4.2.4. Zeta potential (ζ) measurements

The ζ potential value of the TAMI ceramic membrane was determined from electrophoretic mobility measurements using a commercially available electrophoresis measurement apparatus (ELS-Z, Photal, Electronics, Japan) with a plate sample cell. Polystyrene latex particles (diameter 520 nm, Otsuka Electronics, Japan) coated with hydroxyl propyl cellulose (HPC) and with a molecular weight of

300,000 (Scientific Polymer Products, Japan) were used as mobility-monitoring particles. These were dispersed in a 0.01MKCl solution to prevent interactions with (or adsorption on) the quartz cell surface during measurement.

4.2.5. Computation of membrane flux and resistance (R_m)

Permeate flux (J; L/m^2h) was calculated as the flow rate of permeate water (Q; L/h) divided by the effective surface area of the membrane (A; m^2). Specific flux (J_s; $L/m^2h \cdot bar$), or permeability corresponds to flux normalized to trans-membrane pressure (TMP). Membrane resistance (R_m) was calculated based on Darcy's law and the resistances-in-series model. Assuming that no resistance except for membrane resistance (R_m) occurs when pure water is filtered, R_m is equivalent to total resistance R_t. Therefore, R_m was calculated as TMP divided by the permeate flux (J) and the dynamic viscosity of water (η; Ns/m^2).

4.2.6. Modified fouling index (MFI-MF)

Currently, the existing MFI to predict membrane fouling is based on the occurrence of cake filtration during a distinct part of the test, and on the assumption that cake filtration is the most likely dominant fouling mechanism during filtration for an RO system. It is determined under constant pressure filtration from the slope of the general cake filtration equation in a plot of t/V versus V (Boerlage et al. 2004, Boerlage et al. 1998), when fixed reference values are used at a pressure of 2 bars, a 20°C of temperature, and 13.8×10^{-4} m^2 of membrane surface area with 0.45μm pore size.

$$\frac{t}{V} = \frac{\eta R_m}{\Delta P A} + \frac{\eta \alpha C_b}{2\Delta P A^2} V;\ MFI(\mathrm{s}/L^2) = \frac{\eta \alpha C_b}{2\Delta P A^2} \quad (1)$$

Where V is the filtered volume (m^3), t filtration time (s), ΔP the applied trans-membrane pressure (bar, or Ns/m^2), η the water viscosity (Ns/m^2), R_m the membrane resistance (m^{-1}), A the membrane surface area (m^2), α the specific resistance of the cake per unit weight (m), and C_b the concentration of particles per unit filtrate volume (kg/ m^3).

In this study, MFI was used to identify the effect of precoagulation with MF ceramic membrane filtration under certain operational conditions. Assuming that colloidal or dissolved contaminants including particulates in feed water would be aggregated with a metal coagulant such as Fe^{3+}, MFI can help to predict the efficiency of treatment performance based on dominant cake filtration by coagulation. However, because applied pressure for this study is even lower (e.g., 0.1 bar) than that for the original MFI for a RO system, cake filtration might not occur from the very first stage from when operation starts. Besides, according to previous research, the MFI is also dependant on particle size, thus smaller particles generally result in higher MFI values (Boerlage et al. 2003). For this reason, pore blockage, especially complete blocking of the pore surface, should be considered before occurrence of cake formation on the MF membrane surface. That was why the MFI was computed by equation (2) instead of equation (1), not to exclude pore blockage stage and to minimize experimental errors that might occur at the very first stage of filtration during data acquisition with a digital balance. However, it should be noted that the two equations, (1) and (2), are different from each other, where a constant of 2 in the denominator of equation (1) is removed.

$$\frac{dt}{dV} = \frac{\eta R_m}{\Delta P A} + \frac{\eta \alpha C_b}{\Delta P A^2} V;\ MFI(\mathrm{s}/L^2) = \frac{\eta \alpha C_b}{\Delta P A^2} \quad (2)$$

A MF ceramic membrane (0.14µm) used for this study was directly applied to obtain MFI values. Permeated volume was recorded at 10-second intervals under a certain pressure depending on membrane used over a 30 minutes filtration period. The MFI value was then computed by linear regression from the slope of the linear region of a plot of dt/dV as a function of V. The obtained MFI value was corrected into a normalized MFI by applying a correction factor of standard reference conditions, i.e., a pressure of 2 bars (ΔP_0), a temperature of 20°C ($\eta_{20°C}$), and a membrane surface area of 0.001384 m^2 (A_0) which is termed MFI-$MF_{corrected}$ in equation (3).

$$\text{MFI-MF}_{\text{corrected}} = \frac{\eta_{20°C}}{\eta} \left(\frac{\Delta P}{\Delta P_0}\right) \left(\frac{A}{A_0}\right)^2 \times MFI_{measured} \quad (3)$$

4.2.7. Natural organic matter (NOM) analysis

Dissolved organic carbon (DOC) was measured by a carbon analyser (TOC-V, Shimadzu, Japan). The non-purgeable organic carbon (NPOC) method was employed. All samples were prefiltered through a pre-washed 0.45µm cellulose acetate filter prior to measurement and then acidified with the addition of 2 N HCL to remove inorganic carbon by purging with hydrocarbon free nitrogen gas prior to measuring DOC. UVA absorbance measurement at 254 nm (UVA_{254}), representing the aromatic character of NOM, was measured by a UV-visible spectrophotometer (Shimadzu UV 2501 PC, Japan).

4.3. RESULTS AND DISCUSSION

4.3.1. Pure water permeability (PWP) and membrane resistance (R_m)

Two types of TAMI ceramic disc membranes, i.e., MF (0.14 µm) and UF (50KD), were characterized according to properties such as pure water permeability (PWP) and membrane resistance (R_m). Milli-Q water (≈18 Ω) was applied to the MF membrane. For the UF membrane, ultra-pure water (UPW) that was additionally purified with a granular activated carbon cartridge followed by an RO membrane was employed in order to eliminate the possibility of resistance to the tight UF membrane caused by particles still remaining in the Milli-Q water. New virgin discs were cleaned through backwashing at 2.5 bars for 30 seconds to remove any residual contaminants from the manufacturing process. Thereafter, the discs were conditioned in Milli-Q water to avoid potential air-entrapment in membrane pores. Three disc measurements of each MF and UF were conducted to determine PWPs, allowing computation of their membrane resistances (R_m), corrected to a standard temperature of 20°C.

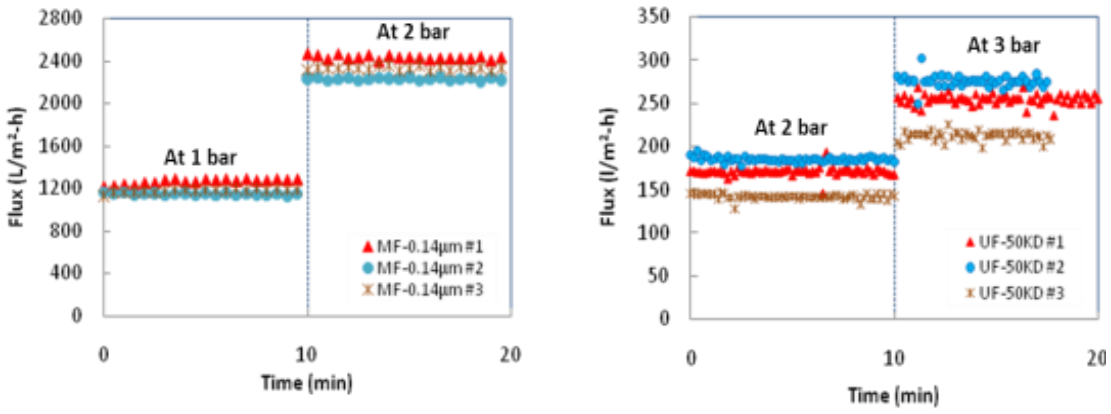

Figure 4.2 - PWP comparison of TAMI MF and UF membranes at different pressures (on the left presents MF; on the right presents UF)

Figure 4.2 presents PWPs of TAMI MF and UF membranes at different TMPs from 1 to 2 bars and from 2 to 3 bars, respectively. The membrane fluxes of both were stable throughout the filtration. When the TMP of the MF membrane increased from 1 to 2 bars, the flux was exactly doubled while a 50 % of increase in flux was observed as TMP of the UF increased from 2 to 3 bars, corresponding to stable specific flux. However, each disc used for the test resulted in a somewhat different PWP, or Rm, under the same conditions as shown in Table 4.2. The difference of MF membranes was ±4.6%, considered as an acceptable error, but UF membrane differences were ±13.8%, representing a larger difference. It is presumed that these differences might be explained. First, membrane discs might be manufactured in different batches. Secondly, if they were made in the same batch, their properties such as porosity and thickness of the top-separation layer were inhomogeneous, which could cause more influence on UF permeability, with UF having relatively smaller pore size or lower molecular weight cut-off than MF.

Table 4.2 - Summary of pure water permeability (PWP) and membrane resistance (R_m) of TAMI MF/UF new membrane discs

Membrane type		PWP	Rm at 20°C [m^{-1}]				
		($L/m^2h \cdot bar$)	Min.	Max.	Ave.	Total Ave.	Deviation
MF	Disc #1	1241±31	1.48E+11	1.59E+11	1.54E+11	1.62E+11	±4.6%
	Disc #2	1105±17	1.65E+11	1.73E+11	1.69E+11		
	Disc #3	1174±17	1.54E+11	1.69E+11	1.62E+11		
UF	Disc #1	170±4	1.98E+12	2.63E+12	2.24E+12	2.34E+11	±13.8%
	Disc #2	184±4	1.90E+12	2.29E+12	2.07E+12		
	Disc #3	141±4	2.48E+12	3.01E+12	2.70E+12		

4.3.2. SEM images of TAMI ceramic membranes

Scanning electronic microscope (SEM) images demonstrated that TAMI ceramic disc membranes were asymmetric as shown in Figure 4.3 and Figure 4.4. TAMI membranes were largely composed of three layers that were the smallest porous active layer at the top supported by an intermediate layer and a macro-porous support at the bottom. However, the UF membrane consisted of a double-coated active layer (Figure 4.4) while the MF represented a single active-separation layer (Figure 4.3). Ceramic membranes are generally fabricated by sintering and a sol-gel process, which can allow them to form thin porous films on top in a simple way that is “dip-coating”, or “withdrawal coating”. SEM images revealed that each layer was not uniform in terms of their thickness, pore shape, and grafting. Because of these inhomogeneous properties that might have resulted from the manufacturing process, differences in membrane resistance (R_m), or pure water permeability, could be observed even though they were fabricated from the same batch. These differences were more distinct for UF, which might be because the double-coated active layers could cause more resistance difference if they are not uniform.

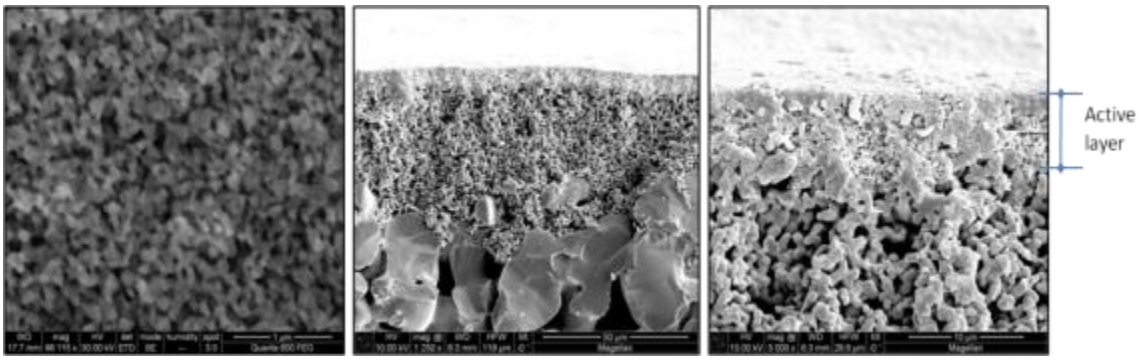

Figure 4.3 - SEM images of a TAMI MF ceramic membrane disc, revealing three different layers which are active top layer, intermediate layer, and support layer (Left: top view; middle: cross section; right: cross section in higher magnification)

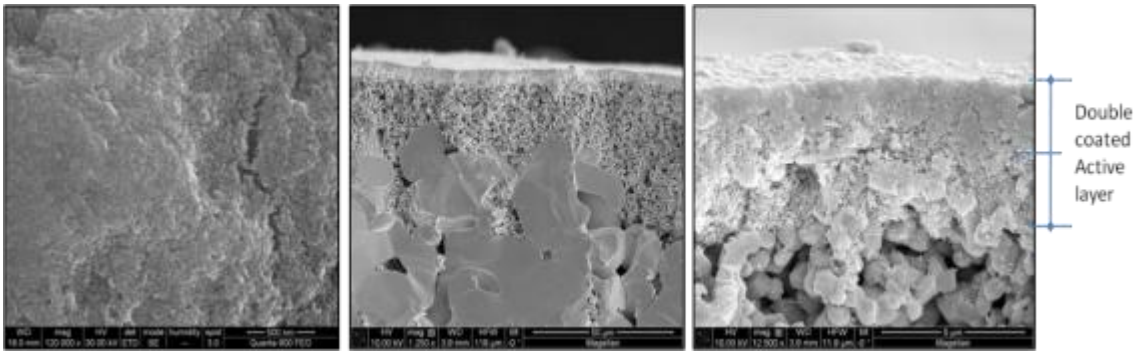

Figure 4.4 - SEM images of a TAMI UF (150KD) ceramic membrane disc, describing double active top layers (Left: top view; middle: cross section; right: cross section in higher magnification)

Ceramic membranes have been shown to exhibit a narrower pore size distribution than those of polymeric ones (Meyn and Leiknes 2010), which results in higher permeability. Nevertheless, homogeneous thickness of the active layer should be effectively controlled in an appropriate way through the manufacturing process to maximize their inherent attributes.

4.3.3. Zeta potential (ζ) measurement

One of the distinctive features of ceramic membranes is an amphoteric oxide surface. The surface charge and sign of the metal oxides vary as a function of pH (Matilainen et al. 2010, Moritz et al. 2001a, Moritz et al. 2001b). For example, Al_2O_3 is reported to have a point of zero charge (PZC) near pH 9 (Nazzal and Wiesner 1994). Hence, alumina membranes are expected to have a net positive charge below or near this pH in the absence of specially adsorbed ions. This feature of the Al_2O_3 membrane at an ambient pH of surface waters with a relatively high NOM content may be decreased in terms of NOM fouling. One of the reasons why coagulation and/or ozone have been generally combined with the alumina membrane filtration for surface water

treatment may be to reduce membrane fouling and the loss of permeability caused by NOM adsorption to the surface (Konieczny et al. 2006, Lehman and Liu 2009, Lerch et al. 2005, Meyn et al. 2008, Meyn and Leiknes 2010).

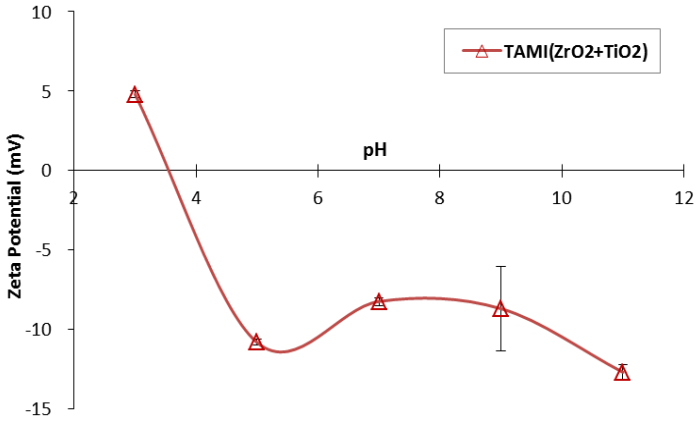

Figure 4.5 – pH dependence of zeta potential in a 0.01MKCl solution; PZC of TAMI ceramic membrane is observed near pH 4

Zeta potential (ζ) of TAMI membrane (made of TiO_2+ZrO_2) used for the study was measured in a 0.01MKCl solution. The TAMI membrane showed pH-dependent surface charge, resulting in having a positive charge below near pH 4 and being negatively charged at higher pH values (i.e., $TAMI_{PZC}$ is near pH 4) as shown in Figure 4.5. Based on the result, the TAMI membrane is expected to relatively reduce NOM binding to the surface, causing an increase in permeability when compared to the alumina-based membrane.

4.3.4. Computation of MFI-MF with dt/dV versus dV curve

Assessment of membrane fouling was carried out using MFI computations as shown in Figure 4.6 and Figure 4.7, which are examples of estimating the MFI. Figure 4.6 represents t/V versus V curves in accordance with different coagulant dosages at pH

5.5. A curve of t/V versus V can help to understand the possibility of combining different fouling mechanisms during the entire filtration period. The curve can be separated in two regions. The very left region depicting a convex trend for a short time corresponds to pore-blockage that generally causes irreversible fouling. The second region represents a cake formation mechanism causing reversible fouling, described by a straight line for a longer time.

The MFI is calculated from the slope of the linear regression curve from the second region instead of the first region, which is illustrated in Figure 4.6. In contrast, Figure 4.7 represents dt/dV versus V curves that describe relatively consistent straight lines from the very first stage unlike Figure 4.6. Even though pore blockage occurs at an early filtration stage, the differential t/V is smoothened as time passes into the next cake filtration region when the curve of dt/dV versus V is plotted. The slope of each linear regression of the dt/dV over V curves was adopted for the MFI computations. A steeper slope means a higher MFI, in other words, more fouling and higher cake resistance that is mostly related to porosity, density and inter-particle cohesive forces of the cake formed on membrane surface.

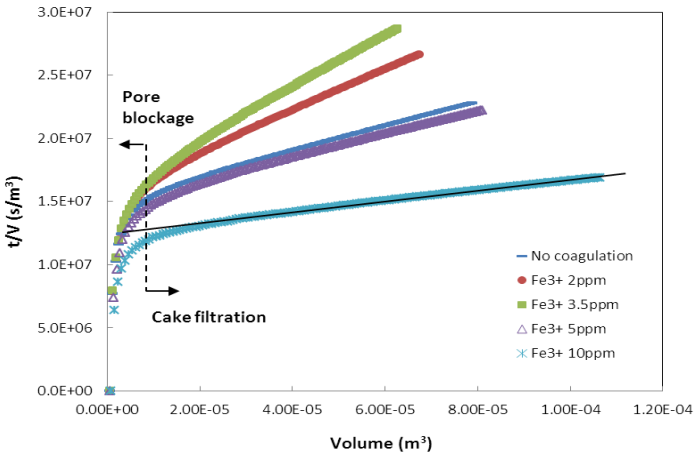

Figure 4.6 - t/V versus V curves according to different coagulant dose at a pH 5.5

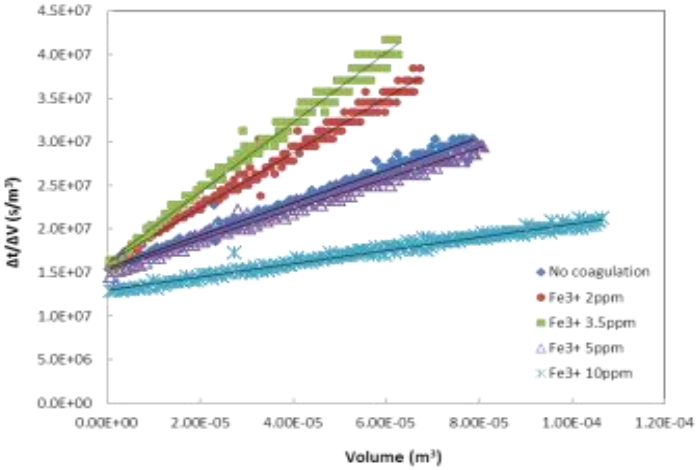

Figure 4.7 - dt/dV versus V curves according to different coagulant dose for MFI-MF calculations that are derived from t/V versus V curves

4.3.5. Membrane fouling reduction with precoagulation

The effect of precoagulation on membrane fouling was investigated. The main focus of this study was to identify the optimal coagulation conditions to enhance filterability and reduce membrane fouling with minimum resistance. Various conditions such as pH, mixing conditions (i.e., velocity gradient (G) and time (T)), and coagulant dosage were considered. TAMI ceramic MF membranes (i.e., a nominal pore size of 0.14μm) were tested. Overall, the ceramic MF membrane exhibited reduced MFI (i.e., membrane fouling) when used with precoagulation. Figure 4.8 and Figure 4.9 show the MFI variation according to pH, G×T, and coagulant dose. Under mixing conditions of G×T of 400 s^{-1} × 30 sec (designated as $G_{400}T_{30}$) and $G_{800}T_{30}$, the MFI variation was not sensitive to pH and dose except for at a pH 5.5 (Figure 4.8) while being very sensitive to pH and dose under mixing condition of $G_{800}T_{10}$ as shown in Figure 4.9. It was observed that at an ambient pH of 7.55 under all mixing conditions, a small amount of dose (i.e., 2 ppm) causes a significantly decreased MFI value. The lowest MFI value was observed at a pH 5.5 with high dose of 10 ppm as Fe^{3+}.

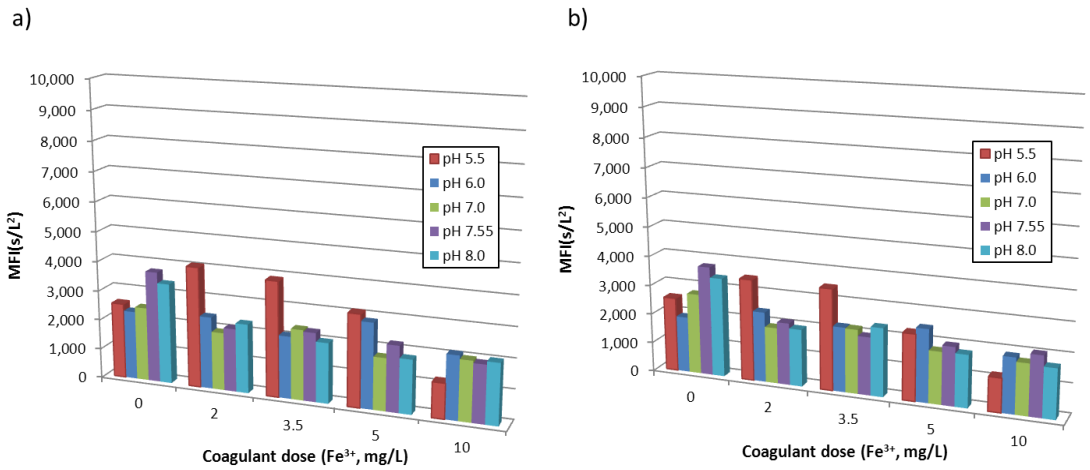

Figure 4.8 - MFI variation as a function of coagulant dose as Fe^{3+} under mixing condition of velocity gradient (G) of 400 and 800 s^{-1} and mixing time (T) of 30 s: (a) and b) results $G_{400}T_{30}$ and $G_{800}T_{30}$, respectively)

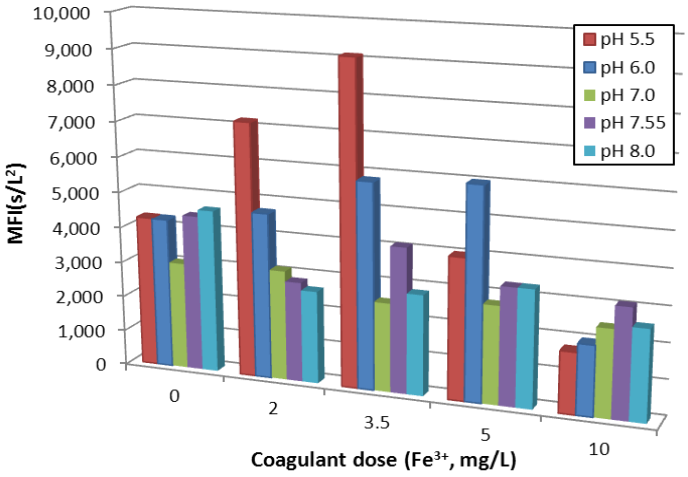

Figure 4.9 - MFI variation as a function of coagulant dose as Fe^{3+} under mixing condition of velocity gradient (G) of 800s^{-1} and mixing time (T) of 10 s

4.3.5.1. The effect of coagulant dosage under mixing condition of $G_{800}T_{10}$

It was clearly observed that mixing condition (G×T) and coagulant dose (as Fe^{3+}) had a significant influence on MFI variation at lower pH range while there was slight variation at higher pH range under the mixing condition of $G_{800}T_{10}$, i.e.(i.e., implying insufficient mixing time) as shown in Figure 4.9. The MFI variation according to

coagulant dosages of 0, 2, 3.5, 5, and 10 mg/L is discussed under mixing condition of $G_{800}T_{10}$. Overall, the MFI tended to decrease according to coagulant dose. It was observed that the MFI increased with an increase in coagulant dose at lower pH conditions of 5.5 and 6, implying more fouling by increased dosage. However, as coagulant dose was increased up to a certain level of 3.5 mg/L (pH 5.5) and 5 mg/L (pH 6) or greater, the MFI rapidly started to decrease back to a considerably lower value. This was more clear at pH 5.5 which is the lowest pH condition applied for this study.

The results can be explained according to two hypotheses. First, coagulant dose less than 3.5mg/L might be too low to neutralize the negatively charged NOM molecules and imparts more resistance onto the membrane surface at a lower pH condition. Secondly, although charge neutralization occurred, relatively small, dense pin-flocs might be formed with insufficient flocculation time. In either case, insufficient coagulant dosage could give rise to increased membrane pore blockage resulting in more severe membrane fouling. Under these conditions, the cake formed on the membrane surface was denser with smaller voids in between particles. Nevertheless, with a certain dose of 5 mg/L or more, there would be more chance for coagulant to induce particles to contact each other and entrap them by bridging and enmeshment. For this reason, larger and more porous flocs can accumulate on the membrane surface, providing less resistance or a lower MFI value. It has also been reported that flocs aggregated by coagulant addition at lower pH ranges are possibly smaller, denser and less porous than those formed at higher pH conditions (Guigui et al. 2002).

On the other hand, it was observed that MFI values slightly decreased with an addition of coagulant at a higher pH condition as shown in Figure 4.9. Even at a high dosage such as 10 mg/L Fe3+, coagulation prior to MF membrane filtration did not play a significant role in reducing membrane fouling. It was assumed that more coagulant dose, flocculation time, or both were required for enough aggregation to improve membrane flux.

4.3.5.2. The effect of mixing intensity and time (G; T)

In order to identify the effect of mixing intensity and time (G; T) on membrane fouling, three different mixing conditions, $G_{800}T_{10}$, $G_{400}T_{30}$, and $G_{800}T_{30}$ were evaluated. It was observed that, at a lower pH range, for mixing conditions adequate to contact NOM with coagulant (i.e., G_{400} and G_{800}), the longer the mixing time the lower the MFI value, corresponding to lower flux decline over time as shown in Figure 4.10. At a mixing time of 10s, such as $G_{800}T_{10}$, MFI was significantly reduced with increasing coagulant dosage, meaning that if mixing time is insufficient for enough flocculation, a high dose of coagulant was needed to decrease membrane fouling.

However, if mixing time is adequate to create pin-flocs (e.g., 30 seconds), membrane fouling could be sharply reduced even at a low dosage of 2 mg/L from about 7,000 s/L^2 to 4,000 s/L^2. In other words, with a low dosage of coagulant (e.g., 2 mg/L), mixing time was a very important factor to improve membrane flux. It is assumed that compared to $G_{400}T_{30}$ and $G_{800}T_{30}$, $G_{800}T_{10}$ was insufficient to create good-quality flocs to reduce the membrane resistance, so that relatively small flocs, or pin-flocs, resulted in more membrane resistance, corresponding to heavier blockage and denser cake

formation at lower pH conditions. Nevertheless, this phenomenon may be diminished with an increasingly higher dosage of coagulant regardless of both G and T.

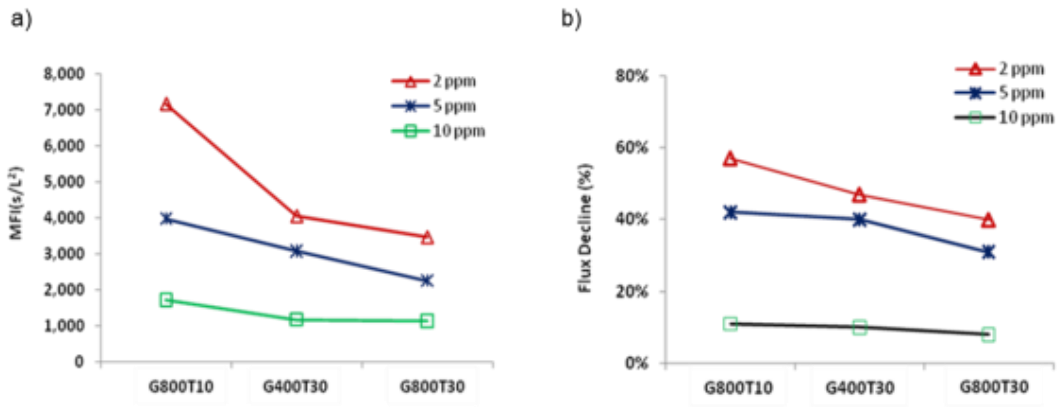

Figure 4.10 - MFI variation (a) and flux decline (b) as a function of different mixing conditions (GT) according to coagulant dose as Fe^{3+} at a pH 5.5

4.3.5.3. The effect of pH conditions under mixing condition of $G_{800}T_{10}$

The pH condition applied for precoagulation with ceramic MF was the most critical factor in terms of membrane fouling or MFI. In application of ferric chloride, a sharp distinction was observed according to the applied pH range as previously mentioned (Figure 4.9). At a lower pH range, mixing conditions and coagulant dose had a significant influence on membrane fouling. That could be because of the dominant coagulation mechanism at a lower pH range (i.e., charge neutralization), suggesting that the optimal operational conditions (i.e., coagulant dose and mixing conditions) should be determined to improve membrane flux.

At a higher pH range, there was little dependence on dose and mixing, but with increased coagulant up to a relatively high dose, membrane fouling was slightly reduced. This was observed at a dosage of 10 mg/L. It can be assumed that if the dosage is higher than 10 mg/L, the MFI would be decreasing. The effect of

coagulation is mostly governed by sweep coagulation or enmeshment instead of charge neutralization at a higher pH range. A hydroxide-precipitate caused by relative over-dosing of coagulant would enmesh NOM and other particles as well, forming larger flocs, but are of little consequence at lower dosage. In spite of this, the enmeshed aggregate by coagulation might not be compact, but porous enough for feed water to penetrate, resulting in an improvement of membrane flux.

The MFI values of precoagulated MF filtration with 2 mg/L and 10 mg/L of coagulant dose were compared at different pH levels as shown in Figure 4.11. It can be clearly observed that the MFI considerably increased with a decrease in pH from 8 to 5.5 at 2 mg/L of dose, meaning that more membrane resistance occurred with a lower pH. However, the MFI gradually decreased at 10 mg/L of dose under the same conditions, implying less fouling at lower pH with an appropriate dosage.

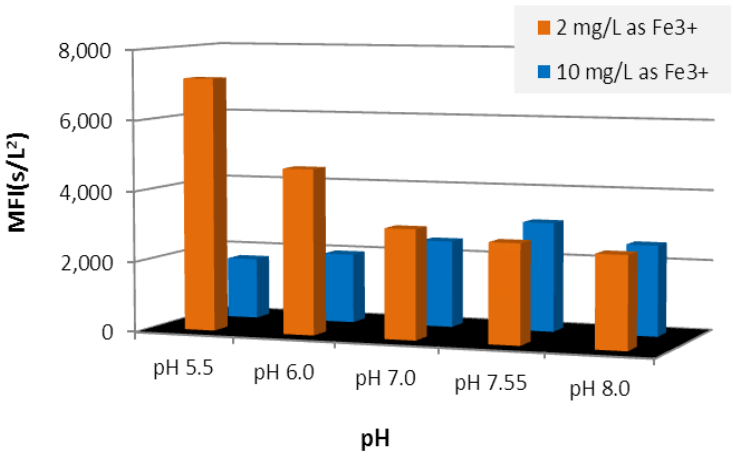

Figure 4.11 - MFI vs. pH in accordance with 2 mg/L and 10 mg/L of coagulant dosage as Fe^{3+} under mixing conditions of $G_{800}T_{10}$

4.3.6. NOM removal improvement with precoagulation

Figure 4.12, Figure 4.13 and Figure 4.14 present the removal of DOC and UVA_{254} as function of pH and coagulant dosage under various mixing conditions of a $G_{400}T_{30}$, $G_{800}T_{300}$ and $G_{800}T_{10}$, respectively. It was observed that the NOM removal efficiency and trend in accordance with coagulant dose and pH was the almost same under all mixing conditions unlike the MFI results as shown in Figure 4.8 and Figure 4.9. At lower pH conditions of 5.5 and 6, coagulation pretreatment significantly enhanced ceramic MF performance in terms of DOC and UVA_{254} removals. The maximum removal was observed at pH 5.5. With 10 mg/L dose as Fe^{3+}, DOC was removed approximately three times as high as that at higher pH conditions of 7, 7.55, and 8 with removals between 41 % and 61 % at the lower pH range, and between 16.8 % and 25.6 % at the higher pH range. It was also observed that while a 3.5 mg/L of coagulant was needed for the removal of 25% of DOC at pH 5.5, a 10 mg/L of dose was required for 17% removal at pH 8, implying that lower pH conditions could allow for a reduction in the dosage to achieve higher DOC removal under mixing condition of $G_{800}T_{10}$.

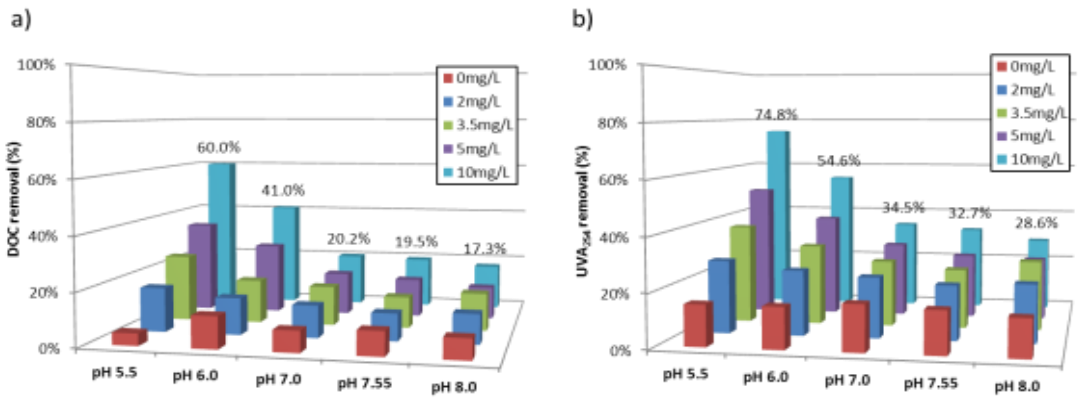

Figure 4.12 - Removal efficiency of NOM in terms of DOC (a) and UVA_{254} (b) as a function of different pH and coagulant dose as Fe^{3+} under mixing condition of $G_{400}T_{30}$

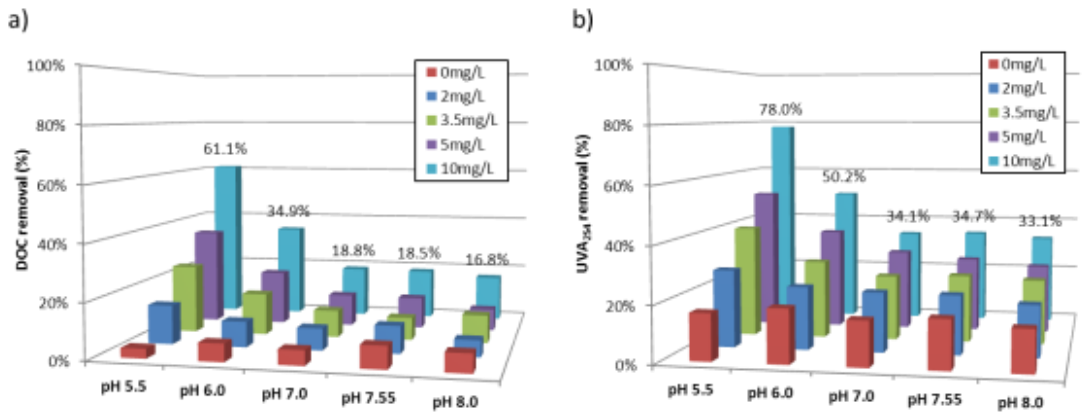

Figure 4.13 - Removal efficiency of NOM in terms of DOC (a) and UVA_{254} (b) as a function of different pH and coagulant dose as Fe^{3+} under mixing condition of $G_{800}T_{300}$

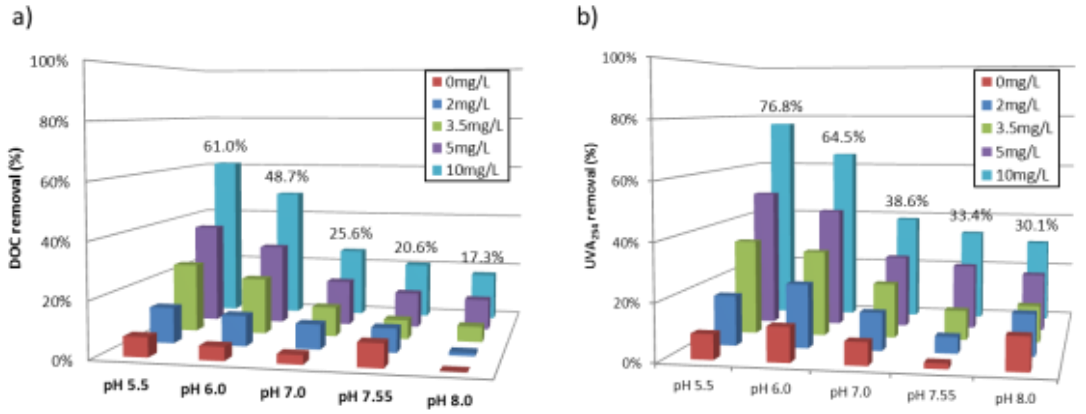

Figure 4.14 - Removal efficiency of NOM in terms of DOC (a) and UVA_{254} (b) as a function of different pH and coagulant dose as Fe^{3+} under mixing condition of $G_{800}T_{10}$

UVA_{254} removal was slightly higher than DOC, implying that coagulation can enhance preferential removal of humics over non-humics. The highest removal was 78% at a pH of 5.5, with a Fe^{3+} dose of 10 mg/L. Especially at lower dosage, the UVA_{254} removal was more significant than the DOC removal with 34% at 3.5 mg/L and 50% at 5 mg/L for UVA_{254} versus 25% and 37% for DOC, respectively, under $G_{800}T_{10}$.

These findings are consistent with the results that were reported in previous research (Konieczny et al. 2006, Lerch et al. 2005). However, the only difference is that the observed removal efficiency was lower than those generally reported results. This is likely due to the absence of additional flocculation, which would allow creation of large hydroxide precipitates adsorbing more NOM, with inter-particle bridging provided by supplementary slow mixing. The pH-dependent NOM removal could also be explained by the enhanced coagulation mechanism in conventional water treatment process. Enhanced coagulation can be achieved at lower pH conditions and higher dose of coagulant than that used in the conventional coagulation process in which coagulation generally focuses on turbidity removal rather than NOM. Furthermore, it was noted that NOM can be effectively removed with in-line coagulation (i.e., flash mixing for very short time) prior to MF ceramic membrane filtration instead of the coagulation/ flocculation process which requires more footprint, energy and cost when used with membrane filtration.

4.4. CONCLUSIONS

The effects of coagulation pretreatment with ceramic membrane filtration on membrane fouling and NOM removal for treating high-organic surface water were investigated with a bench-scale unit. TAMI MF/UF ceramic membrane discs made of TiO_2+ZrO_2 and ferric chloride coagulation were employed in the study. Zeta potential (ζ), PWP and synthetic layer composition of the TAMI ceramic membrane were identified to understand fundamental properties of the TAMI membrane.

Zeta potential (ζ) of the TiO_2+ZrO_2 based membrane was measured. The membrane showed pH-dependent behaviour of surface charge, resulting in having a positive charge below near a pH 4 and being negatively charged at higher pH values (i.e., $TAMI_{PZC}$ is near pH 4). Compared to the alumina based membrane, the TAMI ceramic membrane is expected to reduce NOM binding to the surface attributed to the lower PZC value, promoting an increase in permeability.

At different TMPs, pure water permeability (PWP) of the MF and UF membranes were kept stable throughout the filtration, while each disc resulted in a somewhat different PWP, or membrane resistance (R_m), under the same conditions. The difference in UF was higher than that of MF. SEM images revealed that the UF was composed of a double-coated separation layer, while the MF represented a single separation layer. The separation layers were not uniform in terms of its thickness, pore shape, and surface level. These differences were more distinct for UF, which might come from the double-coating synthesis procedure and have an influence on more resistance difference than MF.

The modified fouling index (MFI) could be effectively employed to predict membrane filterability in accordance with different coagulation conditions. Based on the slope of the linear regression curve that is plotted with dt/dV as function of accumulated volume, MFI was able to represent membrane fouling mechanisms. It is expected that MFI can be a useful tool to compare membrane filterability if many experimental approaches are required to identify the optimal operation conditions such as pretreatment, chemical addition, membrane flux, etc.

Precoagulation was shown to play an important role in both enhancing membrane filterability and NOM removal efficacy. The most critical factors were pH and coagulant dosage, resulting in the highest efficiency for a condition of low pH range (i.e., pH 5.5) and a high dosage (i.e., 10mg/L) corresponding to the enhanced coagulation mechanism. UVA_{254} removal was slightly higher than DOC, implying that precoagulation can improve preferential removal of humics over non-humics. At a low pH range of 5.5 and 6.0, an optimal dosage and proper mixing time was necessary to maximize coagulation effects. At a high pH range of 7.0, 7.5, and 8.0, it was shown that there was no significant influence to enhance MF ceramic membrane performance if coagulant dose was not enough to sweep NOM with precipitating hydroxide.

It is expected that TAMI MF/UF ceramic membrane when used with precoagulation can be effectively applied to treat impaired quality sources such as a high-organic surface water, which might contain problematical NOM foulants. In-line coagulation without an additional flocculation step can effectively play a role in enhancing the TAMI ceramic membrane performance, which is more effective at lower pH and higher dosage.

4.5. REFERENCES

Pontié, M., Thekkedath, A., Kecili, K., Habarou, H., Suty, H. and Croué, J.P. (2007) Membrane autopsy as a sustainable management of fouling phenomena occurring in MF, UF and NF processes. Desalination 204(1-3), 155-169.

Huang, H., Lee, N., Young, T., Gary, A., Lozier, J.C. and Jacangelo, J.G. (2007) Natural organic matter fouling of low-pressure, hollow-fiber membranes: Effects of NOM source and hydrodynamic conditions. Water Research 41(17), 3823-3832.

Lee, E.K., Chen, V. and Fane, A.G. (2008) Natural organic matter (NOM) fouling in low pressure membrane filtration -- effect of membranes and operation modes. Desalination 218(1-3), 257-270.

Lee, N., Amy, G., Croué, J.-P. and Buisson, H. (2004) Identification and understanding of fouling in low-pressure membrane (MF/UF) filtration by natural organic matter (NOM). Water Research 38(20), 4511-4523.

Amy, G. (2008) Fundamental understanding of organic matter fouling of membranes. Desalination 231(1-3), 44-51.

Volk, C., Bell, K., Ibrahim, E., Verges, D., Amy, G. and Lechevallier, M. (2000) Impact of enhanced and optimized coagulation on removal of organic matter and its biodegradable fraction in drinking water. Water Research 34(12), 3247-3257.

Dong, B.-z., Chen, Y., Gao, N.-y. and Fan, J.-c. (2007a) Effect of coagulation pretreatment on the fouling of ultrafiltration membrane. Journal of Membrane Science 19, 278-283.

Matsushita, T., Matsui, Y., Shirasaki, N. and Kato, Y. (2005) Effect of membrane pore size, coagulation time, and coagulant dose on virus removal by a coagulation-ceramic microfiltration hybrid system. Desalination 178(1-3), 21-26.

Lee, N., Amy, G. and Lozier, J. (2005) Understanding natural organic matter fouling in low-pressure membrane filtration. Desalination 178(1-3), 85-93.

Seidel, A. and Elimelech, M. (2002) Coupling between chemical and physical interactions in natural organic matter (NOM) fouling of nanofiltration membranes: implications for fouling control. Journal of Membrane Science 203(1-2), 245-255.

Lee, S. and Cho, J. (2004) Comparison of ceramic and polymeric membranes for natural organic matter (NOM) removal. Desalination 160(3), 223-232.

Burggraaf, A.J. and Cot, L. (1996) Fundamentals of inorganic membrane science and technology, Elsevier.

Dafinov, A., Garcia-Valls, R. and Font, J. (2002) Modification of ceramic membranes by alcohol adsorption. Journal of Membrane Science 196(1), 69-77.

Larbot, A., Gazagnes, L., Krajewski, S., Bukowska, M. and Wojciech, K. (2004) Water desalination using ceramic membrane distillation. Desalination 168, 367-372.

Garmash, E.P., Kryuchkov, Y.N. and Pavlikov, V.N. (1995) Ceramic membrane for ultra- and microfiltration (Review). Glass and Ceramic 52(6), 150-152.

Baruah, G.L., Nayak, A. and Belfort, G. (2006a) Scale-up from laboratory microfiltration to a ceramic pilot plant: Design and performance. Journal of Membrane Science 274(1-2), 56-63.

Konieczny, K., Bodzek, M. and Rajca, M. (2006) A coagulation-MF system for water treatment using ceramic membranes. Desalination 198(1-3), 92-101.

Lerch, A., Panglisch, S., Buchta, P., Tomita, Y., Yonekawa, H., Hattori, K. and Gimbel, R. (2005) Direct river water treatment using coagulation/ceramic membrane microfiltration. Desalination 179(1-3), 41-50.

Mori, Y., Oota, T., Hashino, M., Takamura, M. and Fujii, Y. (1998) Ozone-microfiltration system. Desalination 117(1-3), 211-218.

Lehman, S.G. and Liu, L. (2009) Application of ceramic membranes with pre-ozonation for treatment of secondary wastewater effluent. Water Research 43(7), 2020-2028.

Hong, S., Krishna, P., Hobbs, C., Kim, D. and Cho, J. (2005) Variations in backwash efficiency during colloidal filtration of hollow-fiber microfiltration membranes. Desalination 173(3), 257-268.

Boerlage, S.F.E., Kennedy, M., Tarawneh, Z., De Faber, R. and Schippers, J.C. (2004) Development of the MFI-UF in constant flux filtration. Desalination 161(2), 103-113.

Lee, S., Park, G., Amy, G., Hong, S.-K., Moon, S.-H., Lee, D.-H. and Cho, J. (2002) Determination of membrane pore size distribution using the fractional rejection of nonionic and charged macromolecules. Journal of Membrane Science 201(1–2), 191-201.

Zhao, C., Zhou, X. and Yue, Y. (2000) Determination of pore size and pore size distribution on the surface of hollow-fiber filtration membranes: a review of methods. Desalination 129(2), 107-123.

Hernández, A., Calvo, J.I., Prádanos, P. and Tejerina, F. (1998) Pore size distributions of track-etched membranes; comparison of surface and bulk porosities. Colloids and Surfaces A: Physicochemical and Engineering Aspects 138(2–3), 391-401.

Crispin, T. and Halász, I. (1982) Determination of the pore size distribution, by exclusion chromatography, of ion-exchange polymers which swell in water. Journal of Chromatography A 239(0), 351-362.

Guizard, C., Ayral, A. and Julbe, A. (2002) Potentiality of organic solvents filtration with ceramic membranes. A comparison with polymer membranes. Desalination 147(1–3), 275-280.

Baruah, G.L., Nayak, A. and Belfort, G. (2006b) Scale-up from laboratory microfiltration to a ceramic pilot plant: Design and performance. Journal of Membrane Science 274(1–2), 56-63.

Hong, S. and Elimelech, M. (1997) Chemical and physical aspects of natural organic matter (NOM) fouling of nanofiltration membranes. Journal of Membrane Science 132(2), 159-181.

Kosmulski, M. (2011) The pH-dependent surface charging and points of zero charge: V. Update. Journal of Colloid and Interface Science 353(1), 1-15.

Zhou, J., Zhang, X., Wang, Y., Hu, X., Larbot, A. and Persin, M. (2009) Electrokinetic characterization of the Al2O3 ceramic MF membrane by streaming potential measurements. Desalination 235(1–3), 102-109.

Moritz, T., Benfer, S., Arki, P. and Tomandl, G. (2001a) Investigation of ceramic membrane materials by streaming potential measurements. Colloids and Surfaces A: Physicochemical and Engineering Aspects 195(1–3), 25-33.

Moritz, T., Benfer, S., Árki, P. and Tomandl, G. (2001b) Influence of the surface charge on the permeate flux in the dead-end filtration with ceramic membranes. Separation and Purification Technology 25(1–3), 501-508.

Nazzal, F.F. and Wiesner, M.R. (1994) pH and ionic strength effects on the performance of ceramic membranes in water filtration. Journal of Membrane Science 93(1), 91-103.

Alldredge, A.L., Passow, U. and Logan, B.E. (1993) The abundance and significance of a class of large, transparent organic particles in the ocean. Deep Sea Research Part I: Oceanographic Research Papers 40(6), 1131-1140.

Hernández, A., Calvo, J.I., Prádanos, P., Palacio, L., Rodríguez, M.L. and de Saja, J.A. (1997) Surface structure of microporous membranes by computerized SEM image analysis applied to Anopore filters. Journal of Membrane Science 137(1–2), 89-97.

Boussu, K., Van der Bruggen, B., Volodin, A., Snauwaert, J., Van Haesendonck, C. and Vandecasteele, C. (2005) Roughness and hydrophobicity studies of nanofiltration membranes using different modes of AFM. Journal of Colloid and Interface Science 286(2), 632-638.

Zularisam, A.W., Ahmad, A., Sakinah, M., Ismail, A.F. and Matsuura, T. (2011) Role of natural organic matter (NOM), colloidal particles, and solution chemistry on ultrafiltration performance. Separation and Purification Technology 78(2), 189-200.

Jermann, D., Pronk, W., Kägi, R., Halbeisen, M. and Boller, M. (2008) Influence of interactions between NOM and particles on UF fouling mechanisms. Water Research 42(14), 3870-3878.

Dong, B.-z., Chen, Y., Gao, N.-y. and Fan, J.-c. (2007b) Effect of coagulation pretreatment on the fouling of ultrafiltration membrane. Journal of Environmental Sciences 19(3), 278-283.

Zularisam, A.W., Ismail, A.F., Salim, M.R., Sakinah, M. and Ozaki, H. (2007) The effects of natural organic matter (NOM) fractions on fouling characteristics and flux recovery of ultrafiltration membranes. Desalination 212(1–3), 191-208.

Jung, C.-W., Son, H.-J. and Kang, L.-S. (2006) Effects of membrane material and pretreatment coagulation on membrane fouling: fouling mechanism and NOM removal. Desalination 197(1–3), 154-164.

Perdue, E.M. (2009) Encyclopedia of Inland Waters. Editor-in-Chief: Gene, E.L. (ed), pp. 806-819, Academic Press, Oxford.

Choi, K.Y.-j. and Dempsey, B.A. (2004) In-line coagulation with low-pressure membrane filtration. Water Research 38(19), 4271-4281.

Hatt, J.W., Germain, E. and Judd, S.J. (2011) Precoagulation-microfiltration for wastewater reuse. Water Research 45(19), 6471-6478.

Huang, H., Schwab, K. and Jacangelo, J.G. (2009) Pretreatment for low pressure membranes in water treatment: A review. Environmental Science and Technology 43(9), 3011-3019.

Hofs, B., Vries, D., Siegers, W.G., Beerendonk, E.F. and Cornelissen, E.R. (2012) Influence of water type and pretreatment method on fouling and performance of an Al2O3 microfiltration membrane. Desalination 299(0), 28-34.

Wang, J., Guan, J., Santiwong, S.R. and Waite, T.D. (2010) Effect of aggregate characteristics under different coagulation mechanisms on microfiltration membrane fouling. Desalination 258(1–3), 19-27.

Hofs, B., Ogier, J., Vries, D., Beerendonk, E.F. and Cornelissen, E.R. (2011) Comparison of ceramic and polymeric membrane permeability and fouling using surface water. Separation and Purification Technology 79(3), 365-374.

Meyn, T. and Leiknes, T. (2010) Comparison of optional process configurations and operating conditions for ceramic membrane MF coupled with coagulation/flocculation pre-treatment for the removal of NOM in drinking water production. Journal of Water Supply: Research and Technology - AQUA 59(2-3), 81-91.

Xu, J., Chang, C.-Y. and Gao, C. (2010) Performance of a ceramic ultrafiltration membrane system in pretreatment to seawater desalination. Separation and Purification Technology 75(2), 165-173.

Boerlage, S.F.E., Kennedy, M.D., Aniye, M.P., Abogrean, E.M., Galjaard, G. and Schippers, J.C. (1998) Monitoring particulate fouling in membrane systems. Desalination 118(1-3), 131-142.

Boerlage, S.F.E., Kennedy, M., Aniye, M.P. and Schippers, J.C. (2003) Applications of the MFI-UF to measure and predict particulate fouling in RO systems. Journal of Membrane Science 220(1-2), 97-116.

Matilainen, A., Vepsäläinen, M. and Sillanpää, M. (2010) Natural organic matter removal by coagulation during drinking water treatment: A review. Advances in Colloid and Interface Science 159(2), 189-197.

Meyn, T., Bahn, A. and Leiknes, T.O. (2008) Significance of flocculation for NOM removal by coagulation-ceramic membrane microfiltration, pp. 691-700.

Guigui, C., Rouch, J.C., Durand-Bourlier, L., Bonnelye, V. and Aptel, P. (2002) Impact of coagulation conditions on the in-line coagulation/UF process for drinking water production. Desalination 147(1-3), 95-100.

Chapter 5

Precoagulation Effects on Ceramic Membrane Filtration

Phase 2-2: Effects of enhanced precoagulation on ceramic membrane filtration for treatment of secondary wastewater effluent

Effects of enhanced precoagulation on ceramic membrane filtration for treatment of secondary wastewater effluent[4]

ABSTRACT

When MF and UF membranes are employed to treat wastewater effluent, membrane fouling must be controlled. Due to the robustness of ceramic membranes such as inherent mechanical, thermal, and chemical stability, enhanced coagulation under acidic conditions can be applied to reduce membrane fouling to an acceptable level. This study presents MF ceramic membrane performance with coagulation as a pretreatment, focusing on enhanced coagulation in treating the secondary effluent. A ceramic membrane can play an important role when combined with precoagulation in terms of permeability, filterability, and NOM removal. Enhanced coagulation can significantly reduce membrane fouling which is irreversible by hydraulic cleaning to such a significant extent with even a small coagulant dosage (i.e., 5 mg/L as Fe^{3+}) at pH 5.5. Conventional coagulation is also capable of achieving high membrane performance, observed with a higher coagulant dosage (i.e., 15 mg/L as Fe^{3+}) at pH 7.6. LC-OCD and 3D-FEEM demonstrated that NOM removal is proportion to coagulant dosage and more significantly achieved at a low pH range (i.e., 5.5 or possibly lower), resulting in improved preferential removal of humics over non-humics. Biopolymers responsible for problematical membrane fouling were easily removed by ceramic membrane filtration or with precoagulation.

---

[4] This chapter was submitted to Desalination

Keywords: Ceramic membrane; wastewater reuse; precoagulation; NOM fouling;

5.1. INTRODUCTION

Many communities across the world have frequently been facing water supply challenges because of water scarcity, increasing demand, quality deterioration, and dependence on single source of supply. In the context of a more sustainable water management, as a matter of fact, water reclamation, recycling, and reuse have been recognized as an indispensable alternative to address these challenges (Karnik et al. 2005, Meyn et al. 2008, Tchobanoglous et al. 1998). Membrane processes play a promising role in these water-sector applications. Particularly, ultrafiltration (UF) and microfiltration (MF) to treat secondary or tertiary wastewater effluent has been widely used to enhance water quality compared to conventional treatment processes.

However, one of the main obstacles to further application of the membrane technology for water reuse is the permeate flux decline occurring during a long-term operation, i.e. membrane fouling (Lehman and Liu 2009). Wastewater effluent by membrane filtration is characterized by organic foulants with a biological background, which interact with high elevated concentration of colloids and micro-particles in the source water, and membrane surface. The organic foulant accumulated on the membrane surface is a major constraint, causing irreversible fouling, and eventually deteriorating sustainable membrane performance (Amy 2008, Huang et al. 2007, Lee et al. 2004). Optimization of pretreatment (e.g. coagulation), operation flux, and backwashing interval have been identified as key factors to maintain the sustainable membrane performance (Konieczny et al. 2006).

Ceramic membranes are expected to play a promising role in addressing those inevitable problems instead of polymeric ones which have been mostly used in water reuse applications for the past couple of decades. Ceramic membranes have recently been introduced in water sectors because of the robustness of the materials in terms of their inherent mechanical, thermal and chemical stability (Burggraaf and Cot 1996). As a result of these attributes, it is expected that ceramic membranes are able to operate at high permeate flux, at high feed water recovery, and with less frequent chemical cleaning. Especially, these features could help effectively achieve enhanced filtration performance when treating wastewater effluent, providing excellent backwash efficiency and mitigating NOM fouling with incorporation of various chemical treatments such as coagulation and ozone (O_3) (Konieczny et al. 2006, Lehman and Liu 2009).

This study presents MF ceramic membrane filtration in combination with coagulation as a pretreatment, especially, focusing on enhanced precoagulation to treat secondary wastewater effluent. In previously on-going study, it was found that ceramic membranes could play a role in treating impaired water quality source as surface water with an elevated level of organic matter when combined with precoagulation. It was also found that the most critical factors for coagulation was pH and coagulant dosage, with highest performance observed at low pH range (i.e. 5.5 or lower) and high coagulant dosage (i.e. 10 mg/L or more as Fe^{3+}), which is designated as *enhanced coagulation*. It was notable that precoagulation improved preferential removal of humics over non-humics. It is expected that enhanced coagulation which is processed under strong acid condition and high coagulant dosage is highlighted when used with ceramic membranes due to their robustness.

The research aimed to investigate effects of enhanced precoagulation on ceramic membrane (i.e. a nominal pore size of 0.14 μm) filtration for treating secondary wastewater effluent in terms of permeability, recoverability, and NOM removal by means of various analytical methods. Time-dependant flux and modified fouling index (MFI) were assessed under different pH and coagulant dosage; foulant resistances against the membrane before and after backwashing were determined, focusing on reversible (i.e. cake-layer-causing fouling) or irreversible fouling (i.e. pore-blockage-causing fouling); natural organic matter (NOM) was characterized to understand the effect on organic foulant with liquid chromatography – organic carbon detection (LC-OCD) and 3D-fluorescence excitation-emission matrix (FEEM), both of which are component-specific NOM analyses.

5.2. MATERIALS AND METHODS

5.2.1. Source water

Raw water used for this study was taken from the secondary wastewater treatment plant effluent in Jeddah, Saudi Arabia, treated by an anoxic-oxic (AO) activated sludge process. The pH of samples ranged from 7.6 to 7.75. The DOC was between 5 mg/L to 7 mg/L and UVA_{254} from 10.0 m^{-1} to 17.5 m^{-1}, corresponding to SUVA values from 2.0 L/mg·m to 2.5 L/mg·m. Throughout the experimental period, feed water used for all experiments was adjusted to room temperature between 19.5°C and 20.5°C, which had been established after taking the sample out of a cold storage for a half-day before a set of test started.

5.2.2. Ceramic membrane specification

A MF ceramic membrane with a nominal pore size of 0.14μm, manufactured by TAMI INDUSTRIS was adopted for this study. The ceramic membrane is asymmetric, composed of a surface layer of titanium dioxide-zirconium dioxide (TiO_2 + ZrO_2) and a support layer of titanium dioxide (TiO_2). A disc membrane of 47mm in diameter with an effective area of 0.00131 m^2 and a thickness of 2.2mm was employed with a special holder, where feed waters – raw water and coagulated water – were penetrated through the ceramic MF membrane disc placed inside the holder in a dead-end filtration mode.

5.2.3. Experimental configuration

Raw water (i.e. secondary wastewater effluent) which had been prefiltered with a 20μm of coarse sieve, and coagulated waters under different conditions penetrated TAMI MF ceramic disc membrane placed in the special holder for 40 minutes (mode 1 in Figure 5.1), and then the membrane fouled after filtration was backwashed using Milli-Q water (≈ 18Ω) in normal backwash pressure of twice as high as operation pressure (mode 2 in Figure 5.1). Finally, the flushed membrane was re-filtered for 20 minutes to identify irreversible fouling and reveal the fouling mechanisms. A membrane pressure applied for ceramic MF membrane filtration was exactly fixed at a 0.15 bar, leading to initial membrane flux between 300 L/m^2h to 380 L/m^2h, dependant on individual membrane properties (i.e. the thickness, homogeneity, and porosity) and feed waters characteristics. The reason why the initial flux was set very high was to demonstrate ceramic membrane performance under extreme conditions,

based on that it has been reported that ceramic membrane could achieve enhanced filtration performance and when incorporated with chemical pretreatments, it could greatly mitigate fouling by natural organic matter (Garmash et al. 1995, Karnik et al. 2005). The permeate was accumulated in a beaker under which a digital balance is placed, acquiring time-dependent data of throughput per 10 seconds to evaluate flux, foulant resistance, and MFI. In addition, the filtrate was collected to characterize natural organic matter (NOM) after the completion of the data acquisition.

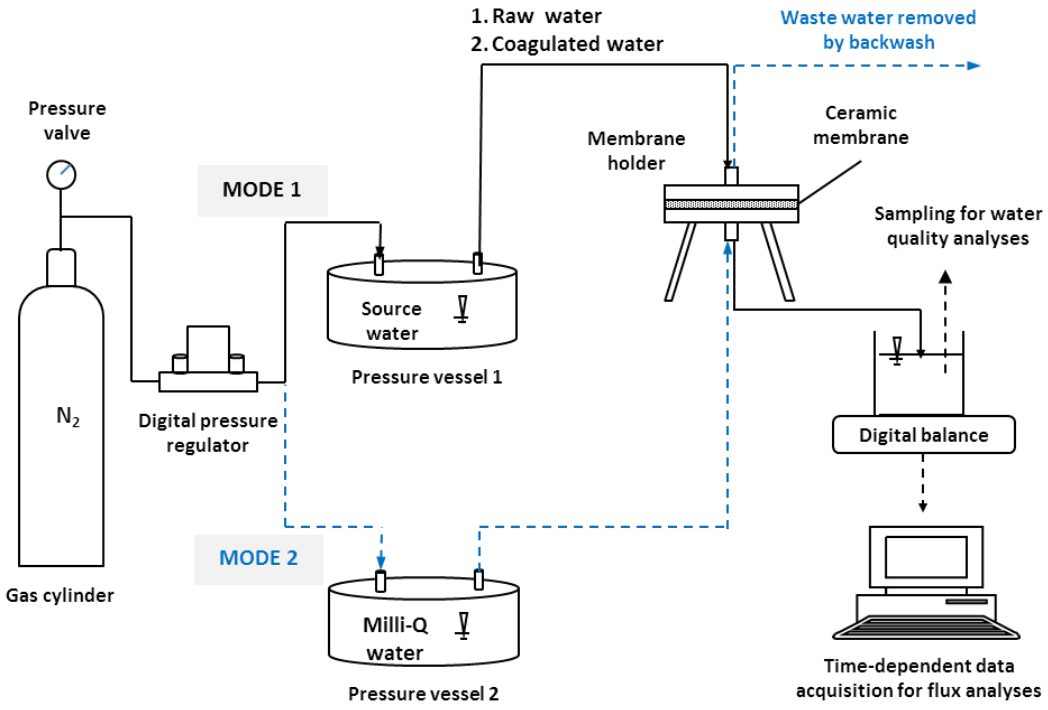

Figure 5.1 - Schematic of ceramic membrane filtration test unit: raw water or coagulated water is filtered with TAMI MF ceramic disc membrane placed in the special holder (mode 1); after filtration for 40 minutes, the fouled membrane is backwashed using pure water under normal backwash pressure of twice as high as operation one (mode 2)

5.2.4. Precoagulation experiment

Prior to ceramic membrane filtration, raw water was coagulated using a jar test unit (PHIPPS & BIRD, USA) that consists of six rectangular jars of 2.0 L and a flat-

bladed stainless steel mixer in each jar, where mixing intensity was controlled by rotational speed set as rpm. Mixing condition was set as follow: 400 s^{-1} of the velocity gradient (G) and 45 seconds of mixing time (T), where no additional flocculation was applied. Ferric chloride ($FeCl_3 \cdot 6H_2O$) was used as a coagulant, and pH was adjusted with nitric acid. First, coagulant dosage increased up to 10 mg/L from 0 as Fe^{3+} at an ambient pH of 7.6 (i.e. conventional coagulation), and the pH was adjusted into 5.5 with high coagulant dosage of 5 mg/L and 10 mg/L (i.e. enhanced coagulation). Finally, coagulant dosage was raised up to 15 mg/L at an ambient pH, compared with the results obtained from enhanced coagulation. Table 5.1 shows parameters and conditions for coagulation experiments in details. Low doses of coagulants (i.e. 0, 2, and 3.5 mg/L) were not carried out for enhanced coagulation, because it has been already observed that a low dosage of coagulant at a pH 5.5 caused more severe fouling, but improved NOM removal in previous study. As soon as a set of coagulation test was completed, the coagulated water was carried in a pressure vessel 1 (Figure 5.1), immediately performing ceramic membrane filtration.

Table 5.1 - Parameters/conditions for coagulation as a pretreatment, aiming to comparing effects of conventional coagulation and enhanced coagulation on ceramic MF membrane filtration (ferric chloride ($FeCl_3 \cdot 6H_2O$) was used as a coagulant)

Conditions/parameters	G; T (s-1; second)	pH	Dosage (mg/L as a Fe3+)
Conventional coagulation	400; 45	7.6 ~ 7.75	0, 2, 3.5, 5, 10, 15
Enhanced coagulation	400; 45	5.5	5, 10

5.2.5. Modified fouling index (MFI-MF)

The MFI-MF was used to identify the effect of enhanced coagulation prior to MF ceramic membrane filtration in terms of membrane fouling. It is determined under constant pressure filtration from the slope of the general cake filtration equation in the plot of dt/dv versus V (Boerlage et al. 2004, Boerlage et al. 1998), when fixed reference values are used at a 2 bar of pressure, a 20°C of temperature, and 13.8×10^{-4} m^2 of membrane surface area with 0.45µm pore size.

$$\frac{dt}{dV} = \frac{\eta R_m}{\Delta P\, A} + \frac{\eta \alpha C_b}{\Delta P A^2} V;\; MFI = \frac{\eta\, \alpha C_b}{\Delta P A^2} \quad (1)$$

Where V is the filtered volume (m^3), t filtration time (s), ΔP the applied trans-membrane pressure (bar, or Ns/m^2), η the water viscosity (Ns/m^2), R_m the membrane resistance (m^{-1}), A the membrane surface area (m^2), α the specific resistance of the cake per unit weight (m), and C_b the concentration of particles per unit filtrate volume (kg/ m^3). A MF ceramic membrane (0.14µm) used for this study was directly applied to obtain the MFI values. Permeated volume was recorded at 10 second intervals under a certain pressure depending on a membrane used over a 40 minutes filtration period. The MFI value was then computed by linear regression from the slope of the linear region of a plot of dt/dv as function of V. The measured MFI value was corrected into a normalized MFI by applying a correction factor of standard reference conditions, i.e. a pressure of 2 bars (ΔP_0), a temperature of 20°C ($\eta_{20°C}$), and a membrane surface area of 0.001384 m^2 (A_0) which is termed MFI-MF in equation (2).

$$\text{MFI-MF}_{\text{corrected}} = \frac{\eta_{20℃}}{\eta}\left(\frac{\Delta P}{\Delta P_0}\right)\left(\frac{A}{A_0}\right)^2 \times MFI_{measured} \quad (2)$$

5.2.6. Determination of fouling mechanisms

The resistance-in-series model was employed to determine the fouling mechanism of ceramic MF membranes with precoagulation (equation 1), based on that particles, or foulants retained by membrane filtration increase total resistance (R_t; m^{-1}) against the membrane, causing the reduction in flux. Initially, membrane itself provides a resistance to water flux (R_m; m^{-1}) caused by the membrane properties such as the thickness, homogeneity, and porosity. As filtration goes on, foulants are deposited inside pores, or block pore entry, leading to declining the membrane flux by increase in resistance (R_b; m^{-1}). When the membrane is fully or partially blocked, particles might be accumulated on the membrane surface as a cake layer, causing the additional resistance (R_c; m^{-1}).

$$J = \frac{\Delta P}{\mu \cdot R_t} = \frac{\Delta P}{\mu(R_m + R_b + R_c)} \; ; \; R_t = R_m + R_b + R_c \quad (3)$$

Where J is the permeate flux (J; L/m^2h) through the membrane, ΔP the applied trans-membrane pressure (TMP) (bar, or N/m^2), η the water viscosity (NS/m^2). The permeate flux was calculated as the flow rate of permeate water (Q; L/h) divided by the effective surface area of the membrane (A; m^2). Specific flux (J_s; $L/m^2h \cdot bar$), or permeability corresponds to flux normalized to trans-membrane pressure (TMP). Total resistance, R_t was calculated by using a final flux of a ceramic membrane which is fouled after 40 minutes filtration (J_{40}), and then resistance due to cake formation, R_c

was acquired with the very first flux of the membrane cleaned after backwashing ($J_{flushed\ initial}$). It is hypothesized that a cake layer formed on the membrane surface can be easily rejected by hydraulic cleaning, or backwashing (i.e. reversible fouling), but foulants still blocked inside membrane pores (i.e. irreversible fouling) cause resistance against membrane. Finally, the resistance due to pore blockage, R_b was obtained by subtracting R_c from R_t, where inherent membrane resistance, R_m was eliminated.

5.2.7. Natural organic matter (NOM) characterization

Liquid (size exclusion) chromatography with organic carbon detection (OCD) and UV detection (UVD), known as LC-OCD-UVD based on the Gräntzel thin-film UV-reactor, was used to characterize NOM in terms of chromatographic peaks that are observed with a special column. On-line purified mobile phase (phosphate buffer solution exposed to UV-irradiation in an annular UV-reactor) is delivered with an HPLC pump (S-100, Knauer, Berlin, Germany) at a flow rate of 1.1 mL/min to an auto-sampler (MLE, Dresden, Germany, 1mL injection volume) followed by chromatographic column (250mm × 20mm, TSK HW 50S, 3000 theoretical plates, Toso, Japan). A sample passes through a 0.45µm in-line PES filter (Sartorius, Germany, # 16537) prior to chromatographic separation. The first detector after column separation is a non-destructive, fixed wavelength UV-detection (UVD 254nm, type S-200, Knauer, Berlin, Germany) prior to the organic carbon detector (OCD). At the inlet of the OCD, the solution is acidified at a flow rate of 0.2 mL/min to convert carbonates to carbonic acid. DOC is analysed at the dead volume time of each chromatographic run by by-passing before the column. Finally, for data acquisition

and data processing, a customized software program is used (ChromCALC, DOC-LABOR, Karlsruhe, Germany) (Guigui et al. 2002, Huber et al. 2011).

3D fluorescence excitation-emission matrix (EEM) spectra was analysed to help characterize NOM in terms of protein-like and humic-like OM with a Fluoromax-4 spectrofluorometer (HORIBA scientific, Japan) in a 4 mL quartz cuvette cell, where temperature was adjusted at 20°C. Fluorescence EEMs were measured in the excitation range of $\lambda_{ex} = 240{\sim}450$ nm and the emission of $\lambda_{em} = 290{\sim}500$ nm at a 5 nm increment with a slit width of 5 nm for both. A number of single wavelength pair intensities were extracted from the EEMs and analysed as: primary humic-like ($\lambda_{ex/em} = 300{\sim}370/380{\sim}480$ nm); secondary humic-like ($\lambda_{ex/em} = 237{\sim}260/380{\sim}460$ nm); protein-like ($\lambda_{ex/em} = 275/310{\sim}340$ nm) (Baker and Genty 1999, Coble 1996, Henderson et al. 2009, Liu et al. 2007). Milli-Q water blank EEM was subtracted to eliminate water Raman peaks from samples.

5.3. RESULTS AND DISCUSSION

5.3.1. Effects of enhanced precoagulation on membrane flux and resistance

Enhanced precoagulation was found to have a significant influence on not only improving ceramic membrane flux of MF, but also reducing membrane resistance as shown in Figure 5.2. Zone I and III in Figure 5.2 denote ceramic membrane filtration results that are performed after coagulation at an ambient pH of 7.6, corresponding to

conventional coagulation condition while Zone II results at a pH 5.5, representing enhanced coagulation conditions). Overall, it was observed that membrane flux improved according to increase in coagulant dosage. With coagulant dosage of 0, 2, 3.5, 5, and 10 mg/L as a Fe^{3+}, normalized fluxes of 0.36, 0.46, 0.44, 0.48, and 0.52 after 40 minutes filtration were respectively remained (Zone I). Under enhanced coagulation condition, normalized fluxes of 0.61 and 0.60 were achieved with 5 and 10 mg/L, resulting in 25% and 15% improvement from 0.48 and 0.52, respectively (Zone II). Even if coagulant dosage increased up to 15mg/L at an ambient pH, membrane flux was not enhanced beyond enhanced coagulation results, observing a normalized flux of 0.60. It was noteworthy that 5 mg/L at a pH 5.5 resulted in the highest improvement among others, implying that if pH is adjusted for enhanced coagulation, coagulant dosage can be significantly reduced with improving membrane flux.

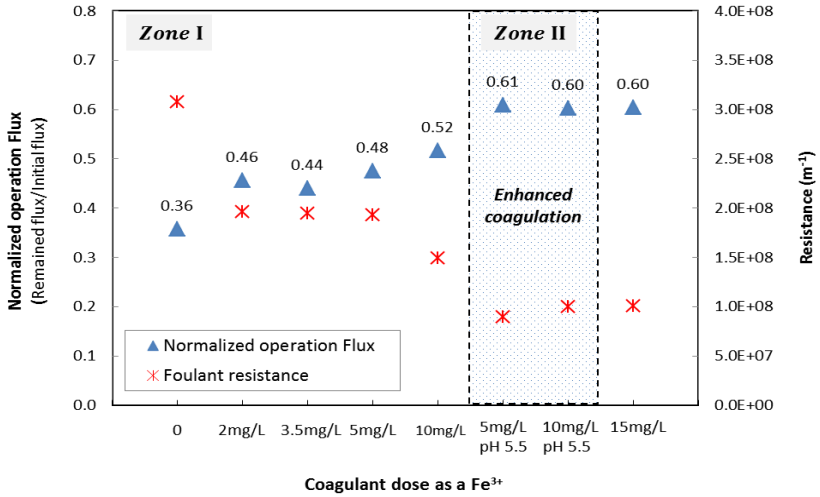

Figure 5.2 - Normalized flux and foulant resistance (R_f) remained after 40 minutes of filtration as function of coagulant dose as a Fe^{3+} at an ambient pH of 7.6 and 5.5

Resistance due to foulants which are accumulated on/inside a ceramic membrane was computed by means of the resistance-in-series model. The foulant resistance ($R_f = R_b + R_c$) was obtained by subtracting the inherent membrane resistance (R_m) from the total resistance (R_t) fouled after 40 minutes filtration. Figure 5.2 shows that the foulants resistance, R_f decreases in inversely proportional to coagulant dosage, and significantly becoming weak by lowering pH by 5.5. It was observed that the R_f decreased by about 36, 37 and 37% with 2, 3.5 and 5 mg/L of coagulant as a Fe^{3+}, and by 51 and 67% with 10 and 15 mg/L, respectively, at an ambient pH of 7.6 (i.e. under conventional coagulation condition). According to the result, it was analysed that just small amount of coagulant of 2 mg/L was able to reduce the foulant resistance against membrane, but large amount of coagulant such as 10 and 15 mg/L was required to achieve over 50 % reduced resistance. However, the resistance significantly became down by 71% with just 5 mg/L at a pH 5.5 (i.e. enhanced coagulation), which was beyond the result from 15 mg/L at an ambient pH as shown in Figure 5.2.

In theory, enhanced coagulation can be accomplished with higher dosage and lower pH range that those of conventional coagulation. The mechanism is dominated by charge neutralization associated with enmeshment at low pH range, while conventional coagulation is done by sweep coagulation mechanism at over neutral pH. The enhanced coagulation mainly aims to increase in NOM removal efficiency. It has been frequently reported that enhanced coagulation resulted in achieving high removal of natural organic matter (NOM), which is difficult to be removed by conventional coagulation. However, it was noticeable that another critical benefit of enhanced coagulation was capable of significantly improving membrane flux with

reducing membrane resistance by small amount of coagulation dosage instead of high dosage, which was also satisfied without additional flocculation step.

5.3.2. Effects of enhanced precoagulation on membrane fouling

5.3.2.1. Computation of MFI and t/V versus V curve

Assessment of MF ceramic membrane fouling combined with precoagulation at different pH and coagulant dosage was carried out by means of modified fouling index (MFI), compared before and after backwashing as shown in Figure 5.3. The both of MFIs were reduced as coagulant dosage increased, and significantly decreased at lower pH of 5.5. It was observed that 2 mg/L of coagulant as Fe^{3+} significantly led to MFI reduction from 4,082 and 3,796 s/L^2 to 1,715 and 1,883 s/L^2 which are of before and after backwashing, respectively (Zone I), implying that only small amount of coagulant dosage can help reduce membrane fouling as previously discussed. Enhanced coagulation (Zone II) allowed for reduction in ceramic membrane fouling with the lowest MFI values of 641/469 s/L^2 before/after backwashing observed at a pH 5.5 with a 5mg/L. It was noteworthy that the MFIs obtained after backwashing resulted in the same trend as those before backwashing, implying that coagulation prior to ceramic membrane filtration can potentially continue to mitigate membrane fouling for long term operation.

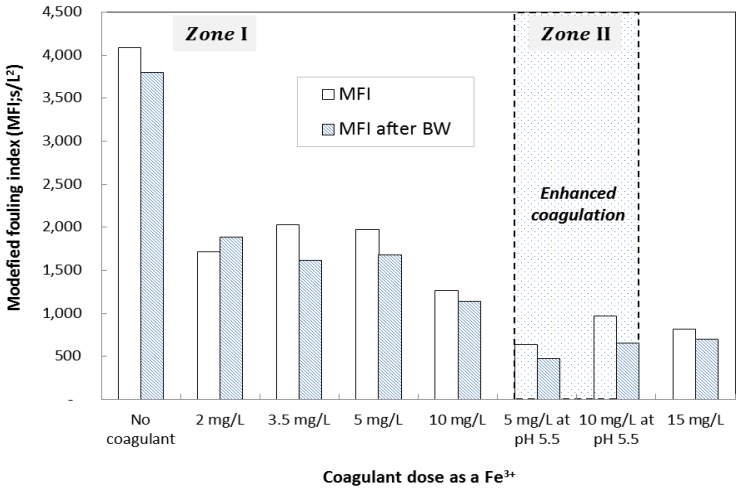

Figure 5.3 – Comparison of modified fouling index (MFI) before/after backwashing as function of coagulant dose as a Fe^{3+} at pH 7.6 and 5.5

The t/V curves as function of filtered volume V after backwashing were assessed to understand the possibility of combining fouling mechanisms during the entire filtration period, as shown in Figure 5.4. The curve can be divided into two regions of pore-blocking and cake filtration portion sequent from left to right as shown in Figure 5.4. The very left region depicts a steep and convex trend while the second region shows rather a gentle and straight linear trend, implying that pore blockage causes flux to significantly go down as soon as filtration starts, and followed by relatively gentle flux-down as cake layer becomes formed as pores are completely or partially blocked. The curves of t/V as function of V are classified in to three groups as shown in Figure 5.4. First, a group of 15 mg/L at a pH 7.6, 5 and 10 mg/L at a pH 5.5 describes the gentlest jump-up amongst other groups, followed by second group of 10, 3.5, 5 and 2 mg/L at an ambient pH of 7.6 and lastly no coagulant. These results indicates that enhanced coagulation, e.g. 10 mg/L and 5 mg/L at a pH 5.5 significantly might mitigate pore blocking with lower coagulant addition than that required for convention coagulation. In spite of that, when coagulant dosage becomes higher up to 15 mg/L or potentially more, pore blocking could be also reduced to the same level as

shown in Figure 5.4. The second region, a cake filtration part also shows consistency in the first pore-blockage region.

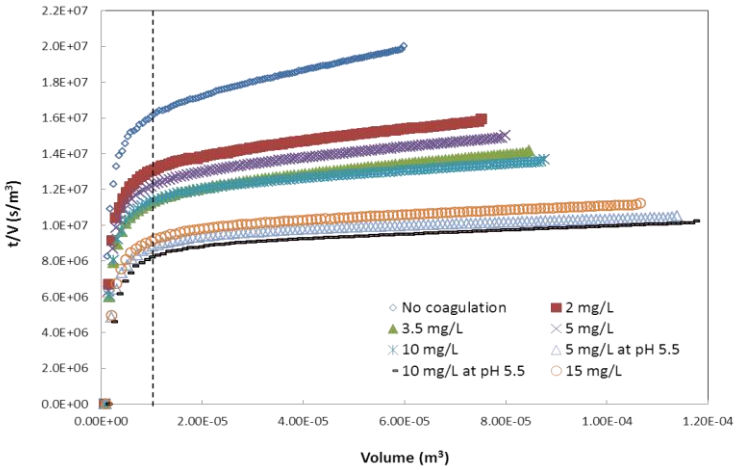

Figure 5.4 – t/V curves as function of filtered volume V after backwashing: each curve was obtained according to different coagulant doses at pH 7.6 (ambient) and 5.5

5.3.2.2. Determination of fouling mechanisms

In order to confirm fouling mechanisms of ceramic membrane filtration with precoagulation, foulants resistance (R_f) was differentiated into pore-blocking-caused resistance (R_b) and cake-formation-caused resistance (R_c) as shown in Figure 5.5. Assuming that foulants accumulated on membrane can be rejected by hydraulic backwashing, the membrane fouling can be defined as a reversible fouling, while the rest of foulants which are still remained inside membrane pores can be described as an irreversible fouling. As previously mentioned in section 5.2.6, R_c is first acquired after backwashing a fouled membrane, and then R_b is calculated by subtracting R_c from total resistance R_t that is already obtained from a membrane fouled through 40 minutes filtration before backwashing.

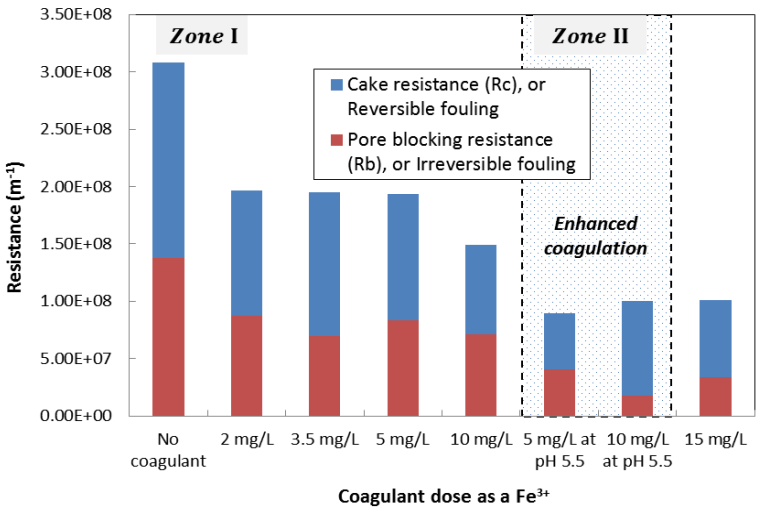

Figure 5.5 - Differentiation of membrane resistances caused by pore blocking and cake formation as function of coagulation dose as Fe^{3+} at pH 7.6 (ambient) and 5.5

Enhanced precoagulation significantly reduced the resistance caused by pore blockage, or irreversible fouling with the lowest resistance observed with a 10 mg/L of coagulant dose at a pH 5.5 as shown in Figure 5.5 (Zone II). It was noticeable that even if 10 mg/L at a pH 5.5 resulted in higher resistance than 5 mg/L at the same pH, the pore-blocking-caused-resistance (R_b) was even smaller than the result from 5 mg/L dosage, reconfirming the observance in the very first region in t/V versus V curves in Figure 5.4. A higher coagulant dose of 15 mg/L at an ambient pH of 7.6 (Zone III) was capable of achieving the resistance which is close to the result from 10 mg/L at a pH 5.5, however, the irreversible fouling, or R_b was higher than 10 mg/L at a pH 5.5 (Zone II).

In summary, enhanced coagulation was found to allow ceramic membrane fouling to significantly decrease in terms of not only pore-blockage, but cake filtration, leading to improvement of membrane performance with significantly small amount of coagulant dosage of 5 mg/L as Fe^{3+} at a pH 5.5. The result corresponded to 15 mg/L

of the dosage under conventional coagulation condition, i.e. at pH 7.6. However, a higher dosage of 10 mg/L at a pH 5.5 resulted in the lowest pore-blocking-caused-resistance (R_b) associated with the least irreversible fouling.

5.3.3. NOM characterization

To understand the effects of coagulation pretreatment, particularly enhanced coagulation on organic foulants, natural organic matter (NOM) in various pretreated waters – raw and coagulated at different pH of 7.6 and 5.5 – prior to MF ceramic membrane filtration was characterized using LC-OCD and 3-dimentional FEEM spectrophotometry.

5.3.3.1. LC-OCD analyses

Figure 5.6 compares LC-OCD chromatographic peaks after various coagulation pretreatments. The chromatographic peaks can be classified into five fractions with respect to retention time, peak shape and detector ratio of NOM (Huber et al. 2011): fraction A - higher molecular weight (MW) biopolymers such as polysaccharides (PS) and proteins, the MW range of which should be 10 KD or higher as the column has a separation range of 0.1-10 KD; fraction B - medium MW humic substances (HS) consisting of humic and fulvic acids; fraction C – building blocks (Volk et al.) reflecting breakdown products of HS or HS-like material of lower molecular weight; fraction D – low molecular-weight (LMW) acids co-eluted with LMW-HS; fraction E – LMW neutrals corresponding to LMW alcohols, aldehydes, ketones, sugars, and amino acids.

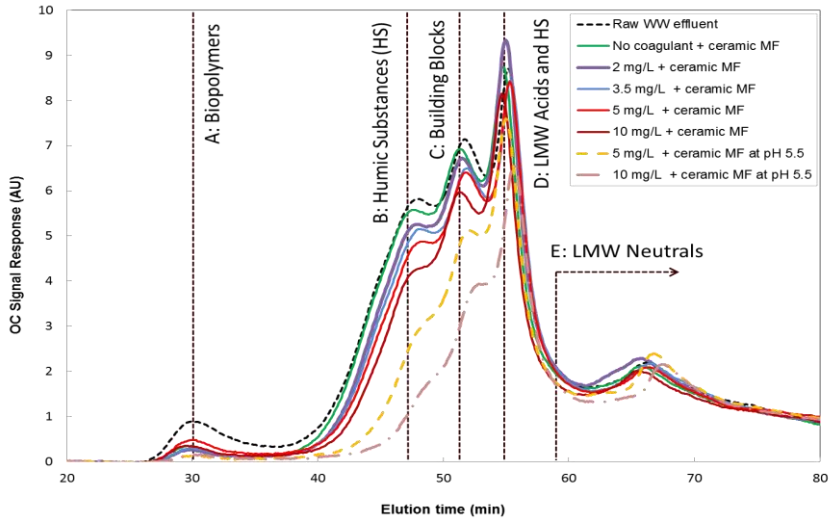

Figure 5.6 - NOM characterization of treated waters by different doses (as Fe^{3+}) of coagulation prior to ceramic membrane filtration at pH 7.6 (ambient) and 5.5 using size exclusion chromatography

As shown in Figure 5.6, a majority of the organic materials remained the same as raw WW effluent when only MF membrane filtration was used. However, the rejection of NOM was observed for the fraction of biopolymers (A) that have been reported as the problematical foulants for low pressure membranes (Amy 2008). With increased coagulant dose, NOM removal was improved in proportion to the dosage in terms of biopolymers (A), HS (B), building blocks (C), and LMW acids (D). Especially, the removal efficiency was significantly enhanced at a pH 5.5 compared with those of an ambient pH of 7.6. This might occur because both mechanisms, which are charge neutralization and sweep coagulation, dominated interactions of NOM with hydrolysis species and precipitating hydroxide in sequence at a low pH of 5.5, corresponding to enhanced coagulation condition.

Figure 5.7 shows the removal efficiency of DOC, biopolymers, and humic substances (HSs) by coagulation prior to ceramic MF membrane filtration in accordance with different coagulant dosage and pH. Overall, DOC removal was improved as coagulant

dosage increased, and remarkably enhanced as pH was lowered to 5.5 from 7.5, resulting in by 22% and 32% removal with 3.5 mg/L and 10 mg/L of the dosage as Fe^{3+} at pH 7.5, respectively, and by 50% with 10 mg/L at pH 5.5. Biopolymers was found to be easily removed up to 60 ~ 71% by ceramic MF itself or in combination with precoagulation, and by 85% with enhanced coagulation. Humic substances (HSs) removal relied on coagulant dosage and pH with the highest efficiency observed at pH 5.5 with 10 mg/L if the dosage, resulting in 67% removal.

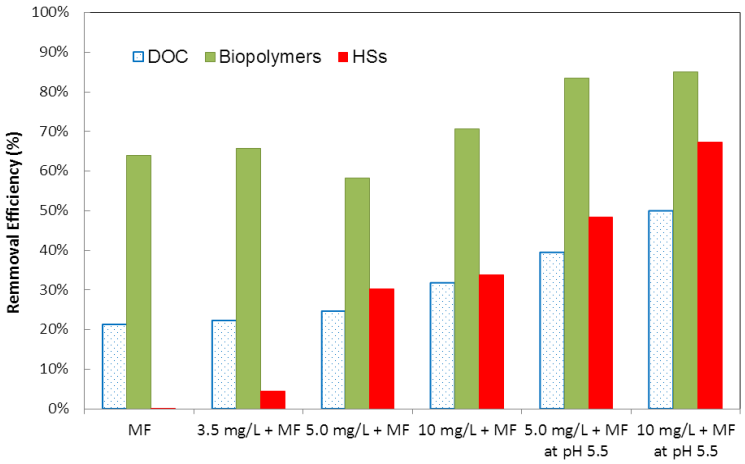

Figure 5.7 – NOM removal efficiency by coagulation prior to ceramic MF membrane filtration in terms of DOC, biopolymers, and humic substances (HS) as a function of different coagulant doses as Fe^{3+} at pH 7.6 and 5.5

Figure 5.8 represents another example which is characterized with LC-OCD containing a higher fraction of biopolymers than other fractions. It is demonstrated that if biopolymers occur at a high proportion wastewater effluent, especially when dominating NOM composition, MF membrane filtration itself can satisfy effective removal without any other additional treatments. It is hypothesized that the majority of biopolymers might be bigger than the pore size of MF (i.e. 0.14 μm), so that they could be easily rejected with the MF membrane itself by size exclusion. Another possible hypothesis is that there might be adsorption of biopolymers onto the ceramic

membrane. However, the membrane fouled with biopolymers may cause severe membrane fouling which is irreversible with backwashing. On the other hand, other NOM fractions (i.e. HS, building blocks, and LMW acids and LMW-HS) still remain using MF filtration alone but are reduced to a certain extent with 10 mg/L coagulant dose as Fe^{3+} as observed in Figure 5.6.

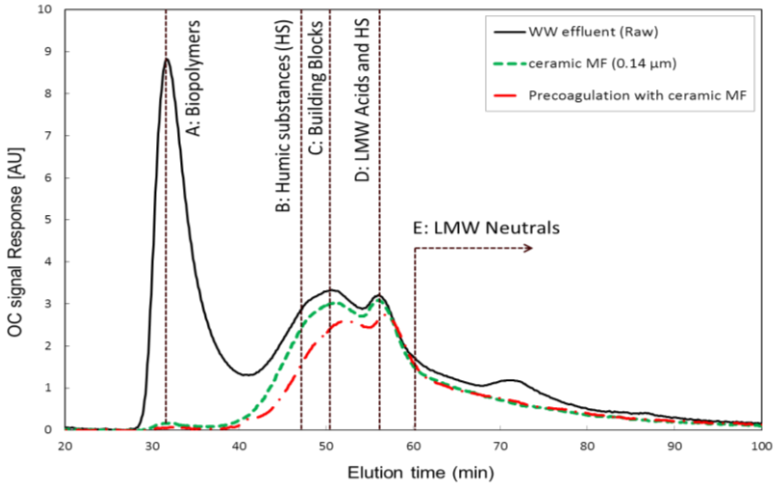

Figure 5.8 – NOM characterization of three waters – raw which comprises a high concentration of biopolymers, MF treated, and precoagulation with MF treated - using size exclusion chromatography with organic carbon detection (LC-OCD), where coagulant dose is 10 mg/L as Fe^{3+} at an ambient pH of 7.5

In summary, biopolymers can be relatively easy to remove than other NOM fractions with MF membrane itself even though causing problematical fouling of the membrane. However, humic substances (HSs) could not be removed by MF alone, but effectively removed with precoagulation treatment to a great extent, which was more significant at a pH 5.5.

5.3.3.2. Fluorescence 3-dimentional EEM analyses

3-dimentional fluorescence excitation-emission matrix (EEM) spectrophotometry was applied to investigate the characterization of dissolved organic matter (DOM) where the same samples as those for LC-OCD (Figure 5.6) were analysed. Three distinctively different types of fluorescence signals were observed from raw WW effluent, including humic-like and protein-like NOM as follows: peak A represents secondary humic-like ($\lambda_{ex/em} = 237{\sim}260/380{\sim}460$ nm); peak C presents primary humic-like ($\lambda_{ex/em} = 300{\sim}370/380{\sim}480$ nm); peak T denotes protein-like ($\lambda_{ex/em} = 275/310{\sim}340$ nm) as shown in Figure 5.9 (Baker and Genty 1999, Coble 1996, Henderson et al. 2009, Liu et al. 2007).

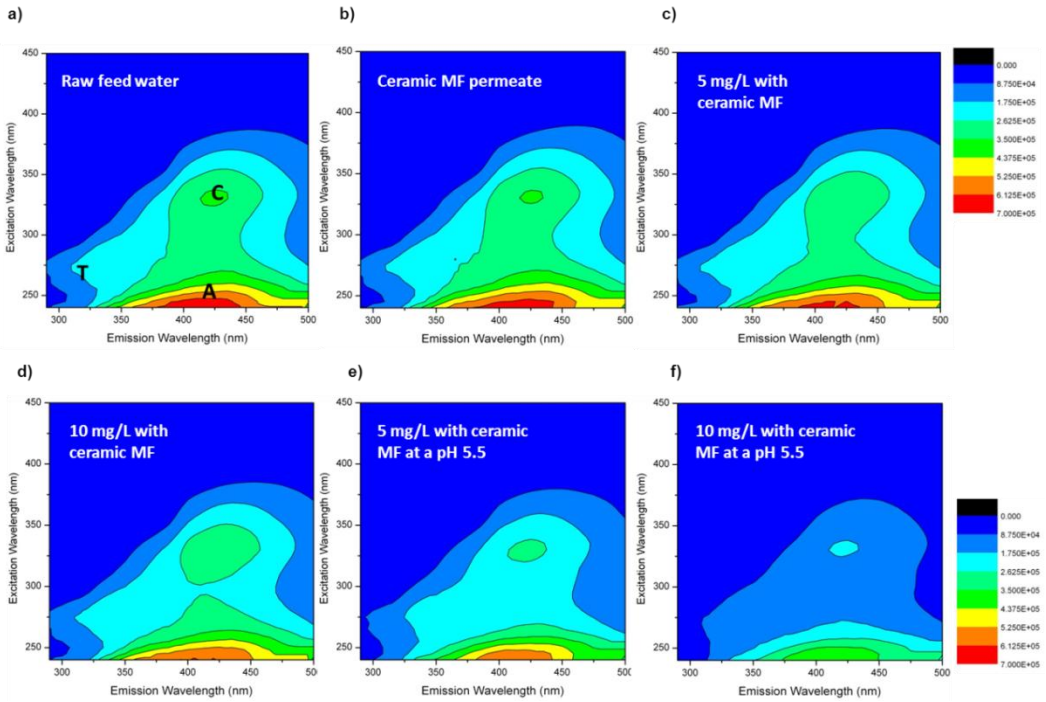

Figure 5.9 – NOM characterization of treated waters by different doses (as Fe^{3+}) of coagulation prior to ceramic membrane filtration at pH 7.6 (ambient) and 5.5 using 3D fluorescence excitation-emission matrixes (FEEM)

Permeate from MF ceramic membrane filtration exhibited similar fluorescent properties to raw WW effluent and little difference between them was observed as shown in Figure 5.9-a and-b, indicating that MF membrane filtration itself was not effective in removing NOM. However, when precoagulated waters with 5 mg/L and 10 mg/L as Fe3+ were fed prior to the MF membrane, the intensity of peaks A and C were lowered, as shown in Figure 5.9 c and d. It was observed that when pH was adjusted to 5.5, both intensities of A and C were decreased down to two times less than those at ambient pH 7.5, as shown in Figure 5.9 e and f. Regarding the peak T of protein-like NOM, there was little influence at ambient pH, but significant effect on the fluorescence intensity at pH 5.5 was observed. This was more distinct under the condition of a higher dosage of 10mg/L at lower pH range. These were consistent with results that were characterized using LC-OCD.

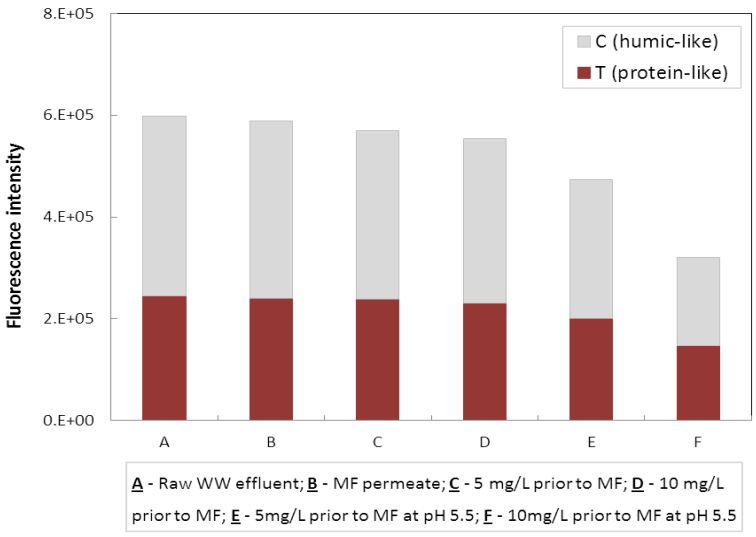

Figure 5.10 - Fluorescence intensities (and T/C ratio) which are measured with 3D-FEEM at peak T ($\lambda_{ex/em} = 275/340$ nm) and peak C ($\lambda_{ex/em} = 325/425$ nm) for treating wastewater effluent by coagulation prior to ceramic MF membrane filtration as function of different coagulant dosage and pH of 7.5 and 5.5

Specific wavelength pair intensities were extracted from EEMs, such as tryptophan-like ($\lambda_{ex/em} = 275/340$ nm) and humic-like ($\lambda_{ex/em} = 325/425$ nm), and analysed as a ratio (T:C) to reveal the relative changes in fluorescence EEM character for each treated water sample. The reason why tryptophan-like peaks were specifically chosen was because NOM originating from microbial activity in an anoxic-oxic (AO) process that was sampled for this study was richer in tryptophan-like than the other protein-like OM (Hambly et al. 2010). Overall, the ratio of tryptophan-like (T) to humic-like (C) fluorescence (T:C) was between 0.69 and 0.84 from raw WW effluent (A) through coagulation pretreatment with a 10 mg/L of Fe3+ at pH 5.5 prior to MF permeate (F) in spite of decreases in fluorescence intensity as shown in Figure 5.10. This finding was the same as that of LC-OCD, indicating that humic-like OM were relatively more plentiful than protein-like OM, which are associated with humic substances (HS) and biopolymers in LC-OCD, respectively. It was noted that not only the fluorescence intensities of samples at pH 5.5 (E, F) were significantly decreased in terms of both T and C, but also more reduced humic-like fluorescence intensity was observed, showing an increase in the T:C ratio from about 0.70 to 0.74 (E) and 0.84 (F), as shown in Figure 5.10.

5.4. CONCLUSIONS

Ceramic MF membrane could play an important role in treating secondary wastewater effluent when combined with precoagulation, leading to enhanced membrane performance in terms of permeability, filterability, and NOM removal. The most

critical parameters for precoagulation were found to be pH in association with coagulant dosage.

Ceramic membrane flux increased in proportion to coagulant dosage with the highest permeability observed at 15 mg/L of the dosage as Fe^{3+} at pH 7.6 (i.e. under conventional coagulation condition). At low pH range of 5.5 or possibly lower (i.e. under enhanced coagulation condition) the membrane flux was capable of significantly being improved with small amount of the dosage (i.e. 5 mg/L), which was better than 15 mg/L at pH 7.6.

Foulants resistance against a ceramic membrane was reduced by precoagulation, which was inversely proportional to coagulant dosage, in particular, enhanced coagulation under low pH of 5.5 led to significantly reduced resistance with the lowest resistance observed with 5 mg/L as Fe^{3+} at a pH 5.5. This result corresponded to 15 mg/L of the dosage under conventional coagulation condition, (i.e. at pH 7.6). However, a higher dosage of 10 mg/L at a pH 5.5 resulted in the lowest pore-blocking-caused-resistance (R_b) associated with the least irreversible fouling.

Both LC-OCD and 3D-fluorescence excitation-emission matrix, which are component-specific analysers demonstrated that NOM was effectively able to be removed by coagulation prior to MF ceramic membrane filtration. Especially, biopolymers could be easily eliminated to a significant extent by ceramic membrane itself or with precoagulation under any pH states. Moreover, with decreased pH and increased dosage, humic substances, which are difficult to treat and pass through a MF membrane, could also be effectively rejected to such a level.

In conclusion, it is expected that because of the robustness of ceramic membrane, enhanced coagulation as a pretreatment which is treated under strongly acid state can be used to successfully treat impaired-quality source waters such as wastewater effluent in water reuse application, resulting in significantly improved membrane performance and NOM removal with even smaller amount of coagulant dosage than that under conventional coagulation condition. Nonetheless, Precoagulation with ceramic membrane filtration under any pH states could achieve preferential removal of humics over non-humics.

5.5. REFERENCES

Amy, G. (2008) Fundamental understanding of organic matter fouling of membranes. Desalination 231(1-3), 44-51.

Baker, A. and Genty, D. (1999) Fluorescence wavelength and intensity variations of cave waters. Journal of Hydrology 217(1-2), 19-34.

Boerlage, S.F.E., Kennedy, M., Tarawneh, Z., De Faber, R. and Schippers, J.C. (2004) Development of the MFI-UF in constant flux filtration. Desalination 161(2), 103-113.

Boerlage, S.F.E., Kennedy, M.D., Aniye, M.P., Abogrean, E.M., Galjaard, G. and Schippers, J.C. (1998) Monitoring particulate fouling in membrane systems. Desalination 118(1-3), 131-142.

Burggraaf, A.J. and Cot, L. (1996) Fundamentals of inorganic membrane science and technology, Elsevier.

Coble, P.G. (1996) Characterization of marine and terrestrial DOM in seawater using excitation-emission matrix spectroscopy. Marine Chemistry 51(4), 325-346.

Garmash, E.P., Kryuchkov, Y.N. and Pavlikov, V.N. (1995) Ceramic membrane for ultra- and microfiltration (Review). Glass and Ceramic 52(6), 150-152.

Guigui, C., Rouch, J.C., Durand-Bourlier, L., Bonnelye, V. and Aptel, P. (2002) Impact of coagulation conditions on the in-line coagulation/UF process for drinking water production. Desalination 147(1-3), 95-100.

Hambly, A.C., Henderson, R.K., Storey, M.V., Baker, A., Stuetz, R.M. and Khan, S.J. (2010) Fluorescence monitoring at a recycled water treatment plant and associated dual distribution system - Implications for cross-connection detection. Water Research 44(18), 5323-5333.

Henderson, R.K., Baker, A., Murphy, K.R., Hambly, A., Stuetz, R.M. and Khan, S.J. (2009) Fluorescence as a potential monitoring tool for recycled water systems: A review. Water Research 43(4), 863-881.

Huang, H., Lee, N., Young, T., Gary, A., Lozier, J.C. and Jacangelo, J.G. (2007) Natural organic matter fouling of low-pressure, hollow-fiber membranes: Effects of NOM source and hydrodynamic conditions. Water Research 41(17), 3823-3832.

Huber, S.A., Balz, A., Abert, M. and Pronk, W. (2011) Characterisation of aquatic humic and non-humic matter with size-exclusion chromatography - organic carbon detection - organic nitrogen detection (LC-OCD-OND). Water Research 45(2), 879-885.

Karnik, B.S., Davies, S.H.R., Chen, K.C., Jaglowski, D.R., Baumann, M.J. and Masten, S.J. (2005) Effects of ozonation on the permeate flux of nanocrystalline ceramic membranes. Water Research 39(4), 728-734.

Konieczny, K., Bodzek, M. and Rajca, M. (2006) A coagulation-MF system for water treatment using ceramic membranes. Desalination 198(1-3), 92-101.

Lee, N., Amy, G., Croué, J.-P. and Buisson, H. (2004) Identification and understanding of fouling in low-pressure membrane (MF/UF) filtration by natural organic matter (NOM). Water Research 38(20), 4511-4523.

Lehman, S.G. and Liu, L. (2009) Application of ceramic membranes with pre-ozonation for treatment of secondary wastewater effluent. Water Research 43(7), 2020-2028.

Liu, R., Lead, J.R. and Baker, A. (2007) Fluorescence characterization of cross flow ultrafiltration derived freshwater colloidal and dissolved organic matter. Chemosphere 68(7), 1304-1311.

Meyn, T., Bahn, A. and Leiknes, T.O. (2008) Significance of flocculation for NOM removal by coagulation-ceramic membrane microfiltration, pp. 691-700.

Tchobanoglous, G., Darby, J., Bourgeous, K., McArdle, J., Genest, P. and Tylla, M. (1998) Ultrafiltration as an advanced tertiary treatment process for municipal wastewater. Desalination 119(1–3), 315-321.

Volk, C., Bell, K., Ibrahim, E., Verges, D., Amy, G. and Lechevallier, M. (2000) Impact of enhanced and optimized coagulation on removal of organic matter and its biodegradable fraction in drinking water. Water Research 34(12), 3247-3257.

Chapter 6

Ozone-Ceramic Membrane Hybrid for Filtration of Impaired-Quality Source Waters

Phase 3-1: Effects of ozone-induced flocculation of particles on ceramic membrane filtration in the presence of calcium (Ca^{2+}) and magnesium (Mg^{2+})

Effects of ozone-induced flocculation of particles on ceramic membrane filtration in the presence of calcium (Ca^{2+}) and magnesium (Mg^{2+})

ABSTRACT

Ceramic membranes have many attractive advantages in terms of their inherent mechanical, thermal and chemical stability, allowing them to have a higher permeability and a longer lifetime than polymeric membranes. Because of the robustness of ceramic membranes, strong oxidants such as ozone (O_3) can be employed as a pretreatment to improve membrane performance reducing the membrane fouling. This study aimed to assess ozone effects on MF/UF ceramic membrane filtration for treatment of impaired-quality source waters (e.g., seawater and wastewater). Bench-scale experiments demonstrated that due to the ozone-resistance nature of the ceramic membranes, preozonation allows the ceramic membranes to operate at sustainably higher flux for filtration of impaired-quality source waters, such as seawater and WW effluent. It was noteworthy that preozonation led to more significant flux improvement when treating seawater rather than WW effluent, which was attributed to the high presence of calcium and magnesium acing as a positive factor to reduce membrane resistance. Several analytical methods such as SEM-EDX, AFM, UVA_{254}, TEP visualization and zeta potential (ζ) revealed that not only does O_3 degrade NOM molecules (particularly transparent exopolymeric particles (TEP)) which mostly cause problematical fouling into smaller fragments, but it also help to form microflocs as a result of ozone-

induced organic matter binding with divalent cations, such as calcium and magnesium in seawater. In particular, SEM-EDX and AFM confirmed that the aggregation of ozone-induce particles porous and loose resulted in cake filtration instead of pore blockage. It is expected that these attractive features help to effectively achieve sustainable flux when ceramic membranes are applied for treating impaired-quality source waters, especially more significant for seawater pretreatment.

Keywords: ceramic membrane, seawater pretreatment, ozone, TEP

6.1. INTRODUCTION

Increasing demand on water resources for domestic, industrial and agricultural purposes, along with water quality deterioration, scarcity and other negative impacts caused by a climate change, have been becoming the major factors that many countries face challenges of drinking water supply. Especially, fresh waters relying on capturing surface water have been critically limited in many countries of Middle East area, Europe, USA, Australia and other regions (Wade Miller 2006). Impaired-quality source waters, such as wastewater and seawater instead of depleted fresh source waters, have been gradually exploited as one of the alternative solutions to address these challenges for the past several decades (Casani et al. 2005, Crook and Surampalli 1996, Fähnrich et al. 1998). Wastewater treatment plant (WWTP) effluent is characterized by organic membrane foulants with a biological signature, which interact with the high concentrations of colloids and micro-particles in the feed water source, and the membrane surface (Tchobanoglous et al. 1998, Zularisam et al. 2011), while seawater is characterized as high salt concentration, presence of refractory organic foulants, and biological activity.

Microfiltration (MF) and Ultrafiltration (UF) have been widely employed as preferred pretreatment technologies for treatment of seawater and WW effluent (Voutchkov 2010). In spite of the excellent retention characteristics of membrane filtration, an inevitable problem that constrains its growth is fouling, which is a main factor increasing the cost of operation and maintenance by deteriorating sustainable membrane performance and shortening their lifetime (Lee et al. 2005b, Lehman and Liu 2009, Seidel and Elimelech 2002). Particularly, it has been shown that one of the

major obstacles to slow down further application of membrane technology is organic fouling associated with bulk natural organic matter (NOM), further influenced by interactions between NOM and particles causing rapid and problematical fouling of polymeric membranes (Amy 2008, Huang et al. 2007, Lee et al. 2008, Lee et al. 2004, Zularisam et al. 2011).

Membrane fouling is usually minimized by pretreatments such as precoagulation and/or powdered activated carbon or, alternatively, a very conservative membrane flux and a short backwashing interval (Konieczny et al. 2006). The emerging use of ozone (O_3) oxidation can offer new opportunities because O_3 is able to efficiently transform the physico-chemical characteristics of NOM to reduce membrane fouling and increase permeability (Van Geluwe et al. 2011). Some researchers have observed that ozonation could decompose NOM molecules that are present in natural surface waters and WW effluents into smaller fragments (Kim et al. 2008, Lee et al. 2005c, Lehman and Liu 2009, Nissinen et al. 2001, Song et al. 2004, Song et al. 2010). On the other hand, it has been reported that ozone (O_3) when used as a preoxidant in water treatment can assist in the destabilization and aggregation of particles by one or a combination of several hypothesized mechanisms as follows (Chandrakanth et al. 1996, Nguyen et al. 2013, Oh et al. 2009): (1) increase in carboxylic acid content by ozonation, leading to greater metal (calcium, magnesium and aluminium) association with the ozone-induced NOM; (2) reduction in the molecular weight of adsorbed organics, causing desorption of stabilized organic coatings from the surface of clay; (3) polymerization of NOM leading to particle aggregation via bridging reactions; (4) rupture of complexes of iron and manganese, resulting in an in situ production of coagulant; (5) algae lysis and biopolymers liberation, acting as coagulating polymer.

Ceramic membranes are expected to play an important role in both drinking water and water reuse applications instead of polymeric membranes that have been predominantly used for the past couple of decades. Ceramic membranes have many attractive attributes in terms of their inherent mechanical, thermal and chemical stability (Lee and Cho 2004). The principal chemical properties are their hydrophilicity (Dafinov et al. 2002, Larbot et al. 2004) and amphoteric surface charge due to the presence of hydroxyl (OH^-) groups on their surface, contributing to high permeability and influencing separation ability and fouling potential (Dafinov et al. 2002). Furthermore, ceramic membranes can provide excellent backwash efficiency and mitigate NOM fouling with incorporation of various chemical treatments such as coagulation under low pH range and/or ozone (O_3) treatment (Konieczny et al. 2006, Lehman and Liu 2009, Meyn and Leiknes 2010).

An ozone (O_3) – ceramic membrane *hybrid* can be effectively applied for treatment of impaired-quality source waters because of the combination of the strong oxidation ability of ozone (O_3) and the robustness of the ceramic material. It is hypothesized that not only does ozone (O_3) degrade NOM molecules which mostly cause problematical membrane fouling into smaller fragments, but it also helps to form microflocs as a result of ozone-induced NOM binding with divalent inorganic cations, such as calcium and magnesium highly present in seawater. Eventually, these features are expected to help effectively achieve enhanced performance when treating impaired-quality source waters (e.g., high-organic surface water, WW effluent, brackish water and seawater).

This study aimed to investigate the effects of ozone (O_3) as a pretreatment when combined with ceramic membrane filtration for seawater and WW effluent. The bench-scale test focused on assessing aggregation effects of ozone-induced particles on membrane permeability and demonstrating fouling mechanisms in the presence of metal ions such as calcium and magnesium. The specific objectives of the research are 1) to assess the filterability of two different kinds of ceramic membranes as a function of ozone dose for treatment of both seawater and WW effluent; 2) to characterize membranes fouled with/without ozonation using a scanning electron microscopy (SEM) with energy-disperse X-ray spectroscopy (EDX) and atomic force microscopy (AFM) as membrane autopsy tools; 3) to identify trans exopolymer particles (TEP) accumulated on the membrane surface and measure zeta potential (ζ) of particles transformed by ozone; 4) to understand fouling mechanisms (i.e., foulants behaviours) when ozone is applied for seawater pretreatment.

6.2. MATERIALS AND METHODS

6.2.1. Source waters

Seawater and secondary WW effluent sampled from the Red Sea and a local WW treatment plant in Jeddah, Saudi Arabia, respectively, were used for experiments. Throughout the whole experimental period, feed water was adjusted to room temperature between 19.5°C and 22.5°C, which was established after the waters had been removed from cold storage for a half-day before starting each set of tests. The seawater sample was collected about 1.5 m above the bottom near the intake of a local

desalination treatment plant. The water quality analysis is provided in Table 6.1. The secondary WWTP effluent is treated by an anoxic-oxic (AO) activated sludge process. The pH ranged from 7.6 to 7.75. The DOC was between 5.5 mg/L to 6 mg/L and UVA_{254} from 0.15 cm^{-1} to 0.175 cm^{-1}, corresponding to SUVA values from 2.7 L/mg·m to 2.9 L/mg·m. Calcium concentration was 76 mg/L. Both seawater and secondary WW effluent were prefiltered with a 0.45μm filter.

Table 6.1 –Seawater quality analysis at experiment site

Parameter	Concentration	Parameter	Concentration
pH	7.8	Calcium, mg/L Ca	527
Turbidity, NTU	< 1	Chlorides, mg/L Cl	22,199
SDI	2	Copper, µg/L Cu	10
DOC, mg/L	≈ 1.0	Fluoride, mg/L F	1.6
UVA_{254}, cm^{-1}	≈ 0.012	Iron, µg/L Fe	< 2
SUVA L/mg·m	1.2±0.2	Magnesium, mg/L Mg	1,436
TDS, mg/L	≈ 41,000	Manganese, µg/L, Mn	< 1
Aluminium, µg/L Al	90	Silica, mg/L SiO_2	0.4
Barium, µg/L Ba	6	Sodium, mg/L Na	12,470
Boron, µg/L	87	Strontium, mg/L Sr	7.99
Bromides, mg/L Br	67.8	Sulphate, mg/L, SO_4	3,330

6.2.2. Experimental setup

6.2.2.1. Ceramic membrane specifications

Two types of ceramic membrane discs, designated as TAMI and AAO, were used for bench-scale tests. The commercially available TAMI ceramic membrane (INSIDE DISRAM™, TAMI INDUSTRIES, France) is fabricated by sintering, while the AAO membrane (Anodisc™, Whatman, USA) is obtained by means of anodic oxidation process. Simple specifications of the membranes are summarized in Table 6.2.

Table 6.2 – Description of two ceramic membrane discs used for experiments

	TAMI		AAO	
	MF	UF	MF	UF
Pore size, or MWCO	0.14μm	150KD	0.1μm	20nm
Materials	$ZrO_2 + TiO_2$	$ZrO_2 + TiO_2$	Al_2O_3	Al_2O_3
Effective surface area (cm^2)	17.4	17.4	17.4	3.14

6.2.2.2. Membrane filtration and ozonation unit

Figure 6.1 shows the scheme of the ceramic membrane filtration unit which is capable of being operated in two different modes. Two types of ceramic membrane discs were employed with a special holder, where feed waters – raw water and preozonated water – were filtered through each membrane disc placed inside the holder in a dead-end filtration mode (mode 1 for AAO; mode 2 for TAMI). The permeated water was monitored as function of time and filtered volume (i.e., flux).

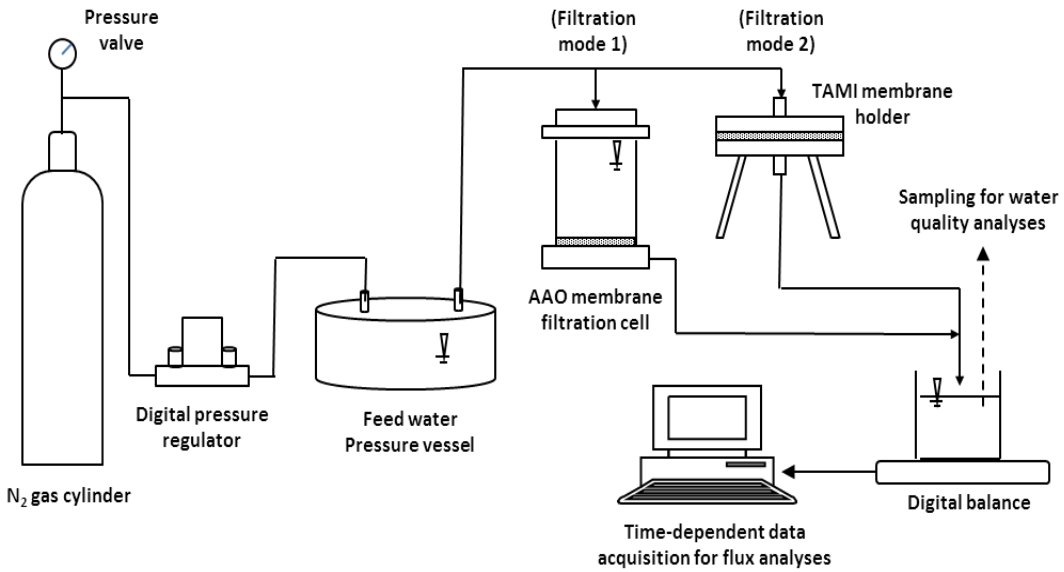

Figure 6.1 - Scheme of ceramic membrane filtration unit in two different modes that are separately operated for AAO membranes (mode 1) and TAMI membranes (mode 2)

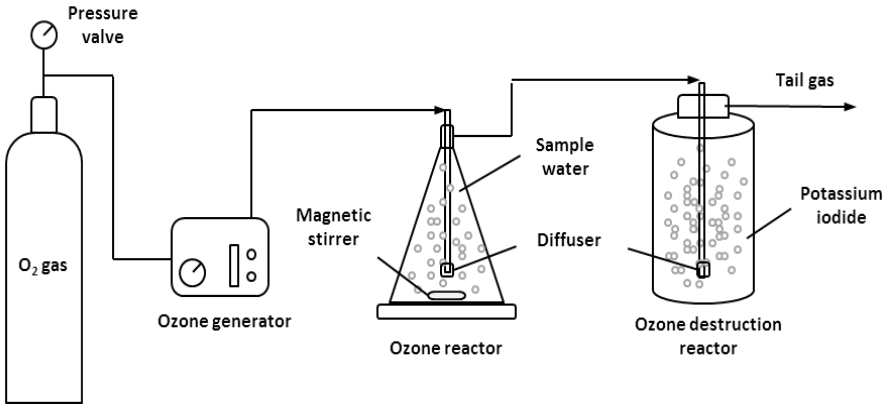

Figure 6.2 – Schematic diagram of ozone pretreatment setup carried out prior to ceramic membrane filtration

Figure 6.2 shows the ozone pretreatment setup used for the study, consisting of an ozone generator (Degremont Technologies- Triogen, Scotland), a static reactor flask (2L), and a gas destruction reactor with potassium iodide. Pure oxygen gas from a gas cylinder was fed to the ozone generator. Ozone dose was controlled through adjusting ozone contact time. A magnetic stirrer at the bottom of the ozone reactor was used with a diffuser, increasing ozone diffusivity in water as shown in Figure 6.2. Exhausted ozone gas was captured with a 4% KI solution. Dissolved ozone in the ozone reactor was measured by the indigo method. As soon as a set of ozonation test was completed, the ozonated water was transferred in a pressure vessel 1 (Figure 6.1), immediately performing ceramic membrane filtration.

6.2.3. Analytical methods

6.2.3.1. Flux calculation

Permeate flux (J; L/m^{2}h) was calculated as the flow rate of permeate water (Q; L/h) divided by the effective surface area of the membrane (A; m^2). The filtered water was monitored as function of time (t; s) and filtered volume (V; m^3), where the permeated

volume was recorded at 10 second intervals under a certain pressure over 30 minutes of filtration. Specific flux (J_s; $L/m^2h \cdot bar$) refers to the filtrate flux (J) that has been normalized by the transmembrane pressure (TMP). Normalized flux (J/J_0) is calculated as the ratio of flux to the initial flux at the beginning of the filtration (J_0; L/m^2h).

6.2.3.1. Scanning electron microscopy (SEM)

Membrane specimens were cryogenically preserved in slush nitrogen at –210°C followed by controlled dehydration in a freeze drying instrument (K775X Turbo; Quorum, UK). A scanning electron microscope (SEM) (FEI, USA) equipped with a cryo stage and cryo preparation chamber (Quorum, UK) was used to image virgin ceramic membranes. Focused Ion Beam (FIB) technique in combination with SEM was used for cross sectional imaging of the samples. Energy Dispersive X-ray Spectroscopy (EDS or EDX) was used for elemental analysis conducted as spot or mapping analysis.

6.2.3.2. Atomic force microscopy (AFM)

AFM scans the material surface with a very fine tip and generates three-dimensional maps by detection of deflection of a laser beam reflected by a cantilever (Alldredge et al.). The AFM employed is made by digital instruments, and data are analyzed with built-in software in the analyzer. The tip size is 4~10 nm made of etched single crystal silicon. AFM was performed with a tapping mode. Tapping brings several advantages: higher lateral resolution on most samples, lower forces and less damage to soft samples imaged in air, and lateral forces are virtually eliminated (there is no scraping); however, it provides a slightly slower scan speed than contact mode AFM. Clean

membrane specimens were prepared with MQ water (≈18Ω) filtration and dried at room temperature to obtain an actual surface. Sample specimens were fixed on a glass slide and scanned over 5μm × 5μm for membranes. Images were obtained in amplitude mode and height mode at the same time. Amplitude mode provides a more detailed topographical view of the membrane surface in voltage units of the *Z*-axis range, and height mode offers nanometer scaled image analysis. A scan rate of 1~2 Hz was applied considering image features, membranes, and scan sizes.

6.2.3.3. Contact angle

Contact angle of ceramic membrane surfaces was measured using an optical tensiometer (Theta Lite, attention, Finland). The sessile drop method was selected for the measurement because it is a highly accurate and reproducible optical method, especially for contact angle measurement. The optical tensiometer records drop images and automatically analyzes the drop shape as a function of time; The captured images are analyzed with a drop-profile fitting method in order to determine contact angle.

6.2.3.4. Transparent exopolymer particles (TEP) visualization

TEP was visualized by microscopic pictures of stained TEP particles on the AAO ceramic MF membrane films that were used for real membrane performance. Alcian blue (0.025% solution), used to stain TEP, was prepared by mixing a 300 mL of ultrapure water with 0.075 g of Alcian blue 8GX powder (SIGMA-ALDRICH®) for 18 hours at 1000 rpm. Before adding the Alcian blue powder, the pH of the ultrapure water was adjusted to 2.5 by adding several drops of acetic acid. For staining TEP, 1) a piece of a ceramic membrane sample (47 mm in diameter) fouled after each

experiment was placed on a petri-dish; 2) The sample was soaked in ultrapure water for about 1 minute and then the water was carefully discarded; 3) The sample was soaked in the 0.025% Alcian blue solution for about 10 minutes, with the solution then discarded; 4) Finally, the sample was rinsed one last time with ultrapure water for 1 minute and the water was discarded. The membrane samples stained were transferred to glass slides and then viewed and photographed using an optical microscope. The microscope used was an Olympus DP72 optical microscope set at 200 times magnification.

6.2.3.1. Zeta potential (ζ)

The electrophoretic mobility of particles was measured using a Zetasizer Nano instrument (Zetasizer Nano ZS90, Malvern Instruments Ltd, UK). 0.75ml of sample is placed in a folded capillary cell and zeta potential is measured using Laser Doppler Microelectrophoresis. For each sample, a minimum of five replicate measurements were made and the average of these measurements was reported. The standard deviation of replicate measurements was also described with error bars.

6.3. RESULTS AND DISCUSSION

6.3.1. Preozonation effects on membrane permeability

The effect of preozonation on TAMI and AAO ceramic MF/UF membrane filtration was investigated to treat both seawater and WW effluent. With ozone doses of 0, 3 and 6 mg/L, the membrane performance was evaluated by comparing the trend of

normalized flux decline as a function of filtered volume for 30 minutes of operation. The TAMI ceramic membrane was mainly employed for most tests, with the AAO ceramic membrane additionally tested for autopsies of fouled membranes.

6.3.1.1. Performance 1 - ozone dose of 3 mg/l (3mg O_3/mg DOC) for seawater

The flux variation of the TAMI MF and UF membranes with 3 mg/L of preozone was observed. The initial membrane flux was set to about 240 L/m^2h for UF and 580 L/m^2h for MF at 0.4 bar, corresponding to a specific flux of 600 L/m2h·bar and 1,450 L/m2h·bar, respectively.

As shown in Figure 6.3, fouling of each membrane with/without ozonation was evaluated by comparing the trend of normalized flux decline. The MF and UF membranes experienced different fouling behaviour with 3 mg/L of preozone treatment. Results showed that with 3 mg/L ozone dose, the normalized UF membrane flux increased to 88% of the initial flux from 73% without ozone, while the normalized MF flux conversely decreased to 74% of the initial flux from 89% without ozone.

When directly treating seawater without ozone, the MF membrane experienced less fouling than the UF membrane. From the result, it is assumed that the majority of particles in seawater might be distributed closer to the UF pore size (a molecular cut-off of 150 KDa) or slightly larger, causing severe fouling of the UF membrane by pore-blocking while there was less fouling of the MF membrane by, predominantly, cake filtration.

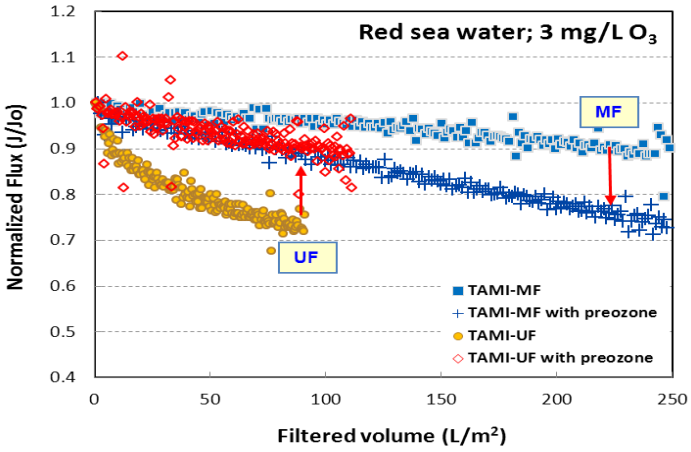

Figure 6.3 – Pre-ozone treatment effects on TAMI MF (0.14µm) and UF (150KD) ceramic membranes flux for seawater - ozone dose of 3 mg/L as O_3 (3 mg O_3/mg DOC)

It is hypothesized that ozone treatment shifted particle size distribution differently in its influence on the MF and UF ceramic membrane performances. There is no doubt that ozone decomposed NOM molecules into smaller MW fragments, however, the degraded particles did not play a role in increase of the MF flux, rather resulting in the flux decrease. Based on this result, degradation of NOM particles might not dominantly affect membrane fouling, because the majority of NOM foulants already are small enough to pass through the MF membrane pores with no ozonation.

Another fouling mechanism is that ozone might assist in the destabilization or aggregation of particles in the presence of calcium and magnesium in the Red Sea water (Ca^{2+} 527 mg/L and Mg^{2+} 1,436mg/L), leading to a shift in particle size distribution toward larger sizes. The aggregates induced by ozone would cause severe fouling for the MF, but less fouling for the UF, resulting in flux decrease versus flux improvement, respectively. The majority size of aggregated particles would be close to the pore size of the TAMI MF membrane, causing an increase in filtration resistance by pore blockage. Conversely, the aggregates might be big enough for the

UF membrane, leading to decrease in filtration resistance, or flux improvement by cake filtration as shown in Figure 6.3. Hypothesized fouling mechanisms for both TAMI MF and UF membrane filtration by ozonation are summarized in Table 6.3.

Table 6.3 – Hypothesized ozone effects on the TAMI ceramic membrane performance for seawater treatment, where ozone dose was a 3 mg/L)

Microfiltration (MF): 0.14µm	Ultrafiltration (UF): 150KDa
- Causing more pore blocking - Less cake filtration - Particles aggregated by ozone cause severe fouling, which is still not big enough for cake formation, but rather close to the pore size, leading to pore blockage	- Less pore blocking - More cake filtration - Particles micro-flocculated by ozone are large enough to form cake layer on the surface, causing less membrane resistance
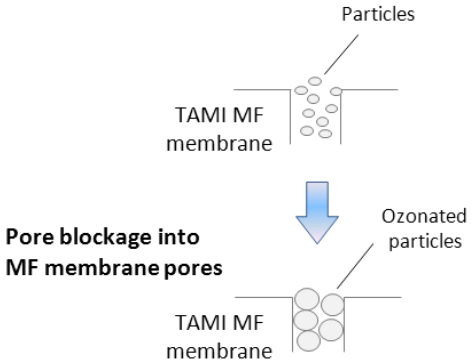	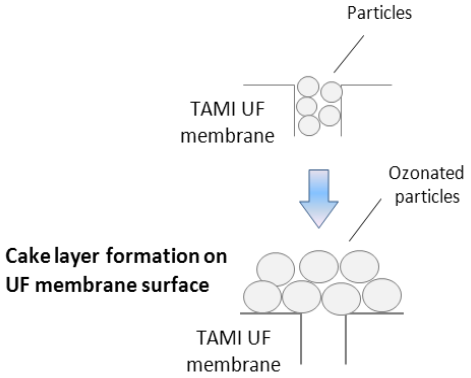

6.3.1.2. Performance 2 - ozone dose of 3 mg/l (0.5 mg O_3/ mg DOC) for WW effluent

WW effluent was studied under the same ozone dose and operational conditions with the TAMI MF and UF membranes. Results showed that preozonation at 3 mg/L (0.5 O_3/DOC) showed little influence on both MF and UF membrane filtration for WW effluent, showing slight flux improvement and no variation, respectively, as shown in Figure 6.4. In order to identify the degradation of humic substances (HS) versus non-

humics even if raw WW effluent contains relatively non-humic NOM (SUVA ≈ 2.7 ~ 2.9 L/mg·m), UVA_{254} removals of three waters – MF membrane filtered, ozone treated and ozone prior to MF filtered waters – were analysed as shown in Figure 6.5.

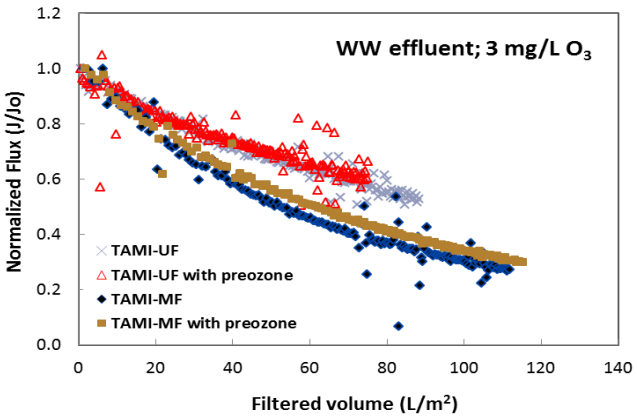

Figure 6.4 - Flux variation of TAMI MF/UF ceramic membranes with/without preozone treatment (3 mg/L as O3) for filtration of WW effluent

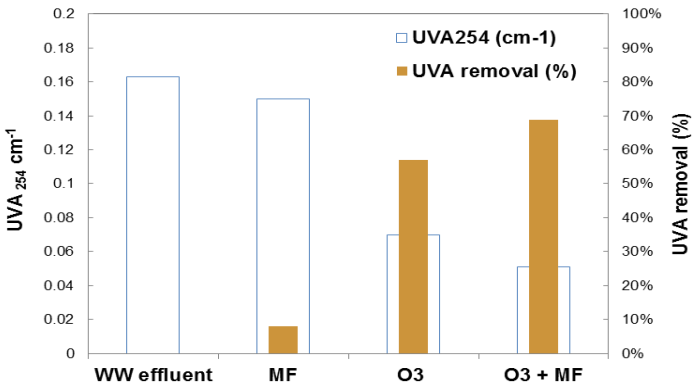

Figure 6.5 – UVA_{254} removal of three waters - TAMI MF treated, ozone treated and ozone prior to TAMI MF treated - for filtration of WW effluent with ozone dose of 3 mg/L (0.5 O_3/DOC)

Figure 6.5 compares removal of humic substances (HS) by TAMI MF membrane filtration, ozone treatment only, and ozone prior to TAMI MF filtration. The MF membrane only removed less than 10% of HS, while ozone and ozone with the MF achieved 57% and 70% removal of HS, respectively. Taking these results into account,

even though HS molecules in WW effluent are decomposed by ozone oxidation, they are already small enough to permeate both TAMI MF/UF ceramic membranes. Besides, there was no aggregation effect induced by ozonation on both MF and UF membrane fluxes observed, because there was no or little association with metal ions (Ca^{2+} 76 mg/L and Mg^{2+} 0mg/L).

6.3.1.3. Performance 3 - ozone dose of 6 mg/l (6 mg O_3/ mg DOC) for seawater

With increased ozone dose of 6 mg/L from 3 mg/L, AAO MF and UF ceramic membranes that have uniform pore-structure were additionally employed for filtration of seawater, comparing with TAMI ceramic membrane performances. Both TAMI and AAO membranes experienced less fouling with an ozone dose of 6 mg/L, showing significantly improved membrane flux as shown in Figure 6.6. In particular, the AAO MF and UF ceramic membranes experienced fully controlled fouling for the entire 30 minutes of operation, showing that the normalized flux of both MF and UF membranes was stabilized at 92~100% of the initial flux.

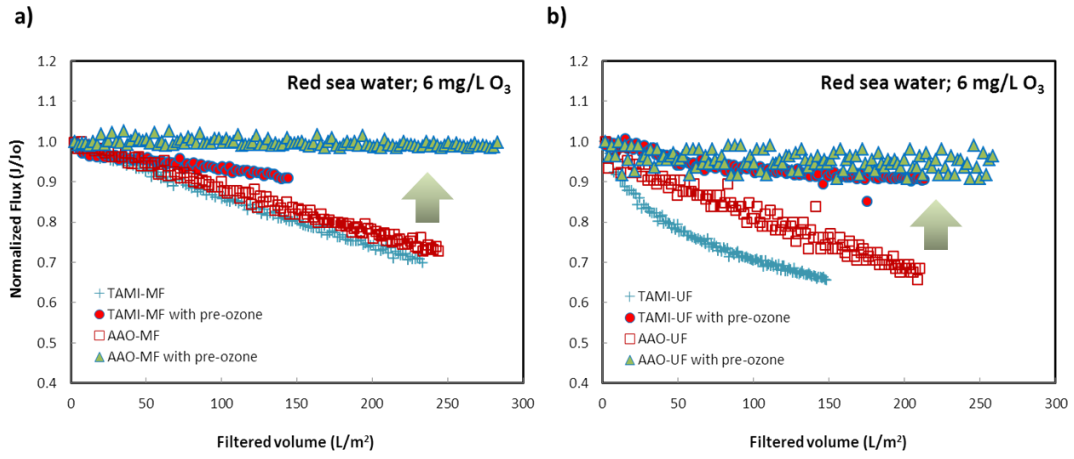

Figure 6.6 – Flux decline of TAMI and AAO MF/UF ceramic membranes with/without pre-ozone treatment (6 mg/L as O_3) in seawater filtration (Figure a) and b) represent MF and UF flux variation, respectively)

It was noteworthy that with increase ozone dose to 6 mg/L, both TAMI and AAO MF membranes experienced significantly improved flux, while with 3 mg/L ozone, the TAMI MF membrane experienced severe fouling caused by pore blockage as shown in (Figure 6.3). As a result, it is hypothesized that an ozone dose of 6 mg/L was enough to assist in aggregation of particles binding with calcium and magnesium, forming cake layer (porous and loose) on the ceramic membrane surface, resulting in leading to minimum membrane resistance, stabilizing membrane flux sustainably as shown in Figure 6.6.

6.3.1.4. Performance 4 - ozone dose of 6 mg/l (1 O_3/DOC) for WW effluent with additional Ca^{2+}

WW effluent was studied as a feed water with an artificial calcium of 15 mM, corresponding to the same concentration in the seawater sampled to identify effects of the calcium association with ozonated particles on membrane performance.

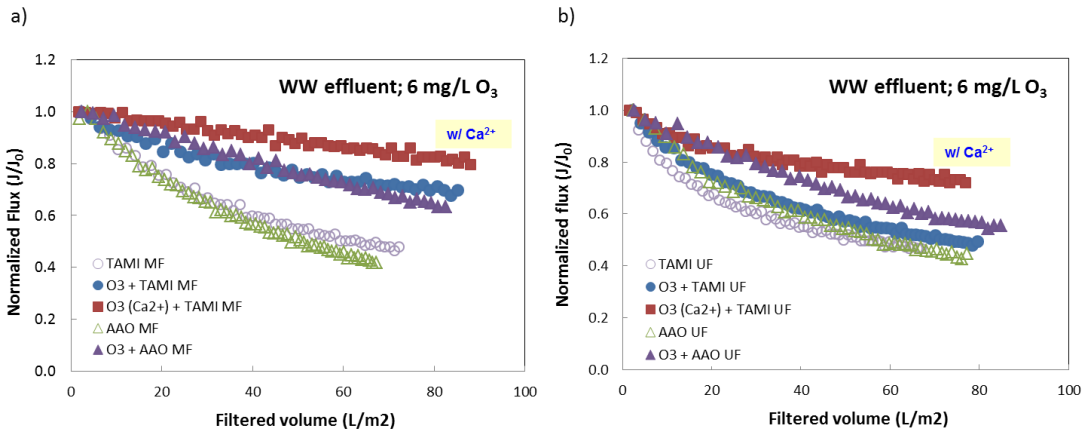

Figure 6.7 - Flux decline of TAMI and AAO MF/UF ceramic membranes for filtration of three waters - raw WW effluent, preozonated WW effluent, and preozonated WW effluent mixed with Ca^{2+} solution - with ozone dose of 6 mg/L: Figure a) and b) represent MF and UF flux variation, respectively

Both TAMI and AAO ceramic MF and UF membranes experienced improved permeability with an ozone dose of 6 mg/L for WW effluent, and better permeability of TAMI MF and UF membranes with the same ozone dose for calcium-augmented WW effluent as shown in Figure 6.7. With an ozone dose of 6 mg/L, the normalized fluxes of both TAMI and AAO MF membranes increased to 69% and 62% of the initial fluxes from 47% and 41%, respectively, after 30 minutes of filtration as shown in Figure 6.7-a). On the other hand, both TAMI and AAO UF membranes experienced less reduced fouling than both MF membranes, showing that the normalized fluxes increased to 50% and 55% of the initial fluxes from 43% and 42%, respectively. It was noteworthy that although both TAMI and AAO MF and UF membrane fouling decreased as ozone dose increased to 6 mg/L from 3 mg/L, the normalized fluxes were relatively less improved compared to the flux variation in seawater treatment (Figure 6.7-b).

With an ozone dose of 6 mg/L and calcium addition of 15mM, both the TAMI MF and UF membranes experienced less fouling than ozonation only, showing that the normalized flux decline of the MF and UF was improved up to 80% and 72% of the initial fluxes from 69% and 50% observed with ozonation only, respectively, as shown in Figure 6.7. This result confirms that the presence of calcium in feed solution is one of the important factors for the ozone-ceramic membrane hybrid to further improve the membrane filterability, sustainably maintaining the flux as clearly observed in seawater application.

6.3.2. Membrane autopsies

6.3.2.1. SEM images of foulant layer morphology

Scanning electron microscopy (SEM) was used to visually reveal the morphology of the foulant layer on the AAO MF membrane surface fouled with seawater and WW effluent through performance 3 and 4 in previous section 6.3.2, respectively. Figure 6.8 and Figure 6.9 compare foulant layer morphologies on membrane surfaces fouled with seawater and ozonated seawater, respectively.

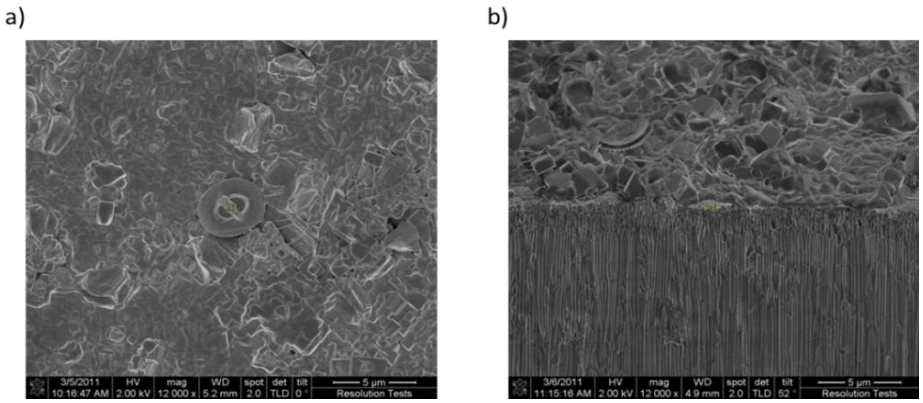

Figure 6.8 – SEM Images of AAO MF ceramic membranes fouled with seawater: a) presents the top view: b) shows the cross section

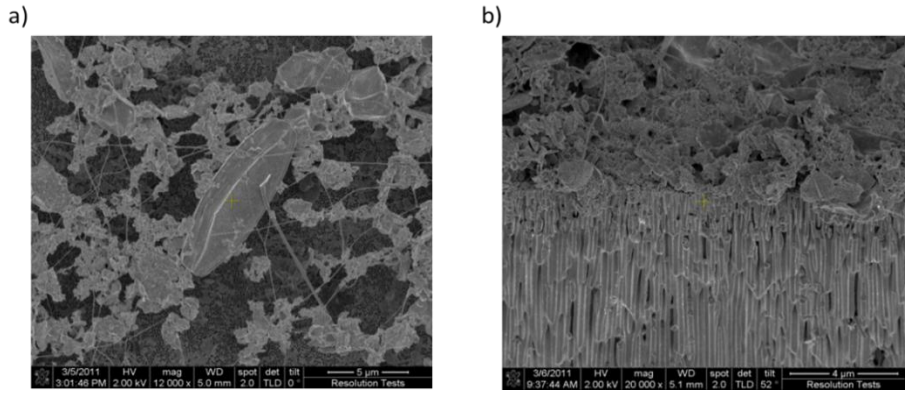

Figure 6.9 – SEM Images of AAO MF ceramic membranes fouled with ozonated seawater: a) presents the top view: b) shows the cross section

It was observed that when seawater was filtered with the AAO ceramic MF membrane, thick and sticky cake-like foulants fully covered the membrane surface as shown in Figure 6.8-a). The foulants accumulated on the surface appear to be non-

porous and compact as shown in Figure 6.8-b). On the other hand, when preozonated seawater with an ozone dose of 6 mg/L was filtered with the AAO ceramic MF membrane, coagulated foulants that are linked with adjacent aggregates above/on the membrane surface were observed as shown in Figure 6.9-a). However, the aggregated foulants were porous and even looser than non-ozonated foulants as shown in Figure 6.9-b).

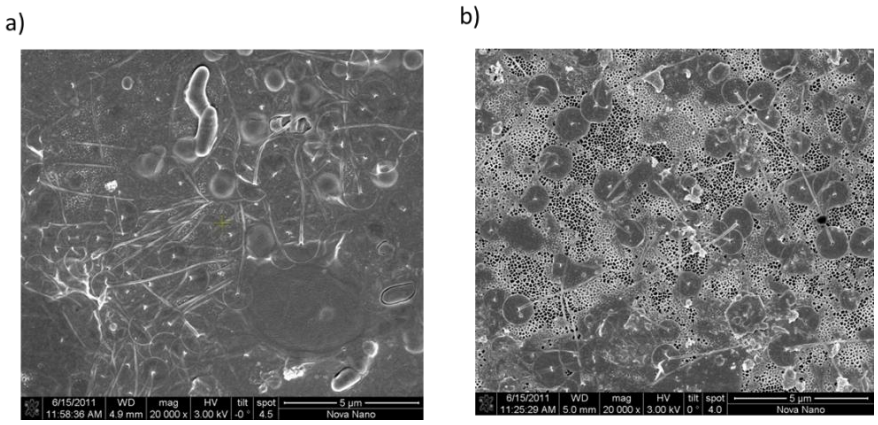

Figure 6.10 – Top views of SEM images of AAO MF ceramic membranes fouled with WW effluent (a) and ozonated WW effluent

Figure 6.10 shows SEM images of foulant layers on the AAO MF that are fouled with raw WW effluent and ozonated WW effluent. For the WW effluent-fouled membrane, thin and compact foulants including several diatoms were accumulated on the membrane surface as shown in Figure 6.10-a). Pretreatment by an ozone dose of 6 mg/L oxidized some particles and less foulants remained on membrane surface, but a majority of the membrane pores were still covered with the foulants including the number of round-objects with long tail as shown in Figure 6.10-b). However, no aggregation of ozone-induced particles binding with others was observed, not forming a porous cake layer to lead to an associated additional increase in filterability.

6.3.2.2. SEM-EDX mapping images

In addition to SEM, Energy-disperse X-ray Spectroscopy (EDX) was used to characterize specific elements in terms of calcium and magnesium that may be deposited on the membrane surface. Figure 6.11 and Figure 6.12 compare EDX mapping images of a seawater-fouled membrane and a preozonated seawater-fouled membrane. As shown in Figure 6.11, small amounts of calcium and magnesium on the AAO ceramic MF membrane fouled with seawater were observed, while larger amounts of the metal ions were accumulated on the membrane surface fouled with preozonated seawater (ozone dese of 6 mg/L) as shown in Figure 6.12.

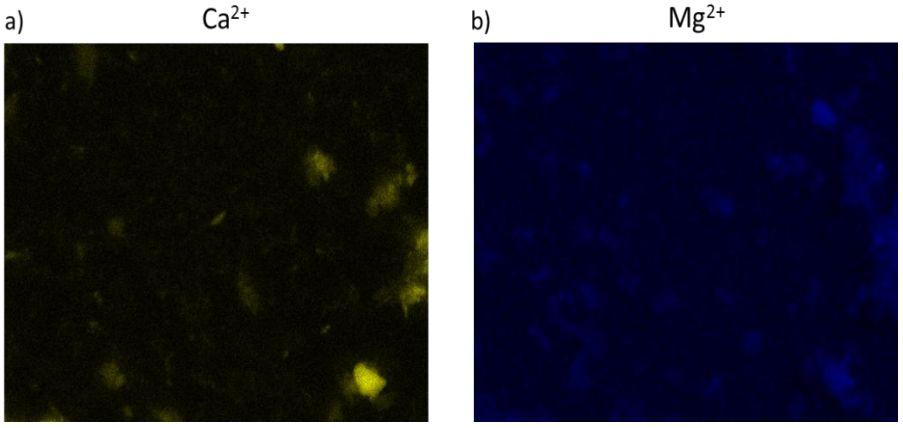

Figure 6.11 – SEM-EDX mapping images of Ca^{2+} (a) and Mg^{2+} (b) on the AAO MF ceramic membrane surfaces fouled with seawater

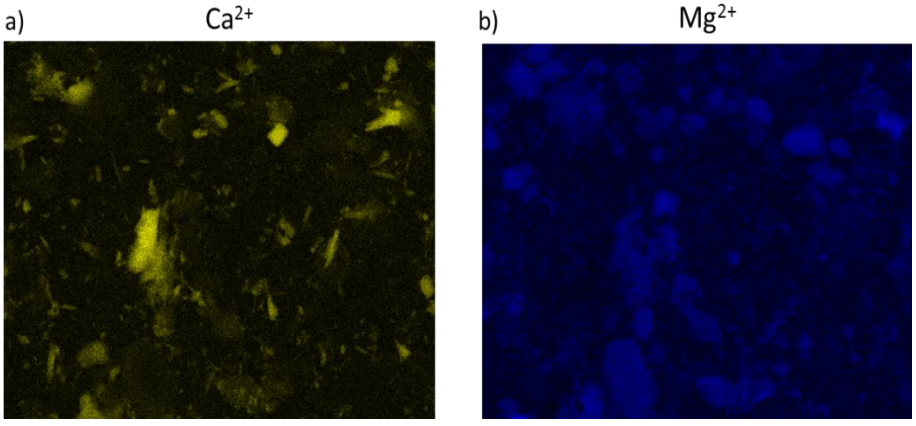

Figure 6.12 – SEM-EDX mapping images of Ca^{2+} (a) and Mg^{2+} (b) on the AAO MF ceramic membrane surface fouled with ozonated seawater (6 mg/L as O_3)

The SEM-EDX mapping results verified that preozonation causes metal ions (i.e., calcium and magnesium) present in bulk seawater solution to bind with some organic matter that is transformed by ozone treatment, and as filtration continues, more precipitates of the metal-humate complexes are being accumulated on the membrane surface as shown in Figure 6.12.

6.3.2.3. Atomic force microscopy (AFM)

AFM images revealed that the membrane fouled with non-ozonated seawater was fully covered with foulants and there was no open-surface observed, while some aggregates and non-blocked pores were observed for the membrane surface fouled with ozonated seawater as shown in Figure 6.13. As previously discussed in SEM image analysis in Figure 6.8-b), foulants covering the membrane surface fouled with seawater were dense and compact, while foulants on the membrane fouled with ozonated seawater were loose and porous as shown in Figure 6.9-b).

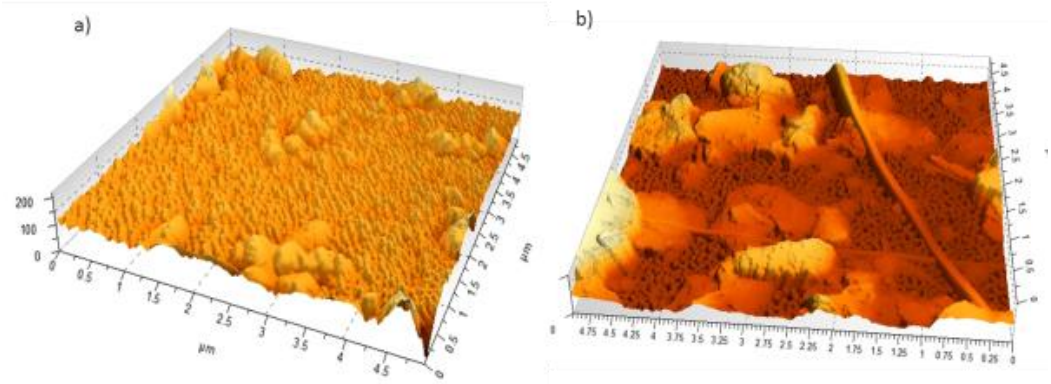

Figure 6.13 – AFM images of AAO MF ceramic membranes fouled with seawater (a) and preozonated seawater (b)

Table 6.4 compares roughness of three membrane surfaces that are virgin, fouled with seawater, and fouled with ozonated seawater. Differences in roughness distribution

and deviation among the three membrane surfaces were observed. The roughness of the membrane surface fouled with seawater was similar to the virgin membrane surface, implying that roughness of non-ozonated foulants covering membrane surface slightly increased compared with a virgin membrane, while the roughness of a membrane surface fouled with ozonated seawater (i.e., ozonated foulants) significantly increased to about three times as high as a virgin membrane as shown in Table 6.4.

Table 6.4 – Comparison of roughness of three membrane surfaces that are virgin, fouled with seawater, and fouled with ozonated seawater; Ra is arithmetic mean deviation and Rq root-mean-square deviation

Roughness		*Virgin*	*Fouled with seawater (SW)*	*Fouled with ozonated SW*
Distribution (nm)		30 ~ 120	50 ~ 150	130 ~ 500
Deviatio	Ra (nm)	6.94	5.39	18.9
n	Rq (nm)	8.72	7.28	27.6

Consequently, both AFM and SEM cross-section images confirmed that preozonation caused foulants to decompose, and the decomposed foulants are coagulated on membrane surface. However, the aggregated foulant are porous, allowing membrane flux to be stabilized without decline as shown in Figure 6.6.

6.3.2.4. Transparent exopolymer particles (TEP) visualization

TEP have been known as one type of extracellular polymeric substances (ESP) formed from acidic polysaccharides, mainly originating from many aquatic organisms, including phytoplankton and bacteria, especially from diatoms (Passow 2002). TEP are very sticky particles that exhibit the characteristics of gels, and amorphous

substances which may appear in different forms and sizes (Villacorte et al. 2009). Because of high abundances, large size and high stickiness of TEP, it can enhance or even facilitate the aggregation of solid and non-sticky particles (Alldredge et al. 1993, Passow 2002), causing severe NOM fouling onto MF and UF membrane surface difficult to remove by general backwashing. TEP are formed spontaneously from dissolved precursor substances, which contribute appreciably to the colloidal NOM pool in aquatic systems (Alldredge et al. 1993, Passow 2012).

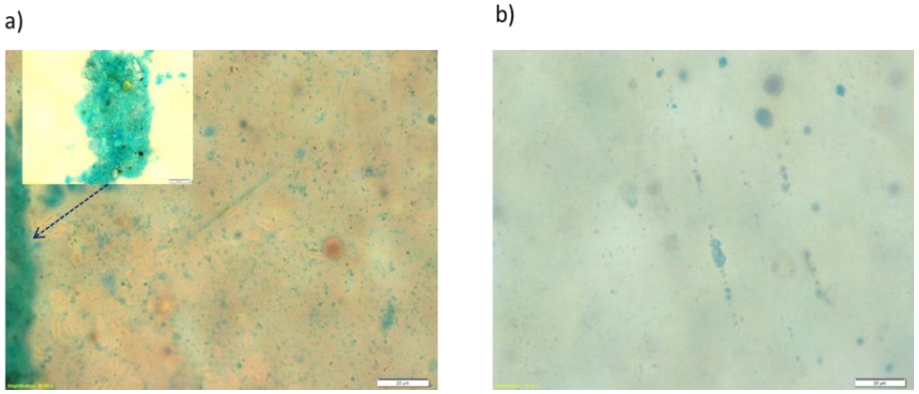

Figure 6.14 – Visualized TEP on AAO MF membranes fouled with seawater (a) and ozonated seawater (b)

TEP on AAO ceramic MF membranes that filtered two water samples – seawater and ozonated seawater – for 30 minutes were visualized using an optical microscope after staining with Alcian Blue. There was a noticeable difference between the two membranes fouled by seawater and ozonated seawater. As shown in Figure 6.14, the size ranges of TEP being accumulated on the seawater-fouled membrane surface were observed (Figure 6.14-a), while smaller amounts of TEP deposited on the ozonated seawater-fouled membrane were revealed (Figure 6.14-b). Gel-like TEP aggregates were observed on the seawater-fouled membrane which is considered to cause severe flux decline by added resistance. It has been known that the formation of gel-like TEP

aggregates is promoted or stabilized by cations, especially Ca^{2+}, as macromolecules bound by cationic bridge formation and hydrogen bonding (Logan et al. 1995, Verdugo et al. 2004). The degradation of TEP was observed on an ozonated seawater-fouled membrane, showing smaller amounts of TEP on the surface, demonstrating that ozone can play an important role in reducing membrane fouling, or improving flux by degrading NOM including TEP as shown in Figure 6.6.

From this result, ozone causes TEP degradation by which calcium is separated from the TEP aggregate, resulting in diminishing its gel-like properties and reducing membrane fouling and an associated increase in permeability. The ozone-induced particles including fragments unbound from the TEP by ozonation, such as poly-amino carboxylic acids led to greater association with divalent cations (i.e., Ca^{2+} and Mg^{2+}) which are not only present in bulk seawater solution, but also removed from the TEP aggregates. Nevertheless, the degradation and the subsequent association caused by preozonation contributed to formation of more porous and looser NOM foulants as shown in Figure 6.8.

6.3.2.5. Contact angle (CA)

Table 6.5 presents CA results of AAO ceramic membranes fouled with seawater and preozonated seawater. CA values of the original MF and UF membranes were 24°~26° and 35°~36°, respectively. Membranes fouled with no ozone showed a significant increase in CA of 84°~88° for MF and 47°~48° for UF, while CA values of ozonated seawater-fouled membranes were measured to be below that of virgin membranes, decreasing down to 17°~20° and 29°~30° for MF and UF, respectively. The result demonstrated that the ozone-induced hydrophilic porous foulants caused AAO MF

and UF membrane permeability to significantly increase with stabilized membrane flux at 92~100% of the initial flux as shown in Figure 6.6.

Table 6.5 – Variation of contact angles of three membranes that are virgin, fouled with seawater and fouled with ozonated seawater

	Virgin membrane	*Seawater-fouled membrane*	*preozonated seawater-fouled membrane*
MF	24~26	84~88	17~20
UF	35~36	47~48	29~30

6.3.3. Discussion of fouling mechanisms by ozonation

Zeta potentials (ζ) of ozonated particles in seawater and WW effluent were compared as function of ozone contact time as shown in Figure 6.15.

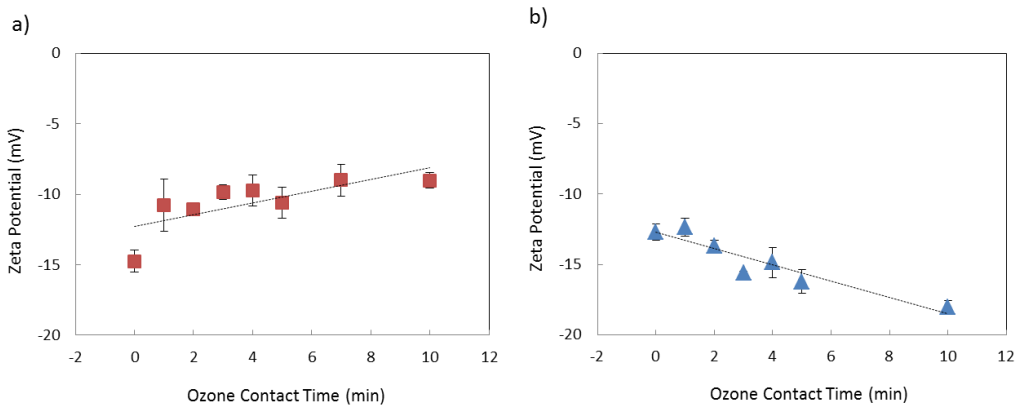

Figure 6.15 – Zeta potentials (ζ) of two ozonated waters (a) presents ozonated seawater; b) shows ozonated WW effluent)

The ζ of particles in seawater became less negatively charged with increased ozone contact time, while the ζ of particles in WW effluent was more negatively charged with increased contact time from 2 min to 10 min. Results verified that calcium (Ca^{2+}) and magnesium (Mg^{2+}) binding with ozone-induced NOM in seawater led to increase

in zeta potential (ζ) (less negative). However, because there was no or little metal ions in WW effluent, the ζ of particles did not increase but rather slightly decreased.

Figure 6.16 and Figure 6.17 illustrate hypothesized fouling mechanisms of a ceramic MF membrane that are fouled with non-ozonated seawater and ozonated seawater, respectively. For seawater-fouled membrane, particles in association with TEP are accumulated on the ceramic membrane surface, blocking the pores and forming a dense/sticky fouling layer on the membrane surface as shown in Figure 6.16. The foulants accumulated on the membrane result in severe membrane fouling, causing significant flux decline.

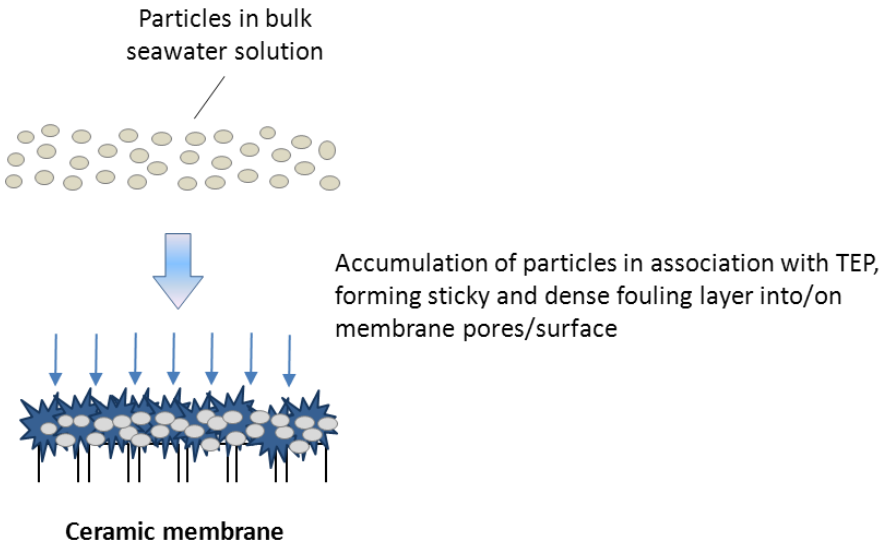

Figure 6.16 – A hypothesized fouling mechanism for filtration of seawater, focusing on foulants behaviour onto a ceramic membrane

On the other hand, when ozone is used prior to ceramic membrane filtration, particles in seawater are decomposed by ozone oxidation and then the ozone-induced particles are aggregated in association with divalent cations (e.g., Ca^{2+} and Mg^{2+}) which are present in seawater bulk solution and extracted from TEP. While the micro-

flocculated foulants are being filtered through a ceramic membrane, greater metal association with ozone-induced particles via bridging reactions on the membrane surface occurs, forming a porous/loose fouling layer which acts as a another filter media as described in Figure 6.17. As a result, the ozonated seawater foulants contribute to decrease irreversible fouling, leading to sustainable membrane performance.

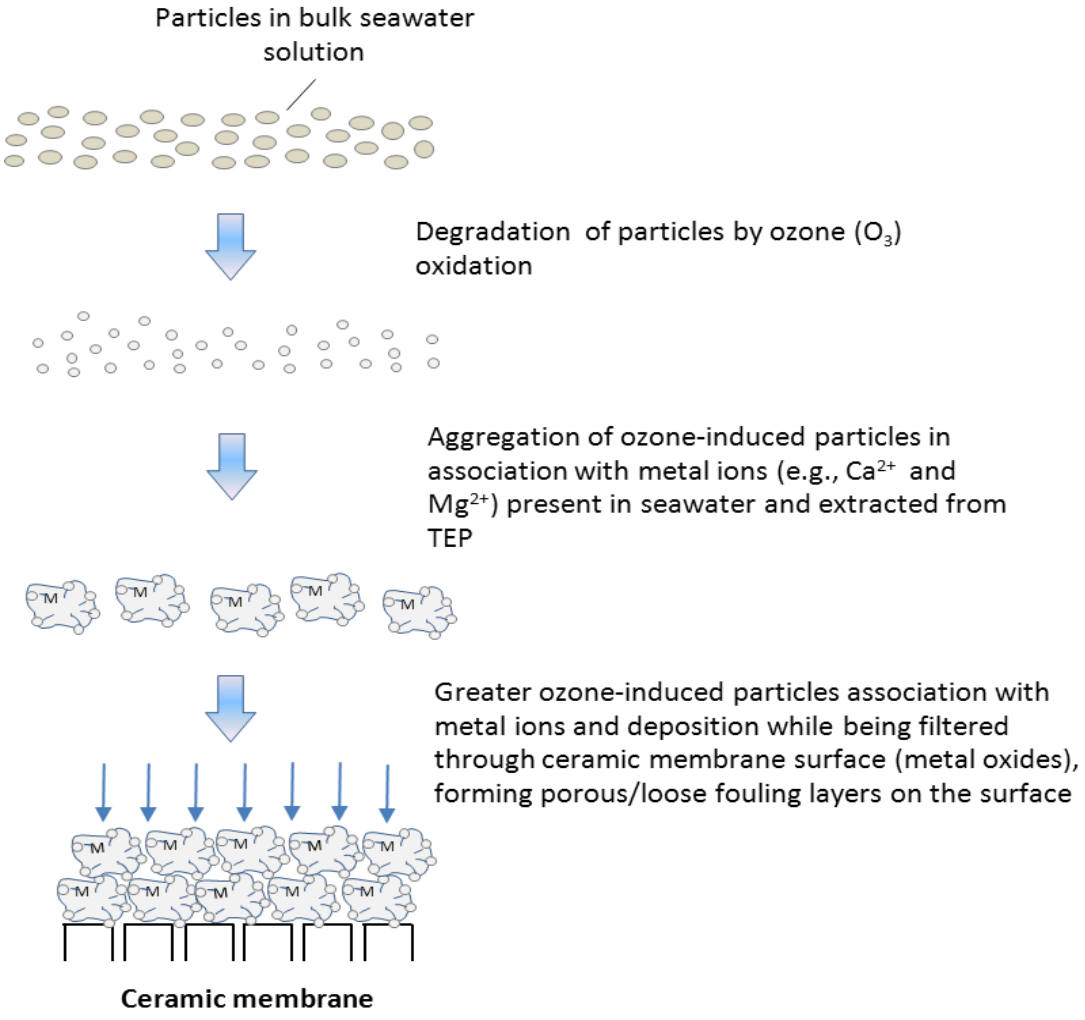

Figure 6.17 – A hypothesized fouling mechanism for filtration of ozonated seawater

6.4. CONCLUSIONS

A new generation of ceramic membranes which have unique advancements and properties over currently available polymeric membranes has been gradually introduced in both drinking water and wastewater applications. Ceramic membranes are physically superior to polymeric membranes and more resistant to severe chemical environments, allowing them to operate successfully under more rigorous conditions, such as higher filtration flux, higher feed water recoveries, extended backwash intervals, lower chemical cleaning requirements, and longer membrane life without breakage.

Bench-scale experiments demonstrated that due to the ozone-resistance nature of the ceramic membranes, preozonation allows the ceramic membranes to operate at sustainably higher flux for filtration of impaired-quality source waters, such as seawater and WW effluent.

It was noteworthy that preozonation led to significant flux improvement when treating seawater rather than WW effluent, which was attributed to the high presence of calcium and magnesium acting as a positive factor. In particular, it was revealed that not only does O_3 degrade NOM molecules (particularly TEP) which cause problematical fouling into smaller fragments, but it also helps to form microflocs as a result of ozone-induced NOM binding with divalent cations, such as calcium (Ca^{2+}) and magnesium (Mg^{2+}) present in seawater.

SEM with EDX and AFM images confirmed that when treating seawater without preozonation, sticky cake-like foulants covered the entire ceramic membrane surface and the foulants appear to be compact and non-porous, while for preozonated seawater, it was observed that foulants are coagulated and linked with adjacent aggregates on the membrane surface, however, they were porous and looser than non-ozonated ones.

Consequently, it is expected that an ozone-ceramic membrane hybrid can be successfully applied for filtration of impaired-quality source waters (i.e., seawater and wastewater), leading to stabilized high membrane flux sustainably. Especially, ozone prior to ceramic MF or UF membrane filtration can play a significant role in maintaining sustainable flux in seawater pretreatment applications before reverse osmosis (RO) production.

6.5. REFERENCES

Alldredge, A.L., Passow, U. and Logan, B.E. (1993) The abundance and significance of a class of large, transparent organic particles in the ocean. Deep Sea Research Part I: Oceanographic Research Papers 40(6), 1131-1140.

Amy, G. (2008) Fundamental understanding of organic matter fouling of membranes. Desalination 231(1-3), 44-51.

Casani, S., Rouhany, M. and Knøchel, S. (2005) A discussion paper on challenges and limitations to water reuse and hygiene in the food industry. Water Research 39(6), 1134-1146.

Chandrakanth, M.S., Honeyman, B.D. and Amy, G.L. (1996) Modeling the interactions between ozone, natural organic matter, and particles in water treatment. Colloids and Surfaces A: Physicochemical and Engineering Aspects 107(0), 321-342.

Crook, J. and Surampalli, R.Y. (1996) Water reclamation and reuse criteria in the U.S. Water Science and Technology 33(10–11), 451-462.

Dafinov, A., Garcia-Valls, R. and Font, J. (2002) Modification of ceramic membranes by alcohol adsorption. Journal of Membrane Science 196(1), 69-77.

Fähnrich, A., Mavrov, V. and Chmiel, H. (1998) Membrane processes for water reuse in the food industry. Desalination 119(1–3), 213-216.

Huang, H., Lee, N., Young, T., Gary, A., Lozier, J.C. and Jacangelo, J.G. (2007) Natural organic matter fouling of low-pressure, hollow-fiber membranes: Effects of NOM source and hydrodynamic conditions. Water Research 41(17), 3823-3832.

Kim, J., Davies, S.H.R., Baumann, M.J., Tarabara, V.V. and Masten, S.J. (2008) Effect of ozone dosage and hydrodynamic conditions on the permeate flux in a hybrid ozonation–ceramic ultrafiltration system treating natural waters. Journal of Membrane Science 311(1–2), 165-172.

Konieczny, K., Bodzek, M. and Rajca, M. (2006) A coagulation-MF system for water treatment using ceramic membranes. Desalination 198(1-3), 92-101.

Larbot, A., Gazagnes, L., Krajewski, S., Bukowska, M. and Wojciech, K. (2004) Water desalination using ceramic membrane distillation. Desalination 168, 367-372.

Lee, E.K., Chen, V. and Fane, A.G. (2008) Natural organic matter (NOM) fouling in low pressure membrane filtration -- effect of membranes and operation modes. Desalination 218(1-3), 257-270.

Lee, N., Amy, G., Croué, J.-P. and Buisson, H. (2004) Identification and understanding of fouling in low-pressure membrane (MF/UF) filtration by natural organic matter (NOM). Water Research 38(20), 4511-4523.

Lee, N., Amy, G. and Lozier, J. (2005a) Understanding natural organic matter fouling in low-pressure membrane filtration. Desalination 178(1-3), 85-93.

Lee, S. and Cho, J. (2004) Comparison of ceramic and polymeric membranes for natural organic matter (NOM) removal. Desalination 160(3), 223-232.

Lee, S., Lee, K., Wan, W.M. and Choi, Y. (2005b) Comparison of membrane permeability and a fouling mechanism by preozonation followed by membrane filtration and residual ozone in membrane cells. Desalination 178(1–3), 287-294.

Lehman, S.G. and Liu, L. (2009) Application of ceramic membranes with preozonation for treatment of secondary wastewater effluent. Water Research 43(7), 2020-2028.

Logan, B.E., Passow, U., Alldredge, A.L., Grossartt, H.-P. and Simont, M. (1995) Rapid formation and sedimentation of large aggregates is predictable from coagulation rates (half-lives) of transparent exopolymer particles (TEP). Deep Sea Research Part II: Topical Studies in Oceanography 42(1), 203-214.

Meyn, T. and Leiknes, T. (2010) Comparison of optional process configurations and operating conditions for ceramic membrane MF coupled with coagulation/flocculation pre-treatment for the removal of NOM in drinking water production. Journal of Water

Nguyen, T.L., Lee, D.J., Chang, J.S. and Liu, J.C. (2013) Effects of ozone and peroxone on algal separation via dispersed air flotation. Colloids and Surfaces B: Biointerfaces 105(0), 246-250.

Nissinen, T.K., Miettinen, I.T., Martikainen, P.J. and Vartiainen, T. (2001) Molecular size distribution of natural organic matter in raw and drinking waters. Chemosphere 45(6–7), 865-873.

Oh, B.S., Jang, H.Y., Cho, J., Lee, S., Lee, E., Kim, I.S., Hwang, T.M. and Kang, J.-W. (2009) Effect of ozone on microfiltration as a pretreatment of seawater reverse osmosis. Desalination 238(1–3), 90-97.

Passow, U. (2002) Transparent exopolymer particles (TEP) in aquatic environments. Progress in Oceanography 55(3–4), 287-333.

Passow, U. (2012) The abiotic formation of TEP under different ocean acidification scenarios. Marine Chemistry 128–129(0), 72-80.

Seidel, A. and Elimelech, M. (2002) Coupling between chemical and physical interactions in natural organic matter (NOM) fouling of nanofiltration membranes: implications for fouling control. Journal of Membrane Science 203(1-2), 245-255.

Song, W., Ravindran, V., Koel, B.E. and Pirbazari, M. (2004) Nanofiltration of natural organic matter with H2O2/UV pretreatment: fouling mitigation and membrane surface characterization. Journal of Membrane Science 241(1), 143-160.

Song, Y., Dong, B., Gao, N. and Xia, S. (2010) Huangpu River water treatment by microfiltration with ozone pretreatment. Desalination 250(1), 71-75.

Tchobanoglous, G., Darby, J., Bourgeous, K., McArdle, J., Genest, P. and Tylla, M. (1998) Ultrafiltration as an advanced tertiary treatment process for municipal wastewater. Desalination 119(1–3), 315-321.

Van Geluwe, S., Braeken, L. and Van der Bruggen, B. (2011) Ozone oxidation for the alleviation of membrane fouling by natural organic matter: A review. Water Research 45(12), 3551-3570.

Verdugo, P., Alldredge, A.L., Azam, F., Kirchman, D.L., Passow, U. and Santschi, P.H. (2004) The oceanic gel phase: a bridge in the DOM–POM continuum. Marine Chemistry 92(1–4), 67-85.

Villacorte, L.O., Kennedy, M.D., Amy, G.L. and Schippers, J.C. (2009) The fate of Transparent Exopolymer Particles (TEP) in integrated membrane systems: Removal through pretreatment processes and deposition on reverse osmosis membranes. Water Research 43(20), 5039-5052.

Voutchkov, N. (2010) Considerations for selection of seawater filtration pretreatment system. Desalination 261(3), 354-364.

Wade Miller, G. (2006) Integrated concepts in water reuse: managing global water needs. Desalination 187(1–3), 65-75.

Zularisam, A.W., Ahmad, A., Sakinah, M., Ismail, A.F. and Matsuura, T. (2011) Role of natural organic matter (NOM), colloidal particles, and solution chemistry on ultrafiltration performance. Separation and Purification Technology 78(2), 189-200.

Chapter 7

Ozone-Ceramic Membrane Hybrid for Filtration of Impaired-Quality Source Waters

Phase 3-2: Effects of ozone on ceramic membrane fouling as a pretreatment and chemically enhanced backwashing (CEB)

Effects of ozone on ceramic membrane fouling as a pretreatment and chemically enhanced backwashing (CEB)

ABSTRACT

Ozone can be aggressively and successfully combined with ceramic membranes for filtration of impaired-quality source waters such as seawater and wastewater effluent because of the robustness of ceramic membranes in terms of mechanical and chemical stability. This study aimed to demonstrate the effects of ozone not only as a pretreatment, but also as a chemically enhanced backwashing (CEB) when applied with ceramic membrane filtration for seawater and wastewater effluent. Parachlorobenzoic (pCBA), as a hydroxyl (˙OH) radical probe compound, demonstrated that dissolved ozone in contact with a TAMI ceramic membrane surface (based on TiO_2+ZrO_2) accelerated the formation of ˙OH radicals in WW effluent treatment, showing flux improvement as a result of breaking down organic matter. On the other hand, there was no acceleration of the formation of ˙OH radical observed in seawater application; however, the membrane flux was significantly improved. Flux restoration of the TiO_2+ZrO_2-based TAMI and Al_2O_3-based AAO membrane, fouled with seawater and WW effluent, was efficiently achieved by high BW pressure and ozone-CEB. This was attributed to the robustness of ceramic membrane in terms of mechanical and chemical stability. Assimilable organic carbon (AOC) production was observed when ozone is applied prior to ceramic membrane filtration for seawater and WW effluent, transforming dissolved organic carbon (DOC) into AOC, nevertheless, as ozone dose increased to a certain level, AOC started to become mineralized. It is

expected that ozone plays a dual role to oxidize organic matter leading to less fouling and to clean the membrane by inhibiting the rise in TMP.

Keywords: Ceramic membranes, ˙OH radical, Ozone, AOC

7.1. INTRODUCTION

In the context of water quality deterioration, scarcity, and other negative impacts caused by a climate change, multi-barrier methods to treat various kinds of source waters must be adopted to provide reliable recycled water quality to industrial, agricultural and domestic users. An ozone and membrane filtration hybrid is one of the classical technologies in the multi-barrier suite (Lee et al. 2005c, Oh et al. 2009, Park 2002, Song et al. 2010, Wang et al. 2007, Zhu et al. 2010, Zhu et al. 2008). Ozone, however, can damage polymeric membranes that are currently being used for both drinking water and wastewater application.

Ceramic membranes are superior to polymeric membranes and are more resistant to severe thermal and chemical environments (Garmash et al. 1995, Lee and Cho 2004), allowing them to operate at high permeate fluxes, high feed water recoveries, and with less frequent chemical cleaning as compared to conventional polymeric membranes (Amy 2008, Huang et al. 2007, Lee et al. 2004, Lehman and Liu 2009, Pontié et al. 2007). Due to the robustness of ceramic membranes in terms of mechanical and chemical stability, ozone can be more aggressively and successfully combined with ceramic membranes. Several studies have demonstrated that ozone prior to ceramic membrane filtration could be employed to reduce membrane fouling and increase permeability for treatment of seawater and WWTP effluent (Karnik et al. 2005, Kim et al. 2008, Lehman and Liu 2009, Xu et al. 2010)

The principal chemical properties of ceramic membranes are their hydrophilicity (Dafinov et al. 2002, Larbot et al. 2004) and amphoteric surface charge due to the

presence of hydroxyl (OH^-) groups on their surface. These characteristics contribute to high permeability, and influence separation ability and fouling potential as well (Dafinov et al. 2002). In particular, when treating impaired-quality source waters, such as seawater and WWTP effluent, ceramic membranes can effectively achieve enhanced performance for mainly two reasons: First, the ceramic membrane provides excellent backwashability because the material itself can withstand high backwash pressure (Kim et al. 2007); Second, it has been reported that the incorporation of chemical treatment as a pretreatment and a CEB (i.e., ozone pretreatment) with ceramic membranes can greatly mitigate fouling by natural organic matter (NOM) (Konieczny et al. 2006, Lehman and Liu 2009, Meyn and Leiknes 2010, Van Geluwe et al. 2011).

During ozonation, organic contaminants are oxidized in two ways (Hoigné and Bader 1983, Rosenfeldt et al. 2006, Van Geluwe et al. 2011, von Gunten 2003). Ozone itself can directly react with dissolved chemicals (mainly with double bonds, activated aromatic systems and non-protonated amines), at varying rates, and is a highly selective oxidant. In addition to direct oxidation, ozone decomposes via a chain reaction mechanism to form $^{\cdot}OH$ radicals, which in turn can oxidize the pollutant (von Gunten 2003). The two pathways can lead to different products and display different transformation kinetics. Furthermore, it is expected that when ceramic membranes are employed with ozone treatment, the decomposition of ozone into OH radicals can be accelerated by dissolved ozone in contact with the ceramic surface, providing not only degradation of organic matter, but disinfection of microbes. The ozone can work in role to clean the membrane by way of inhibiting the rise in trans-membrane pressure, providing the unique feature for ‘chemical-free’ performance as

compared to costly waste generation clean-in-place operations mandatory for polymeric membranes.

Ozone causes the formation of low molecular weight (LMW) oxygen-containing organic by-products. These compounds arise from the oxidative breakdown of complex natural organic matter (NOM). Typical examples of such LMW compounds are carboxylic acids, benzoic compounds, aldehydes, ketones, and keto-acids (Huang et al. 2005). Many of these molecules constitute easily assimilable organic carbon (AOC). AOC is one of the most important quality parameters responsible for microbiological stability in drinking water (Escobar and Randall 2001, Escobar et al. 2001, Hammes et al. 2007). Therefore, ozone-oxidative water treatment is generally followed by a biological filtration step to remove AOC.

In the previous Chapter 6, a series of ceramic membrane performances and various analytical methods including SEM-EDX, AFM, UVA_{254}, TEP visualization and zeta potential (ζ) demonstrated that ozone in combination with ceramic membrane filtration was capable of being effectively applied for treatment of impaired-quality source waters, providing sustainable membrane performance with stabilized flux. It is also demonstrated that not only does ozone (O_3) degrade NOM molecules which mostly cause problematical membrane fouling into smaller fragments, but it also helps to form microflocs as a result of ozone-induced OM binding with divalent inorganic cations, such as calcium and magnesium, highly present in seawater. As a result, these attractive features are expected to help effectively achieve enhanced performance when treating impaired-quality source waters (e.g., high-organic surface water, WW effluent, brackish water and seawater).

Following the previous Chapter 6, this study aimed to understand the effects of ozone as a pretreatment and chemically enhanced backwashing (CEB) for filtration of impaired-quality source waters (i.e., seawater and WW effluent), focusing on hydroxyl (˙OH) radical acceleration in contact with the ceramic oxide surface by measuring the degradation of a commonly utilized hydroxyl radical (ozone-resistant) probe compound, parachlorobenzoic acid (pCBA), and flux restoration, respectively. The specific objectives of this study were to i) identify the formation of ˙OH radical reacting with ceramic membrane surface during preozonation with TiO_2+ZrO_2-based membrane filtration in both seawater and WW effluent applications. With increase ozone dosage, the percentage of ˙OH radical formation produced by dissolved ozone in contact with the TAMI membrane surface was assessed by pCBA as the probe compound for ˙OH radical exposure. pCBA is an ideal probe compound for this study because it displays slow reaction rates with ozone ($k_{O3} < 1\ M^{-1}\ s^{-1}$), but rapid oxidation kinetics with the ˙OH radical ($k_{OH,\ pCBA} = 5 \times 10^9\ M^{-1}\ s^{-1}$) (Rosenfeldt et al. 2006); ii) to investigate the transformation of assimilable organic carbon (AOC) as function of ozone dose; iii) to assess the recovery rate of fouled ceramic membranes with high BW pressure and ozone-CEB; iv) finally, to characterize natural organic matter (NOM) in WW effluent using LC-OCD for understanding ozone effects on decomposition of organic foulants.

7.2. MATERIALS AND METHODS

7.2.1. Source waters

Two different impaired-quality source waters that were sampled from the Red Sea and the Jeddah wastewater treatment plant in Saudi Arabia, respectively, were used for experiments. Throughout the whole experimental period, the feed water was adjusted to room temperature between 19.5°C and 20.5°C, which was established after the waters had been removed from cold storage for a half-day before starting each set of tests.

Table 7.1 – Summary of water quality analysis

Parameter	*Red Sea Water*	*Jeddah WW effluent*
DOC	≈ 1 mg/L	5.5 ~ 6 mg/L
SUVA	1.2±0.2 L/mg·m	2.7 ~2.9 L/mg·m
Ca^{2+}	527 mg/L	79 mg/L
Mg^{2+}	1,436 mg/L	-
pH	7.8 ~ 8.2	7.6 ~ 7.75

The Red Sea water sample was collected about 1.5 m above the bottom near the intake of a local desalination treatment plant. The DOC measured was about 1.0 mg/L. The JWTP secondary effluent is treated by an anoxic-oxic (AO) activated sludge process. The DOC was between 5.5 mg/L to 6 mg/L. Both seawater and secondary WW effluent were prefiltered with a 0.45μm filter. Water quality analysis of two feed water sources is summarized in Table 7.1.

7.2.2. Experimental set-up

7.2.2.1. Ceramic membranes

Two different types of ceramic membranes, designated as TAMI and AAO, were used for bench-scale tests. The TAMI ceramic membrane (INSIDE DISRAM™, TAMI INDUSTRIES, France) is fabricated by means of sintering, while the AAO ceramic

membrane (AnodiscTM, Whatman, USA) is obtained by anodic oxidation process. Simple specifications of the two ceramic membranes are summarized in Table 3.1.

Table 7.2 – Specifications of two ceramic membranes used for experiments

	TAMI		AAO	
	MF	UF	MF	UF
Pore size, or MWCO	0.14μm	150KD	0.10μm	20nm
Materials	$ZrO_2 + TiO_2$	$ZrO_2 + TiO_2$	Al_2O_3	Al_2O_3
Effective surface area (cm^2)	17.4	17.4	17.4	3.14

7.2.2.1. Ozonation test setup

Two ozone experimental setups were employed. First, to measure AOC transformation as function of ozone dose, 100 mL beakers for seawater and 50mL beakers for WW effluent were prepared. Ozone stock solution prepared was added to the each beaker, setting at the proper concentration for both seawater (0.35, 1.0, 1.7, 2.3, and 3.2 mg/L as O_3) and WW effluent (1.3, 3.2, 5.8, and 8.1 mg/L as O_3).

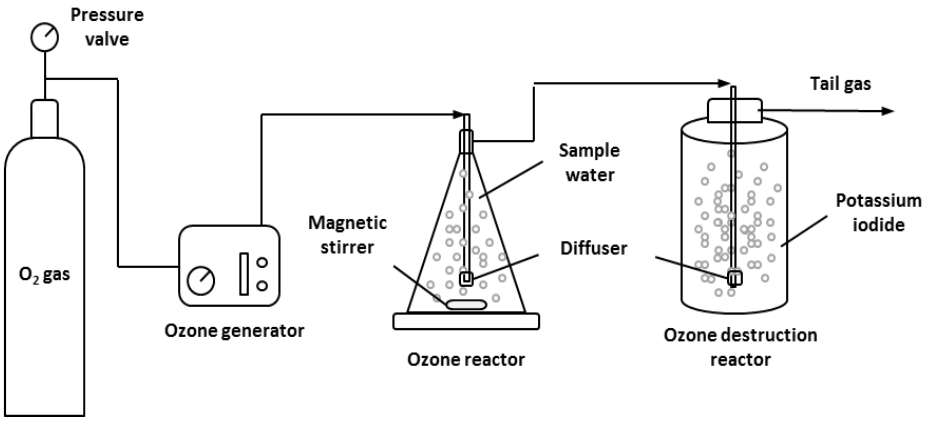

Figure 7.1 – Schematic of ozonation experimental setup

To identify ˙OH radical formation in contact with ceramic membrane surface with increased ozone dosage and to characterize natural organic matter (NOM) in the

ozonated waters using LC-OCD, a dynamic ozone experimental setup was employed as shown in Figure 7.1. The bench-scale setup is comprised of an ozone generator (Degremont Technologies- Triogen, Scotland), a static batch-reactor flask (2L), and a gas destruction reactor with potassium iodide. Pure oxygen gas from a gas cylinder was fed to the ozone generator. Ozone dose was controlled by adjusting ozone contact time, where a magnetic stirrer at the bottom of the ozone reactor was used in combination with a diffuser in order to mix the water, increasing ozone diffusivity. As soon as a set of ozonation test was completed, the ozonated water was transferred in pressure vessel 1 and 2 (Figure 7.2), immediately performing ceramic membrane filtration and backwashing tests, respectively.

7.2.2.2. Membrane filtration and backwashing test setup

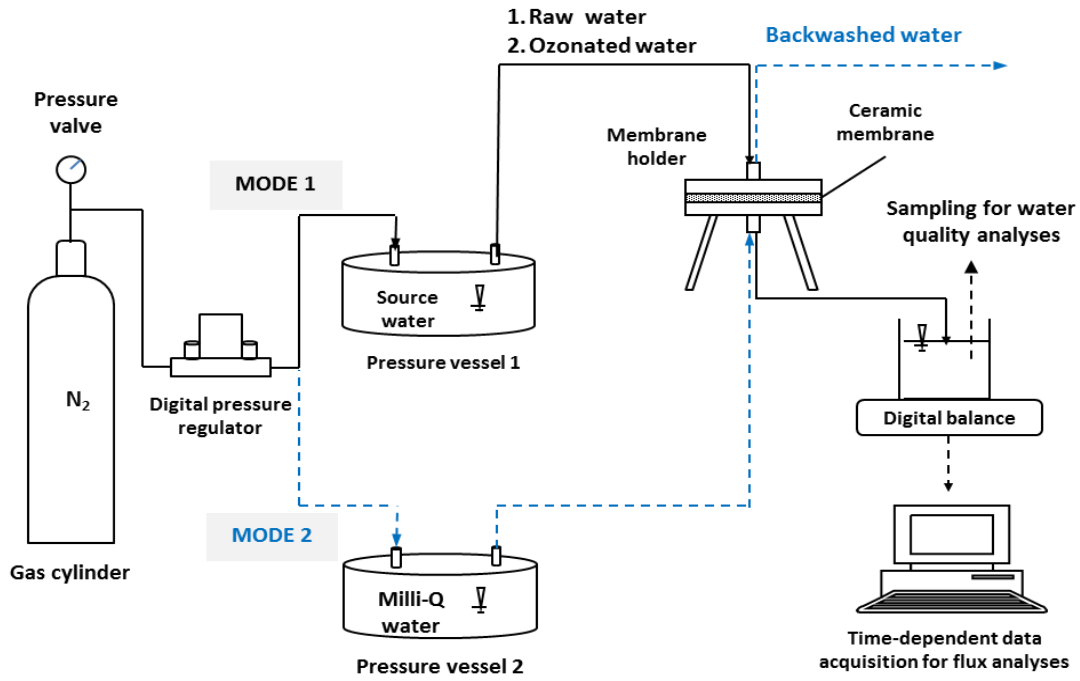

Figure 7.2 - Schematic of ceramic membrane filtration and backwashing test unit: raw water or ozonated water is filtered in a mode 1; the membrane fouled after filtration is backwashed in a mode 2

Figure 7.2 shows the scheme of the ceramic membrane filtration setup which is capable of being operated in both filtration and backwashing in two modes, where two different ceramic membrane discs are set in a special holder for the TAMI ceramic membranes and an Amicon unstirred cell for the AAO ceramic membranes. Feed waters – raw water and preozonated water – are filtered through each membrane disc placed inside the holder or the cell in a dead-end filtration mode. Each of filtered waters is accumulated in a beaker under which a digital balance is placed, monitoring the filtered volume as function of time, every 10 seconds (i.e., permeate flux).

In addition to the time-dependent behaviour, ˙OH radical formation data was generated using para-chlorobenzoic acid (pCBA) to identify ˙OH radical acceleration in contact with the TAMI ceramic membrane surface by measuring the degradation of the ˙OH radical probe compound. The pCBA stock solution was prepared to the following concentration: 1g/L tetra-borate and 20mg/L pCBA which was kept at 15°C. After ozonation tests with different ozone contact time according to the schematic of the ozonation experimental setup as shown in Figure 7.1, ozone in the gas phase in treated water was completely removed by purging with nitrogen (N_2) gas for 5 minutes. And then the ozonated water was moved into a pressure vessel 1 in Figure 7.2 and immediately spiked 5mL of the pCBA stock in the vessel. After each set of filtration test, both ozonated water in the vessel and filtered water through the TAMI ceramic membrane were collected to assess the percentage of ˙OH radical formation produced by dissolved ozone in contact with the TAMI oxide surface.

7.2.3. Analytical methods

7.2.3.1. Ozone residual and ˙OH radical measurements

The indigo method was used for ozone residual analysis. To detect pCBA, a Waters 1525 Micro binary HPLC pump with a Waters 2489 UV visible detector was used, with an Agilant Eclipse XDB-C18 4.6mm ID × 150mm (5 μm) column was used for separation of pCBA. An eluent (mobile phase) consisted of 40% of acetonitrile and 60% of phosphoric acid (0.3%). UV absorbance at a wavelength of 240 nm was applied to detect pCBA.

7.2.3.2. Assimilable organic carbon (AOC) measurement

AOC is usually measured by measuring the total concentration of a pure culture inoculum that has grown into stationary phase in a water sample. In this AOC assay, AOC determination was made using a naturally present bacterium as inoculum. The advantage of this method is that the natural microbial community gives a realistic interpretation of the AOC content, because it represents their cultures. A seawater (SW) sample was collected from the Red Sea and wastewater (WW) effluent from the Jeddah WW plant. Two water sources (SW and WW) were incubated onto marine agar and LB agar, respectively, overnight. Then, a fast-grown and dominant colony was isolated from each incubated plate. The isolated colony was sub-cultured in artificial seawater (ASW) and synthetic WW (SWW) for AOC tests and sequencing. 16S-rRNA based sequencing results showed that a bacterium in SW is *Pseudoalteromonas atlantica* (*P. atlantica*) and a bacterium in WW is *Escherichia fergusonii* (*E. fergusonii*).

ASW was prepared by dissolving various salts (13.5 g NaCl, 1.96g Na_2SO_4, 0.107 g $NaHCO_3$, 0.33 g KCl, 0.053 g KBr, 2.5 g $MgCl_2{\cdot}6H_2O$, 0.55 g $CaCl_2{\cdot}2H_2O$, 0.0107 g

$SrCl_2 \cdot 6H_2O$ and 0.0107 g H_3BO_3 and adjusted to pH 7.5) in 1,000 ml Milli-Q water. The ASW medium was fortified with 9.52 mM NH_4Cl, 1.32 mM K_2HPO_4 and 0.2 % glucose (as a carbon source) for growth. SWW was made by dissolving compounds (2.5 g glucose, 0.5g NH_4Cl, 0.25g KH_2PO_4, 0.25g K_2HPO_4, 0.3 $MgCl_2 \cdot 6H2O$, 0.025 g FeCl3, 0.0105g $CuCl_2$, 0.005g $CaCl_2$ and 0.015g $MnCl_2$) into 1L Milli-Q water. AOC assays typically measure growth of inoculums in a water sample from which the natural bacterial community has first been removed and inactivated through sterilization. The inoculums grow until stationary phase, with the assumption that the growing bacteria have assimilated all the AOC in the water. The net growth of the bacteria is measured and then converted to an AOC (or AOC equivalent) concentration.

In the AOC method, samples were filtered through a 0.22-µm PES filter to remove particulate organic matter and microbes before autoclaving at 70 °C for 30 min to inactivate the bacterial community. Then, 6.2 (±0.2) x 10^4/mL of *P. atlantica* and 1.6 (±0.1) x 10^5/mL of *E. fergusonii* were spiked into glucose samples of different concentration (0, 0.025, 0.050, 0.100 and 1.000 µg/mL) with ASW and SWW to measure AOC using a standard curve. The samples were incubated at 25 °C (based on membrane system operation temperature) for 3 d and then monitored over time until peaks become stationary. Cell growth was measured by using plate count with marine agar for marine samples and LB agar for WW samples over the time.

7.2.3.3. Flux calculation

Permeate flux (J; L/m^2h) was calculated as the flow rate of permeate water (Q; L/h) divided by the effective surface area of the membrane (A; m^2). The filtered water was

monitored as function of time (t; s) and filtered volume (V; m^3), where the permeated volume was recorded every 10 second intervals under a certain pressure for filtration. Normalized flux (J/J_0) was calculated as the ratio of flux to the initial flux at the beginning of the filtration (J_0; L/m^2h).

7.3. RESULTS AND DISCUSSION

7.3.1. ˙OH radical formation by ozone residual

In order to identify how much ˙OH radical is produced by residual ozone in contact with TAMI MF ceramic membrane surface (made of TiO_2+ZrO_2), bench scale ˙OH radical formation data as function of dissolved ozone concentration were generated by indirect measurement of the ˙OH radicals using para-chlorobenzoic acid (*p*CBA) as an ˙OH radical probe compound. The decrease of an added probe compound which does not react with ozone but does rapidly with OH radicals was analyzed as a function of the ozone dosage. Two water samples, WW effluent and seawater, were used for tests. In addition, the effects of ozone residual on the ceramic MF membrane performance were estimated to understand the relationship between ˙OH radical formation and fouling reduction (i.e., flux variation).

7.3.1.1. Performance for WW effluent according to increased ozone dose

Figure 7.3 compares the trend of normalized flux decline of the TAMI MF ceramic membranes for 10 min. of operation as function of increased ozone contact time of 0, 1, 2 and 3 minutes for WW effluent. Results showed that with no ozone, the

normalized flux decreased to 70% of the initial flux after 10 minutes of operation, while with ozonation for 1 min. contact time, the normalized flux decreased to 82% of the initial flux, revealing less fouling. However, no further flux improvement was observed with increased ozone contact time to 2 and 3 min., where the normalized flux decreased to 85% and 82% of the each initial flux, respectively.

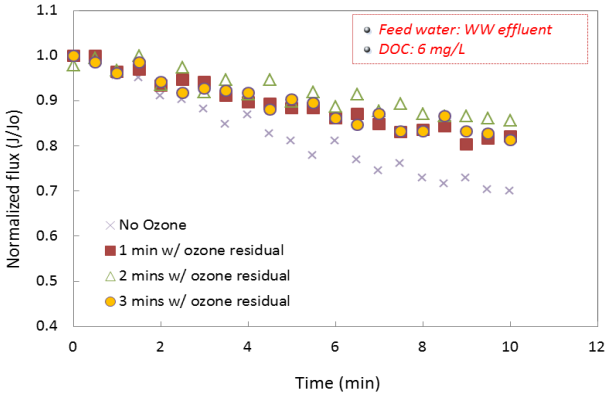

Figure 7.3 – Ozonation effects on TAMI ceramic MF membrane flux as function of ozone contact time for filtration of WW effluent: DOC measured is 6 mg/L

The percentage of ˙OH radical formation which is produced by dissolved ozone in contact with the TAMI membrane surface was assessed as summarized in Table 7.3. Results showed that dissolved ozone in contact with the TiO_2+ZrO_2-based membrane surface produces ˙OH radical which played a role in improving the permeability as shown in Figure 7.3. With increased ozone residual to 3.42 mg/L from 1.47 mg/L, the ˙OH radical formation was increased up to 18.6% from 14.5%. However, increase in ozone residual to 6.93 mg/L did not lead to further increase in the formation of ˙OH radicals, but decrease to 14.3% which was unexpected. The results corresponded to the normalized flux decline to 82% from 85%, when ozone contact time increased to 3 min from 2 min as previously discussed in Figure 7.3.

Table 7.3 – Formation of ˙OH radicals by dissolved ozone in contact with TAMI ceramic membranes (made of TiO_2+ZrO_2) while filtration of WW effluent

Ozone contact time	*Dissolved ozone*	*˙OH radical formation*
1 min	1.47 mg/L	14.5%
2 min	3.42 mg/L	18.6%
3 min	6.93 mg/L	14.3%

Taking the results of both the flux decline and the formation rate of ˙OH radicals into account, there may have been an error for carrying out the experiment with 3 min. of ozone contact time. Nevertheless, it was clearly observed that the TAMI ceramic membrane fouling was controlled in proportion to the formation rate of ˙OH radicals.

7.3.1.2. Performance for seawater according to increased ozone residual

Seawater was fed and the trend of normalized flux decline of the TAMI MF ceramic membranes according to increased ozone contact time from 0 to 1, 2, and 3 minutes were assessed as shown in Figure 7.4.

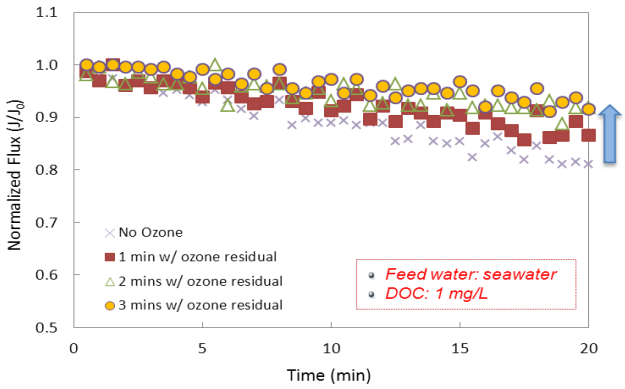

Figure 7.4 – Ozonation effects on TAMI ceramic MF membrane flux as function of ozone contact time for filtration of seawater: DOC measured is 1 mg/L

Overall, the normalized membrane flux was proportionally improved with an increased ozone contact time. Results showed that without ozone treatment, the normalized flux decreased to 81% of its initial flux after 20 minutes of operation, while with ozone dose for 1 min contact time, the normalized flux declined to 88% as a result of reduced fouling by ozonation. Further flux improvement was observed with increased ozone contact time to 2 and 3 min., showing the normalized flux decrease to 90% and 92% of the initial flux, respectively.

For seawater, the percentage of ˙OH radical formation produced by ozone residual was estimated and ozone residual was measured as well after 20 min. of operation as a function of ozone contact time as summarized in Table 7.4.

Table 7.4 - Formation of ˙OH radical accelerated by dissolved ozone in contact with TAMI ceramic membrane (made of TiO_2+ZrO_2) for seawater

Ozone contact time	*Dissolved ozone*	*˙OH radical formation*
1 min	5.0 mg/L	1.7%
2 min	6.2 mg/L	1.5%
3 min	6.4 mg/L	0.1%

Results showed that dissolved ozone in contact with the TAMI ceramic surface had an no influence on the formation of ˙OH radical for seawater. Even if dissolved ozone increased from 5.0 mg/L to 6.2 mg/L and 6.4 mg/L, there was slight formation of ˙OH radicals observed, showing the formation rate from 1.7% to 1.5% and 0.1%, respectively. It is hypothesized that CO_3^{2-} and HCO^{3-} in seawater scavenges ˙OH radical formation while dissolved ozone is in contact with the TiO_2+ZrO_2-based membrane surface. Nevertheless, it was observed that the normalized membrane flux

improved with an increase in ozone contact time as shown in Figure 7.4 although ˙OH radical formation was inhibited in seawater.

Consequently, dissolved ozone in contact with the TAMI ceramic membrane surface accelerated the formation of ˙OH radicals in WW effluent treatment, showing flux improvement as a result of breaking down organic matter. On the other hand, there was no formation of ˙OH radical observed in seawater application, but improved flux was shown.

7.3.2. Effects of ozone as CEB on membrane fouling reversibility

7.3.2.1. Performance of train 1 – increased BW pressure and ozone-CEB

Recovery of the TAMI MF membranes fouled with WW effluent was assessed by hydraulic backwashing (BW). Initial membrane flux was set to 200 LMH at a 0.15 bar and filtered for 30 minutes and backwashed using Milli-Q water for 2 min., 1 min., and 30 sec. in accordance with increased pressure from two times (i.e., 0.3 bar) to five times (i.e., 0.75 bar) and ten times (i.e., 1.5 bar) as high as membrane operation pressure, respectively. In addition to high BW pressure, ozone as a chemically enhanced backwashing was employed, where 2 mg/L of ozone dissolved in Milli-Q water was applied for 2 min. at a twice higher than the membrane operation pressure.

As shown in Figure 7.5, as BW pressure increased from twice to five times and ten times higher, the recovery rate of the TAMI membranes fouled increased to 47%, 69% and 78% of their initial fluxes, respectively. Moreover, ozone as a CEB played a significant role in flux restoration with almost complete recovery of the fouled TAMI

ceramic membrane, showing that the normalized flux recovered to 93% of the initial flux.

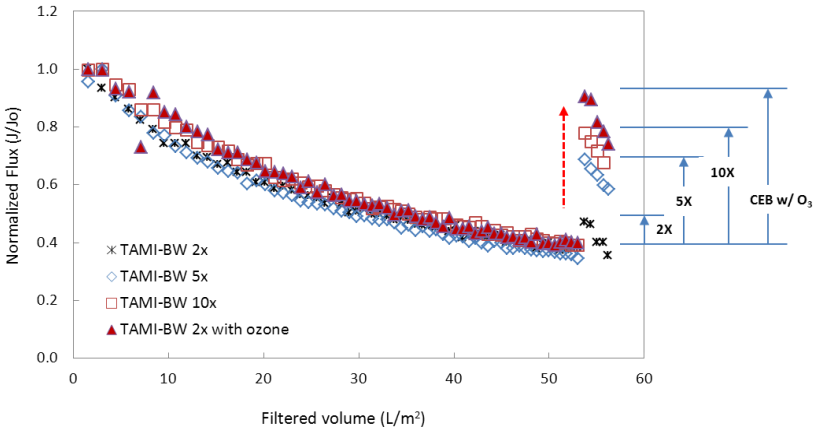

Figure 7.5 – Flux restoration of TAMI ceramic MF membranes fouled with WW effluent as function of backwashing (BW) pressure with ozone-CEB

Recovery of the TAMI MF membranes fouled with seawater was investigated under the same conditions that were performed for the WW effluent, setting 200 LMH as the initial flux at a pressure of 0.15 bar for 30 minutes filtration, and backwashed using Milli-Q water as function of increased pressure with ozone-CEB. Results showed the same trend of flux restoration in accordance with increased pressure and ozone. WW effluent-fouled membranes were recovered to 74%, 84%, and 94% of their initial fluxes with twice, five times, and ten times higher pressure, respectively. Moreover, ozone (2 mg/L) as a CEB allowed the normalized membrane flux to restore by 95% of the initial flux as shown in Figure 7.6.

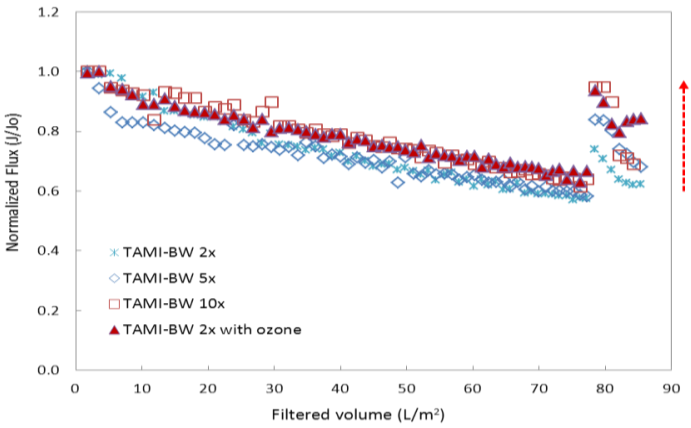

Figure 7.6 - Flux restoration of TAMI ceramic MF membranes fouled with seawater as function of BW pressure with ozone-CEB

Consequently, the TAMI MF ceramic membranes fouled during filtration of seawater and WW effluent could be effectively recovered to such an extent (i.e., up to about 95% of the initial flux) by a high BW pressure for a short time and with ozone as a CEB, which is attributed to the inherent robustness of ceramic membranes in terms of mechanical and chemical stability.

7.3.2.1. Performance of train 2 – continual operation after BW under high pressure and ozone-CEB

Assessment of the AAO MF membrane recovery while treating WW effluent was studied as function of BW pressure. BW pressure was applied to 20 times from 10 times as high as operation pressure. Initial membrane flux was set to 300 LMH at 0.075 bar, which is much higher than the TMP applied for normal MF membrane operation. After 30 minutes filtration, the fouled AAO MF membrane was backwashed at 0.75 bar (i.e., 10 times higher than TMP) and then filtered again for 30 minutes. The fouled membrane was backwashed at 1.5 bar (i.e., 20 times higher), filtered again for 30 minutes as shown in Figure 7.7.

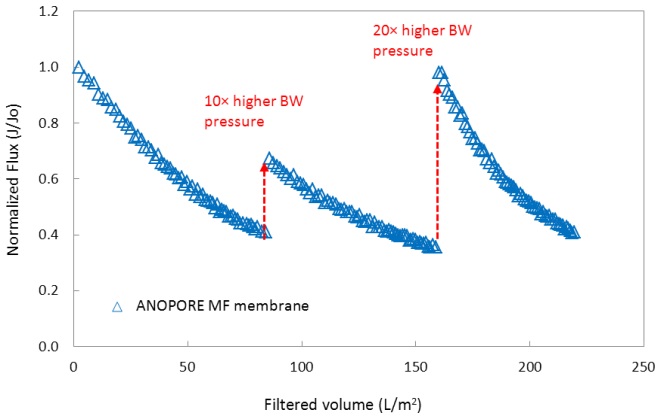

Figure 7.7 – Flux restoration of an AAO ceramic MF membrane fouled with WW effluent by BW pressure of 10 and 20 times as high as operation pressure

Chemically enhance backwashing (CEB) using 2mg/L of ozone dissolved in Milli-Q water was employed to assess the flux restoration rate of the AAO MF ceramic membranes fouled with WW effluent. Initial flux and TMP was applied the same as in previous experiments, corresponding to an initial membrane flux of 300 LMH at 0.075 bar. With ozone-CEB, BW duration was controlled from 4 minutes to 30 seconds under twice higher pressure than operation TMP (i.e., at a 0.15 bar).

As shown in Figure 7.8, while filtering WW effluent for 30 minutes, the AAO MF membrane experienced significant flux decline, showing that the normalized flux decreased to 27% of the initial flux. However, the fouled membrane was almost completely recovered by 4 minutes of BW with ozone, resulting in a normalized flux restoration up to 96% of the initial flux. Again, the membrane was operated for 20 minutes and backwashed for 2 minutes without ozone at this time. The result, however, showed that the flux was just recovered by 58% of the initial flux from 45%. Finally, ozone-CEB tests with reduced time to 2 minutes from 30 seconds were carried out. The results showed that AAO MF membrane fouled with WW effluent experienced almost complete flux restoration by ozone-CEB with reduced BW time to

2 minutes and 30 seconds, showing the normalized flux recovery to 96% and 97% of the initial flux, respectively, as shown in Figure 7.8.

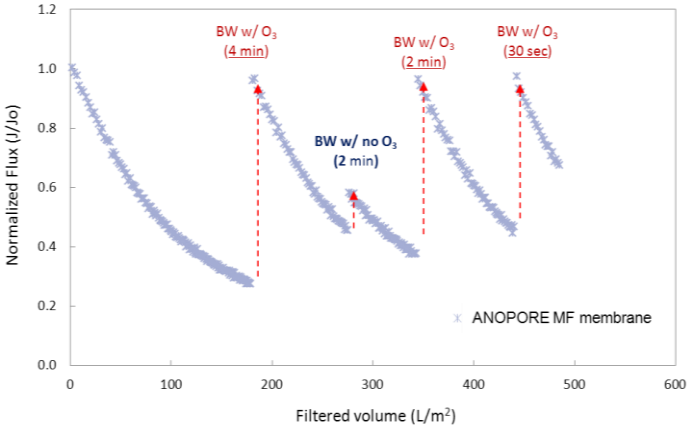

Figure 7.8 – Effects of backwashing duration with ozone-CEB on the flux restoration of AAO ceramic MF membrane fouled with WW effluent

Consequently, it was clearly observed that for both TAMI and AAO ceramic membranes that are fouled with impaired-quality source waters, such as seawater and WW effluent, could be effectively recovered by high BW pressure with short time or ozone-CEB performance regardless of BW time.

7.3.3. Ozone effects on assimilable organic carbon (AOC)

Effects of ozone dose on transformation of AOC in seawater and WW effluent were assessed. Experiments were carried out measuring AOC as function of ozone dose, where bacteria species directly extracted from SW and WW effluent were used for the AOC measurements. Figure 7.9 shows results of AOC variation for seawater with increased ozone dose from 0 to 3.2 mg/L. The AOC concentration increased to 252µg/L from 21µg/L with an increase in ozone dose to 1.0 mg/L from zero. However, as ozone dose increased up to a certain level of 1.7 mg/L, the AOC started

to decrease back to 223µg/L, and further decreased to a lower value of 80µg/L at 2.3 mg/L ozone dose. Finally, as the ozone dose reached to 3.2 mg/L, the AOC was completely oxidized to zero as shown in Figure 7.9.

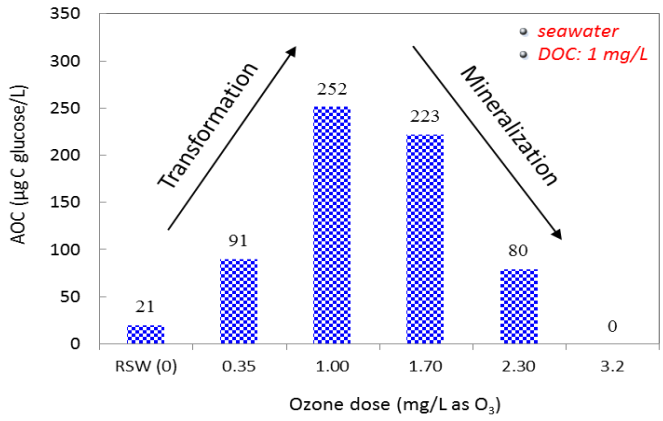

Figure 7.9 - Effects of ozone dose on assimilable organic carbon (AOC) in seawater

The same tests were carried out for WW effluent as shown in Figure 7.10. Results showed that the AOC significantly increased to 3,629 µg/L at an ozone dose of 1.3 mg/L, but as ozone dose increased to 3.2 mg/L, the AOC concentration sharply started to decrease down to 316 µg/L, which was similar to the trend observed in SW experiments. When ozone dose increased to a higher level of 5.8 mg/L and 8.1 mg/L, the AOC concentration decreased to 23 µg/L and 3 µg/L, respectively.

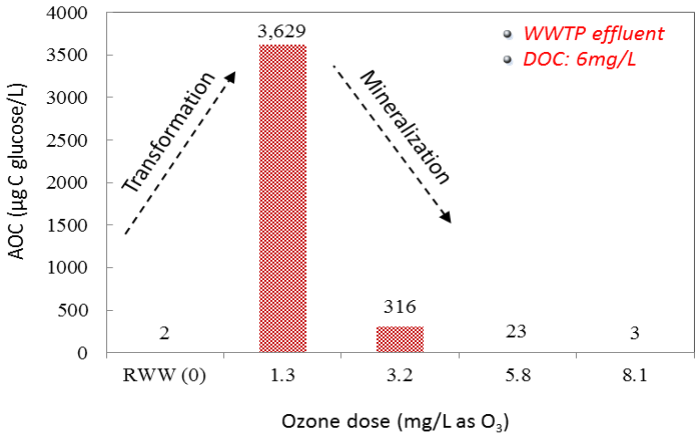

Figure 7.10 – Effects of ozone dose on AOC in WW effluent

Consequently, it was observed that significant AOC production cannot be avoided when ozone is applied as a pretreatment with ceramic membrane filtration for seawater and WW effluent. It was demonstrated that ozone transformed dissolved organic carbon (DOC) into assimilable organic carbon (AOC), so a suitable process to control this parameter (AOC) after ozonation would be indispensable. However, as ozone dose increased to a certain level, AOC started to become mineralized as shown in Figure 7.9 and Figure 7.10.

7.3.4. Discussion of NOM fouling mechanism for WW effluent

To understand ozone effects on organic foulants in WW effluent, natural organic matter (NOM) in four waters – raw, AAO MF treated, 3 mg/L ozone prior to AAO MF treated, and 6 mg/L ozone prior to AAO MF treated – were characterized with liquid (size exclusion) chromatography with organic carbon detection (LC-OCD). Figure 7.11 compares the LC-OCD chromatographic peaks of the four waters. The chromatographic peaks were classified into five fractions with respect to retention time, peak shape and detector ratio of NOM (Huber et al. 2011): fraction A - higher molecular weight (MW) biopolymers such as polysaccharides (PS) and proteins; fraction B - medium MW humic substances (HS) consisting of humic and fulvic acids; fraction C – building blocks (BB) (Volk et al.) reflecting breakdown products of HS or HS-like material of lower molecular weight; fraction D – low molecular weight (LMW) acids co-eluted with LMW-HS; fraction E – LMW neutrals corresponding to LMW alcohols, aldehydes, ketones, sugars, and amino acids.

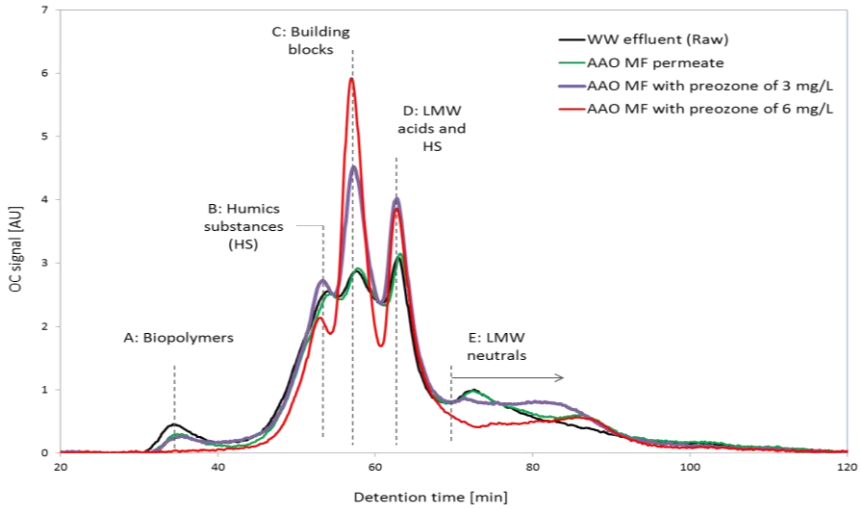

Figure 7.11 - NOM characterization using size exclusion chromatography with organic carbon detection (LC-OCD) for AAO ceramic MF membrane filtration of WW effluent as function of ozone dose

In the case of the AAO MF membrane filtration only, a majority of the organic fractions remained the same as in raw WW effluent. The most significant reduction in NOM was observed in the biopolymer portion (fraction A). With a 3 mg/L dose of preozonation, the biopolymer portion was not decomposed, showing the same as in the MF only; conversely, HS, building blocks and LMW humic acids increased, presumably caused by degradation of biopolymers and passing through the AAO MF membrane. With an increased ozone dose to 6 mg/L, the biopolymers were completely removed; HS were reduced but other portions (i.e., building blocks and LMW humic acids) increased. It is hypothesized that ozone decomposed PS and HS that are relatively higher MW into building blocks and LMW humic acids, which are small enough to pass through AAO MF membrane.

7.4. CONCLUSIONS

pCBA as a ˙OH radical probe compound demonstrated that dissolved ozone in contact with the TAMI ceramic membrane surface (based on TiO_2+ZrO_2) caused the formation of ˙OH radical in WW effluent treatment, showing flux improvement as a result of breaking down organic matter. On the other hand, there was no formation of ˙OH radical observed in seawater application; however, the membrane flux was significantly improved.

Flux restoration of two ceramic membranes, AAO and TAMI, was assessed. Results showed that both ceramic membranes, fouled with impaired-quality source waters (i.e., seawater and WW), could be effectively recovered by high BW pressure and ozone as a chemically enhanced backwash (CEB). This was attributed to the robustness of ceramic membrane in terms of mechanical and chemical stability.

Significant AOC production cannot be avoided when ozone is applied as a pretreatment with ceramic membrane filtration for seawater and WW effluent. The measurements demonstrated that ozone transformed dissolved organic carbon (DOC) into assimilable organic carbon (AOC), so a suitable process to control this parameter (AOC) after ozonation would be indispensable. However, as ozone dose increased to a certain level, AOC started to become mineralized.

To understand ozone effects on organic foulants in WW effluent, natural organic matter (NOM) in four waters – raw, AAO MF treated, 3 mg/L ozone prior to AAO MF treated, and 6 mg/L ozone prior to AAO MF treated – were characterized with

liquid (size exclusion) chromatography with organic carbon detection (LC-OCD). LC-OCD demonstrated that ozone decomposed polysaccharides and humic substances that are relatively higher MW compared to other fractions into building blocks and LMW humic acids, with increasing chromatographic peaks passing through the AAO MF membrane.

It is expected that ozone plays a dual role in oxidizing organic matter leading to less fouling, and cleaning the membrane by inhibiting the rise in TMP.

7.5. REFERENCES

Dafinov, A., Garcia-Valls, R. and Font, J. (2002) Modification of ceramic membranes by alcohol adsorption. Journal of Membrane Science 196(1), 69-77.

Escobar, I.C. and Randall, A.A. (2001) Assimilable organic carbon (AOC) and biodegradable dissolved organic carbon (BDOC):: complementary measurements. Water Research 35(18), 4444-4454.

Escobar, I.C., Randall, A.A. and Taylor, J.S. (2001) Bacterial growth in distribution systems: Effect of assimilable organic carbon and biodegradable dissolved organic carbon. Environmental Science and Technology 35(17), 3442-3447.

Garmash, E.P., Kryuchkov, Y.N. and Pavlikov, V.N. (1995) Ceramic membrane for ultra- and microfiltration (Review). Glass and Ceramic 52(6), 150-152.

Hammes, F., Meylan, S., Salhi, E., Köster, O., Egli, T. and von Gunten, U. (2007) Formation of assimilable organic carbon (AOC) and specific natural organic matter (NOM) fractions during ozonation of phytoplankton. Water Research 41(7), 1447-1454.

Hoigné, J. and Bader, H. (1983) Rate constants of reactions of ozone with organic and inorganic compounds in water—I: Non-dissociating organic compounds. Water Research 17(2), 173-183.

Huang, W.-J., Fang, G.-C. and Wang, C.-C. (2005) The determination and fate of disinfection by-products from ozonation of polluted raw water. Science of The Total Environment 345(1–3), 261-272.

Huber, S.A., Balz, A., Abert, M. and Pronk, W. (2011) Characterisation of aquatic humic and non-humic matter with size-exclusion chromatography - organic carbon detection - organic nitrogen detection (LC-OCD-OND). Water Research 45(2), 879-885.

Karnik, B.S., Davies, S.H.R., Chen, K.C., Jaglowski, D.R., Baumann, M.J. and Masten, S.J. (2005) Effects of ozonation on the permeate flux of nanocrystalline ceramic membranes. Water Research 39(4), 728-734.

Kim, J.-O., Jung, J.-T., Yeom, I.-T. and Aoh, G.-H. (2007) Effect of fouling reduction by ozone backwashing in a microfiltration system with advanced new membrane material. Desalination 202(1–3), 361-368.

Kim, J., Davies, S.H.R., Baumann, M.J., Tarabara, V.V. and Masten, S.J. (2008) Effect of ozone dosage and hydrodynamic conditions on the permeate flux in a hybrid ozonation–ceramic ultrafiltration system treating natural waters. Journal of Membrane Science 311(1–2), 165-172.

Konieczny, K., Bodzek, M. and Rajca, M. (2006) A coagulation-MF system for water treatment using ceramic membranes. Desalination 198(1-3), 92-101.

Larbot, A., Gazagnes, L., Krajewski, S., Bukowska, M. and Wojciech, K. (2004) Water desalination using ceramic membrane distillation. Desalination 168, 367-372.

Lee, S. and Cho, J. (2004) Comparison of ceramic and polymeric membranes for natural organic matter (NOM) removal. Desalination 160(3), 223-232.

Lee, S., Lee, K., Wan, W.M. and Choi, Y. (2005) Comparison of membrane permeability and a fouling mechanism by preozonation followed by membrane filtration and residual ozone in membrane cells. Desalination 178(1–3), 287-294.

Lehman, S.G. and Liu, L. (2009) Application of ceramic membranes with preozonation for treatment of secondary wastewater effluent. Water Research 43(7), 2020-2028.

Oh, B.S., Jang, H.Y., Cho, J., Lee, S., Lee, E., Kim, I.S., Hwang, T.M. and Kang, J.-W. (2009) Effect of ozone on microfiltration as a pretreatment of seawater reverse osmosis. Desalination 238(1–3), 90-97.

Park, Y.G. (2002) Effect of ozonation for reducing membrane-fouling in the UF membrane. Desalination 147(1–3), 43-48.

Rosenfeldt, E.J., Linden, K.G., Canonica, S. and von Gunten, U. (2006) Comparison of the efficiency of OH radical formation during ozonation and the advanced oxidation processes O3/H2O2 and UV/H2O2. Water Research 40(20), 3695-3704.

Song, Y., Dong, B., Gao, N. and Xia, S. (2010) Huangpu River water treatment by microfiltration with ozone pretreatment. Desalination 250(1), 71-75.

Meyn, T. and Leiknes, T. (2010) Comparison of optional process configurations and operating conditions for ceramic membrane MF coupled with

coagulation/flocculation pre-treatment for the removal of NOM in drinking water production. Journal of Water

Van Geluwe, S., Braeken, L. and Van der Bruggen, B. (2011) Ozone oxidation for the alleviation of membrane fouling by natural organic matter: A review. Water Research 45(12), 3551-3570.

Volk, C., Bell, K., Ibrahim, E., Verges, D., Amy, G. and Lechevallier, M. (2000) Impact of enhanced and optimized coagulation on removal of organic matter and its biodegradable fraction in drinking water. Water Research 34(12), 3247-3257.

von Gunten, U. (2003) Ozonation of drinking water: Part I. Oxidation kinetics and product formation. Water Research 37(7), 1443-1467.

Wang, X., Wang, L., Liu, Y. and Duan, W. (2007) Ozonation pretreatment for ultrafiltration of the secondary effluent. Journal of Membrane Science 287(2), 187-191.

Xu, J., Chang, C.-Y. and Gao, C. (2010) Performance of a ceramic ultrafiltration membrane system in pretreatment to seawater desalination. Separation and Purification Technology 75(2), 165-173.

Zhu, H., Wen, X. and Huang, X. (2010) Membrane organic fouling and the effect of preozonation in microfiltration of secondary effluent organic matter. Journal of Membrane Science 352(1–2), 213-221.

Zhu, H.T., Wen, X.H. and Huang, X. (2008) Preozonation for dead-end microfiltration of the secondary effluent: suspended particles and membrane fouling. Desalination 231(1–3), 166-174.

Chapter 8

Phase 4: Comparison of Two Ceramic Membranes on pH-Dependent Filterability for Impaired-Quality Source Waters

Comparison of two ceramic membranes on pH-dependent filterability for impaired-quality source waters

ABSTRACT

The effects of pH on permeate flux of two different types of ceramic membranes that are based on TiO_2+ZrO_2 (i.e., TAMI) and Al_2O_3 (i.e., AAO) for filtration of impaired-quality source waters (e.g., seawater and wastewater effluent) were studied. Bench-scale tests were carried out focusing on assessment of filterability, and membrane fouling under acidic and basic pH conditions. The point of zero charge (PZC) of the TAMI ceramic membrane was near pH 4, while PZC of the AAO ceramic membrane was near pH 9~10. The AAO ceramic membranes showed the highest PWP, followed by TAMI ceramic membranes. Both amphoteric ceramic membranes experienced pH-dependence of permeate flux for filtering WW effluent, showing reduced fouling with increased pH. Flux variation of the Al_2O_3-based AAO membrane was very sensitive to pH value, showing the higher pH, the better permeate flux, while the TiO_2+ZrO_2-based TAMI membrane showed stable flux decline at low pH range (i.e., pH 4.1 ~ 8.1), and became sensitive at the high pH range, resulting in better permeate flux. On the other hand, when filtering seawater, there was a big difference in permeate flux between AAO and TAMI membranes under basic pH conditions. The TAMI membrane flux was stable regardless of change in pH, while the AAO membrane flux significantly decreased down to below 10% of the initial flux as pH increased to 10. The difference in flux between the two ceramic membranes at a pH 10 might be attributed to the ceramic material. The Al_2O_3-based AAO ceramic membrane might

adsorb some metal-hydroxide complexes, causing complete pore-blocking cake formation on the membrane surface, but these chemical reactions are not expected to occur in contact with the TiO_2+ZrO_2-based TAMI ceramic membrane, maintaining stabilized flux at an increased pH level of 10. Ozone played a role in reducing membrane fouling, maximizing chemically stable advantages of the ceramic membranes. Especially, the AAO ceramic membranes showed fully controlled fouling by preozonation, attributed to uniform pore structure/smooth surface roughness of the membranes, helping ozone-treated foulants to be uniformly and loosely formed on the surface.

Keywords: zeta potential, ceramic membranes, impaired-quality source waters

8.1. INTRODUCTION

With rapidly increased applications of polymeric membranes in water sectors, ceramic membranes have been applied in a growing scale because of their inherent mechanical, thermal, and chemical stability, leading to higher permeability, better cleaning conditions, and a longer lifetime that those of polymeric ones (Lee and Cho 2004, Lehman and Liu 2009, Moritz et al. 2001b). The retention of the membranes in filtration processes cannot only be attributed to pure size exclusion effects by the pore structure. Furthermore, electrochemical interactions influence the formation of fouling layers on the membrane surface causing flux decline during the filtration process, and as a result, the filtration efficiency is sharply decreased. Membrane fouling mechanisms (i.e., mainly cake formation and pore blockage) which cause a permeate flux decline in the filtration process are strongly influenced by the surface charge of the membrane (Moritz et al. 2001b).

Ceramic membranes are made of metal oxides, such as Al_2O_3, ZrO_2, TiO_2 and various combinations, and generally asymmetric structures, consisting of a supporting layer with large pores (low flow resistance) of sufficient mechanical strength on top of which are layers with gradually decreasing pore size (Burggraaf and Cot 1996). This can be an advantage for obtaining relatively higher fluxes from thin separation layers. The principal chemical properties of ceramic membranes are their hydrophilicity (Dafinov et al. 2002, Larbot et al. 2004) and amphoteric surface charge because of the presence of hydroxyl (OH^-) groups on their surface. Generally, amphoteric behaviour of metal oxides (i.e., ceramic membranes) is caused by protonation and de-protonation of hydroxyl groups on the material surface (Kosmulski 2012, Moritz et al.

2001a). The surface charge of amphoteric ceramic membranes is able to dissociate when the surface is exposed to polar liquids. The dissociation of amphoteric surface groups strongly depends on the pH value of feed solutions for the membrane filtration, expressed by following two equations of (1) and (2):

$$MOH + H^+ \rightarrow MOH_2^+ \leftrightarrow M^+ + H_2O \qquad (1)$$

$$MOH + OH^- \rightarrow M(OH)_2^- \leftrightarrow MO^- + H_2O \qquad (2)$$

The net surface charge density and potential of the ceramic membrane changes as pH varies because the protonation degree of functional groups on the membrane surface is greatly dependent on the pH value (Kosmulski 2011, Zhou et al. 2009). The pH and ionic strength of the feed waters to membrane units are often altered in conjunction with pretreatment practices aimed at optimizing (i.e., enhancing) membrane performance. Feed waters may be acidified to avoid precipitation of scale, iron or aluminum salts may be added to precipitate soluble species, such as phosphorus and arsenic, and to assist in coagulating colloidal materials and improving permeate flux.

It has been frequently reported that the coagulation process with monolithic Al_2O_3-based ceramic MF membranes was able to be optimized to such an extent that their employment was competitive with polymeric hollow fibre membranes (Konieczny et al. 2006, Lerch et al. 2005). In addition, research have shown that in terms of irreversible fouling development, coagulation pretreatment was effective for Al_2O_3-based MF membrane fouling control in the advanced treatment of secondary effluents (Xu et al. 2010). Coagulation and flocculation prior to ceramic MF membrane filtration is essential as an effective alternative for maintaining higher permeate flux, resulting in efficient removal of NOM (Meyn and Leiknes 2010). Based on these results, coagulation might be necessary for sustainable operation when the Al_2O_3-

based ceramic membrane is applied for filtration of a high-organic surface water or wastewater effluent to inhibit charge neutralization, or adsorption of NOM on the membrane surface.

The aim of this study was to investigate effects of pH on permeate flux of two different types of ceramic membranes that are based on TiO_2+ZrO_2 and Al_2O_3 for filtration of impaired-quality source waters (e.g., seawater and wastewater effluent). Bench-scale tests were carried out focusing on assessment of filterability of the two ceramic membranes under acidic and basic pH conditions. The specific objectives of this study were i) to identify fundamental properties of two ceramic membranes (i.e., pore morphology and layer composition, surface roughness, pure water permeability (PWP), contact angle (CA), and zeta potential (ζ)); ii) to characterize water quality of seawater and WW effluent that are used for tests in terms of natural organic matter (NOM); iii) to compare pH-dependent behaviour in terms of membrane permeability for filtration of both seawater and WW effluent; iv) to compare preozonation effects on filterability of two membranes having different surface morphologies for seawater treatment. In this work, Hermia's models (Hermia 1982) for dead-end filtration were used to investigate the fouling mechanisms involved in the TAMI and AAO MF and UF membrane filtration with or without pre-ozonation for treatment of seawater.

8.2. MATERIALS AND METHODS

8.2.1. Source water

Samples from two different impaired-quality source waters, the Red Sea and the Jeddah wastewater treatment plant (JWTP) in Saudi Arabia, were used for experiments. Throughout the whole experimental period, the feed water was adjusted to room temperature between 19.5°C and 20.5°C, which was established after the waters had been removed from cold storage for a half-day before starting each set of tests. The Red Sea water sample was collected about 1.5 m above the bottom near the intake of a local desalination treatment plant. The DOC measured was about 1.0 mg/L. The secondary JWTP effluent is treated by an anoxic-oxic (AO) activated sludge process. The DOC was between 5.5 mg/L to 6 mg/L. Both seawater and secondary WW effluent were prefiltered with a 0.45μm filter. Water quality analysis of two feed water sources is summarized in Table 8.1. The raw water samples were prefiltered with a 0.45μm filter to remove all particulates.

Table 8.1 – Summary of water quality analysis

Parameter	*Red Sea Water*	*Jeddah WW effluent*
DOC	≈ 1 mg/L	5.5 ~ 6 mg/L
SUVA	1.2±0.2 L/mg·m	2.7 ~2.9 L/mg·m
Ca2+	527 mg/L	79 mg/L
Mg2+	1,436 mg/L	-
pH	7.8 ~ 8.2	7.6 ~ 7.75

8.2.2. Experimental set-up

8.2.2.1. Ceramic membranes

Two different types of ceramic membranes, designated as TAMI and AAO were used for bench-scale tests. The TAMI ceramic membrane (INSIDE DISRAM^{TM}, TAMI INDUSTRIES, France) is fabricated by means of sintering, while the AAO ceramic

membrane (AnodiscTM, Whatman, USA) is obtained by anodic oxidation process. Simple specifications of the two ceramic membranes are summarized in Table 8.2.

Table 8.2 – Simple specification of two ceramic membrane discs used for bench-scale experiments

	TAMI		AAO	
	MF	UF	MF	UF
Pore size, or MWCO	0.14μm	150KD	0.10μm	20nm
Materials	ZrO_2 + TiO_2	ZrO_2 + TiO_2	Al_2O_3	Al_2O_3
Effective surface area (cm^2)	17.4	17.4	17.4	3.14

8.2.2.2. Experimental set-up

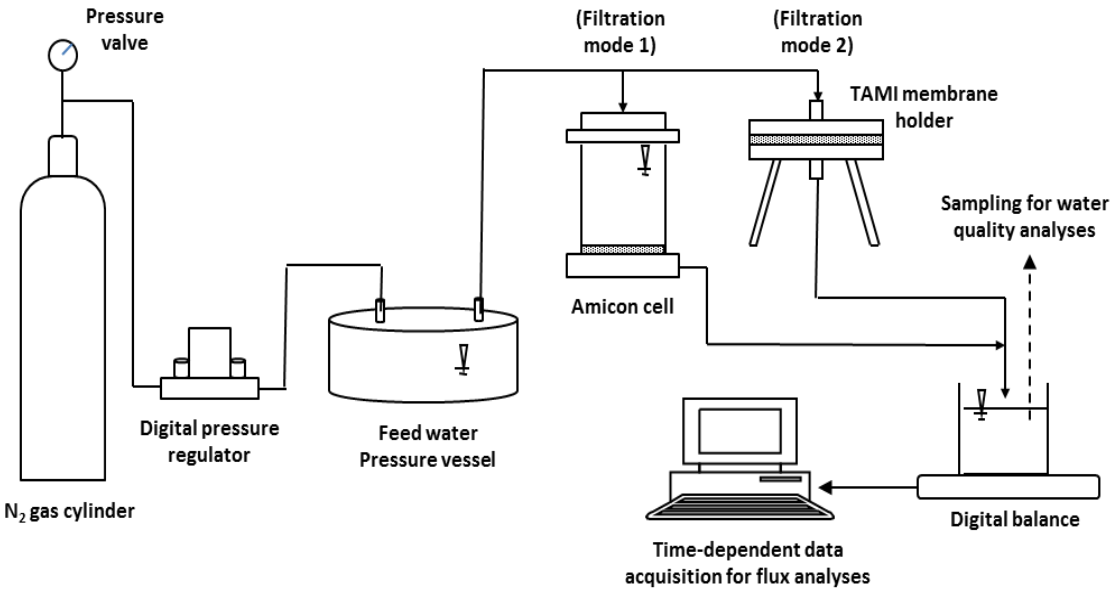

Figure 8.1 - Scheme of ceramic membrane filtration unit that can be separately operated for AAO membranes (mode 1) and TAMI membranes (mode 2)

Figure 8.1 shows the scheme of the ceramic membrane filtration setup which is capable of being operated for both filtration and backwashing in two modes, where two different ceramic membrane discs are set in a special holder for TAMI ceramic

membranes and an Amicon unstirred cell for AAO ceramic membranes. Feed waters – raw water and preozonated water – are filtered through each membrane disc placed inside the holder or the cell in a dead-end filtration mode. Each of filtered waters is accumulated in a beaker under which a digital balance is placed, monitoring the filtered volume as a function of time, every 10 seconds (i.e., permeate flux).

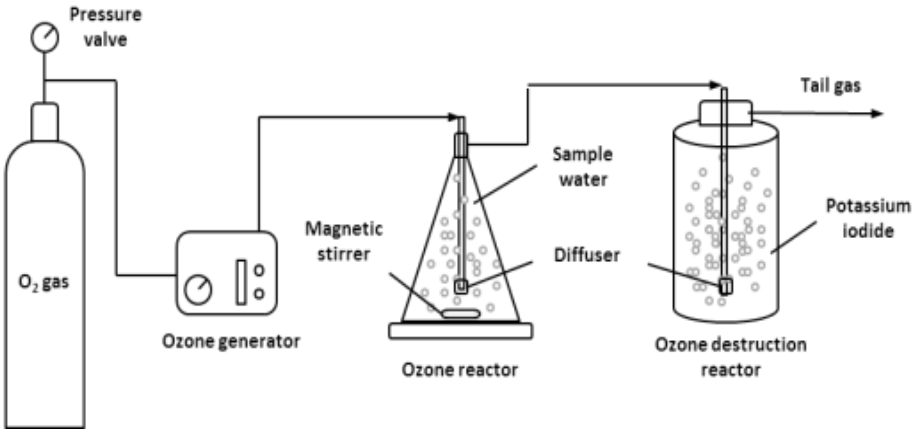

Figure 8.2 – Schematic diagram of ozone pretreatment setup which are carried out prior to ceramic membrane filtration

Figure 8.2 shows the ozone pretreatment setup used for the study. The bench-scale setup is comprised of an ozone generator (Degremont Technologies- Triogen, Scotland), a static batch-reactor flask (2L), and a gas destruction reactor with potassium iodide. Pure oxygen gas from a gas cylinder was fed to the ozone generator. Ozone dose was controlled by adjusting ozone contact time, where a magnetic stirrer at the bottom of the ozone reactor was used in combination with a diffuser in order to mix the water, increasing ozone diffusivity. As soon as a set of ozonation test was completed, the ozonated water was transferred in a pressure vessel 1 (Figure 8.1), immediately performing ceramic membrane filtration.

8.2.3. Flux calculation

Permeate flux (J; L/m^{2}h) was calculated as the flow rate of permeate water (Q; L/h) divided by the effective surface area of the membrane (A; m^2). The filtered water was monitored as a function of time (t; s) and filtered volume (V; m^3), where the permeated volume was recorded at 10 second intervals under a certain pressure over 30 minutes of operation. Specific flux (J_s; L/m^{2}h·bar) refers to the filtrate flux (J) that has been normalized by the transmembrane pressure (TMP). Normalized flux (J/J_0) is calculated as the ratio of flux to the initial flux at the beginning of the filtration (J_0; L/m^{2}h).

8.2.4. Modelling

Four empirical models developed by Hermia (Hermia 1982) that correspond to complete blocking, intermediate blocking, standard blocking and cake layer formation were used for characterization of fouling mechanisms. The parameters considered by these models have a physical meaning and contributed to the comprehension of the mechanisms of membrane fouling. These models were developed for dead-end filtration mode at a constant pressure (equation (1)).

$$\frac{d^2t}{dV^2} = k\left(\frac{dt}{dV}\right)^n \quad (1)$$

Where, V is the filtered volume (m^3), t filtration time (s), k rate (constant depending on n), and n constant (parameter depending on the fouling mechanism). The parameter *n* takes different values for each type of fouling.

8.2.4.1. Complete blocking model (n=2)

According to this model, every model molecule that reaches the membrane surface completely blocks the entrance of the membrane pores. Moreover, a molecule never settles on another molecule that have previously deposited on the membrane surface. Hermia (Hermia 1982) concluded that n was equal to 2 in this model. For n=2, equation (1) linearized and expressed in terms of the permeate flux versus time results in equation (2) (Lim and Bai 2003).

$$\ln J_p = \ln J_0 - k_c\, t \qquad (2)$$

Where J_p is the permeate flux (L/m^2h), J_0 the initial permeate flux (L/m^2h), k_c constant corresponding to complete blocking model (s^{-1}) and t time (s). The parameter k_c can be expressed as a function of the membrane surface blocked per unit of the total volume that permeates through the membrane and the initial permeate flux, J_o (Bowen et al. 1995).

8.2.4.2. Intermediate blocking model (n=1)

This model considers that solute molecules block membrane pores as the molecules approach the open membrane pores. However, every molecule that arrives to the membrane surface dose not block a membrane pore. For the intermediate blocking model (n=1), equation (1) linearized and expressed in terms of the permeate flux as function of time results in equation (3) (Mohammadi et al. 2003).

$$\frac{1}{J_p} = \frac{1}{J_0} + k_i\, t \qquad (3)$$

Where, k_i is constant corresponding to the intermediate blocking model (m^{-1}).

The parameter k_i can be expressed as a function of the membrane surface blocked per unit of the total volume that permeates through the membrane (Bowen et al. 1995).

8.2.4.3. Standard blocking model (n=1.5)

This model considers that molecules deposit over the pore walls. As a result, the volume of membrane pores decreases proportionally to the filtered volume. For the standard blocking model, permeate flux as a function of time is given by the linearized equation (4) (Bowen et al. 1995).

$$\frac{1}{{J_p}^{1/2}} = \frac{1}{{J_o}^{1/2}} + k_s\, t \qquad (4)$$

Where, k_s is constant corresponding to the standard blocking model ($m^{-1/2}$ $s^{-1/2}$). This type of fouling is caused by molecules smaller than the membrane pore size and pore blocking occurs inside the membrane pores (Mohammadi et al. 2003).

8.2.4.4. Cake layer formation (n=0)

In this case, a cake layer forms on the membrane surface. Solutes molecules are greater that the membrane pores and do not penetrate inside them. However, the concentration of solutes is high and they can deposit on the membrane surface and on the previously deposited solute molecule layer. The linearized equation (5) for permeate flux over time is the following (Lim and Bai 2003):

$$\frac{1}{{J_p}^{2}} = \frac{1}{{J_o}^{2}} + k_{cl}\, t \qquad (4)$$

Where, K_{cl} is constant corresponding to the cake layer formation model (s/m^2).

8.2.5. Membrane autopsy and characterization

8.2.5.1. Scanning electron microscopy (SEM)

Membrane specimens were cryogenically preserved in slush nitrogen at −210°C followed by controlled dehydration in a freeze drying instrument (K775X Turbo; Quorum, UK). A scanning electron microscope (SEM) (FEI, USA) equipped with cryo stage and cryo preparation chamber (Quorum, UK) was used to image virgin ceramic membranes. Focused Ion Beam (FIB) technique in combination with SEM was used for cross sectional imaging of the samples. Energy Dispersive X-ray Spectroscopy (EDS or EDX) was used for elemental analysis conducted as spot or mapping analysis.

8.2.5.2. Atomic force microscopy (AFM)

AFM scans the material surface with a very fine tip and generates three-dimensional maps by detection of deflection of a laser beam reflected by a cantilever (Alldredge et al.). The AFM employed is made by Digital Instruments, and data are analyzed by built-in software in the analyzer. The tip size is 4~10 nm made of etched single crystal silicon. AFM was performed with a tapping mode. Tapping provides several advantages: higher lateral resolution on most samples, lower forces and less damage to soft samples imaged in air, and lateral forces are virtually eliminated (there is no scraping), but it provides slightly slower scan speed than contact mode AFM. Clean membrane specimens were prepared with MQ water (≈18Ω) filtration and dried at room temperature to obtain an actual surface. Sample specimens were fixed on a glass slide and scanned over 5μm × 5μm for membranes. Images were obtained in amplitude mode and height mode at the same time. Amplitude mode provides a more

detailed topographical view of the membrane surface in voltage units of the *Z*-axis range, and height mode offers nanometer scaled image analysis. A scan rate of 1~2 Hz was applied considering image features, membranes, and scan sizes.

8.2.5.3. Contact angle (CA)

Contact angle of ceramic membrane surfaces was measured using an optical tensiometer (Theta Lite, attention, Finland). The sessile drop method was selected for the measurement because it is a highly accurate and reproducible optical method, especially for contact angle measurement. The optical tensiometer records drop images, and automatically analyzes the drop shape as a function of time; the captured images are analyzed with a drop-profile fitting method in order to determine contact angle.

8.2.5.4. Zeta potential (ζ)

The ζ potential value of ceramic membranes were determined from electrophoretic mobility measurements using a commercially available electrophoresis measurement apparatus (ELS-Z, Photal, Electronics, Japan) with a plate sample cell. Polystyrene latex particles (diameter 520 nm, Otsuka Electronics, Japan) coated with hydroxyl propyl cellulose (HPC) with a molecular weight of 300,000 (Scientific Polymer Products, Japan) were used as mobility-monitoring particles. These were dispersed in a 0.01MKCl solution to prevent the interactions with (or adsorption on) the quartz cell surface during measurement. The ζ potential of polymeric membranes such as a PVDF MF and MCE UF membrane was measured by SurPASS (Anton Paar, GambH, Graz, Austria) electro-kinetic analyzer across a range of pH values, using electrolyte

solution of 10 mM KCl, respectively. The zeta potential was calculated using Helmholtz–Smoluchowski equation, using streaming potential approach.

8.3. RESULTS AN D DISCUSSION

8.3.1. Fundamental membrane properties

8.3.1.1. Surface morphology and layer composition

Pore morphology and synthetic layer composition of two different types of ceramic membranes (i.e., TAMI and AAO MF and UF membranes) were compared using scanning electron microscopy (SEM). The TAMI ceramic membrane that is obtained by sintering/sol-gel process was asymmetric with multilayered structure with interconnected pores as shown in Figure 9.4 and **Error! Reference source not found.**. The TAMI ceramic membrane was composed of three layers that were the smallest porous active layer at the top supported by an intermediate layer and a macro-porous supporting layer at the bottom. Differences in an active layer composition between MF and UF were observed. The MF had a single active-separation layer, while the UF consisted of a double-coated active layer. SEM images revealed that TAMI ceramic membranes was characterized by pore network obtained by a packing of particles in each layer of the multi-layered system, but each layer was not uniform in terms of thickness and level.

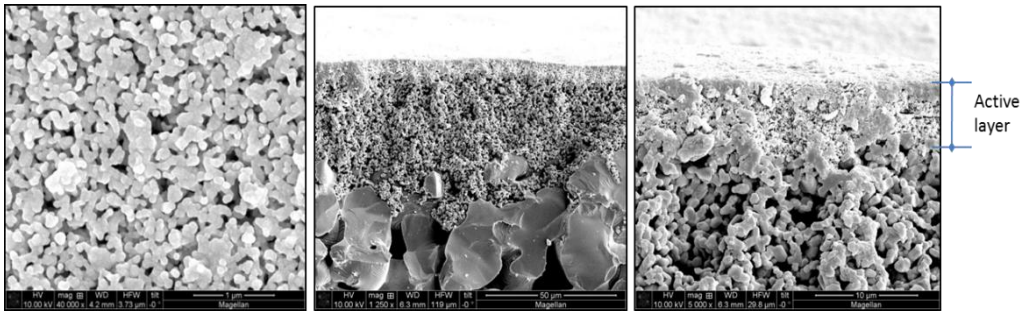

Figure 8.3 – SEM images of a TAMI MF ceramic membrane (left: top view; middle: cross section; right: cross section in higher magnification)

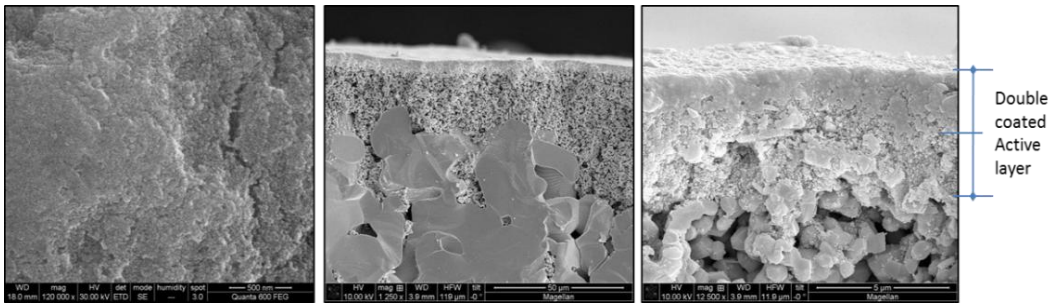

Figure 8.4 – SEM images of a TAMI UF ceramic membrane (left: top view; middle: cross section; right: cross section in higher magnification)

Figure 9.5 presents SEM images of AAO ceramic membranes in terms of top view and cross section. SEM photographs revealed that the AAO ceramic membrane consisted of simple pore morphology, which was different from TAMI ceramic membranes. AAO ceramic membranes are obtained by anodic oxidation process, immersing a piece of aluminum foil in an acidic electrolyte batch, and applying an appropriate potential across it. Different acids yield membranes with different pore size because the rate of field assisted dissolution that results in pore formation depends upon the nature of the electrolyte. Phosphoric and oxalic acids are generally used to produce the commercially available anodic alumina membranes of AAO (Hernández et al. 1997).

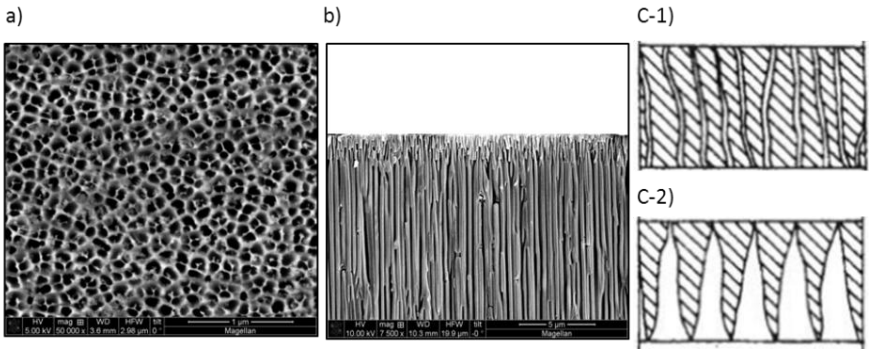

Figure 8.5 - SEM images of an AAO MF ceramic membrane (based on Al_2O_3) which is fabricated by anodic oxidation process: a) top view; b) cross section; c-1) illustration of the MF cross section; c-2) illustration of the UF cross section

As shown in Figure 9.5, the AAO ceramic membranes were characterized by uniform pore-structure that had straight cylindrical-shaped pores and conical-shaped pores for the MF and UF, respectively. SEM cross section images revealed that pore shapes of the AAO MF membrane were symmetrical, showing a single wall without intermediate/supporting layer, while the AAO UF membrane was asymmetric with a conical pore shape. Figure 9.5-c-1) and c-2) illustrate pore shapes of AAO MF and UF membranes.

8.3.1.2. Surface roughness deviation/distribution

Surface roughness and distribution of TAMI and AAO membranes were determined with atomic force microscopy (AFM). There are three commonly used AFM techniques: contact mode, noncontact mode, and tapping mode. In this study, *tapping mode* AFM was used because this mode allows high-resolution topographic imaging of sample surfaces by alternately bringing the tip into contact with the surface to provide high resolution and then lifting it off the surface to avoid dragging the tip across the surface (Boussu et al. 2005). Figure 9.6 shows a comparison of AFM topographical section images of TAMI and AAO MF membrane. AFM section

images revealed that the TAMI membrane surface is rough and relatively deep, having a large roughness deviation, while the AAO membrane resulted in having smoother surface and smaller roughness deviation.

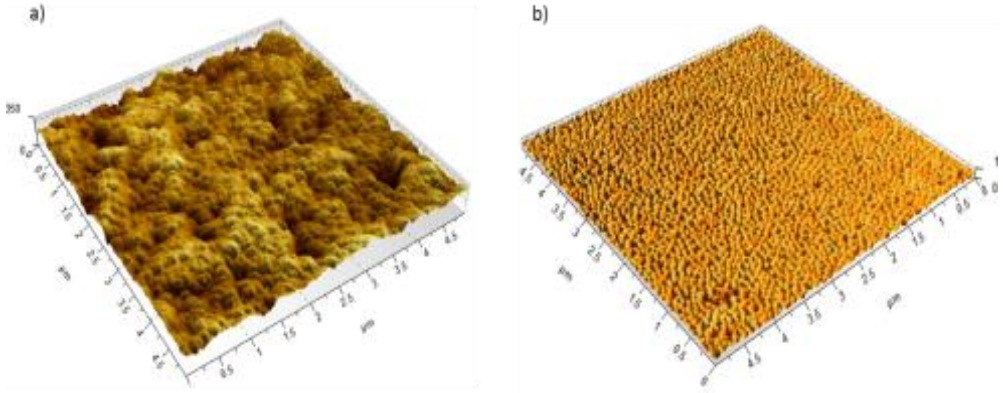

Figure 8.6 – AFM section images of TAMI MF (a) and AAO MF (b): a) 0.5 × 0.5 µm; b) 0.5 × 0.5 µm; note that z-scale of a) and b) is 250 and 1 µm, respectively

Table 8.3 summarizes surf ace roughness deviation of two MF membranes in terms of arithmetic mean deviation (Ra) and root-mean-square deviation (Rq), confirming that the AAO MF surface is smoother than TAMI. The surface roughness profile and distribution measurement were obtained as shown in Figure 8.7. The TAMI MF surface showed wide roughness distribution ranging from 30nm to 320nm and a deep surface, while the AAO MF showed narrow distribution ranging from 30nm to 120 nm and was less deep.

Table 8.3 – Surface roughness deviation of TAMI MF and AAO MF membrane

	Roughness Deviation	*TAMI-MF 140nm*	*AAO-MF 100nm*
Ra	Arithmetic mean deviation	19.4 nm	6.94 nm
Rq	Root-mean-square deviation	24.4 nm	8.72 nm

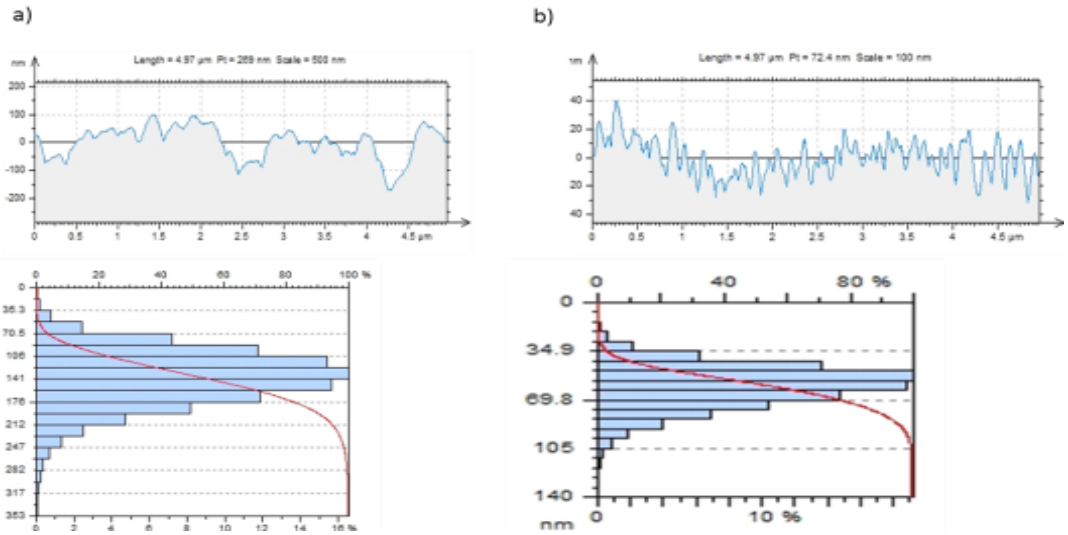

Figure 8.7 – Surface roughness profile/distribution of TAMI MF (a) and AAO MF (b)

AFM surface section images of the TAMI and AAO UF membrane were obtained with the same approach as tried for the AAO MF. As shown in Figure 8.8, AFM images revealed that the TAMI UF membrane surface (Figure a.) was rough with a larger deviation, while the AAO UF membrane (Figure b.) has a relatively smoother surface and smaller deviation, the same as observed in the AAO MF membrane (Lee et al. 2005a).

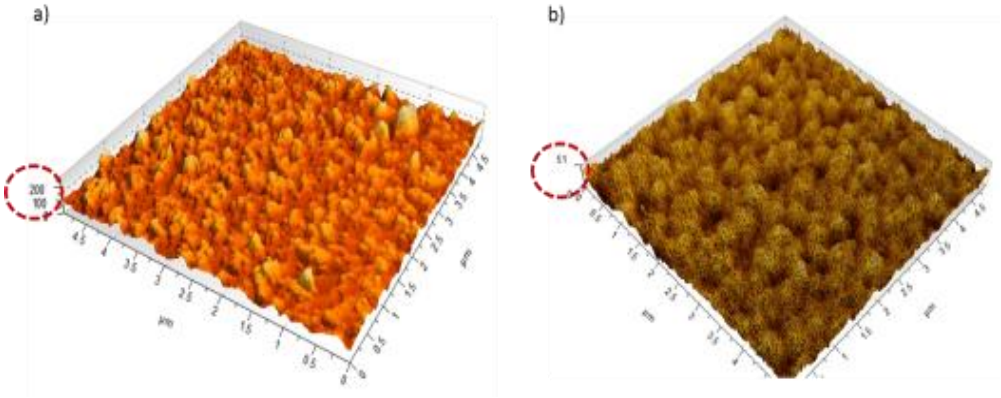

Figure 8.8 - AFM section images of TAMI UF (a) and AAO UF (b): a) 0.5 × 0.5 µm; b) 0.5 × 0.5 µm; note that z-scale of a) and b) is 200 and 51 µm, respectively

Surface roughness deviation of TAMI and AAO UF membranes in terms of arithmetic mean deviation (Ra) and root-mean-square deviation (Rq) were measured, resulting in 12.4 nm and 15.4 nm for TAMI UF and 2.78 nm and 3.45 nm for AAO UF, respectively. The surface roughness profile of both UF membranes was obtained as shown in Figure 8.9. The TAMI UF surface roughness was widely distributed ranging from 50nm to 250nm, while the AAO UF presented a narrower distribution from 10nm to 45 nm and less deeper than the TAMI.

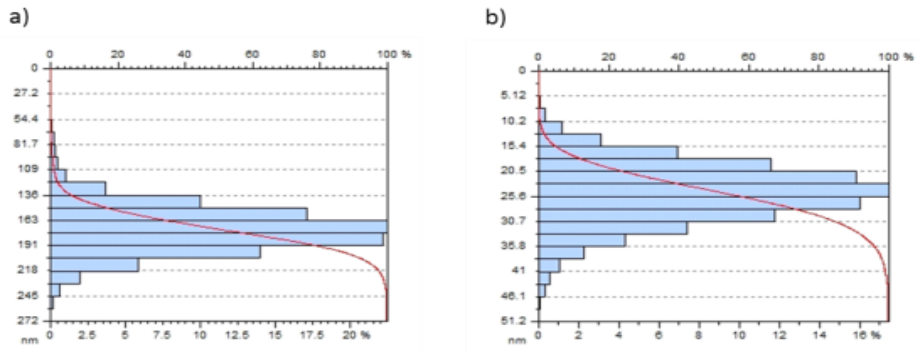

Figure 8.9 – Surface roughness distribution of TAMI UF (a) and AAO UF (b) ceramic membranes

Taking results on SEM and AFM analyses in terms of surface morphology and topology into account, it can be hypothesized that the reason why the AAO membrane exhibited a much higher permeability than the TAMI membrane as shown in Figure 8.10, is that the AAO membrane has a narrower surface roughness distribution and possesses a more uniform pore-structure.

8.3.1.3. Pure water permeability (PWP) and contact angle (CA)

Pure water permeability (PWP) of two ceramic membranes (i.e., TAMI and AAO) with MQ water (≅18Ω) was investigated. Both the TAMI and AAO membrane provided stable operation at TMP of 1 bar, experiencing constant flux without any

fluctuation as shown in Figure 8.10. The AAO MF membrane with a uniformed pore-structure provided higher permeability than the TAMI membrane, resulting in 4,500 L/m^{2}h·bar and 1,500 L/m^{2}h·bar for the AAO and TAMI, respectively. For the UF membranes, results showed that the AAO permeability was significantly higher than the TAMI membrane, performing 2,200 L/m^{2}h·bar and 250 L/m^{2}h·bar for the TAMI and the AAO, respectively. It is hypothesized that the highest permeability resulted from several structural properties, including a uniform pore-structure (i.e., cylindrical and conical-shaped pores, respectively, of MF and UF), a narrower pore distribution, smoother surface roughness and shorter deviation, which are revealed by SEM and AFM analyses in previous sections of 8.3.1.1 and 8.3.1.2.

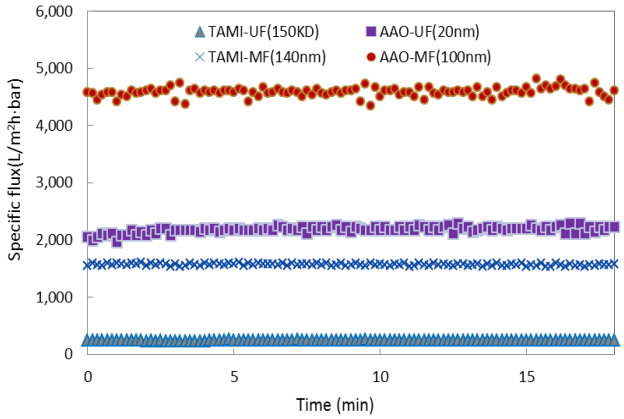

Figure 8.10 – PWP measurement of TAMI and AAO ceramic membranes

Contact angles (CA) were measured. Results showed that both AAO and TAMI membranes were hydrophilic, resulting in 35° (UF) and 25° (MF) for the AAO and 42° (UF) and 50° (MF) for the TAMI. The AAO showed slightly higher hydrophilicity. Table 3.2 summarizes PWP and CA measurement of the TAMI and AAO ceramic membranes, compared to polymeric membranes reported from a literature (Lee et al. 2004).

Table 8.4 – Specifications and properties of TAMI and AAO ceramic membranes, compared with polymeric membranes

	Ultrafiltration (UF) membranes				Microfiltration (MF) membranes			
	AAO	TAMI	PES, Orelis	YM100, Millipore	AAO	TAMI	GVHP, Millipore	GSWP, Millipore
Pore size	20nm	150KDa	100KDa	100KDa	0.1µm	0.14µm	0.22µm	0.22µm
Materials	Al_2O_3	ZrO_2+ TiO_2	PES	Re-generated cellulose	Al_2O_3	ZrO_2+ TiO_2	PVDF	Mixed cellulose ester
PWP ($L/m^2h \cdot bar$)	2200	250	122	372	4500	1500	856	3770
CA (°)	35	42	58	18	25	50	83	19

8.3.1.4. Zeta potential (ζ)

Zeta potential (ζ) of a TAMI (based on TiO_2+ZrO_2) and AAO (based on Al_2O_3) MF ceramic membrane used for the study were measured, compared with a GSWP polymeric MF membrane (based on mixed cellulose ester) as shown in Figure 8.11. Results showed that surface charges of both ceramic MF membranes varied as a function of pH from 3 to 11, resulting in a decrease in zeta potentials (ζ) as pH increased. The TAMI ceramic membrane was positively charged below near pH 4 and negatively charged at higher pH values, while the AAO membrane is positively charged below near pH 10 and negatively charged above the value.

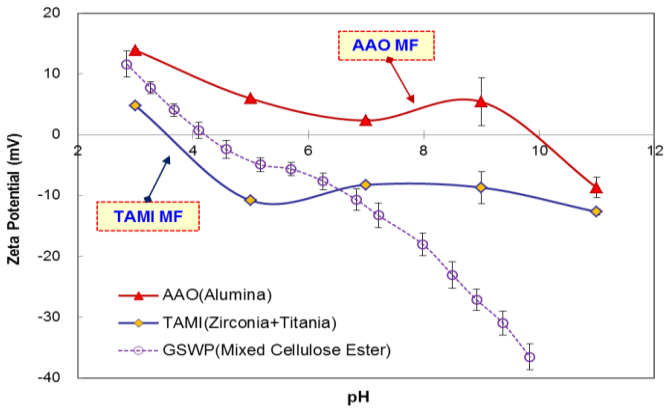

Figure 8.11 – pH dependence of zeta potential of AAO, TAMI and GSWP membranes in a 0.01M KCl solution

Consequently, it was observed that point of zero charge (PZC) of the TAMI ceramic membrane was very low, i.e., near pH 4, which was similar to the PZC of the GSWP membrane, while the PZC of an AAO membrane was very high (i.e., near pH 9~10) as expected due to the alumina-based property of AAO membranes.

8.3.2. Effects of pH on filterability for impaired-quality source waters

Effects of pH on the performance of AAO and TAMI ceramic MF and UF membranes while filtering seawater and secondary wastewater (WW) effluent were evaluated. The pH was adjusted with nitric acid and sodium hydroxide.

8.3.2.1. NOM characterization

To provide basic background information for understanding pH-dependent flux behaviour of TAMI and AAO ceramic membranes, natural organic matter (NOM) in raw seawater and WW effluent was characterized using LC-OCD and 3-dimentional FEEM spectrophotometry.

Wastewater effluent

Figure 8.12 shows LC-OCD chromatographic peaks of raw WW effluent. The chromatographic peaks were clearly classified into five fractions with respect to retention time, peak shape and detector ratio of NOM (Huber et al. 2011): fraction A - higher molecular weight (MW) biopolymers such as *polysaccharides* (PS) and *proteins*, the MW range of which should be 10 KD or higher as the column has a separation range of 0.1~10 kDa; fraction B - medium MW humic substances (HS) consisting of *humic* and *fulvic acids*, with a MW of 1 ~ 10 kDa; fraction C – building

blocks (BB) (Volk et al.) reflecting breakdown products of HS or HS-like material of lower molecular weight; fraction D – low molecular-weight (LMW) acids co-eluted with LMW-HS; fraction E – LMW neutrals corresponding to LMW alcohols, aldehydes, ketones, sugars, and amino acids.

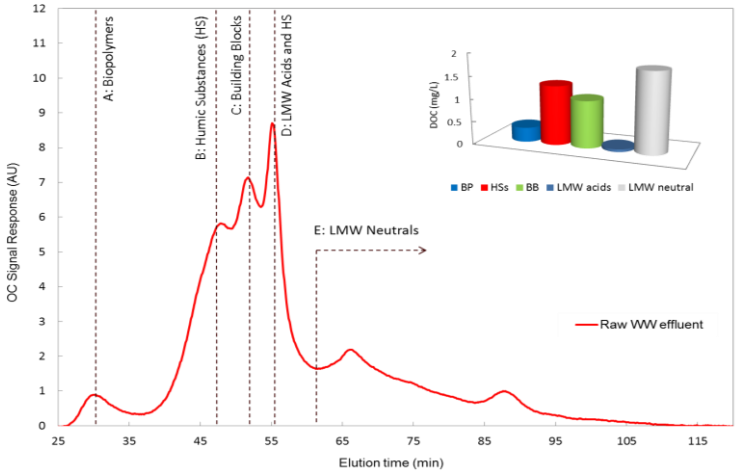

Figure 8.12 - NOM characterization using size exclusion chromatography with organic carbon detection (LC-OCD) for raw wastewater effluent

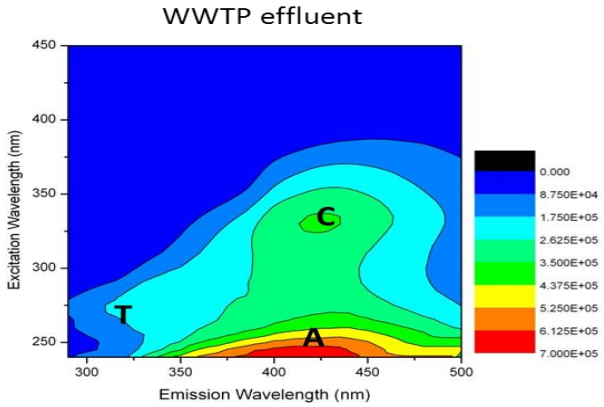

Figure 8.13 - NOM characterization using 3D fluorescence excitation-emission matrix (FEEM) for raw wastewater effluent.

3-dimentional fluorescence excitation-emission matrix (FEEM) spectrophotometry was used to characterize NOM in terms of protein-like and humic-like organic matter. As shown in Figure 8.13, three distinctive fluorescence signals were observed as

follows: peak A, secondary humic-like ($\lambda_{ex/em}$ = 237~260/380~460 nm); peak C, primary humic-like ($\lambda_{ex/em}$ = 300~370/380~480 nm); peak T, protein-like ($\lambda_{ex/em}$ = 275/310~340 nm) as shown in Figure 8.13 (Baker and Genty 1999, Coble 1996, Henderson et al. 2009, Liu et al. 2007).

Seawater

Figure 8.14 shows LC-OCD chromatographic peaks and 3D-FEEM spectrophotometric images of raw seawater. Similar to WW effluent, the LC-OCD chromatographic peaks were classified into five fractions, but showing lower OC signal responses (i.e., lower DOC concentration). Focusing on BP and HS, the peaks signal responded to 0.6 and 1.5 area unit (AU), respectively, while responding to 1.0 and 6.0 AU, respectively, in WW effluent. In particular, only a small amount of protein-like and humic-like NOM was detected as shown in 3D-FEEM spectrometric photograph

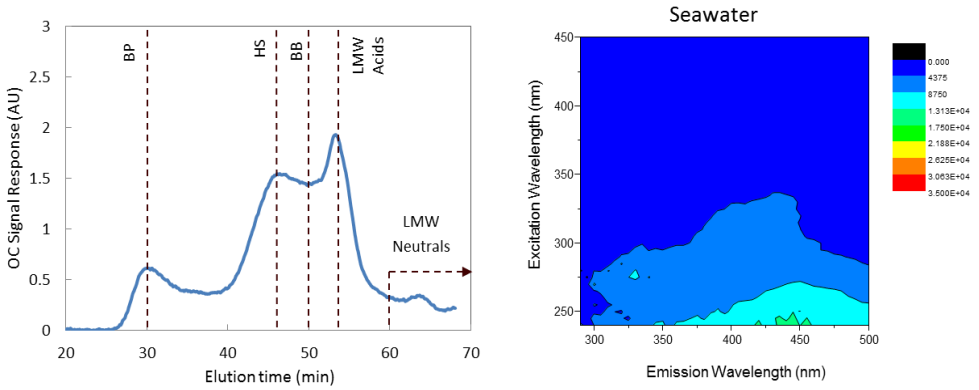

Figure 8.14 - NOM characterization using LC-OCD and 3D fluorescence excitation-emission matrix (FEEM) for raw seawater.

8.3.2.2. pH dependence of permeate flux for WW effluent

For secondary WW effluent, permeate fluxes of AAO and TAMI ceramic MF and UF membranes were compared under various pH conditions. Figure 8.15 shows the normalized flux declines of AAO MF and UF membranes as a function of pH for 30 min. of filtration, where initial fluxes were set between 220 to 250 LMH at 0.1 bar for the MF and at 0.25 bar for the UF. Results showed that with increased pH from pH 4.1 to 10.1, both membrane fluxes improved accordingly. AAO MF membranes experienced significantly reduced fouling with pH increase, showing at a pH 4.1 the normalized flux decreased to 31% of the initial flux; as pH increased to 5.1, 6.1, 7.1, 8.1, 9.1 and 10.1, the normalized fluxes improved to 33%, 38%, 45%, 50%, 74% and 83% of the initial fluxes, respectively. In addition, AAO UF membranes experienced less fouling, showing normalized flux increasing to 44%, 49%, 53%, 59%, 84% and 89% from 43% of the initial fluxes as pH increased to 5.1, 6.1, 7.1, 8.1, 9.1 and 10.1 from 4.1, respectively. Significant differences in flux between low pH range (i.e., 4.1, 5.1, 6.1, 7.1, and 8.1) and higher pH range (i.e., 9.1 and 10.1) were observed.

Consequently, AAO ceramic membrane permeate fluxes completely depended on pH variation of wastewater effluent containing high-elevated organic matter, and the normalized flux significantly improved above pH 9.1. This observation demonstrated that fouling of the Al_2O_3-based AAO membrane which is amphoteric was dependent on pH, showing the higher pH the higher permeability. It was noteworthy that as pH increased to above the PZC of the AAO membrane (i.e., near pH 9), the AAO permeate flux was significantly enhanced, which is attributed to charge repulsion between the membrane surface turned to negative charge and NOM (i.e., especially, polysaccharides and humics) present in WW effluent.

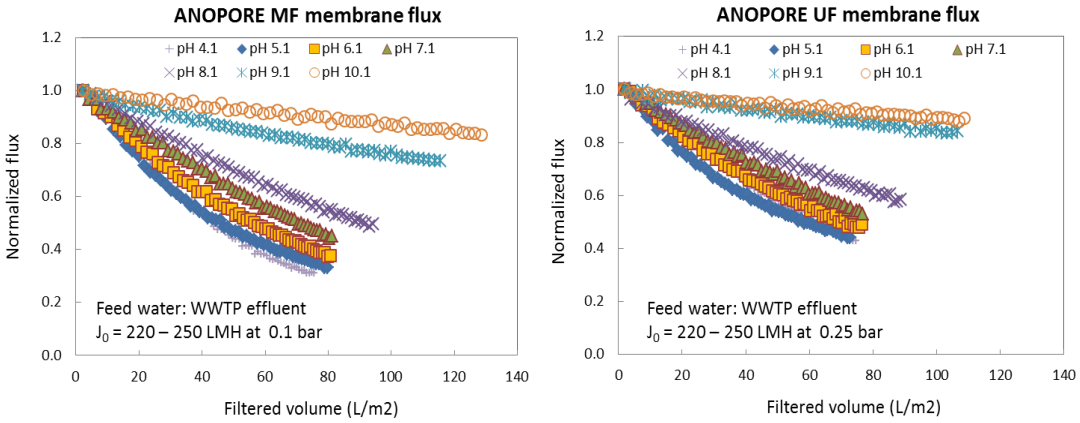

Figure 8.15 – Effects of pH on permeate flux of AAO MF and UF ceramic membranes while filtering secondary WW effluent

Effects of pH on permeate flux of TAMI MF/UF ceramic membranes were assessed. As shown in Figure 8.16, the TAMI membranes experienced differences in flux between low pH range (i.e., 4.1, 5.1, 6.1, 7.1, and 8.1) and high pH range (i.e., 9.1 and 10.1). At the low pH range, there was no remarkable variation in flux of both MF and UF even though the pH increased. Results showed that the normalized fluxes of MF membranes declined to 47, 50, 55, 55, and 50% of the initial fluxes at a pH 4.1, 5.1, 6.1, 7.1, and 8.1, respectively, and similarly the normalized fluxes of UF membranes declined to 59, 57, 61, 62, and 66% of the initial fluxes at a pH 4.1, 5.1, 6.1, 7.1, and 8.1, respectively. On the other hand, as pH increase up to 9.1, both MF and UF membranes experienced significantly less fouling, showing the normalized fluxes increased to 78% and 72%, respectively. Nevertheless, when pH increased higher to 10.1 from 9.1, there was no flux variation of both membranes observed.

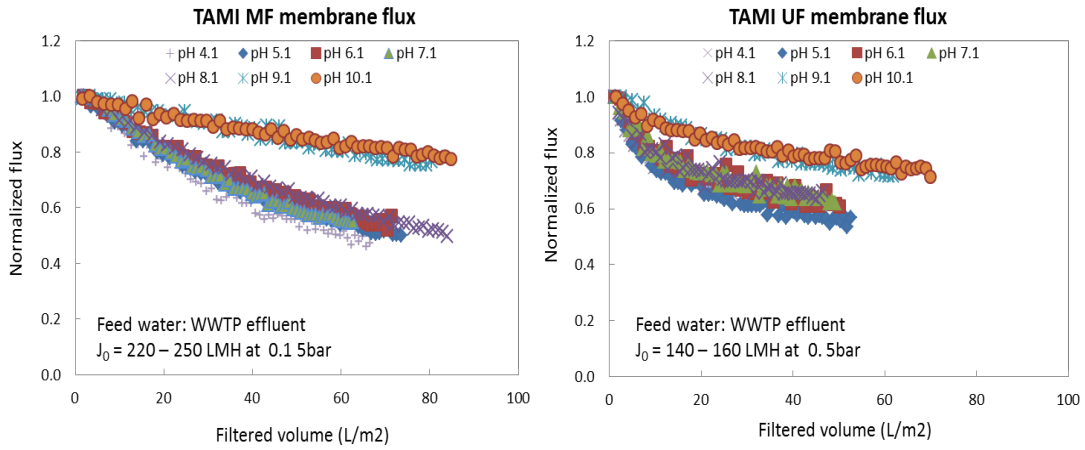

Figure 8.16 - pH-dependent flux variation of TAMI MF and UF ceramic membrane for secondary WW effluent

It was observed that as pH increased from 4.1 to 8.1 (i.e., at low pH range), the normalized fluxes of TAMI membranes were not significantly improved ranging from 47% to 55% for the MF and from 57% to 66% for the UF, however, they were higher than the normalized fluxes of AAO membranes measured at pH 8.1 showing 50% and 59% of the initial fluxes of MF and UF, respectively. Especially, at a pH 4.1, there was a distinctive difference in flux between AAO and TAMI membranes, showing the normalized fluxes of TAMI MF and UF remained at 47% and 59%, respectively, while the normalized fluxes of AAO MF and UF decreased to 31% and 43%, respectively. A potential reason why AAO ceramic membranes experienced more severe flux decline (i.e., more fouling) than TAMI ceramic membranes at low pH range is because the PZC of the AAO membrane is much higher than the TAMI membrane, measuring near pH 9 and pH 4, respectively.

Consequently, both amphoteric ceramic membranes (i.e., TAMI and AAO) experienced pH-dependent flux behavior while filtering wastewater effluent, showing reduced fouling with increased pH, which was more distinctive at high pH range of

9.1 and 10.1. Flux variation of the Al_2O_3-based AAO membrane was very sensitive to pH values from 4.1 to 10.1, resulting in the higher the pH, the better the permeate flux, while the TiO_2+ZrO_2-based TAMI membrane showed stable flux decline at low pH range from 4.1 to 8.1, and started to become sensitive at a higher pH range of 9.1 and 10.1 resulting in better permeate flux.

8.3.2.3. pH dependence of permeate flux for seawater

While treating seawater, permeate fluxes of AAO and TAMI MF and UF membranes were estimated under different pH conditions of 5.0, 8.2 and 10. Figure 8.17 shows the normalized flux decline curves of the AAO MF and UF ceramic membranes as a function of filtered volume. Both AAO MF and UF membranes experienced the same result, showing significant flux decline as pH increased to 10 from 5 and 8.2, which was the complete opposite of results observed in WW effluent treatment. There was no or slight flux variation observed at pH 5.0 and 8.2, while both MF and UF experienced severe fouling as pH increased to 10.

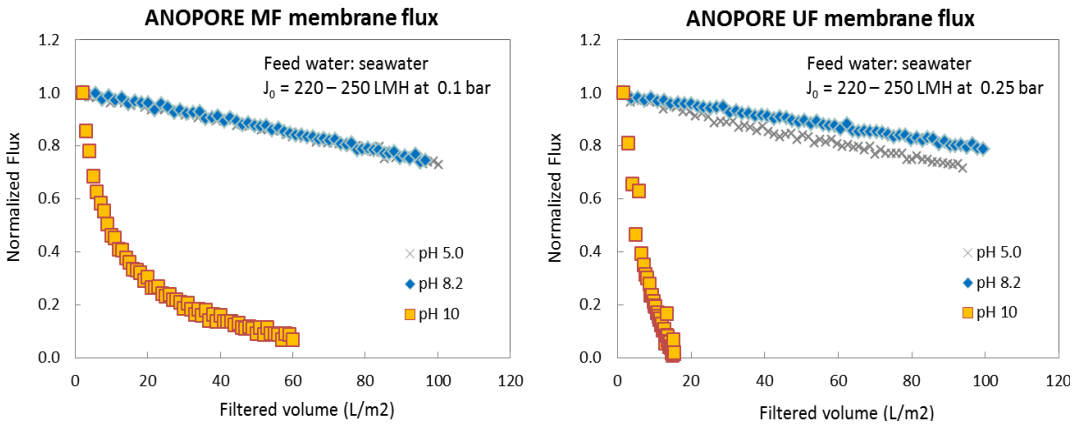

Figure 8.17 - Flux variation of AAO ceramic membrane as a function of pH in seawater treatment application

Results showed that the normalized flux of the AAO MF membrane decreased to 7% of the initial flux from 73% and 75% as pH increased to 10 from 5 and 8.2, respectively. The AAO UF ceramic membrane exhibited more severe fouling, showing the the normalized flux decreased to 2% of the initial flux from 71% and 79% with increased pH to 10 from 5 and 8.2, respectively. From the point of view of the AAO membrane fouling while treating seawater, it can be assumed that the AAO membrane filtration was dominated by complete pore blocking followed by cake formation, causing significant flux decline as pH increased to 10 above the ZPC for AAO (i.e., near pH 9).

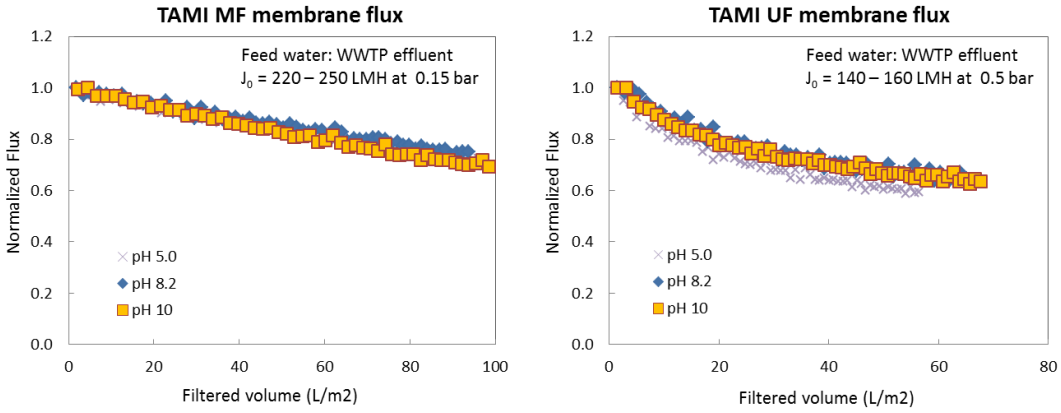

Figure 8.18 - Flux variation of TAMI MF/UF ceramic membrane as a function of pH in seawater treatment application

Effects of pH on permeate fluxes of TAMI MF and UF membranes for filtration of seawater were investigated as shown in Figure 8.18. Results showed that the normalized fluxes of both the MF and UF membranes were maintained stable although pH increased from 5.0 to 8.2 and 10.0. It was observed that the normalized fluxes of MF membranes remained at 72%, 73%, and 70% at a pH 5.0, 8.2 and 10, respectively, as well as the UF membrane fluxes stabilized at 60%, 64%, and 65% of the initial fluxes at a pH 5.0, 8.2, and 10, respectively. It was noteworthy that there

was a big difference in permeate flux between AAO membranes made of Al_2O_3 and TAMI membranes made of TiO_2+ZrO_2 while filtering seawater at a pH 10. The TAMI membrane flux was stable without any fluctuation, while the AAO membrane flux significantly decreased down to below 10% of the initial flux when pH increased to 10.

8.3.2.4. Discussion of fouling mechanisms

It can be hypothesized that the difference in flux between the two ceramic membranes under basic condition of pH 10 might be attributed to the ceramic material. In other words, while filtering seawater at a pH 10 (i.e., under basic pH condition), the Al_2O_3-based AAO ceramic membrane might adsorb some metal-hydroxide complexes, causing severe pore blocking, but such chemical reaction between the TiO_2+ZrO_2-based TAMI ceramic membrane and the metal-hydroxide complexes might not occur.

Based on the results, hypothesized fouling mechanisms of two ceramic membranes (i.e., AAO and TAMI) for filtration of seawater under basic pH condition (i.e., at a pH 10) can be summarized as follows: i) because of high presence of metal ions such a s Ca^{2+} and Mg^{2+} in seawater, metal-hydroxide complexes and metal carbonates (e.g., calcium hydroxide, magnesium hydroxide and calcium carbonate) are formed at a pH 10; ii) these metal-hydroxides bind with the Al_2O_3-based oxide (i.e., the AAO ceramic membrane) while filtering, causing completely pore blocking and cake formation on the membrane surface; iii) but, these chemical reactions do not occur in contact with the TiO_2+ZrO_2-based oxide (i.e., the TAMI ceramic membrane), maintaining stabilized flux at an increased pH level of 10.

In addition to the difference between AAO and TAMI membranes for filtering seawater, an interesting question arises: why do ceramic membranes show a difference in permeate flux behaviour between WW effluent and seawater? First, there are significant differences of water quality, i.e., elevated levels of NOM present in WW effluent versus high concentrations of metal ions (e.g., calcium, magnesium, boron, etc.) present but a low amount of NOM in seawater. Second, NOM dominates flux behaviour for filtering WW effluent, resulting in adsorption of NOM molecules and adhesion of colloids on the membrane surface and pores as a function of pH versus some other dominant behaviour such as crystallization of salts at the pore entrances (i.e., scaling) because of an increased ion concentration on membrane surface resulting in exceeding of the solubility product for filtering seawater. Third, the surface charge of TAMI and AAO ceramic membranes has an influence on the permeate flux according to pH for WW effluent versus no influence on the permeate flux as a function of pH for seawater.

8.3.3. Effects of pre-ozone on ceramic membrane filtration for seawater

8.3.3.1. Permeate flux variation

Effects of preozonation on TAMI and AAO ceramic membrane filtration for seawater were compared. Figure 8.19 shows flux variation of the TAMI and AAO membrane with a preozone dose of 6 mg/L for filtration of seawater. As shown in the figure, permeate fluxes of both TAMI and AAO membrane improved with preozone treatment, which was possible because of the robustness of the ceramic membranes in terms of chemical durability. In particular, the AAO ceramic membranes experienced less membrane fouling than the TAMI membranes (i.e., gentler flux decline), showing

the normalized fluxes were stabilized at 98% ~100% of the initial flux for the MF and at 92% ~100% of the initial flux for the UF. The reason why the AAO membrane flux is fully controlled by preozonation might be attributed to uniform pore structure/smooth surface roughness of the AAO membranes, helping ozone-treated foulants to be uniformly and loosely formed on the surface, while the TAMI membranes are multi-layered with an interconnected pore structure and uneven and deep surface roughness. It is hypothesized that the uniform pore-structured AAO membrane could help to play an important role in stabilizing the flux and controlled fouling when treating preozonated seawater.

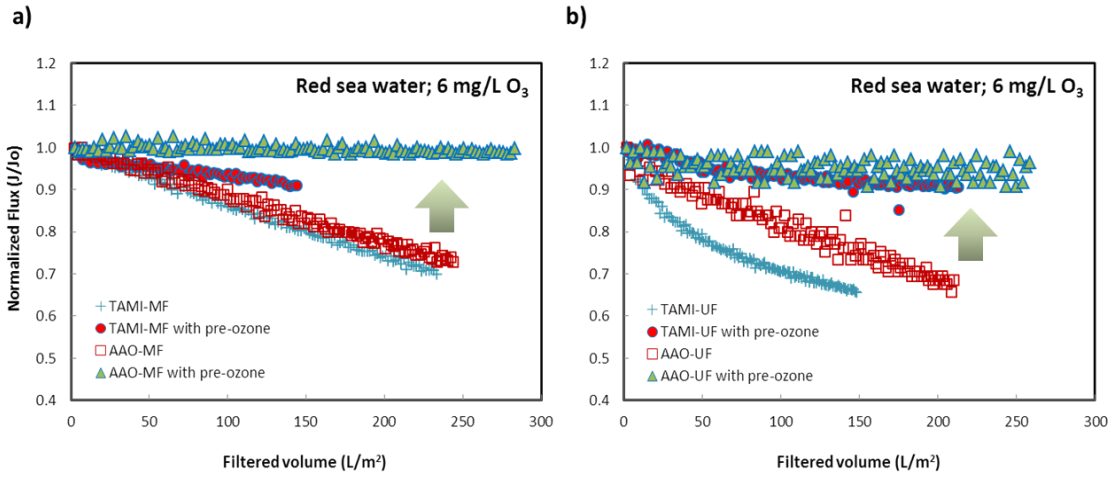

Figure 8.19 – Flux variation of TAMI and AAO ceramic membranes by preozonation for filtration of seawater

8.3.3.2. Characterization of fouling mechanisms

Hermia's models were used to interpret the fouling phenomenon occurring in the TAMI and AAO ceramic MF filtration with or without pre-ozonation experimental test for treatment of seawater. The fitting of experimental data to these models permits to characterize if permeate flux decline is controlled by cake layer formation or pore blocking.

Figure 8.20, Figure 8.21, Figure 8.22 and Figure 8.23 show the fitting of the experimental results to the complete blocking model, the intermediate blocking model, the standard blocking model and the cake layer formation model, respectively, according to equation (2), (3), (4) and (5), respectively. As shown in these Figures, almost no deviation between experimental and predicted flux decline was observed to all types of fouling models (i.e., pore blocking models and a cake layer formation model) for all experimental tests that are the TAMI and AAO ceramic MF membrane filtration with and without pre-ozonation.

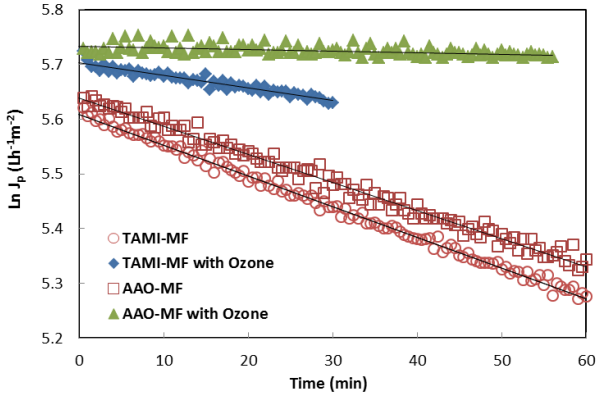

Figure 8.20 – Permeate flux predicted by the complete blocking model for the TAMI and AAO ceramic MF membrane filtration with or without pre-ozonation for filtration of seawater (lines: predicted data; symbols: experimental results)

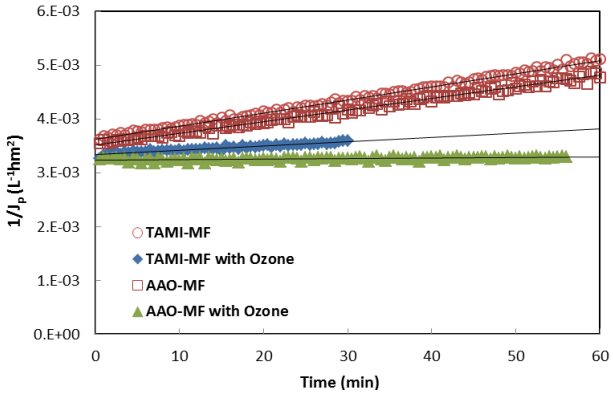

Figure 8.21 - Permeate flux predicted by the intermediate blocking model for the TAMI and AAO ceramic MF membrane filtration with or without pre-ozonation for filtration of seawater (lines: predicted data; symbols: experimental results)

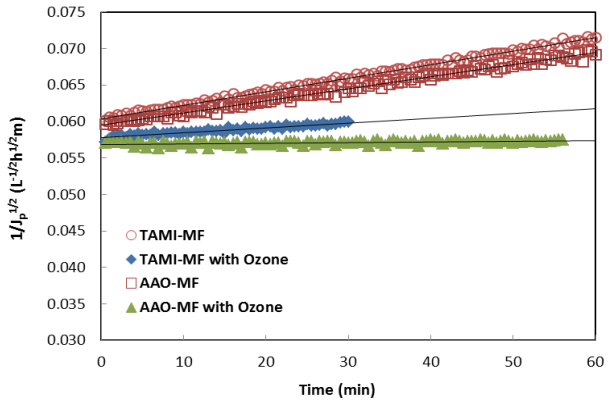

Figure 8.22 - Permeate flux predicted by the standard blocking model for the TAMI and AAO ceramic MF membrane filtration with or without pre-ozonation for filtration of seawater (lines: predicted data; symbols: experimental results)

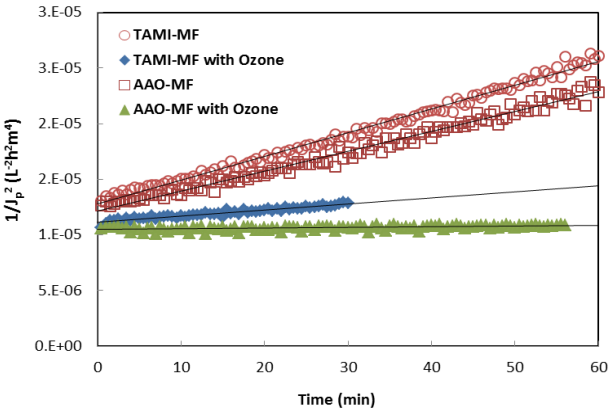

Figure 8.23 - Permeate flux predicted by the cake layer formation model for the TAMI and AAO ceramic MF membrane filtration with or without pre-ozonation for filtration of seawater (lines: predicted data; symbols: experimental results)

Table 8.5 shows the measures of fit to the experimental data obtained with the TAMI and AAO ceramic MF membrane filtration with or without pre-ozonation for Hermia's model. The result shows that fouling of the TAMI and AAO MF membrane filtration without pre-ozone was dominated by standard blocking and all three pore blocking (i.e., complete, intermediate and standard pore blocking), respectively, resulting in the highest R^2 value of 0.996 and 0.987, respectively. However, with pre-

ozonation, both ceramic MF membrane foulings were predominated by cake layer formation, showing the highest R^2 value of 0.924 and 0.236, respectively.

Table 8.5 – Measures of fit to the experimental data obtained with the TAMI and AAO ceramic MF membrane filtration with or without pre-ozonation for Hermia's model: values of R^2

Membrane filtration	*Complete*	*Intermediate*	*Standard*	*Cake layer*
TAMI MF	0.995	0.995	0.996	0.991
O_3 - TAMI MF	0.921	0.922	0.922	0.924
AAO MF	0.987	0.987	0.987	0.983
O_3 - AAO MF	0.233	0.235	0.234	0.236

Table 8.6 shows the values of the fitted Hermia's model parameters for the experimental data obtained with the TAMI and AAO ceramic MF membranes filtration with or without pre-ozonation. According to the physical meaning and the definitions of Hermia's model parameter (i.e., equation (2), (3), (4) and (5)), the values of these parameters should be higher for the filtration tests that correspond to a more severe fouling of the membranes. The result demonstrated that with pre-zonation, both ceramic membrane fouling decreased and consequently, the fitted model parameters were smaller, as expected.

Table 8.6 – Fitted Hermia's model parameters for the TAMI and AAO ceramic MF membrane filtration with or without pre-ozonation

Membrane filtration	$K_c \times 10^4 (s^{-1})$	$K_i \times 10^6 (m^{-1})$	$K_s \times 10^5$ $(s^{-0.5}\ m^{-0.5})$	$K_{cl} \times 10^8 (s\ m^{-2})$
TAMI MF	56.17	24.41	18.50	21.34
O_3 - TAMI MF	22.96	7.93	6.75	5.48
AAO MF	51.56	21.44	16.61	17.91
O_3 - AAO MF	2.80	0.91	0.80	0.59

8.3.3.3. Membrane autopsies

AAO MF membranes fouled with seawater and preozonated seawater were autopsied using AFM and SEM in order to characterize the fouled membranes. The AFM images revealed that the membrane fouled with non-ozonated seawater was fully covered with foulants and there was no open-surface observed, while some aggregates and non-blocked pores were observed at the membrane surface fouled with ozonated seawater as shown in Figure 6.13. Cross-sections of two fouled membranes were photographed using SEM analysis. As shown in Figure 8.25-a), foulants covering the membrane surface that is fouled with seawater were dense and compact, while foulants on the membrane fouled with preozonated seawater were loose and porous as shown in Figure 8.25-b). Both AFM and SEM cross-section images demonstrated that preozonation caused foulants to decompose and while the decomposed foulants are filtered through the AAO MF ceramic membrane, and they were coagulated on membrane surface. However, the aggregated foulants are porous, allowing membrane flux to stabilize sustainably as shown in Figure 8.19.

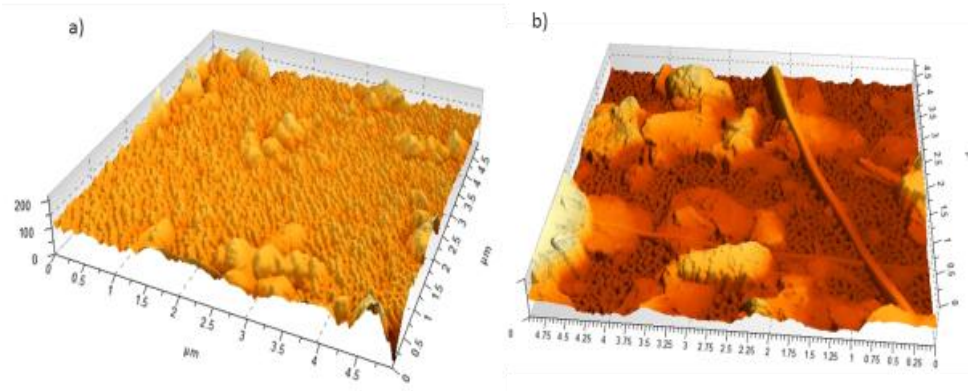

Figure 8.24 – AFM images of AAO MF ceramic membranes which are fouled with raw seawater (a) and preozonated seawater (b)

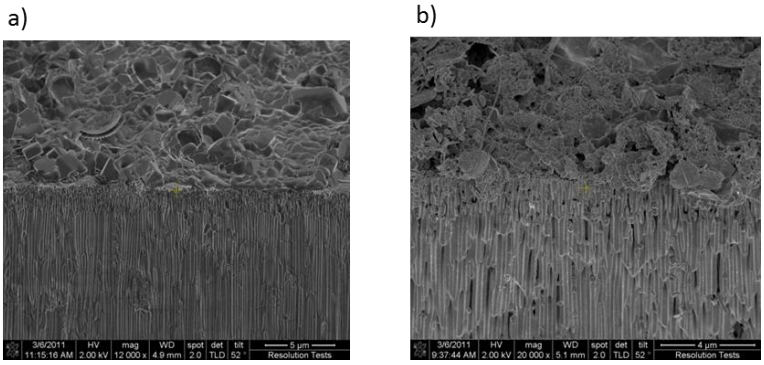

Figure 8.25 - SEM cross-section images of AAO MF ceramic membranes which are fouled with raw seawater (a) and preozonated seawater (b)

In addition, contact angles (CA) of both TAMI and AAO membranes fouled with seawater and preozonated seawater were compared as summarized in Table 8.7. CA values of virgin MF/UF membranes measured were 49°~54° and 40°~42° for TAMI MF and UF, respectively, and 24°~26° and 35°~36° for AAO MF and UF, respectively. Both ceramic membranes fouled without preozonation showed an increase in CA, which was more distinct than for AAO ceramic membranes, while CA values of both membranes fouled with preozonation was lowered to below the level of virgin membranes, resulting in 27°~31° and 42°~45° for TAMI MF and UF and 17°~20° and 29°~30° for AAO MF and UF, respectively. From the point of view of CA variation, it is considered that preozone treatment causes foulants that are hydrophobic to become hydrophilic and, as a result, allows the membrane permeability to significantly improve and stabilize with fully controlled fouling.

Table 8.7 – Contact angle (°) of TAMI and AAO ceramic membranes fouled with seawater and pre-ozonated seawater

		Virgin membrane	*Seawater-fouled membrane*	*Preozonated seawater-fouled membrane*
MF	TAMI	49~54	47~50	27~31
	AAO	24~26	84~88	17~20
UF	TAMI	40~42	68~72	42~45

AAO	35~36	47~48	29~30

8.4. CONCLUSIONS

Effects of pH on permeate flux of two different types of ceramic membranes that are based on TiO_2+ZrO_2 (i.e., TAMI) and Al_2O_3 (i.e., AAO) for filtration of impaired-quality source waters (e.g., seawater and wastewater effluent) were studied. Bench-scale tests were carried out focusing on assessment of filterability, or membrane fouling under acidic and basic pH conditions. Fundamental properties (i.e., pore morphology and layer composition, surface roughness, pure water permeability (PWP), contact angle (CA), and zeta potential (ζ)) and water quality in terms of NOM were identified using various analytical methods to provide information for understanding the pH dependence of permeate flux for seawater and WW effluent. In addition, the effects of ozone prior to TAMI and AAO MF and UF ceramic membranes were compared.

Zeta potential (ζ) measurement demonstrated that the point of zero charge (PZC) of the TAMI ceramic membrane was very low, measured near pH 4, similar to the PZC of the GSWP membrane, while the PZC of the AAO ceramic membrane was near pH 9~10 which was expected because of the alumina-based material.

The PWP of various kinds of membranes were compared. AAO ceramic membranes showed the highest PWP among others followed by TAMI ceramic membranes,

which were higher than polymeric membranes. SEM, AFM, and contact angle revealed that the highest permeability resulted from several structural properties including a uniform pore-structure (i.e., cylindrical and conical-shaped pores, respectively, of MF and UF), a narrower pore distribution, smoother surface roughness and shorter deviation, and a higher hydrophilicity.

Both amphoteric ceramic membranes (i.e., TAMI and AAO) exhibited pH-dependence of permeate flux behavior while filtering wastewater effluent, showing reduced fouling with increased pH and which was more distinctive at high pH range (i.e., pH 9.1 and 10.1). Flux variation of the Al_2O_3-based AAO membrane was very sensitive to pH values from 4.1 to 10.1, showing the higher the pH, the better the permeate flux, while the TiO_2+ZrO_2-based TAMI membrane showed stable flux decline at a low pH range (i.e., pH 4.1 to 8.1), starting to improve at the higher pH range.

While filtering seawater, there was a big difference in permeate flux between AAO and TAMI membranes observed under basic pH conditions. The TAMI membrane flux was stable regardless of change in pH, while the AAO membrane flux significantly decreased down to below 10% of the initial flux as pH increased to 10. The difference in flux between the two ceramic membranes at a pH 10 might be attributed to the ceramic material. When filtering seawater, the Al_2O_3-based AAO ceramic membrane might adsorb some metal-hydroxide complexes, causing pore-blocking cake formation on the membrane surface, but these chemical reactions do not occur in contact with the TiO_2+ZrO_2-based TAMI ceramic membrane, maintaining stabilized flux at an increased pH level of 10

Ozone played a role in improving membrane performance, maximizing chemically stable advantages of the ceramic membranes when treating seawater. Especially, AAO ceramic membranes experienced fully controlled fouling by preozonation, which might be attributed to uniform pore structure/smooth surface roughness of the AAO membranes, helping ozone-treated foulants to be uniformly and loosely formed on the surface, while TAMI membranes are multi-layered with interconnected pore structure with uneven and deep surface roughness.

8.5. REFERENCES

Alldredge, A.L., Passow, U. and Logan, B.E. (1993) The abundance and significance of a class of large, transparent organic particles in the ocean. Deep Sea Research Part I: Oceanographic Research Papers 40(6), 1131-1140.

Baker, A. and Genty, D. (1999) Fluorescence wavelength and intensity variations of cave waters. Journal of Hydrology 217(1-2), 19-34.

Boussu, K., Van der Bruggen, B., Volodin, A., Snauwaert, J., Van Haesendonck, C. and Vandecasteele, C. (2005) Roughness and hydrophobicity studies of nanofiltration membranes using different modes of AFM. Journal of Colloid and Interface Science 286(2), 632-638.

Bowen, W.R., Calvo, J.I. and Hernández, A. (1995) Steps of membrane blocking in flux decline during protein microfiltration. Journal of Membrane Science 101(1-2), 153-165.

Burggraaf, A.J. and Cot, L. (1996) Fundamentals of inorganic membrane science and technology, Elsevier.

Coble, P.G. (1996) Characterization of marine and terrestrial DOM in seawater using excitation-emission matrix spectroscopy. Marine Chemistry 51(4), 325-346.

Dafinov, A., Garcia-Valls, R. and Font, J. (2002) Modification of ceramic membranes by alcohol adsorption. Journal of Membrane Science 196(1), 69-77.

Henderson, R.K., Baker, A., Murphy, K.R., Hambly, A., Stuetz, R.M. and Khan, S.J. (2009) Fluorescence as a potential monitoring tool for recycled water systems: A review. Water Research 43(4), 863-881.

Hermia, J. (1982) CONSTANT PRESSURE BLOCKING FILTRATION LAWS - APPLICATION TOPOWER-LAW NON-NEWTONIAN FLUIDS. TRANS INST CHEM ENG V 60(N 3), 183-187.

Hernández, A., Calvo, J.I., Prádanos, P., Palacio, L., Rodríguez, M.L. and de Saja, J.A. (1997) Surface structure of microporous membranes by computerized SEM image analysis applied to Anopore filters. Journal of Membrane Science 137(1–2), 89-97.

Huber, S.A., Balz, A., Abert, M. and Pronk, W. (2011) Characterisation of aquatic humic and non-humic matter with size-exclusion chromatography - organic carbon detection - organic nitrogen detection (LC-OCD-OND). Water Research 45(2), 879-885.

Konieczny, K., Bodzek, M. and Rajca, M. (2006) A coagulation-MF system for water treatment using ceramic membranes. Desalination 198(1-3), 92-101.

Kosmulski, M. (2011) The pH-dependent surface charging and points of zero charge: V. Update. Journal of Colloid and Interface Science 353(1), 1-15.

Kosmulski, M. (2012) IEP as a parameter characterizing the pH-dependent surface charging of materials other than metal oxides. Advances in Colloid and Interface Science 171–172(0), 77-86.

Larbot, A., Gazagnes, L., Krajewski, S., Bukowska, M. and Wojciech, K. (2004) Water desalination using ceramic membrane distillation. Desalination 168, 367-372.

Lee, N., Amy, G., Croué, J.-P. and Buisson, H. (2004) Identification and understanding of fouling in low-pressure membrane (MF/UF) filtration by natural organic matter (NOM). Water Research 38(20), 4511-4523.

Lee, N., Amy, G., Croué, J.-P. and Buisson, H. (2005) Morphological analyses of natural organic matter (NOM) fouling of low-pressure membranes (MF/UF). Journal of Membrane Science 261(1–2), 7-16.

Lee, S. and Cho, J. (2004) Comparison of ceramic and polymeric membranes for natural organic matter (NOM) removal. Desalination 160(3), 223-232.

Lehman, S.G. and Liu, L. (2009) Application of ceramic membranes with pre-ozonation for treatment of secondary wastewater effluent. Water Research 43(7), 2020-2028.

Lerch, A., Panglisch, S., Buchta, P., Tomita, Y., Yonekawa, H., Hattori, K. and Gimbel, R. (2005) Direct river water treatment using coagulation/ceramic membrane microfiltration. Desalination 179(1-3), 41-50.

Lim, A.L. and Bai, R. (2003) Membrane fouling and cleaning in microfiltration of activated sludge wastewater. Journal of Membrane Science 216(1-2), 279-290.

Liu, R., Lead, J.R. and Baker, A. (2007) Fluorescence characterization of cross flow ultrafiltration derived freshwater colloidal and dissolved organic matter. Chemosphere 68(7), 1304-1311.

Meyn, T. and Leiknes, T. (2010) Comparison of optional process configurations and operating conditions for ceramic membrane MF coupled with coagulation/flocculation pre-treatment for the removal of NOM in drinking water production. Journal of Water Supply: Research and Technology - AQUA 59(2-3), 81-91.

Mohammadi, T., Kazemimoghadam, M. and Saadabadi, M. (2003) Modeling of membrane fouling and flux decline in reverse osmosis during separation of oil in water emulsions. Desalination 157(1-3), 369-375.

Moritz, T., Benfer, S., Arki, P. and Tomandl, G. (2001a) Investigation of ceramic membrane materials by streaming potential measurements. Colloids and Surfaces A: Physicochemical and Engineering Aspects 195(1–3), 25-33.

Moritz, T., Benfer, S., Árki, P. and Tomandl, G. (2001b) Influence of the surface charge on the permeate flux in the dead-end filtration with ceramic membranes. Separation and Purification Technology 25(1–3), 501-508.

Volk, C., Bell, K., Ibrahim, E., Verges, D., Amy, G. and Lechevallier, M. (2000) Impact of enhanced and optimized coagulation on removal of organic matter and its biodegradable fraction in drinking water. Water Research 34(12), 3247-3257.

Xu, J., Chang, C.-Y. and Gao, C. (2010) Performance of a ceramic ultrafiltration membrane system in pretreatment to seawater desalination. Separation and Purification Technology 75(2), 165-173.

Zhou, J., Zhang, X., Wang, Y., Hu, X., Larbot, A. and Persin, M. (2009) Electrokinetic characterization of the Al2O3 ceramic MF membrane by streaming potential measurements. Desalination 235(1–3), 102-109.

Chapter 9

Phase 5: Effects of Three Natural Organic Matter (NOM) Types on fouling of TiO_2+ZrO_2 and Al_2O_3-based Ceramic Membrane Filtration

Effects of three natural organic matter (NOM) types on fouling of TiO_2+ZrO_2-and Al_2O_3-based ceramic membrane filtration

ABSTRACT

The objectives of this study were to identify the impacts of three natural organic matter (NOM) types, in the presence and absence of calcium ions, on both MF and UF ceramic membrane filtration in terms of permeability and removal efficiency, compared to polymeric membranes. Sodium alginate (SA), humic acid (HA) and bovine serum albumin (BSA) solutions were used as NOM models. Two different types of ceramic membranes which are fabricated by sintering (TAMI, based on TiO_2+ZrO_2) and anodic oxidation process (AAO, based on Al_2O_3), and polymeric membranes such as polyvinylidene difluoride (PVDF) and mixed cellulose ester (MCE) for MF and UF, respectively, were applied for bench-scale experiments. The normalized flux declines of the membranes while filtering the three NOM solutions and the rejection rates (%) were compared. Overall, both TAMI and AAO MF and UF ceramic membranes showed better performance compared to the PVDF MF and MCE UF membranes in terms of rejection of the three NOM types. Sodium alginate (SA) solution among the three NOM types caused the most significant fouling and exhibited the highest rejection by both the MF and UF ceramic membranes, followed by HA and BSA. These observations demonstrated that polysaccharides (i.e., hydrophilic NOM) might be the most problematical fouling species in both drinking water (DW) and wastewater (WW) membrane applications compared to humic acid and proteins. Calcium (Ca^{2+}) played an important role in significantly improving

removal efficiency of sodium alginate and humic acid by both ceramic and polymeric MF and UF membranes, while little impact on bovine serum albumin was observed except for the TAMI UF membrane.

Keywords: Ceramic membranes, sodium alginate, humic acid, bovine serum albumin

9.1. INTRODUCTION

One of the critical factors to more widespread use of low-pressure membrane (LPM) technologies such as microfiltration (MF) and ultrafiltration (UF) for both drinking water (DW) and wastewater (WW) treatment is membrane fouling associated with bulk organic matter (Amy 2008, Yuan and Zydney 1999). It has been reported that both hydrophobic (HPO) NOM components such as humic substances (Badis et al. 2010, Katsoufidou et al. 2005, Lee et al. 2006, Maartens et al. 1998, Ruohomäki et al. 1998, Sutzkover-Gutman et al. 2010, Yuan and Zydney 2000), and hydrophilic (HPI) NOM components such as polysaccharides and protein-like substances (Amy 2008, Katsoufidou et al. 2010, Kelly and Zydney 1995, Lee et al. 2004), contributed to membrane fouling. It has been also reported that mixtures (synergy) between HPO and HPI NOM (Kim and Dempsey 2013) or NOM and inorganic constituents (Jermann et al. 2008, Salehi and Madaeni 2010) affected LPM membrane fouling.

The use of MF and UF in both DW and WW applications has been almost exclusively focused on polymeric membranes, while little research has been performed with ceramic membranes. It is generally known that ceramic membranes are physically superior to polymeric membranes and are more resistant to severe chemical environments (Garmash et al. 1995, Lee and Cho 2004). As a result, ceramic membranes have been found to be able to operate at high permeate fluxes, high feed water recoveries, and with less frequent chemical cleaning as compared to conventional polymeric membranes (Amy 2008, Huang et al. 2007, Lee et al. 2004, Lehman and Liu 2009, Pontié et al. 2007).

Due to the robustness of ceramic membranes in terms of mechanical and chemical stability, it is expected that the ceramic membranes can be effectively employed to treat impaired-quality source waters (e.g., seawater and wastewater effluent) in combination with coagulation, especially enhanced coagulation under acidic conditions, and/or ozone (O_3) (Karnik et al. 2005, Kim et al. 2008, Lehman and Liu 2009, Xu et al. 2010). Differences in fouling behaviour of ceramic and polymeric membranes are expected because their surface functional groups are different. The principal chemical properties of ceramic membranes are their hydrophilicity (Dafinov et al. 2002, Larbot et al. 2004) and amphoteric surface charge due to the presence of hydroxyl (OH^-) groups on their surface. These characteristics contribute to high permeability, and influence separation ability and fouling potential as well (Dafinov et al. 2002).

Surrogate organic materials have frequently been used to represent natural organic matter (NOM) and wastewater effluent organic matter (EfOM) in treatment processes for studies of membrane fouling. Commercially available organic foulants include humic acid (HA), sodium alginate (SA) and bovine serum albumin (BSA) extracted from soils or water, representing humic substances, polysaccharides and proteins, respectively. These materials contain organic carbon and are negatively charged at neutral pH. Alginate is a polymer of α-L-guluronate and β-D-mannuronate and from 10 to 600kDa in size depending on the extent of hydrolysis during alkaline extraction from brown algae. BSA is a 66.5 kDa protein with pH_{iep} of 4.7 (Haberkamp et al. 2008). Most of the studies on membrane fouling by different surrogate materials have focused on polymeric UF membranes (Alazmi et al. 2010, Fu et al. 2008, Hao et al. 2013, Hashino et al. 2011a, Hashino et al. 2011b, Jones and O'Melia 2000,

Katsoufidou et al. 2008, Katsoufidou et al. 2010, Salehi and Madaeni 2010), while a few studies on MF membranes have been carried out (Kelly and Zydney 1995, Yang et al. 2011, Yuan and Zydney 1999).

Some researchers have reported that calcium affects membrane fouling and rejection of organic matter, by inducing aggregation and precipitation depending on the calcium concentration (Alazmi et al. 2010, Hao et al. 2013, Katsoufidou et al. 2005, Shao et al. 2011). Divalent cation bridging (DCB) theory emphasizes the role of cations such as calcium and magnesium in bridging between the negatively charged functional groups that exist on extracellular polymeric substances (EPS). This bridging allows biopolymers to aggregate and encourages bio-flocculation (Sobeck and Higgins 2002). The role of divalent cations in membrane fouling is unclear and controversial. Some researchers have reported a reduction in membrane fouling resulting from the formation of larger flocculated particles with increased calcium cation concentration (Aspelund et al. 2008, Kim and Jang 2006). On the other hand, several studies on the interactions of cations, especially divalent calcium cations and EPS components, have reported that the cations form complexes with the organic molecules, which form a compacted fouling layer on the membrane surface and cause severe flux decline (Alazmi et al. 2010, Costa et al. 2006, Hong and Elimelech 1997).

The objectives of this study were to identify the impacts of three NOM types, in the presence and absence of calcium ions, on both MF and UF ceramic membrane filtration in terms of permeability and removal efficiency, compared to polymeric membranes. Sodium alginate (SA), humic acid (HA) and bovine serum albumin (BSA) solutions were used as NOM models. Two different kinds of ceramic membranes

which are fabricated by sintering (TAMI, based on TiO_2+ZrO_2) and anodic oxidation process (AAO, based on Al_2O_3), and polymeric membranes such as polyvinylidene difluoride (PVDF) and mixed cellulose ester (MCE) for MF and UF, respectively, were applied for bench-scale experiments. The normalized flux decline of the membranes while filtering the three NOM solutions and the rejection rate (%) were compared.

9.2. MATERIALS AND METHODS

9.2.1. Materials

The humic acid (HA) (SIGMA-ALDRICH Chemical Co.) solution was prepared by mixing with sodium bicarbonate (SIGMA-ALDRICH Chemical Co.) as a buffer, which was prefiltered with a 0.45 μm cellulose acetate filter. The sodium alginate solution was also prepared with sodium bicarbonate (all regents from SIGMA-ALDRICH Chemical Co.) The bovine serum albumin (BSA) solution was prepared by mixing BSA with a sodium dihydrogen phosphate/disodium hydrogen phosphate buffer solution at pH 7 (all regents from SIGMA-ALDRICH Chemical Co.). The SA and BSA were used without further purification. The calcium-mixed solution was prepared by adding calcium chloride ($CaCl_2 \cdot 2H_20$) (Fisher Scientific Co.) in each NOM solution of SA, HA and BSA.

9.2.2. Experimental setup

9.2.3. Membranes

Two different types of ceramic membranes and polymeric membranes were used for bench-scale tests, as summarized in Table 3.1. The TAMI ceramic membranes (INSIDE DISRAM^{TM}, TAMI INDUSTRIES, France) are fabricated by sintering, and the AAO ceramic membranes (AnodiscTM, Whatman, Germany) are obtained by anodic oxidation process. The polyvinylidene difluoride (PVDF) polymeric membranes (GVHP, Millipore, Germany) and the mixed cellulose ester (MCE) polymeric membranes (VSWP, Millipore, Germany) were used for comparing with the two ceramic membranes. All membranes are hydrophilic.

Table 9.1 – Simple specification of membranes used for bench-scale experiments

	TAMI		AAO		PVDF	MCE
	MF	UF	MF	UF	MF	UF
Pore size, or MWCO	0.14μm	150kDa	0.1μm	20nm	0.1μm	25nm
Materials	ZrO_2 + TiO_2	ZrO_2 + TiO_2	Al_2O_3	Al_2O_3	polyvinylidene difluoride	mixed cellulose ester
Effective surface area (cm^2)	17.4	17.4	17.4	17.4	17.4	17.4

Figure 8.1 shows the scheme of the ceramic membrane filtration setup which is capable of being operated in both filtration and backwashing in two modes, where two different ceramic membrane discs are set in a special holder for TAMI ceramic membranes and an Amicon unstirred cell for AAO ceramic membranes and polymeric membranes (i.e., PVDF and MCE). Feed solutions – SA, HA and BSA – in the presence/absence of 4 mmol/L calcium were filtered through each membrane disc placed inside the holder or the cell in a dead-end filtration mode. The HA feed

solution consisted of 50 mg/L sodium alginate in 0.5 mM/L sodium bicarbonate as a buffer solution at pH 8; 50mg/L of SA and BSA solutions were prepared as described in section 9.2.1. Each of filtered water was accumulated in a beaker under which a digital balance is placed, monitoring the filtered volume as a function of time, every 10 seconds.

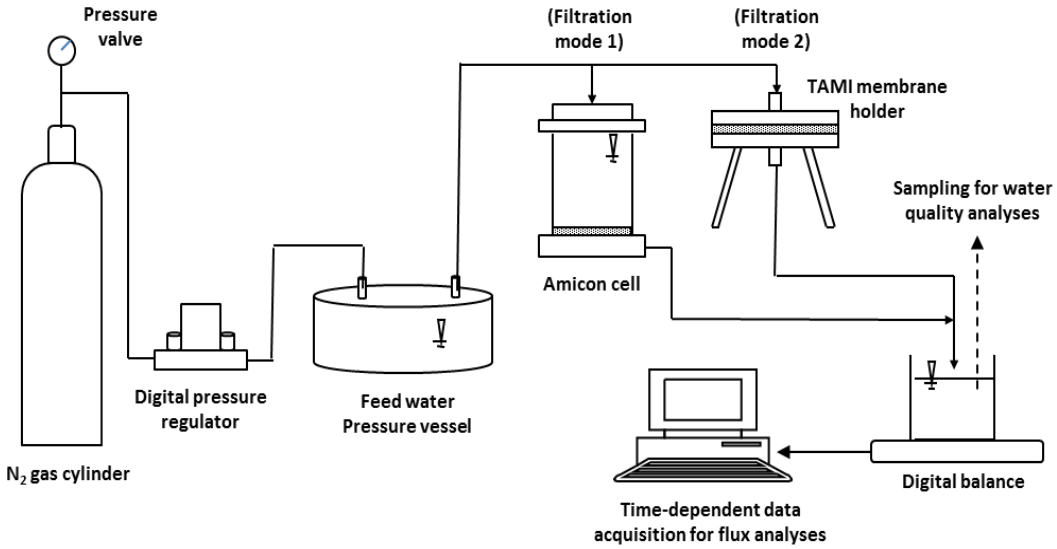

Figure 9.1 - Scheme of ceramic membrane filtration unit that can be separately operated for AAO membranes and polymeric membranes (i.e., PVDF and MCE) (mode 1) and TAMI membranes (mode 2)

9.2.4. Analytical methods

9.2.4.1. Zeta potential (ζ)

The ζ potential values of ceramic membranes were determined from electrophoretic mobility measurements using a commercially available electrophoresis measurement apparatus (ELS-Z, Photal, Electronics, Japan) with a plate sample cell. Polystyrene latex particles (diameter 520 nm, Otsuka Electronics, Japan) coated with hydroxyl propyl cellulose (HPC) and with a molecular weight of 300,000 (Scientific Polymer

Products, Japan) were used as mobility-monitoring particles. These were dispersed in a 0.01M KCl solution to prevent the interactions with (or adsorption on) the quartz cell surface during measurement. The ζ potential of polymeric membranes such as a PVDF MF and MCE UF was measured by SurPASS (Anton Paar, GambH, Graz, Austria) electro-kinetic analyzer across a range of pH values, using electrolyte solutions of 1 mM KCl and 10 mM KCl, respectively. The zeta potential was calculated using Helmholtz–Smoluchowski equation, using the streaming potential approach.

9.2.4.2. Scanning electron microscopy (SEM)

Membrane specimens were cryogenically preserved in slush nitrogen at –210°C followed by controlled dehydration in a freeze drying instrument (K775X Turbo; Quorum, UK). A scanning electron microscope (SEM) (FEI, USA) equipped with cryo stage and cryo preparation chamber (Quorum, UK) was used to image virgin ceramic membranes. Focused Ion Beam (FIB) technique in combination with SEM was used for cross sectional imaging of the samples.

9.2.4.3. Atomic force microscopy (AFM)

AFM scans the material surface with a very fine tip and generates three-dimensional maps by detection of deflection of a laser beam reflected by a cantilever. The AFM employed is made by digital instruments, and data are analyzed with built-in software in the analyzer. The tip size is 4~10 nm made of etched single crystal silicon. AFM was performed with a tapping mode. Tapping brings several advantages: higher lateral resolution on most samples, lower forces and less damage to soft samples imaged in air, and lateral forces are virtually eliminated (there is no scraping); however, it

provides a slightly slower scan speed than contact mode AFM. Clean membrane specimens were prepared with MQ water (≈18Ω) filtration and dried at room temperature to obtain an actual surface. Sample specimens were fixed on a glass slide and scanned over 5μm × 5μm for membranes. Images were obtained in amplitude mode and height mode at the same time. Amplitude mode provides a more detailed topographical view of the membrane surface in voltage units of the *Z*-axis range, and height mode offers nanometer scaled image analysis. A scan rate of 1~2 Hz was applied considering image features, membranes, and scan sizes.

9.2.4.4. NOM analysis

Concentrations of sodium alginate in the feed solution and permeate were measured using a total organic carbon (TOC) meter (TOC-V, Shimadzu Co., Japan). Rejection of sodium alginate was calculated as:

$$\text{Rejection (\%)} = \frac{C_0 - C}{C_0} \times 100 \quad (1)$$

Where C_0 and C are the TOC in feed and permeate, respectively. The rejection of humic acid and BSA were calculated according to Eq. (1) by measuring UV absorbance at 254nm and 280 nm, respectively, using a UV-visible spectrophotometer (Shimadzu UV 2501 PC, Japan).

Liquid (size exclusion) chromatography with organic carbon detection (OCD) and UV detection (UVD), known as LC-OCD-UVD based on the Gräntzel thin-film UV-reactor, was used to characterize NOM in terms of chromatographic peaks that are observed with a special column. On-line purified mobile phase (phosphate buffer

solution exposed to UV-irradiation in an annular UV-reactor) is delivered with an HPLC pump (S-100, Knauer, Berlin, Germany) at a flow rate of 1.1 mL/min to an auto-sampler (MLE, Dresden, Germany, 1mL injection volume) followed by a chromatographic column (250mm × 20mm, TSK HW 50S, 3000 theoretical plates, Toso, Japan).

3D fluorescence excitation-emission matrix (EEM) spectra was analysed to help characterize NOM in terms of protein-like and humic-like organic matter with a Fluoromax-4 spectrofluorometer (HORIBA scientific, Japan) in a 4 mL quartz cuvette cell, where temperature was adjusted at 20°C. Fluorescence EEMs were measured in the excitation range of $\lambda_{ex} = 240{\sim}450$ nm and the emission range of $\lambda_{em} = 290{\sim}500$ nm at 5 nm increments with a slit width of 5 nm for both.

9.2.4.5. Flux calculation

Permeate flux (J; L/m^{2}h) was calculated as the flow rate of permeate water (Q; L/h) divided by the effective surface area of the membrane (A; m^2). The filtered water was monitored as function of time (t; s) and filtered volume (V; m^3), where the permeated volume was recorded every 10 second intervals under a certain pressure for filtration. Normalized flux (J/J_0) was calculated as the ratio of flux to the initial flux at the beginning of the filtration (J_0; L/m^{2}h).

9.3. RESULTS AND DISCUSSION

9.3.1. Zeta potential (ζ) measurements

Zeta potentials (ζ) of a TAMI (based on TiO_2+ZrO_2) and AAO (based on Al_2O_3) MF ceramic membrane used for this study were measured, comparing with the PVDF and MCE MF membranes as shown in Figure 9.2. Surface charges of both ceramic MF membranes exhibited pH-dependent surface charge, resulting in a decrease in zeta potentials (ζ) with increased pH. Results showed that the TAMI ceramic membrane was positively charged below pH 4 and negatively charged at higher pH values with a point of zero charge (PZC) near pH 4. On the other hand, the AAO membrane has a positive charge below pH 10 and negative charge above the value. It was observed that the PZC of the TAMI ceramic membrane was very low (i.e., near pH 4), similar to PZC of a MCE polymeric membrane, while the PZC of the AAO membrane was high in between pH 8 to 10 as expected due to the alumina-based property. The PVDF membrane was negatively charged from pH 2 to 10.

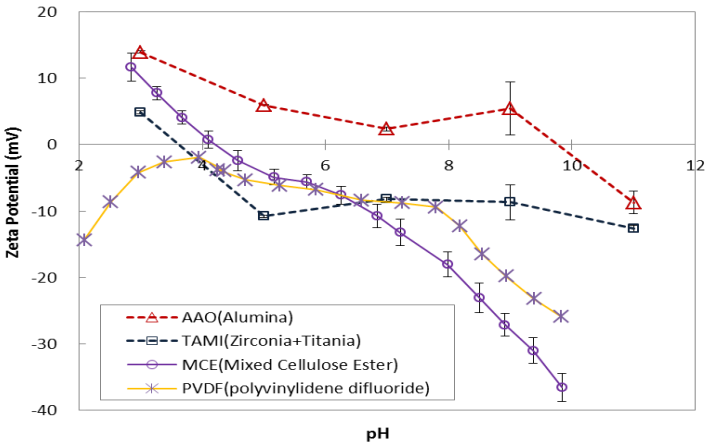

Figure 9.2 – pH-dependent zeta potentials (ζ) of an AAO MF and a TAMI MF ceramic membrane in a 0.01MKCl solution

9.3.2. Surface morphologies and pore structures

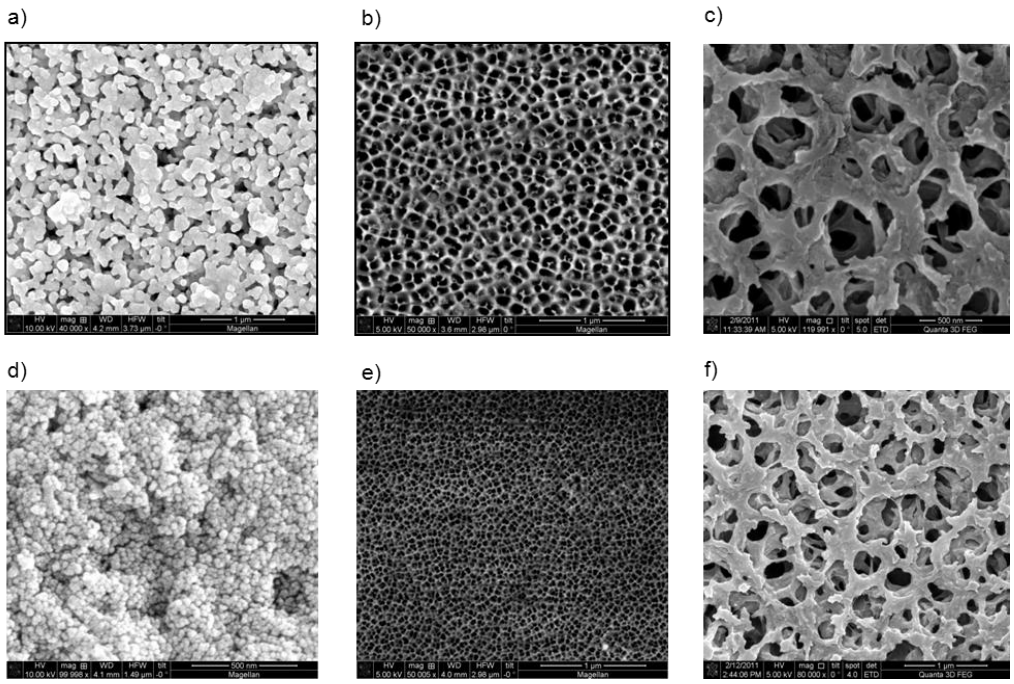

Figure 9.3 – SEM images for the TAMI, AAO, PVDF and MCE membranes: a) and d) the TAMI MF and UF, respectively; b) and e) the AAO MF and UF, respectively; c) the PVDF MF membrane; f) the MCE UF membrane

Figure 9.3 shows SEM images of surface morphologies of two set of ceramic membranes (i.e., TAMI MF and UF membranes and AAO MF and UF membranes) and polymeric membranes (i.e., a PVDF MF membrane and a MCE UF membrane). The differences between all of the membranes were observed. SEM images of the two ceramic membranes demonstrated that the pore shapes of the TAMI MF and UF membranes are irregular and interconnected with each other, while the AAO MF and UF membranes presented a uniform pore-structure. SEM images of both PVDF MF and MCE UF membranes were obtained from the manufacture's websites, showing that both are irregular pore shapes with wide ranges of pore sizes and a surface density which appeared to be looser than both ceramic membranes.

In particular, pore morphology and synthetic layer composition of two ceramic membranes (i.e., TAMI and AAO membranes) were compared. Figure 9.4 represents the TAMI ceramic MF membrane that was asymmetric with multilayered structure with interconnected pores. The TAMI ceramic membrane was composed of three layers that were the smallest porous active layer at the top supported by an intermediate layer and a macro-porous supporting layer at the bottom. Differences in an active layer composition between MF and UF were observed. The MF had a single active-separation layer as shown in Figure 9.4, while the UF consisted of a double-coated active layer. SEM images revealed that TAMI ceramic membranes was characterized by pore network obtained by a packing of particles in each layer of the multi-layered system, but each layer was not uniform in terms of thickness and level.

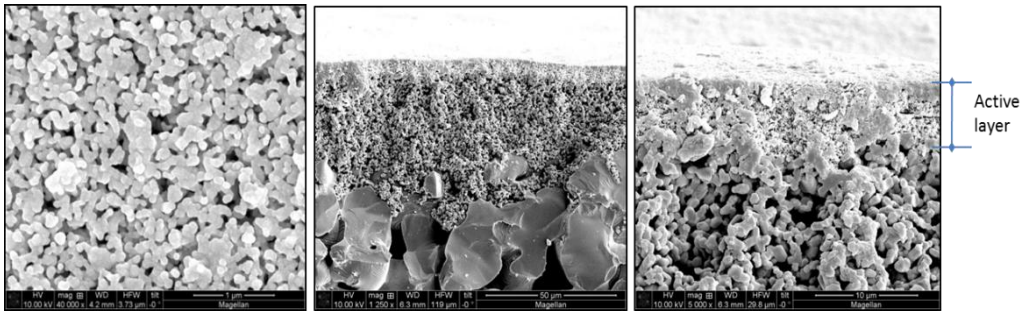

Figure 9.4 – SEM images of a TAMI ceramic MF membrane (left: top view; middle: cross section; right: cross section in higher magnification)

Figure 9.5 presents SEM images of AAO ceramic membranes in terms of top view and cross section. SEM photographs revealed that the AAO ceramic membrane consisted of simple pore morphology, which was different from TAMI ceramic membranes. As shown in Figure 9.5, AAO ceramic membranes were characterized by uniform pore-structure that had straight cylindrical-shaped pores and conical-shaped pores for the MF and UF, respectively. SEM cross section images revealed that pore

shapes of the AAO MF membrane were symmetrical, showing a single wall without intermediate/supporting layer, while the AAO UF membrane was asymmetric with a conical pore shape. Figure 3.6-c-1) and c-2) illustrate pore shapes of AAO MF and UF membranes.

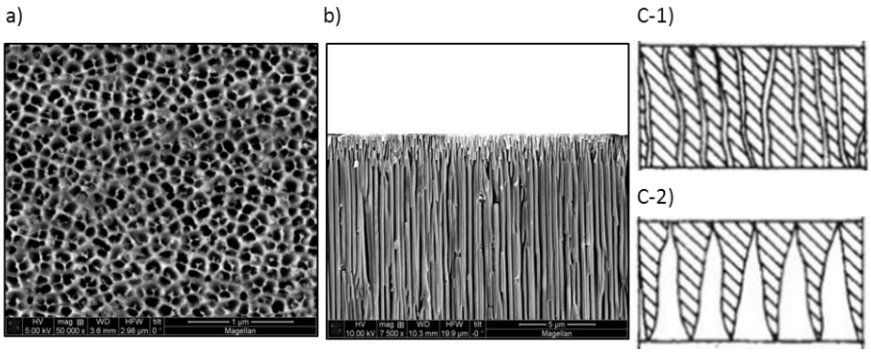

Figure 9.5 - SEM images of an AAO MF ceramic membrane (based on Al_2O_3) which is fabricated by anodic oxidation process: a) top view; b) cross section; c-1) illustration of the MF cross section; c-2) illustration of the UF cross section

9.3.3. Surface roughness deviation/distribution

Surface roughness and distribution of TAMI and AAO membranes were determined with atomic force microscopy (AFM). There are three commonly used AFM techniques: contact mode, noncontact mode, and tapping mode. In this study, *tapping mode* AFM was used because this mode allows high-resolution topographic imaging of sample surfaces by alternately bringing the tip into contact with the surface to provide high resolution and then lifting it off the surface to avoid dragging the tip across the surface (Boussu et al. 2005). Figure 9.6 shows a comparison of AFM topographical section images of TAMI and AAO MF membrane. AFM section images revealed that the TAMI membrane surface is rough and relatively deep, having a large roughness deviation, while the AAO membrane resulted in having smoother surface and smaller roughness deviation.

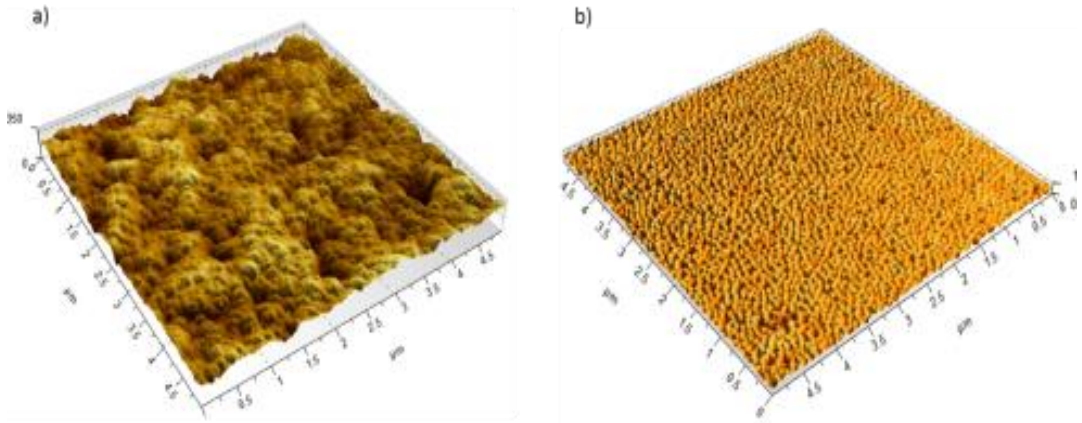

Figure 9.6 – AFM section images of TAMI MF (a) and AAO MF (b): a) 0.5 × 0.5 µm; b) 0.5 × 0.5 µm; note that z-scale of a) and b) is 250 and 1 µm, respectively

Table 9.2 summarizes surface roughness deviation of two MF membranes in terms of arithmetic mean deviation (Ra) and root-mean-square deviation (Rq), confirming that the AAO MF surface is smoother than TAMI.

Table 9.2 – Surface roughness deviation of TAMI MF and AAO MF membrane

	Roughness Deviation	*TAMI-MF 140nm*	*AAO-MF 100nm*
Ra	Arithmetic mean deviation	19.4 nm	6.94 nm
Rq	Root-mean-square deviation	24.4 nm	8.72 nm

AFM surface section images of the TAMI and AAO UF membrane were obtained with the same approach as tried for the AAO MF. As shown in Figure 9.7, AFM images revealed that the TAMI UF membrane surface (Figure a.) was rough with a larger deviation, while the AAO UF membrane (Figure b.) has a relatively smoother surface and smaller deviation, the same as observed in the AAO MF membrane (Lee et al. 2005a).

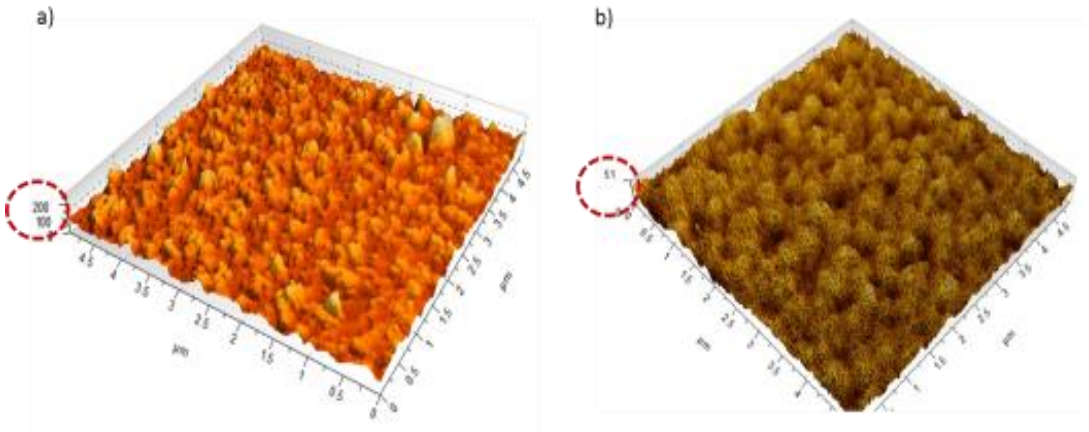

Figure 9.7 - AFM section images of TAMI UF (a) and AAO UF (b): a) 0.5 × 0.5 µm; b) 0.5 × 0.5 µm; note that z-scale of a) and b) is 200 and 51 µm, respectively

Surface roughness deviation of TAMI and AAO UF membranes in terms of arithmetic mean deviation (Ra) and root-mean-square deviation (Rq) were measured, resulting in 12.4 nm and 15.4 nm for TAMI UF and 2.78 nm and 3.45 nm for AAO UF, respectively.

9.3.4. Effects of three NOM types on membrane fouling

Effects of 50 mg/L sodium alginate (SA), humic acid (HA) and bovine serum albumin (BSA) in the presence and absence of calcium ions on fouling of two MF and UF ceramic membranes (i.e., TAMI and AAO) and polymeric membranes (i.e., PVDF for MF and MCE for UF) were evaluated.

9.3.4.1. Characterization of three NOM types

The SA, HA and BSA solutions were characterized using liquid chromatography – organic carbon detection (LC-OCD). The chromatographic peaks of the SA, HA and BSA were classified into mainly four fractions with respect to retention time, peak

shape and detector ratio of NOM (Huber et al. 2011) as shown in Figure 9.8 and Figure 9.9. Results showed that the SA solution mainly contained *biopolymers (BP)* fraction with a high molecular weight with almost no other fractions detected. The MW of this fraction is 10 kDa or higher as the column has a separation range of 0.1 – 10 kDa. The HA solution was characterized by small amounts of *humic substances (HS)* and *LMW neutrals*. Huber et al. reported that the MW of HS and LMW neutrals fractions are about 1 - 10 kDa and below 350 Da, respectively. The BSA solution contained small amounts of *biopolymers (BP)* fraction and *LMW neutrals*. According to some researchers, the MW of alginate ranges from 10 to 600 kDa depending on the extent of hydrolysis during alkaline extraction from brown algae, bovine serum albumin is a 66.5 kDa protein, and humic substances are smaller (Haberkamp et al. 2008). Specific UV absorbance (SUVA) of SA, HA and BSA were 0.49, 12.09, 3.14 L/mg·m.

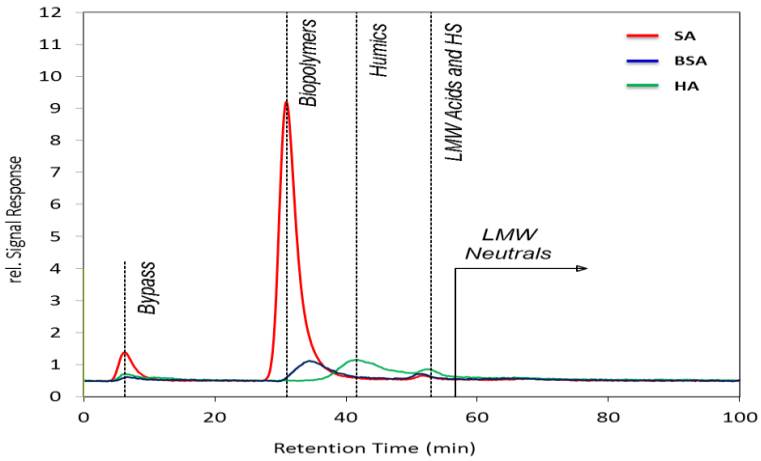

Figure 9.8 – Characterization of three NOM types of SA, BSA, and HA using size exclusion chromatography with organic carbon detection (LC-OCD): note that these results are based on separate injections

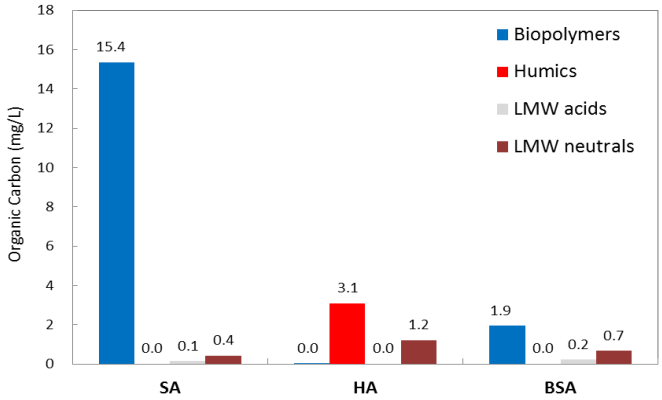

Figure 9.9 – Specific classification of chromatographic peaks of three NOM types (i.e., SA, HA and BSA) using LC-OCD

9.3.4.2. Calcium adsorption on MF/UF membranes

To identify calcium adsorption on membranes, flux decline of two ceramic membranes and polymeric membranes (i.e., designated as TAMI, AAO, PVDF and MCE in order) for filtering calcium-contained solutions were estimated. 4 mM of calcium solution in Milli-Q water (≈18 Ω) was prepared and applied to each MF/UF membrane during 30 minutes, and the filtration tests were replicated twice. As shown in Figure 9.10 and Figure 9.11, results show that all MF and UF membranes were operated with a stable flux throughout the filtration, confirming there was no effects of calcium on fouling of the TAMI, AAO, PVDF, MCE membranes for 30 minutes of operation.

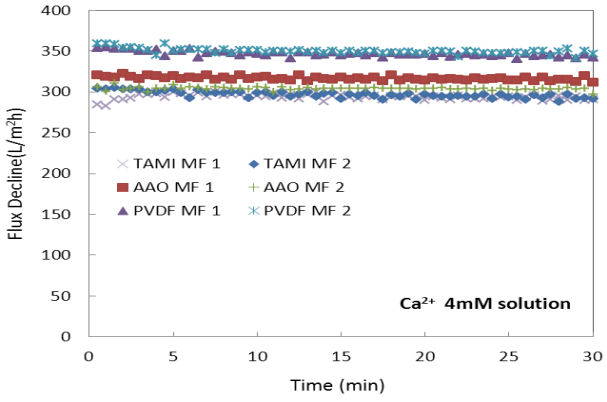

Figure 9.10 – Calcium effects on fouling of three MF membranes: filtration of each membrane was replicated twice (e.g., TAMI MF 1 and 2)

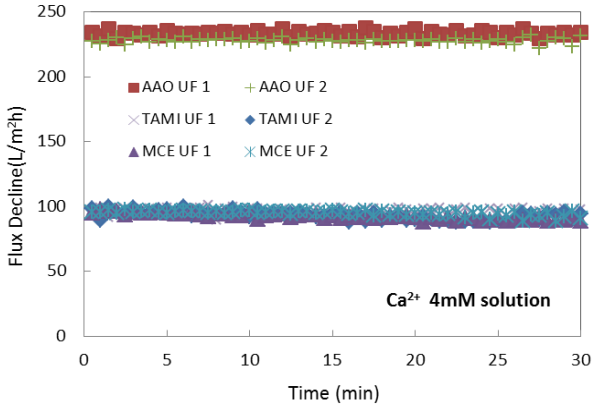

Figure 9.11 - Calcium effects on fouling of three UF membranes: filtration of each membrane was replicated twice (e.g., TAMI UF 1 and 2)

9.3.4.3. Effects of sodium alginate (SA) on membrane fouling

To investigate the impacts of sodium alginate (SA) in the absence/presence of calcium on fouling of MF and UF ceramic membranes, compared with polymeric membranes, the normalized flux decline of the membranes (i.e., TAMI, AAO, PVDF and MCE) were estimated for 30 minutes of operation.

For MF filtration experiments, initial membrane fluxes (J_0) of all MF membranes were set between 130 L/m^{2}h and 210 L/m^{2}h at 0.2 bar. The differences in normalized flux decline between two ceramic membranes (i.e., TAMI and AAO) and a PVDF membrane were observed as shown in Figure 9.12, however, overall the fluxes of all membranes significantly decreased within 5 min. of operation. The results implied that fouling of all membranes may proceed by pore blocking during the early stage of filtration, followed by cake layer formation (Ye et al. 2005). Particularly, in the absence of calcium, both AAO and TAMI ceramic MF membranes experienced severe flux decline, showing that the normalized fluxes were significantly decreased to 4% and 6% of the initial flux, respectively. On the other hands, the PVDF membrane experienced less fouling, showing the normalized flux declined to 36%

after 30 min. of operation. However, in the presence of calcium, the AAO and TAMI MF membrane experienced slightly less fouling, resulting in the normalized flux improvement to 14% and 18%, respectively, while the PVDF membrane showed more fouling, resulting in the normalized flux decline down to 16% from 36% in the absence of calcium as shown in Figure 9.12.

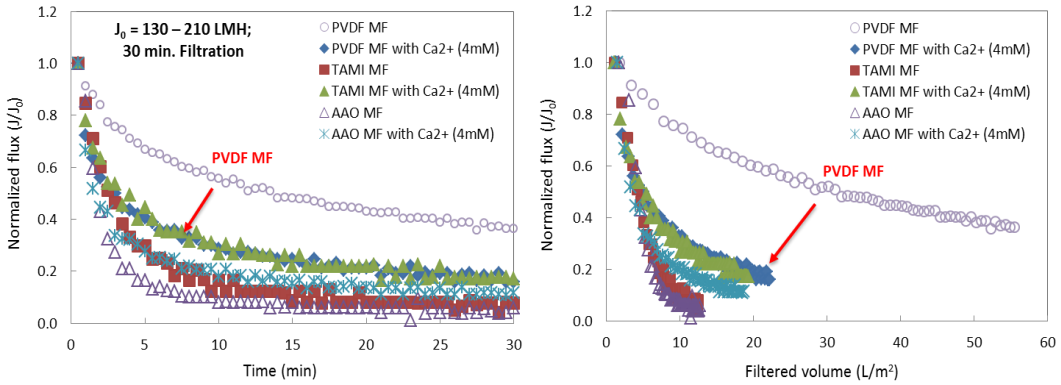

Figure 9.12 - Normalized flux decline of three different MF membranes as a function of time (left) and filtered volume (right) for 50mg/L sodium alginate (SA) solution in the absence/presence of calcium: Arrows in the figure present flux variation of PVDF MF membrane with calcium association

Rejections of sodium alginate achieved by three MF membranes are shown in Figure 9.13. The rejection of SA reached about 40% by both TAMI and AAO MF ceramic membranes, while almost no rejection was achieved by the PVDF MF membrane. The achievement of SA rejection by three membranes was matched to the normalized flux decline (Figure 9.12), showing steeper flux decline of ceramic membranes and gentler flux decline of the PVDF membrane. However, in the presence of calcium, the removal of SA significantly increased to over 80% by all MF membranes. It was noteworthy that even though the rejection of SA by the PVDF MF membrane reached to 80% with calcium association, the normalized flux was significantly decreased, while both AAO and TAMI ceramic membranes resulted in

not only improved flux but an increase in the SA removal with calcium association. Consequently, it was clearly observed that the SA removal by three MF membranes was effectively achieved by pore blocking followed by cake formation in the presence of calcium.

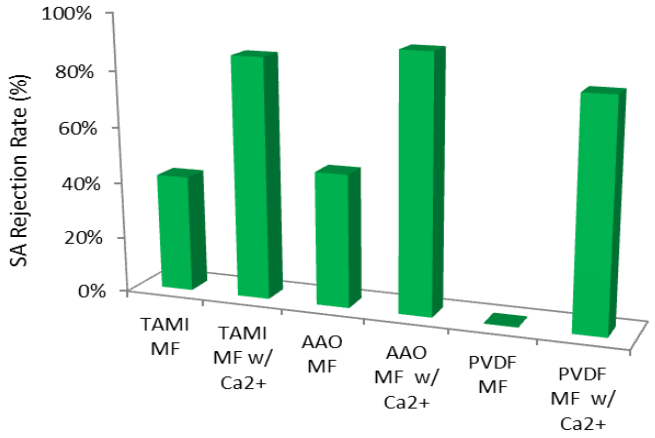

Figure 9.13 – Rejection (%) of sodium alginate in the absence/presence of calcium achieved by the TAMI, AAO and PVDF MF membrane

Considering results from both flux decline and SA rejection in the absence and presence of calcium achieved by three MF membranes, differences in fouling mechanisms between the TAMI and AAO ceramic membranes and the PVDF MF membrane were hypothesized as follows: 1) in the absence of calcium, the SA solution caused pore constriction/blocking for both ceramic MF membranes at the beginning of filtration followed by cake filtration which led to significant flux decline and about 40% SA rejection, while the PVDF MF membrane filtration did not reached cake formation for 30 minutes, leading to almost no rejection of SA; Moreover, for the TAMI and AAO MF filtration, it is concluded that larger size of alginate which ranges from 10 to 600 kDa (Haberkamp et al. 2008) or close to the pore size of the MF membranes caused pore size to reduce pore plugging, and subsequently smaller size of alginate were accumulated on the membrane surface promoting cake formation,

leading to SA removal of about 40 %. However, these fouling mechanisms did not dominate the PVDF MF membrane which is probably attributed to the difference in surface morphology from both ceramic membranes as shown in Figure 9.3; 2) in the presence of 4 mM calcium, the calcium induced molecular binding and aggregation with SA, leading to less fouling (i.e., flux improvement) for the TAMI and AAO MF membranes by promoting cake formation, while leading to more fouling for the PVDF MF membrane by pore blocking.

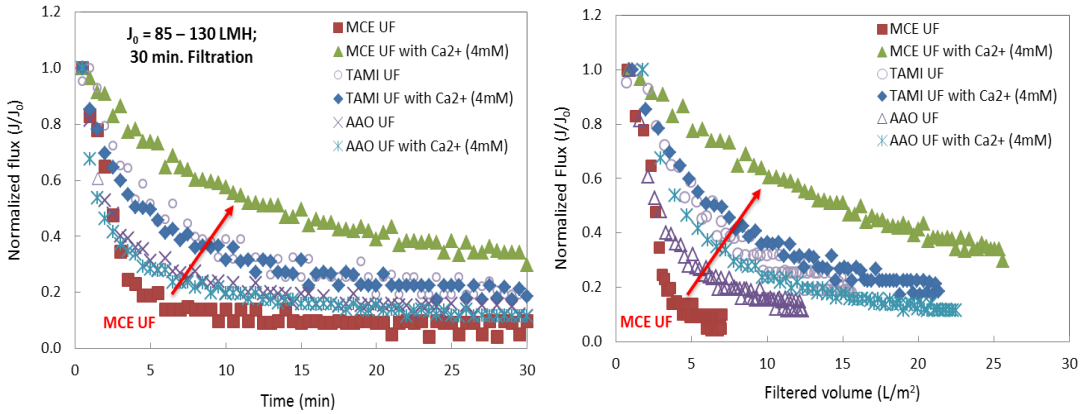

Figure 9.14 - Effects of sodium alginate (SA) with/without 4 mM calcium addition on three different UF membrane permeabilities

Effects of the sodium alginate (SA) on UF membrane fouling were compared. Initial flux (J_0) was set between 85 L/m^{2}h and 130 L/m^{2}h at 0.3 bar for the AAO UF membrane and at 0.6 bar for the TAMI and MCE UF membrane. As shown in Figure 9.14, all UF membranes experienced severe fouling caused by pore blocking followed by cake filtration in the absence of calcium. The most significant fouling was observed for the MCE UF membrane, showing that the normalized flux decreased to 14% of the initial within 5 minutes after operation starts, and decreased down to 10% during 30 minutes. Both AAO and TAMI UF membrane also experienced significant fouling, resulting in normalized flux decline to 15% and 22%

for 30 minutes of operation, respectively. In the presence of 4 mM calcium, there were no remarkable variations in the normalized fluxes of the AAO and TAMI UF membranes. However, difference in flux variation between two ceramic UF membranes and the MCE UF membrane were observed. Compared to the MF membrane performances, the MCE polymeric UF membrane exhibited the most improved flux (i.e., reduced fouling) among others, showing that the normalized flux improved to 34% of the initial flux, which was completely opposite to the result for the PVDF MF membrane filtration as shown in Figure 9.12.

Figure 9.15 shows the SA removal by three UF membranes in the absence and presence of calcium. All UF membranes achieved better removal efficiency of sodium alginate than those of MF membranes, attributed to smaller pore size of the UF membranes than the MF membranes. Results showed that the SA was removed to 66% and 88% by the AAO and TAMI UF ceramic membranes, and rejected to 39% by the MCE UF membrane. An interesting observation was that even if the MCE UF membrane flux were the most sharply decreased, the SA removal was not relatively high compared to both ceramic UF membranes. Calcium addition (4 mM) played a role in improving the SA removal efficiency with increased removal to 86%, 92% and 85% by the TAMI, AAO and MCE UF membrane, respectively. The results confirmed that SA-calcium complexes led to better rejection by all UF membranes, attributed to the effect of calcium on binding and aggregation with the polysaccharide macromolecules (Katsoufidou et al. 2010).

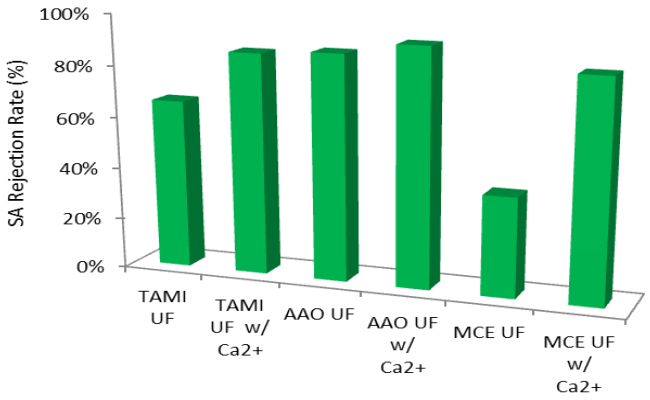

Figure 9.15 - Rejection (%) of sodium alginate in the absence/presence of calcium for the TAMI, AAO and MCE UF membrane

In summary, for both MF and UF filtration, the TAMI and AAO ceramic membranes showed better removal of SA in the absence of calcium than the PVDF MF membrane and the MCE UF membrane. However, in the presence of calcium, all three membranes achieved more than 80% of SA rejection with reduced membrane fouling, attributed to calcium-binding with sodium alginate; and the cake filtration mechanism dominates (Hashino et al. 2011b).

9.3.4.4. Effects of humic acid (HA) with calcium on membrane fouling

Effects of humic acid (HA) in the presence and absence of calcium on fouling of ceramic and polymeric MF and UF membranes were assessed comparing the normalized flux decline of two ceramic membranes (i.e., TAMI ceramic membranes and AAO ceramic membranes) and a PVDF polymeric membrane for 30 minutes of operation.

For MF membrane experiments, initial membrane flux (J_0) was set between 215 L/m^2h and 260 L/m^2h at 0.1 bar for the AAO MF membrane and at 0.15 bar for the TAMI and PVDF MF membranes. Figure 9.16 shows the normalized flux decline of

the three membranes in the presence and absence of calcium. In the absence of calcium, the sharpest flux decline was observed for the AAO MF membrane, followed by TAMI and PVDF MF membranes that follow nearly the same trend. In presence of 4 mM calcium, the AAO MF membrane experienced less fouling, showing that the normalized flux increased to 64% from 47% at a filtered volume of 68 L/m^2, while other MF membranes showed almost no variation for filtering HA solution in the presence of calcium.

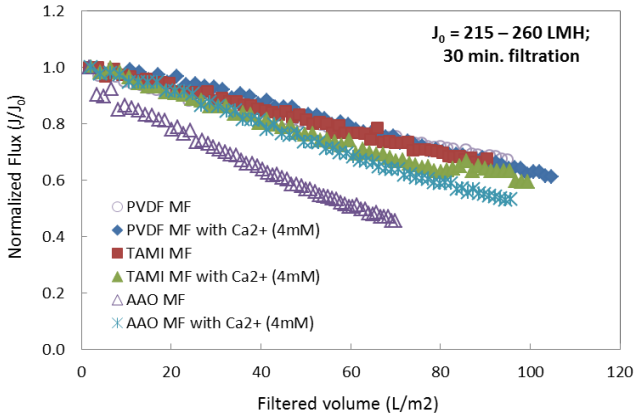

Figure 9.16 – Comparison of normalized flux decline of three MF membranes for filtration of 50 mg/L humic acid (HA) solution with calcium 4mM.

Figure 9.17 compares rejection rate of humic acid (HA) achieved by three membranes. Results showed that in absence of calcium, humic acid removal by all MF membranes were less than 20%, however, the AAO MF ceramic membrane resulted in slightly higher removal, followed by the TAMI MF and the PVDF MF membranes. When calcium was added to the solution, the HA removal efficiency significantly increased to more than 80%. Interestingly, among all results, the AAO MF membrane resulted in slightly higher rejection rate as well, which was relevant to the sharpest flux decline amongst as shown in Figure 9.16. Meaningful observation herein was that calcium (Ca^{2+})-HA complex was easily rejected by all MF membranes.

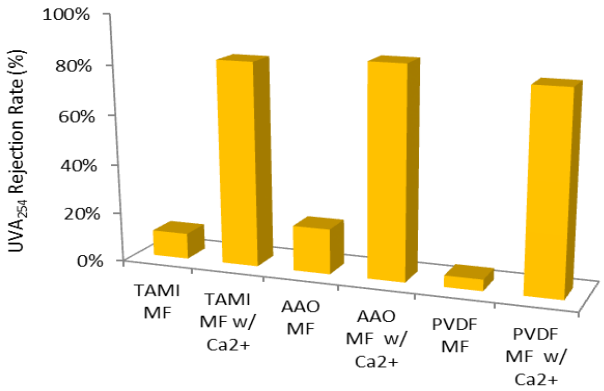

Figure 9.17 – HA rejection rate (%) achieved by the TAMI, AAO and PVDF MF membrane filtration

Effects of HA on UF membrane fouling were assessed. The initial flux (J_0) was set between 100 L/m^{2}h and 120 L/m^{2}h at 0.15 bar (for the AAO UF membrane) and 0.5 bar (for the TAMI and MCE UF membranes). As shown in Figure 9.18, in the absence of calcium, the normalized flux of the TAMI UF membrane sharply decreased to 41% of the initial flux, followed by the AAO UF membrane decreased to 73%, and the MCE UF membrane to 86%. Rejection of humic acid was proportional to the trend of flux decline, showing 90%, 20% and 7% for the TAMI, AAO and MCE UF membranes, respectively. In the presence of calcium, both the normalized membrane flux and humic acid removal were improved. Results showed that the normalized flux of the TAMI UF membrane was improved to 58% from 41% of the initial flux, the AAO UF flux increased to 85% from 73%, and the MCE flux improved to 96% from 86% of the initial flux. HA removal rate also increased to 93%, 86% and 81% for the TAMI, AAO and MCE UF membranes, respectively, in the presence of 4mM calcium

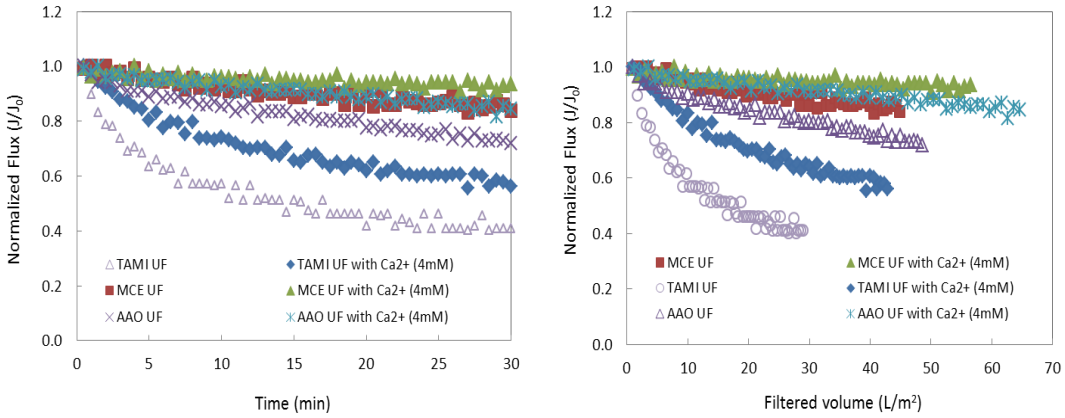

Figure 9.18 - Comparison of normalized flux decline of three UF membranes for filtration of 50 mg/L humic acid (HA) solution with calcium 4mM

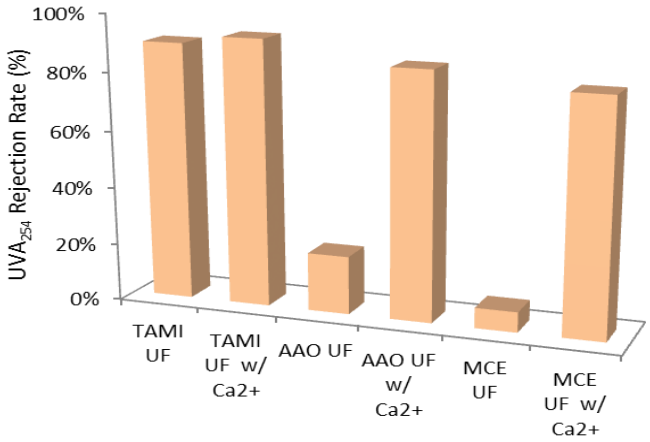

Figure 9.19 - HA rejection rate (%) by TAMI, AAO and MCE UF membrane filtration

Consequently, the differences in both the membrane fouling and the rejections between the SA solution and the HA solution were observed. Results showed that sodium alginate solution caused relatively severe fouling and higher rejection by all types of MF and UF membranes compared to the HA solution, which is considered to be attributed to the MW size differences and gel-like properties of sodium alginate (i.e., polysaccharide). However, in the presence of calcium, both the TAMI and AAO ceramic MF and UF membranes experienced less fouling (i.e., increased flux) and higher removal for filtering both the sodium alginate and humic acid solution. On the

other hand, in the presence of calcium, the PVDF MF membrane experienced an increase in fouling but improved removal for filtering the sodium alginate solution, which is attributed to promoting pore-blocking followed by cake formation by the effect of calcium on binding and aggregation of the SA macromolecules.

9.3.4.5. Effects of bovine serum albumin (BSA) with calcium on membrane fouling

Effects of bovine serum albumin (BSA) in the presence and absence of calcium on fouling of three membranes (i.e., two ceramic membranes and a polymeric membrane) were assessed comparing the normalized flux decline for 30 minutes of operation. Initial flux (J_0) was set between 210 L/m^{2}h and 270 L/m^{2}h at 0.1 bar for AAO MF membranes and at 0.15 bar for TAMI and PVDF MF membranes. As shown in Figure 9.20, there was slight difference in normalized flux decline of three membranes observed, showing the flux decline of the AAO MF membrane to 81% of the initial flux, followed by PVDF and TAMI MF membranes decreasing to 87% and 94%, respectively. In the presence of calcium (4 mM), the normalized flux decline of the PVDF MF membrane was slightly improved, but no flux improvement for two ceramic membranes was observed. Figure 9.21 compares the BSA removal achieved by three MF membranes in the absence and presence of calcium. In absence of calcium, BSA removals determined for two ceramic membranes were less than 10% and almost no removal was observed for the PVDF membrane. The BSA solution was characterized by small amounts of *biopolymers (BP)* fraction and *LMW neutrals* as shown in Figure 9.8. In addition, the size of BSA has been known to be much smaller than the pore size of MF membranes (Haberkamp et al. 2008), therefore the BSA may be adsorbed on the pore surface, leading to a gradual and prolonged normalized flux

decline and little removal. In the presence of calcium, no improvement of BSA removal was measured by all MF membranes. Considering both flux decline and the BSA removal in the presence of calcium, it is concluded that the BSA-calcium association might not occur, or even if the aggregation occurred, the size is still smaller than the pore size.

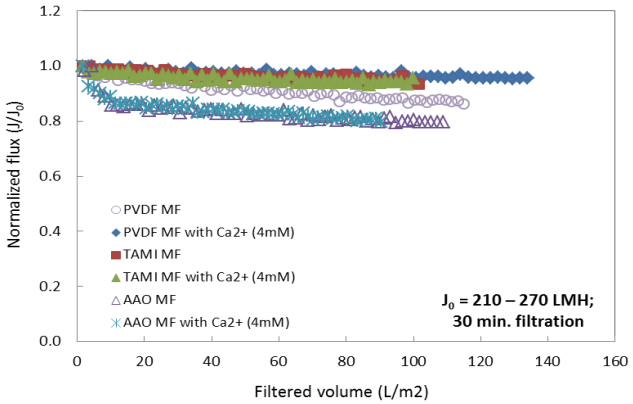

Figure 9.20 - Comparison of normalized flux decline of three MF membranes for filtration of bovine serum albumin (BSA) in absence/presence of 4 mM calcium; feed solution consists of 50 mg/L BSA and 0.5 mM sodium bicarbonate at pH 8

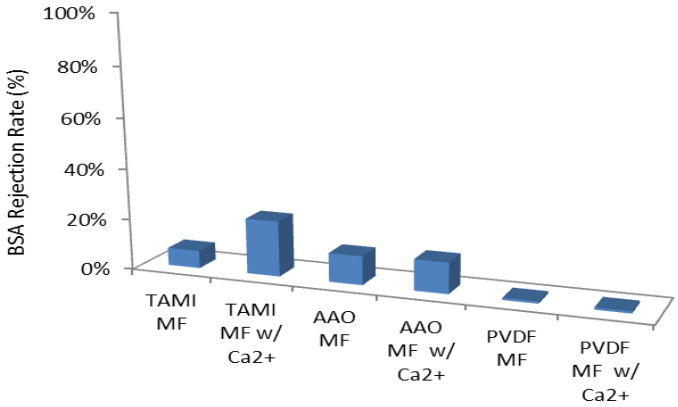

Figure 9.21 - BSA rejection rate (%) for TAMI, AAO (which is named AAO in the figure) and PVDF MF membranes

Effects of BSA on UF membrane fouling were compared as shown in Figure 9.22. Initial fluxes (J_0) were set between 100 L/m^{2}h and 120 L/m^{2}h at 0.15, 0.4 and 0.5 bar

for the AAO, TAMI and MCE UF membrane, respectively. In absence of calcium, normalized fluxes of all membranes gently decreased to about 80% of the initial fluxes, and the BSA removal determined for the TAMI, AAO and MCE UF membranes was not over 20%. In the presence of calcium, the normalized flux of the AAO UF and MCE UF membranes was not varied, showing nearly the same as observed in the absence of calcium. But, the TAMI UF membrane experienced severe fouling (i.e., more flux decline) with calcium association, showing steep flux decline to 36% of the initial flux for 30 min. of filtration.

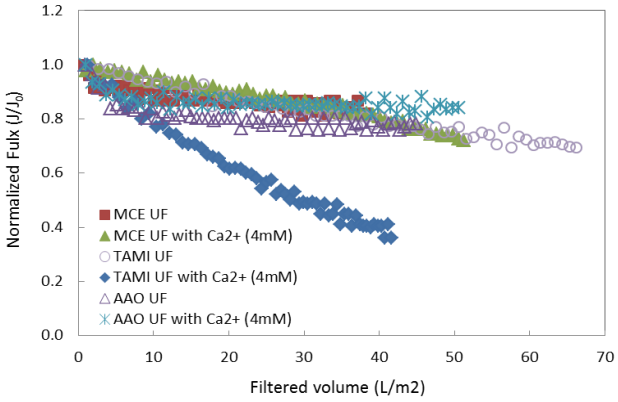

Figure 9.22 - Comparison of normalized flux decline of three UF membranes for filtration of bovine serum albumin (BSA) in absence/presence of calcium

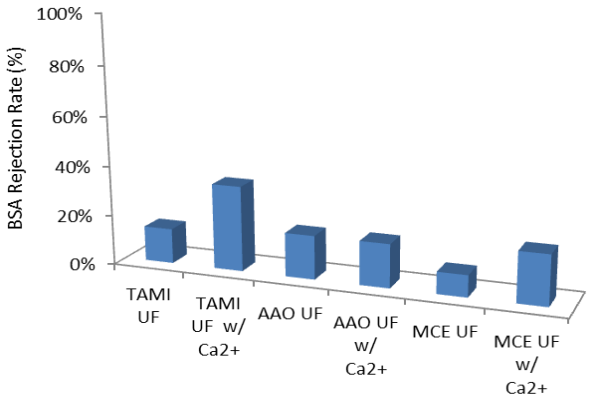

Figure 9.23 - BSA rejection rate (%) for TAMI, AAO (which is named AAO in the figure) and MCE UF membranes

As discussed in MF membrane filtration, the BSA solution characterized by small amounts of *biopolymers (BP)* fraction and *LMW neutrals* has a smaller size than the pore size of UF membranes, so the BSA may be adsorbed on the pore surface, leading to a gradual and prolonged normalized flux decline and little removal. On the other hand, more fouling of the TAMI UF membrane in the presence of calcium were observed, therefore, it is clearly concluded that the BSA-calcium association occurred, however, the majority of aggregates are still smaller than the pore size of the AAO and PVDF UF membranes, but the aggregates are larger or close to the pore size of the TAMI UF membrane.

9.4. CONCLUSIONS

The impacts of three NOM types in the presence and absence of calcium ions on both MF and UF ceramic membrane filtration were evaluated in terms of permeability and removal efficiency, compared to polymeric membranes. Sodium alginate (SA), humic acid (HA) and bovine serum albumin (BSA) solutions were used as NOM models. Two different types of ceramic membranes which are fabricated by sintering (TAMI, based on TiO_2+ZrO_2) and anodic oxidation process (AAO, based on Al_2O_3), and polymeric membranes such as polyvinylidene difluoride (PVDF) and mixed cellulose ester (MCE) for MF and UF, respectively, were tested in bench-scale experiments.

Overall, both TAMI and AAO MF and UF ceramic membranes showed better performance compared to the PVDF MF and MCE UF membranes in terms of rejection of three NOM types. Sodium alginate (SA) solution among the three NOM

types caused the most significant fouling and showed the highest rejection by both the MF and UF ceramic membranes, followed by HA and BSA in order. These observations demonstrated that polysaccharides (i.e., hydrophilic NOM) might be the most problematical fouling species in both DW and WW treatment applications compared to the humic acid and proteins, which is attributed to the MW size difference and gel-like properties of sodium alginate. For the sodium alginate (SA) solution, it was considered that fouling of all membranes may be proceeded by pore blocking during the early stage of filtration, followed by cake layer formation.

For filtration of humic acid (HA), the normalized flux of the TAMI UF membrane sharply decreased, followed by the AAO UF membrane and the MCE UF membrane. The rejection rate of humic acid was proportional to the trend of the flux decline. On the other hand, for the bovine serum albumin (BSA) solution, the normalized fluxes of all membranes gradually decreased over filtration time and there was no distinct difference between all MF and UF membranes.

Calcium (Ca^{2+}) played an important role in significantly improving removal efficiency of sodium alginate and humic acid by both ceramic and polymeric MF and UF membranes, while little impacts on bovine serum albumin was observed except for the TAMI UF membrane. In the presence of calcium, both the TAMI and AAO ceramic MF and UF membranes experienced less fouling (i.e., increased flux) and higher removal in filtering both the sodium alginate and humic acid solutions. However, in the presence of calcium, the PVDF MF membrane experienced an increase in fouling but improved removal for filtering the sodium alginate solution,

which is attributed to pore-blocking followed by cake formation induced by the effect of calcium on binding and aggregation of the SA macromolecules.

9.5. REFERENCES

Alazmi, R., Nassehi, V. and Wakeman, R. (2010) Calcium cation interactions with polysaccharides and proteins in wastewater UF membrane fouling. Membrane Technology 2010(1), 6-12.

Amy, G. (2008) Fundamental understanding of organic matter fouling of membranes. Desalination 231(1-3), 44-51.

Aspelund, M.T., Rozeboom, G., Heng, M. and Glatz, C.E. (2008) Improving permeate flux and product transmission in the microfiltration of a bacterial cell suspension by flocculation with cationic polyelectrolytes. Journal of Membrane Science 324(1–2), 198-208.

Badis, A., Ferradji, F.Z., Boucherit, A., Fodil, D. and Boutoumi, H. (2010) Removal of natural humic acids by decolorizing actinomycetes isolated from different soils (Algeria) for application in water purification. Desalination 259(1–3), 216-222.

Boussu, K., Van der Bruggen, B., Volodin, A., Snauwaert, J., Van Haesendonck, C. and Vandecasteele, C. (2005) Roughness and hydrophobicity studies of nanofiltration membranes using different modes of AFM. Journal of Colloid and Interface Science 286(2), 632-638.

Costa, A.R., de Pinho, M.N. and Elimelech, M. (2006) Mechanisms of colloidal natural organic matter fouling in ultrafiltration. Journal of Membrane Science 281(1–2), 716-725.

Dafinov, A., Garcia-Valls, R. and Font, J. (2002) Modification of ceramic membranes by alcohol adsorption. Journal of Membrane Science 196(1), 69-77.

Fu, X., Maruyama, T., Sotani, T. and Matsuyama, H. (2008) Effect of surface morphology on membrane fouling by humic acid with the use of cellulose acetate butyrate hollow fiber membranes. Journal of Membrane Science 320(1–2), 483-491.

Garmash, E.P., Kryuchkov, Y.N. and Pavlikov, V.N. (1995) Ceramic membrane for ultra- and microfiltration (Review). Glass and Ceramic 52(6), 150-152.

Haberkamp, J., Ernst, M., Makdissy, G., Huck, P.M. and Jekel, M. (2008) Protein fouling of ultrafiltration membranes - Investigation of several factors relevant for

tertiary wastewater treatment. Journal of Environmental Engineering and Science 7(6), 651-660.

Hao, Y., Moriya, A., Ohmukai, Y., Matsuyama, H. and Maruyama, T. (2013) Effect of metal ions on the protein fouling of hollow-fiber ultrafiltration membranes. Separation and Purification Technology 111(0), 137-144.

Hashino, M., Hirami, K., Katagiri, T., Kubota, N., Ohmukai, Y., Ishigami, T., Maruyama, T. and Matsuyama, H. (2011a) Effects of three natural organic matter types on cellulose acetate butyrate microfiltration membrane fouling. Journal of Membrane Science 379(1–2), 233-238.

Hashino, M., Katagiri, T., Kubota, N., Ohmukai, Y., Maruyama, T. and Matsuyama, H. (2011b) Effect of membrane surface morphology on membrane fouling with sodium alginate. Journal of Membrane Science 366(1–2), 258-265.

Hong, S. and Elimelech, M. (1997) Chemical and physical aspects of natural organic matter (NOM) fouling of nanofiltration membranes. Journal of Membrane Science 132(2), 159-181.

Huber, S.A., Balz, A., Abert, M. and Pronk, W. (2011) Characterisation of aquatic humic and non-humic matter with size-exclusion chromatography - organic carbon detection - organic nitrogen detection (LC-OCD-OND). Water Research 45(2), 879-885.

Jermann, D., Pronk, W., Kägi, R., Halbeisen, M. and Boller, M. (2008) Influence of interactions between NOM and particles on UF fouling mechanisms. Water Research 42(14), 3870-3878.

Jones, K.L. and O'Melia, C.R. (2000) Protein and humic acid adsorption onto hydrophilic membrane surfaces: effects of pH and ionic strength. Journal of Membrane Science 165(1), 31-46.

Karnik, B.S., Davies, S.H.R., Chen, K.C., Jaglowski, D.R., Baumann, M.J. and Masten, S.J. (2005) Effects of ozonation on the permeate flux of nanocrystalline ceramic membranes. Water Research 39(4), 728-734.

Katsoufidou, K., Yiantsios, S.G. and Karabelas, A.J. (2005) A study of ultrafiltration membrane fouling by humic acids and flux recovery by backwashing: Experiments and modeling. Journal of Membrane Science 266(1–2), 40-50.

Katsoufidou, K., Yiantsios, S.G. and Karabelas, A.J. (2008) An experimental study of UF membrane fouling by humic acid and sodium alginate solutions: the effect of backwashing on flux recovery. Desalination 220(1–3), 214-227.

Katsoufidou, K.S., Sioutopoulos, D.C., Yiantsios, S.G. and Karabelas, A.J. (2010) UF membrane fouling by mixtures of humic acids and sodium alginate: Fouling mechanisms and reversibility. Desalination 264(3), 220-227.

Kelly, S.T. and Zydney, A.L. (1995) Mechanisms for BSA fouling during microfiltration. Journal of Membrane Science 107(1–2), 115-127.

Kim, H.-C. and Dempsey, B.A. (2013) Membrane fouling due to alginate, SMP, EfOM, humic acid, and NOM. Journal of Membrane Science 428(0), 190-197.

Kim, I.S. and Jang, N. (2006) The effect of calcium on the membrane biofouling in the membrane bioreactor (MBR). Water Research 40(14), 2756-2764.

Kim, J., Davies, S.H.R., Baumann, M.J., Tarabara, V.V. and Masten, S.J. (2008) Effect of ozone dosage and hydrodynamic conditions on the permeate flux in a hybrid ozonation–ceramic ultrafiltration system treating natural waters. Journal of Membrane Science 311(1–2), 165-172.

Larbot, A., Gazagnes, L., Krajewski, S., Bukowska, M. and Wojciech, K. (2004) Water desalination using ceramic membrane distillation. Desalination 168, 367-372.

Lee, N., Amy, G. and Croué, J.-P. (2006) Low-pressure membrane (MF/UF) fouling associated with allochthonous versus autochthonous natural organic matter. Water Research 40(12), 2357-2368.

Lee, N., Amy, G., Croué, J.-P. and Buisson, H. (2004) Identification and understanding of fouling in low-pressure membrane (MF/UF) filtration by natural organic matter (NOM). Water Research 38(20), 4511-4523.

Lee, N., Amy, G., Croué, J.-P. and Buisson, H. (2005) Morphological analyses of natural organic matter (NOM) fouling of low-pressure membranes (MF/UF). Journal of Membrane Science 261(1–2), 7-16.

Lee, S. and Cho, J. (2004) Comparison of ceramic and polymeric membranes for natural organic matter (NOM) removal. Desalination 160(3), 223-232.

Lehman, S.G. and Liu, L. (2009) Application of ceramic membranes with pre-ozonation for treatment of secondary wastewater effluent. Water Research 43(7), 2020-2028.

Maartens, A., Swart, P. and Jacobs, E.P. (1998) Humic membrane foulants in natural brown water: characterization and removal. Desalination 115(3), 215-227.

Ruohomäki, K., Väisänen, P., Metsämuuronen, S., Kulovaara, M. and Nyström, M. (1998) Characterization and removal of humic substances in ultra- and nanofiltration. Desalination 118(1–3), 273-283.

Salehi, E. and Madaeni, S.S. (2010) Adsorption of humic acid onto ultrafiltration membranes in the presence of protein and metal ions. Desalination 263(1–3), 139-145.

Shao, J., Hou, J. and Song, H. (2011) Comparison of humic acid rejection and flux decline during filtration with negatively charged and uncharged ultrafiltration membranes. Water Research 45(2), 473-482.

Sobeck, D.C. and Higgins, M.J. (2002) Examination of three theories for mechanisms of cation-induced bioflocculation. Water Research 36(3), 527-538.

Sutzkover-Gutman, I., Hasson, D. and Semiat, R. (2010) Humic substances fouling in ultrafiltration processes. Desalination 261(3), 218-231.

Xu, J., Chang, C.-Y. and Gao, C. (2010) Performance of a ceramic ultrafiltration membrane system in pretreatment to seawater desalination. Separation and Purification Technology 75(2), 165-173.

Yang, N., Wen, X., Waite, T.D., Wang, X. and Huang, X. (2011) Natural organic matter fouling of microfiltration membranes: Prediction of constant flux behavior from constant pressure materials properties determination. Journal of Membrane Science 366(1–2), 192-202.

Ye, Y., Le Clech, P., Chen, V., Fane, A.G. and Jefferson, B. (2005) Fouling mechanisms of alginate solutions as model extracellular polymeric substances. Desalination 175(1), 7-20.

Yuan, W. and Zydney, A.L. (1999) Humic acid fouling during microfiltration. Journal of Membrane Science 157(1), 1-12.

Yuan, W. and Zydney, A.L. (2000) Humic acid fouling during ultrafiltration. Environmental Science and Technology 34(23), 5043-5050.

Chapter 10

Conclusions and Future Work

10.1. CONCLUSIONS

The objective of this research was to identify the effects of coagulation and/or ozonation on ceramic membrane filtration for impaired-quality source waters (i.e., seawater and WW effluent). Two different types of MF and UF ceramic membranes which are fabricated by sintering (TAMI made of TiO_2+ZrO_2) and anodic oxidation process (AAO made of Al_2O_3) were used for bench-scale tests.

Precoagulation was shown to play an important role in both enhancing membrane filterability and NOM removal efficacy for treating a high-organic surface water. The most critical factors were found to be pH and coagulant dosage with the highest efficiency resulting under a low pH of 5.5 and a high dosage of 10 mg/L, designated as enhanced coagulation conditions. In-line coagulation without an additional flocculation step could effectively play a role in enhancing the TAMI MF ceramic membrane performance, which is also more effective under enhanced coagulation conditions. LC-OCD and 3D-FEEM demonstrated that NOM removal is proportion to coagulant dosage and more significantly achieved at a low pH range (i.e., 5.5 or possibly lower), resulting in improved preferential removal of humics over non-humics. Biopolymers responsible for problematical membrane fouling were easily removed by ceramic MF membrane filtration with precoagulation.

Due to the ozone-resistance nature of the ceramic membranes, preozonation allows the ceramic membranes to be operated at higher flux for filtration of impaired-quality source waters (i.e., seawater and WW effluent), particularly leading to more significant flux improvement when treating seawater rather than WW effluent, which

was attributed to the high presence of calcium and magnesium. Several analytical methods such as SEM-EDX, AFM, UVA_{254}, TEP visualization and zeta potential (ζ) revealed that not only does O_3 degrade NOM molecules (particularly TEP) which mostly cause problematical fouling into smaller fragments, but it also help to form microflocs as a result of ozone-induced flocculation of organic matter through binding with divalent cations, such as calcium and magnesium, in seawater.

pCBA as a ˙OH radical probe compound demonstrated that dissolved ozone in contact with the TAMI ceramic membrane surface allowed the formation of ˙OH radicals in WW effluent treatment, showing flux improvement as a result of breaking down organic matter. On the other hand, there was no formation of ˙OH radical observed in seawater application; however, the membrane flux was significantly improved.

Flux restoration of the TAMI and AAO membranes, fouled with seawater and WW effluent, was efficiently achieved by high BW pressure and ozone-CEB. This was attributed to the robustness of ceramic membranes in terms of mechanical and chemical stability. Assimilable organic carbon (AOC) production was observed when ozone is applied prior to ceramic membrane filtration for seawater and WW effluent, transforming dissolved organic carbon (DOC) into AOC, so a suitable process to control this parameter after ozonation is indispensable. However, as ozone dose increased to a certain level, AOC started to become mineralized.

Both amphoteric ceramic membranes exhibited a pH-dependence of permeate flux while filtering WW effluent, showing reduced fouling with increased pH. Flux variation of the AAO membrane was very sensitive to pH values, showing the higher

the pH, the better the permeate flux. On the other hand, the TAMI membrane showed stable flux decline at a low pH range, starting to become sensitive at the high pH range, resulting in better permeate flux. When filtering seawater, there was a difference in permeate flux between the membranes under basic pH conditions, showing that the TAMI membrane flux was stable regardless of changes in pH, while the AAO membrane flux significantly decreased as pH increased to 10. It was hypothesized that the Al_2O_3-based AAO ceramic membrane adsorbs some metal-hydroxide complexes, causing pore-blocking and cake formation on the membrane surface, but these chemical reactions do not occur with the TiO_2+ZrO_2-based TAMI ceramic membrane, maintaining stabilized flux at an increased pH level of 10.

The impacts of three NOM types in the presence and absence of calcium ions on both MF and UF ceramic membrane filtration were evaluated in terms of permeability and removal efficiency, compared to polymeric membranes. Sodium alginate, humic acid and bovine serum albumin solutions were used as NOM models. The TAMI and AAO MF and UF ceramic membranes showed better performance compared to the PVDF MF and MCE UF membranes in terms of rejection of the three NOM types. Sodium alginate solution among the three NOM types caused the most significant fouling and showed the highest rejection by both MF and UF ceramic membranes, followed by humic acid and bovine serum albumin. These observations demonstrated that polysaccharides (i.e., hydrophilic NOM) might be the most problematical fouling species in both DW and WW treatment applications compared to humic acid and proteins. Calcium (Ca^{2+}) played an important role in significantly improving removal efficiency of sodium alginate and humic acid by both ceramic and polymeric MF and

UF membranes, while little impacts on bovine serum albumin was observed except for the TAMI UF membrane.

In conclusion, ceramic membranes are expected to play an important role in both drinking water and water reuse applications as follows: 1) creation of high productivity by elevating membrane operational flux; 2) significant improvement of membrane filterability by reducing membrane fouling as a result of combination with ozone and/or coagulation pretreatments; 3) increase in flux restoration (i.e., fouling reversibility) by not only high pressurized BW, but also ozone (O_3)-enhanced backwashing in a CEB; 4) especially, high performance in treating impaired-quality source waters (e.g., seawater and wastewater) rather than normal surface waters, leading to successful employment as one of the powerful pretreatments before RO in desalination or water reuse applications.

10.2. FUTURE WORK

This research demonstrated that coagulation and/or ozonation in combination with ceramic membrane filtration can play a significant role in treating impaired-quality source waters such as seawater and wastewater in terms of filterability, permeability and flux restoration. However, the experiments were carried out using bench-scale units with the TAMI and AAO MF and UF ceramic membrane discs. Therefore, pilot tests using the TAMI MF and UF ceramic membranes which are commercially available are necessary to determine operational conditions (e.g., sustainable flux, coagulation parameters, ozone dosage, backwashing duration and pressure) for both drinking water and water reuse applications.

Moreover, a life cycle analysis (LCA) of ceramic membranes compared with polymeric membranes for 20 years for filtration of various impaired-quality source waters instead of normal surface water treatment should be carried out in order to identify whether ceramic membranes are competitive to polymeric membranes in seawater and wastewater reuse applications, leading to increases in the application of membrane processes as an alternative to overcome some limitations of polymeric membranes.